ON PAIRED DECOUPLED QUASI-LINEARIZATION METHODS FOR SOLVING NONLINEAR SYSTEMS OF DIFFERENTIAL EQUATIONS THAT MODEL BOUNDARY LAYER FLUID FLOW PROBLEMS

A THESIS SUBMITTED TO THE UNIVERSITY OF KWAZULU-NATAL
FOR THE DEGREE OF DOCTOR OF PHILOSOPHY
IN THE COLLEGE OF AGRICULTURE, ENGINEERING & SCIENCE

By

Olumuyiwa Otegbeye

School of Mathematics, Statistics & Computer Science

November 2018

Contents

List of Tables

List of Figures

Abstract

Two numerical methods, namely the spectral quasilinearization method (SQLM) and the spectral local linearization method (SLLM), have been found to be highly efficient methods for solving boundary layer flow problems that are modeled using systems of differential equations. Conclusions have been drawn that the SLLM gives highly accurate results but requires more iterations than the SQLM to converge to a consistent solution. This leads to the problem of figuring out how to improve on the rate of convergence of the SLLM while maintaining its high accuracy.

The objective of this thesis is to introduce a method that makes use of quasilinearization in pairs of equations to decouple large systems of differential equations. This numerical method, hereinafter called the paired quasilinearization method (PQLM) seeks to break down a large coupled nonlinear system of differential equations into smaller linearized pairs of equations. We describe the numerical algorithm for general systems of both ordinary and partial differential equations. We also describe the implementation of spectral methods to our respective numerical algorithms. We use MATHEMATICA to carry out the numerical analysis of the PQLM throughout the thesis and MATLAB for investigating the influence of various parameters on the flow profiles in Chapters 4, 5 and 6.

We begin the thesis by defining the various terminologies, processes and methods that are applied throughout the course of the study. We apply the proposed paired methods to systems of ordinary and partial differential equations that model boundary layer flow problems. A comparative study is carried out on the different possible combinations made for each example in order to determine the most suitable pairing needed to generate the most accurate solutions. We test convergence speed using the infinity norm of solution error. We also test their accuracies by using the infinity norm of

the residual errors. We also compare our method to the SLLM to investigate if we have successfully improved the convergence of the SLLM while maintaining its accuracy level. Influence of various parameters on fluid flow is also investigated and the results obtained show that the paired quasilinearization method (PQLM) is an efficient and accurate method for solving boundary layer flow problems. It is also observed that a small number of grid-points are needed to produce convergent numerical solutions using the PQLM when compared to methods like the finite difference method, finite element method and finite volume method, among others. The key finding is that the PQLM improves on the rate of convergence of the SLLM in general. It is also discovered that the pairings with the most nonlinearities give the best rate of convergence and accuracy.

Preface

The studies carried out in this thesis were under the direct supervision of Prof. S. S. Motsa in the School of Mathematics, Statistics and Computer Science, College of Agriculture, Engineering and Science, University of KwaZulu-Natal, Pietermaritzburg, from February 2015 to October 2018.
I hereby declare that the thesis represents the original work of the author except where duly acknowledged and referenced. No portion of the thesis has been submitted to another university or institution of learning for any degree or qualification.

Signature: ....

Olumuyiwa Otegbeye Date

Signature: ....

Prof. S. S. Motsa Date

Declaration 2: Plagiarism

I, Olumuyiwa Otegbeye, declare that:

(i) The studies conducted in this thesis, except where duly indicated and acknowledged, represent my original effort;

(ii) this thesis has not been submitted in full or in part for any degree or examination to any other university;

(iii) this thesis does not contain data, pictures, graphs or other information, that belongs to someone else unless where duly acknowledged;

(iv) this thesis does not contain the writing of others, unless specifically acknowledged as being sourced from other researchers. Where other written sources have been quoted, then:

  (a) their words have been re-written but the general information attributed to them has been referenced;

  (b) where their exact words have been used, their writing has been placed inside quotation marks, and referenced;

(v) this thesis does not contain text, graphics or tables copied and pasted from the Internet, unless specifically acknowledged, and the source being detailed in the thesis and in the References sections.

Signature: ....

Olumuyiwa Otegbeye Date

Declaration 2:Publication

O. Otegbeye and S. S. Motsa. A paired quasilinearization method for solving boundary layer flow problems. *American Institute of Physics conference proceedings, https://doi.org/10.1063/1.5042190.*

O. Otegbeye and S. S. Motsa. A paired spectral-finite difference approach for solving boundary layer flow problems *Afrika Matematika, https://doi.org/10.1007/s13370-019-00658-3*

O. Otegbeye, S. S. Motsa and Md. S. Ansari. An application of paired quasi-linearization on double diffusive convection flow over a cone embedded in a porous medium in the presence of nano-particles. *Submitted to Rendiconti del Circolo Matematico di Palermo*

I worked on the introduction of the paper, discussed the method of solution, conducted the simulation, discussed the results and concluded

Md. S. Ansari, O. Otegbeye, M. Trivedi and S. S. Motsa. A paired quasi-linearization on magnetohydrodynamic flow and heat transfer of Casson nanofluid with Hall effects. *Submitted to Journal of Applied and Computational Mechanics* Manuscript ID: JACM-1812-1435

I contributed to the introduction of the paper, discussed the method of solution, conducted the simulation, discussed the results and concluded

O. Otegbeye, S. S. Motsa and M. S. Ayano. Combined influence of radiation and Hall and ion effects flow past semi-infinite vertical flat plate: Paired quasilinearization method. *Submitted to American Institute of Physics conference proceedings*

I contributed to the introduction of the paper, discussed the method of solution, conducted the simulation, discussed the results and concluded.

Signature: ....

Olumuyiwa Otegbeye Date

Dedication

To the memory of my late father, Dr. G.O. Otegbeye. Your memory lives on.

Acknowledgments

I thank God for giving me the strength to begin and complete this thesis. He kept me all through smooth and turbulent times and I emerged unscathed. I will like to recognize the tremendous effort of my advisor and supervisor Prof. S. S. Motsa in steering me properly down the years. He introduced me to computational numerical methods and has been a mentor and advisor since 2012.

I thank my mother, Moji, Shade, and Dayo for their immense support. You were all there for me emotionally, academically, spiritually and financially. I will definitely not have gotten this far without you all. To Dr. Olorunda Rotimi, Prof. K. Rotimi, Mrs. Adewole, Pa Joe, Aunts Idowu, Dele and Lola and the rest of my extended family members, I will like to thank you all for your continues support and prayers. I cannot name you all but God bless you. A special mention to Sanelisiwe Khanyile and her family for being there for me especially when I was at a really low point, I will forever be grateful.

I recognize the efforts of Sheelagh Halstead in applying a professional touch to this thesis and picking out areas that needed improvement and correction. Thank you. A heartfelt thanks goes to Dr. and Dr. Mrs. Ogunnubi for facilitating my move to UKZN and for always being available to assist when I needed help even with their hectic schedule. To my colleagues in the School of Mathematics, Statistics and Computer Science, I say a big thanks. Patrick, Shina, Rasheed, Faustin, Tirab, Osman, Izuchukwu, Titilayo, Ibukun, Sicelo, Vusi, Gabriel, fluid group, numerical analysis group members, thank you for your individual and collective assistance. I also appreciate my great friends Bayo Adeniyi, Tijani Mukhtar, Cyril Makama and the rest of my wonderful people back in Nigeria. Thanks for always remembering me even though we are miles apart. The school administrator, Ms. C. Barnard, I appreciate your personal effort in making me comfortable throughout the course of my various programs. Thanks to the technical team as well for making equipment and facilities readily available for my every need. I will also like to appreciate the

various sports groups I identified with. They provided me outlets to let off some steam and get my body and soul in check. To the Nigerian students association, my Sudanese friends, South African friends and friends from all over the continent and world, thank you. Finally, I will like to appreciate the efforts of Dr. Ansari and Dr. Ayano for their contributions towards modeling some of the problems investigated in the thesis. Your efforts are duly noted.

Chapter 1

INTRODUCTION

Increasingly complex real-world problems have led to mathematical models that contain many details. Mathematical models have proved useful in fields such as medical research, biological problems, financial modeling and engineering. Constructing mathematical equations that properly model such problems usually results in higher order systems of differential equations that are nearly impossible to solve analytically. These highly nonlinear systems of differential equations then have to be approximated to obtain numerical solutions. Although these solutions are never precise [1], they give valuable insight into real problems. Consequently there is a need to continually improve on such numerical methods, especially with regards to efficiency and accuracy. Over the years, a number of computational methods have been developed to solve nonlinear equations.

Differential equations that model boundary layer flow problems can be difficult or impossible to solve analytically so creating the need to implement semi-analytical or numerical methods. Analytical methods such as the Homotopy Analysis method [2] and Perturbation methods [3] to mention two, are examples of methods that are used to generate closed-form solutions. The difficulty in obtaining analytical solutions for systems of highly nonlinear differential equations, however, limits the use of these methods (see for example [2]). Solving such complex problems prompts the use of numerical methods. This has been achieved over the years with traditional methods such as finite difference methods (FDM), finite element methods (FEM) and finite volume methods (FVM). Amongst these methods, the finite difference method and its variants such as the Keller box method [4] have proved popular due to their simplicity of implementation and their versatility. The finite difference method, introduced by Courant et al. [5] and mathematically structured by Friedrichs

[6], Feng [7] and Friedrichs and Keller [8] amongst others, has over the years, proved to be an efficient method for solving partial differential equations with wide applicability ranging through seismology [9], fluid mechanics [10], diffusion [11] and fractional diffusion equations [12] to mention a few. Although the finite difference method has been useful in solving problems defined under strong shocks, irregular domains or boundary conditions, or modelled with an incomplete understanding of the theoretical aspect of the problem when combined with other numerical techniques [13, 14], it has also been shown to be computationally costly. The FDM is computationally costly because it uses a lot of collocation points that effectively require long computational time to generate convergent solutions. In the light of the limitations of the traditional FDM, a more suitable approach for solving highly nonlinear systems of differential equations was developed with the introduction of spectral methods [14, 15]. The concept of spectral methods is motivated by finite differences [13]. They make use of orthogonal functions in obtaining approximate solutions. They have proved popular because of their relatively simple implementation, which also requires fewer grid-points to obtain convergent and highly accurate results than are needed with traditional methods. With the popularization of spectral methods by Boyd [16], Trefethen [13], Canuto et al. [17], among others, other spectral based numerical techniques have been developed to improve on previous methods, such as the spectral quasilinearization method [18], spectral local linearization method [18], bivariate spectral quasilinearization method [19], paired quasilinearization method [20].

The spectral local linearization method (SLLM), as introduced by Motsa [18], involves linearization of a function and its derivatives in one equation and using the updated solution in subsequent equations of a large system of differential equations. The Chebyshev spectral collocation method is used to solve the decoupled system of linearized equations. This process gives the method some advantages. The SLLM has been shown to be an efficient numerical method for solving systems of differential equations. Motsa et al. [21] considered the problem of natural convection in boundary layer flow with heat transfer using the SLLM. The SLLM was observed to be a highly accurate method and had an easy implementation process. It was extended to partial differential equations

by Motsa and Animasaun [22] where the problem of unsteady heat and mass transfer past a semi-infinite vertical plate with diffusion-thermo and thermophoresis effects in the presence of suction were considered. The results obtained showed the robustness of the SLLM. A comparative study carried out by Otegbeye [23] investigated the SLLM in detail. It was observed that decoupling the system of equations decreased the size of the matrices being inverted hereby leading to a reduction in computational cost. It was also observed that the SLLM needed few grid-points to obtain convergent solutions and gave very high accuracy when compared to the spectral quasilinearization method (SQLM), but was noted to converge slower than the SQLM. The rapid convergence of the SQLM is based on its being a Newton-Raphson type of method, which converges quadratically. The advantages of the SLLM led to further work. It was realized that linearizing a pair of functions and their corresponding derivatives instead of only one function could maintain the high accuracy of the SLLM while improving the speed of convergence. This method, the paired quasilinearization method (PQLM), was introduced by Motsa and Animasaun [20] in studying the motion of the unsteady gravity-induced nanofluid flow containing gyrotactic micro-organisms along a downward vertical convectively heated surface subject to passively controlled nanofluid. The analysis by Motsa and Animasaun [20] suggests the PQLM as an alternative method in solving systems of differential equations that model fluid flow problems.

In this thesis, we aim to thoroughly investigate the recently introduced paired quasilinearization method (PQLM) by observing the different combinations obtained using the PQLM and comparing its performance with another previously known efficient numerical method (SLLM). We perform the comparison by investigating the speed of convergence using the infinity norm of their respective solution errors. We also investigate the computational time in generating solutions that converge to a stipulated number of decimal places. Accuracy is also tested using the infinity norm of the residual error of the different numerical methods. For the remainder of this Chapter, we begin by defining some common processes used during the course of this thesis. We also describe the PQLM, and spectral local linearization method (SLLM) for a general system of N differential equations with N unknowns. In Chapter 2, we introduce the PQLM by solving a system of ordinary differential equations that model the problem of mixed convection in a gravity-driven

nano-liquid film containing both nanoparticles and gyrotactic microorganisms and compare results against those of the SLLM. Chapter 3 focuses on a comparative study of the PQLM introduced recently by Motsa and Animasaun [20]. We investigate the accuracies and speed of convergence of the different pairings of the PQLM and compare these to the bivariate spectral local linearization method (BSLLM). In Chapter 4, we examine the combined influence of radiation, Hall and ion effects on magneto-hydrodynamic free convective heat generating flow past a semi-infinite vertical flat plate using the PQLM. Chapter 5 further gives the use of the PQLM in investigating the effect of thermophoresis, buoyancy ratio, Brownian motion and the Dufour effect on a system of partial differential equations that model an induced Darcy flow of incompressible nanofluid along an inclined isothermal surface embedded in a porous medium. Chapter 6 extends the PQLM to fluid flow problems by examining the double-diffusive mixed convection flow of a nanofluid near a vertical cone embedded in a porous medium with Soret and Dufour effects. In Chapter 7, we introduce the multi-domain paired quasilinearization method (MD-PQLM) for a system of partial differential equations with large time domains.

1.1 Some Definitions

To give insight into a lot of concepts that have been used in this thesis, we begin by explaining some in this section. While some are general knowledge, it is important to briefly state them once more so as to ensure the rest of the thesis is understandable to the reader.

1.2 Taylor series expansion for multivariables

Suppose we have an infinitely differentiable function $f(x_1, x_2, \ldots, x_N) \in \mathbb{R}^n$ in an open neighborhood around $(x_1, x_2, \ldots, x_N) = (k_1, k_2, \ldots, k_N)$. An expansion taken around the points $k_1, k_2, \ldots, k_N$ of the function $f(x_1, x_2, \ldots, x_N)$ is referred to as the Taylor series expansion. The Taylor series of

$f(x_1, x_2, \ldots, x_N)$ is

$$
\begin{aligned}
& f(x_1, x_2, \ldots, x_N) \approx f(k_1, k_2, \ldots, k_N) + f'_{k_1}(k_1, k_2, \ldots, k_N)(x_1 - k_1) \\
& + f'_{k_2}(k_1, k_2, \ldots, k_N)(x_2 - k_2) + \cdots + f'_{k_N}(k_1, k_2, \ldots, k_N)(x_N - k_N) \\
& + \frac{f''_{k_1}(k_1, k_2, \ldots, k_N)}{2!}(x_1 - k_1)^2 + \cdots + \frac{f''_{k_N}(k_1, k_2, \ldots, k_N)}{2!}(x_N - k_N)^2 + \cdots \\
& + \frac{f^{(j)}_{k_1}(k_1, k_2, \ldots, k_N)}{j!}(x_1 - k_1)^j + \cdots + \frac{f^{(j)}_{k_N}(k_1, k_2, \ldots, k_N)}{j!}(x_N - k_N)^j,
\end{aligned} \tag{1.1}
$$

where prime $'$ denotes differentiation with respect to $k_i,\ i = 1, \ldots, N$ and j is the last term of the series.

Throughout the course of this thesis, this process is instrumental in the linearization of nonlinear functions in all the examples used.

1.3 Criteria for convergence

We consider the nonlinear system of equations

$$\mathbf{Fx} = \mathbf{0}, \tag{1.2}$$

that has an iteration scheme of the form

$$\mathbf{Ex}_{r+1} = \mathbf{bx}_r, \tag{1.3}$$

where $\mathbf{x}_{r+1}$ is solution at current iteration level and $\mathbf{x}_r$ is solution at previous iteration level. We say convergence has occurred when

$$||\mathbf{Ex}_{r+1} - \mathbf{bx}_r|| < \delta, \tag{1.4}$$

is satisfied where $||\mathbf{Ex}_{r+1} - \mathbf{bx}_r||$ is a vector norm and $\delta \neq 0$ is an acceptable tolerance level which is set at 10^{-16} and smaller in this thesis.

1.4 Spectral Methods

According to Gottlieb and Orszag [24], spectral methods are used to obtain approximate solutions to differential equations using a series of smooth and known functions. The functions can be orthogonal functions such as the Chebyshev and Legendre polynomials that have truncated series [14, 15, 25, 26]. In essence, spectral approximation entails transforming a function from the physical space to the spectral space. Spectral methods are global methods, in that they make use of global representations to obtain high order approximations [27, 28]. As shown in Gottlieb and Orszag [24], three commonly used types of spectral methods are the Tau spectral method, the collocation spectral method, and the Galerkin spectral method. It has been reported by Gottlieb and Gottlieb [28], Baltensperger and Berrut [29] and Ogundare [30] amongst others, that the Tau and Galerkin spectral methods are weighted residual methods, unlike the collocation spectral method. As reported by Babolian et al. [31], the Tau and Galerkin methods are applied to expansion coefficients while the collocation methods are applied to physical space values of unknown functions. According to Gheorghiu [14] and Boyd [16], important properties of the spectral methods are their ability to transform self-adjoint differential problems into nonsymmetric discrete algebraic problems and their nondispersive nature. As noted by Mantzaris et al. [32], they also exhibit exponential convergence or infinite-order accuracy.

The conditioning of differentiation matrices in spectral methods is explained in Cueto-Felgueroso and Juanes [33] and Trefethen and Trummer [34]. As noted by Baltensperger and Berrut [29], errors occur in the process of calculating the differentiation matrices for Chebyshev nodes. Trefethen and Trummer [34] observed that the stability of spectral methods for problems associated with initial boundary value conditions was quite unknown.

Applications of spectral methods include periodic geometries [27]. According to Boyd [16], they are also applicable to flows with shock waves and fronts. Spectral methods have been applied successfully in multivariable cell population models by Mantzaris et al. [32], in weather forecasting by Juang and Kanamitsu [35] and in many other applications.

1.5 Residual Error

The process of discretizing differential equations gives rise to some errors, which are referred to as the residual errors of the approximations. The residual error occurs as a result of approximating solutions of differential equations [36]. To calculate the residual error, we substitute approximate solutions obtained for differential equations into the original equations. To illustrate, we consider a differential equation of the form

$$Ey = f, \tag{1.5}$$

with approximate solution $\overline{y}$. We obtain the residual error as

$$res(y) = E\overline{y} - f. \tag{1.6}$$

Provided $\overline{y}$ is not a poor approximation of y, we see that the residual error (1.6) of equation (1.5) should be close to but not zero, given that the solutions are approximations. Cheng et al. [37] reported that the residual error does not actually indicate the true error of a solution but rather it captures the closeness of the approximate solution to the exact solution.

1.6 Quasilinearization Method (QLM)

The quasilinearization method (QLM) is a technique that combines computer programming procedures with linear approximation methods. As a generalized form of the Newton-Rhapson method, the QLM was introduced by Bellman and Kalaba [38] to generate solutions to nonlinear ordinary and partial differential equations. The QLM arose from the need to seek solutions to models of the physical processes with a nonlinear nature [39]. It has been shown to possess rapid convergence properties and in most cases, monotonicity [40], among others. Mandelzweig and Tabakin [39] also discovered that the QLM performs differently to other approximation techniques by accounting for the nonlinearity of a problem at the start of every iteration through a change in the differential operator.

The applicability of the QLM cuts across various research interests. Mandelzweig and Tabakin

[39] and Parand et al. [41] applied it to Lame-Eden type equations and found it to be an efficient approach in handling the nonlinearity of physics-based problems. It was also applied by Mandelzweig and Tabakin [39] on the Thomas-Fermi, Blasius, and Duffing equations. Krivec and Mandelzweig [40] also extended the applicability to quantum physics and tested the numerical stability and convergence. They found the QLM to be a powerful tool for such problems. Before this, however, Bellman et al. [42] had applied the QLM on nonlinear multipoint boundary value problems for systems of nonlinear ordinary differential equations. Shazad and Vatsala [43] and Ahmad et al. [44] applied the QLM to a second order ordinary nonlinear differential equation with Neumann boundary conditions while Nieto [45] solved a 2^{nd} order nonlinear ODE with Dirichlet boundary conditions with the QLM and Ahmad et al. [46] extended the QLM to solve the same problem with mixed boundary conditions. Periodic boundary value problems were solved by Lakshmikantham et al. [47] using the QLM. The QLM has been extended to convex functions by Lakshmikantham [48]. Jaddu [49] applied the QLM on nonlinear optimal control problems with some constraints. In physics, the QLM has been applied by Mandelzweig and Tabakin [39] to the Lane-Emden, Thomas-Fermi, Duffing, and Blasius equations and to quantum physics by Krivec and Mandelzweig [40].

1.7 Description of numerical methods

This section shows the steps taken to develop the algorithms of the paired quasilinearization method (PQLM) and spectral local linearization method (SLLM) for a generalized system of N differential equations with N unknowns. We begin by displaying the linearized schemes for the PQLM, SLLM, and SQLM. We note here that the schemes we display are for PDEs, but also cover ODEs by excluding time. We also briefly include the application of domain splitting when dealing with PDEs defined over large time in the description.

Let us consider a partial differential equation that has a highest derivative order m_1 of the form

$$f\left(\mathbf{u}_1\left(\zeta,\tau\right)\right)=0,\ \ \zeta\in[a,b],\ \ \tau\in[0,T], \tag{1.7}$$

where the unknown function $\mathbf{u}_1$ is defined as $\mathbf{u}_1=\{u_1,\frac{\partial u_1}{\partial\zeta},\ldots,\frac{\partial^{m_1-1}u_1}{\partial\zeta},\frac{\partial^{m_1}u_1}{\partial\zeta},\frac{\partial^2 u_1}{\partial\tau\partial\zeta}\}$. Now consider

a system of N partial differential equations in N unknowns of the form

$$\mathbf{F}_l\left(\mathbf{u}_1\left(\zeta,\tau\right),\mathbf{u}_2\left(\zeta,\tau\right),\ldots,\mathbf{u}_N\left(\zeta,\tau\right)\right)=0,\;\; l=1,2,\ldots,N \tag{1.8}$$

which represents a coupled nonlinear system of partial differential equations with each $\mathbf{F}_l,\;\; l=1,\ldots,N$ being a nonlinear operator, $\{\mathbf{u}_1,\mathbf{u}_2,\ldots,\mathbf{u}_N\}$ is a set that contains

$$\left(\{u_1^{(0)},u_1^{(1)},\ldots,u_1^{(m_1)}\},\ldots,\{u_N^{(0)},u_N^{(1)},\ldots,u_N^{(m_N)}\}\right).$$

To maintain uniformity, let $m_{l,q}$ represent the highest partial derivative order of entries in $(\mathbf{u}_1,\mathbf{u}_2,\ldots,\mathbf{u}_N)$ with respect to ζ in the l^{th} equation. The nonlinear system of partial differential equations (1.8) will be used throughout this section in describing the respective algorithms of the SLLM and PQLM.

1.7.1 Spectral Local Linearization Method (SLLM)

In this section, the *SLLM* is described for the general nonlinear system of coupled PDEs given in (1.8).

$$\mathbf{F}_l\left(\mathbf{u}_1\left(\zeta,\tau\right),\mathbf{u}_2\left(\zeta,\tau\right),\cdots,\mathbf{u}_N\left(\zeta,\tau\right)\right)=0,\;\; l=1,2,\ldots,N. \tag{1.9}$$

The spectral local linearization method (SLLM), introduced by Motsa [18], is a method that involves linearizing the l^{th} set of $(\mathbf{u}_1,\mathbf{u}_2,\cdots,\mathbf{u}_N)$ in the l^{th} equation of the system (1.9) using a one step Taylor series and solving the system one equation at a time. To linearize the nonlinear system (1.9) using the SLLM, we expand nonlinear terms of corresponding $\mathbf{u}_l$ of each $\mathbf{F}_l^{th}$ equation.

Approximations $(\mathbf{u}_{1,r}, \mathbf{u}_{2,r}, \cdots, \mathbf{u}_{N,r})$ are chosen such that

$$
\begin{aligned}
&\mathbf{F}_1\left((\mathbf{u}_{1,r}, \cdots, \mathbf{u}_{N,r}) + \Delta(\mathbf{u}_1, \cdots, \mathbf{u}_N)\right) \approx \mathbf{F}_1\left(\mathbf{u}_{1,r}, \cdots, \mathbf{u}_{N,r}\right) \\
&\qquad + \sum_{p=0}^{m_{1,1}} \frac{\partial^{(p)} \mathbf{F}_1\left(\mathbf{u}_{1,r}, \cdots, \mathbf{u}_{N,r}\right)}{\partial \mathbf{u}_1^{(p)}} \left(\Delta \mathbf{u}_1^{(p)}\right), \\
&\mathbf{F}_2\left((\mathbf{u}_{1,r+1}, \mathbf{u}_{2,r}, \cdots, \mathbf{u}_{N,r}) + \Delta(\mathbf{u}_1, \cdots, \mathbf{u}_N)\right) \approx \mathbf{F}_2\left(\mathbf{u}_{1,r+1}, \mathbf{u}_{2,r}, \cdots, \mathbf{u}_{N,r}\right) \\
&\qquad + \sum_{p=0}^{m_{2,2}} \frac{\partial^{(p)} \mathbf{F}_2\left(\mathbf{u}_{1,r+1}, \mathbf{u}_{2,r}, \cdots, \mathbf{u}_{N,r}\right)}{\partial \mathbf{u}_2^{(p)}} \left(\Delta \mathbf{u}_2^{(p)}\right), \\
&\qquad \vdots \\
&\mathbf{F}_N\left((\mathbf{u}_{1,r+1}, \cdots, \mathbf{u}_{N-1,r+1}, \mathbf{u}_{N,r}) + \Delta(\mathbf{u}_1, \cdots, \mathbf{u}_N)\right) \approx \mathbf{F}_N\left(\mathbf{u}_{1,r+1}, \cdots, \mathbf{u}_{N-1,r+1}, \mathbf{u}_{N,r}\right) \\
&\qquad + \sum_{p=0}^{m_{N,N}} \frac{\partial^{(p)} \mathbf{F}_N\left(\mathbf{u}_{1,r+1}, \cdots, \mathbf{u}_{N-1,r+1}, \mathbf{u}_{N,r}\right)}{\partial \mathbf{u}_N^{(p)}} \left(\Delta \mathbf{u}_N^{(p)}\right),
\end{aligned}
\tag{1.10}
$$

where $\Delta \mathbf{u}_l^{(p)} = \mathbf{u}_{l,r+1}^{(p)} - \mathbf{u}_{l,r}^{(p)}$ (with the $r-$subscript denoting the current iteration level and the $r+1-$subscript the next iteration level). The system (1.10) expands to

$$
\begin{aligned}
&\mathbf{F}_1\left((\mathbf{u}_{1,r}, \cdots, \mathbf{u}_{N,r}) + \Delta(\mathbf{u}_1, \cdots, \mathbf{u}_N)\right) \approx \mathbf{F}_1\left(\mathbf{u}_{1,r}, \cdots, \mathbf{u}_{N,r}\right) \\
&+ \sum_{p=0}^{m_{1,1}} \frac{\partial^{(p)} \mathbf{F}_1\left(\mathbf{u}_{1,r}, \cdots, \mathbf{u}_{N,r}\right)}{\partial \mathbf{u}_1^{(p)}} \mathbf{u}_{1,r+1}^{(p)} - \sum_{p=0}^{m_{1,1}} \frac{\partial^{(p)} \mathbf{F}_1\left(\mathbf{u}_{1,r}, \cdots, \mathbf{u}_{N,r}\right)}{\partial \mathbf{u}_1^{(p)}} \mathbf{u}_{1,r}^{(p)}, \\
&\mathbf{F}_2\left((\mathbf{u}_{1,r+1}, \mathbf{u}_{2,r}, \cdots, \mathbf{u}_{N,r}) + \Delta(\mathbf{u}_1, \cdots, \mathbf{u}_N)\right) \approx \mathbf{F}_2\left(\mathbf{u}_{1,r+1}, \mathbf{u}_{2,r}, \cdots, \mathbf{u}_{N,r}\right) \\
&+ \sum_{p=0}^{m_{2,2}} \frac{\partial^{(p)} \mathbf{F}_2\left(\mathbf{u}_{1,r+1}, \cdots, \mathbf{u}_{N,r}\right)}{\partial \mathbf{u}_2^{(p)}} \mathbf{u}_{2,r+1}^{(p)} - \sum_{p=0}^{m_{2,2}} \frac{\partial^{(p)} \mathbf{F}_2\left(\mathbf{u}_{1,r+1}, \cdots, \mathbf{u}_{N,r}\right)}{\partial \mathbf{u}_2^{(p)}} \mathbf{u}_{2,r}^{(p)}, \\
&\vdots \qquad\qquad\qquad\qquad\qquad\qquad\qquad\qquad\qquad\qquad\qquad\qquad \vdots \\
&\mathbf{F}_N\left((\mathbf{u}_{1,r+1}, \cdots, \mathbf{u}_{N-1,r+1}, \mathbf{u}_{N,r}) + \Delta(\mathbf{u}_1, \cdots, \mathbf{u}_N)\right) \approx \mathbf{F}_N\left(\mathbf{u}_{1,r+1}, \cdots, \mathbf{u}_{N-1,r+1}, \mathbf{u}_{N,r}\right) \\
&+ \sum_{p=0}^{m_{N,N}} \frac{\partial^{(p)} \mathbf{F}_N\left(\mathbf{u}_{1,r+1}, \cdots, \mathbf{u}_{N,r}\right)}{\partial \mathbf{u}_N^{(p)}} \mathbf{u}_{N,r+1}^{(p)} - \sum_{p=0}^{m_{N,N}} \frac{\partial^{(p)} \mathbf{F}_N\left(\mathbf{u}_{1,r+1}, \cdots, \mathbf{u}_{N,r}\right)}{\partial \mathbf{u}_N^{(p)}} \mathbf{u}_{N,r}^{(p)},
\end{aligned}
\tag{1.11}
$$

The system (1.9) is now rewritten using the expansion given in (1.11) and we obtain

$$\begin{aligned}
&\sum_{p=0}^{m_{1,1}} \frac{\partial^{(p)}\mathbf{F}_1\left(\mathbf{u}_{1,r},\cdots,\mathbf{u}_{N,r}\right)}{\partial\mathbf{u}_1^{(p)}}\mathbf{u}_{1,r+1}^{(p)} = R_1,\\
&\sum_{p=0}^{m_{2,2}} \frac{\partial^{(p)}\mathbf{F}_2\left(\mathbf{u}_{1,r+1},\mathbf{u}_{2,r},\cdots,\mathbf{u}_{N,r}\right)}{\partial\mathbf{u}_2^{(p)}}\mathbf{u}_{2,r+1}^{(p)} = R_2,\\
&\vdots\\
&\sum_{p=0}^{m_{N,N}} \frac{\partial^{(p)}\mathbf{F}_N\left(\mathbf{u}_{1,r+1},\cdots,\mathbf{u}_{N-1,r+1},\mathbf{u}_{N,r}\right)}{\partial\mathbf{u}_N^{(p)}}\mathbf{u}_{N,r+1}^{(p)} = R_N,
\end{aligned} \tag{1.12}$$

where

$$\begin{aligned}
R_1 &= \sum_{p=0}^{m_{1,1}} \frac{\partial^{(p)}\mathbf{F}_1\left(\mathbf{u}_{1,r},\cdots,\mathbf{u}_{N,r}\right)}{\partial\mathbf{u}_1^{(p)}}\mathbf{u}_{1,r}^{(p)} - \mathbf{F}_1\left(\mathbf{u}_{1,r},\cdots,\mathbf{u}_{N,r}\right),\\
R_2 &= \sum_{p=0}^{m_{2,2}} \frac{\partial^{(p)}\mathbf{F}_2\left(\mathbf{u}_{1,r+1},\mathbf{u}_{2,r},\cdots,\mathbf{u}_{N,r}\right)}{\partial\mathbf{u}_2^{(p)}}\mathbf{u}_{2,r}^{(p)} - \mathbf{F}_2\left(\mathbf{u}_{1,r+1},\mathbf{u}_{2,r},\cdots,\mathbf{u}_{N,r}\right),\\
&\vdots\\
R_N &= \sum_{p=0}^{m_{N,N}} \frac{\partial^{(p)}\mathbf{F}_N\left(\mathbf{u}_{1,r+1},\cdots,\mathbf{u}_{N-1,r+1},\mathbf{u}_{N,r}\right)}{\partial\mathbf{u}_N^{(p)}}\mathbf{u}_{N,r}^{(p)} - \mathbf{F}_N\left(\mathbf{u}_{1,r+1},\cdots,\mathbf{u}_{N-1,r+1},\mathbf{u}_{N,r}\right).
\end{aligned}$$

Multi-domain spectral local linearization method (MD-SLLM)

The multi-domain approach involves decomposing the time interval in (1.12) into smaller non-overlapping sub-intervals $\rho_e = [\tau_{e-1},\tau_e],\ e = 1,2,\ldots,T$ where $\tau \in \rho,\quad \rho = [0,T]$. The system (1.12) is solved in each interval $[\tau_{e-1},\tau_e]$ in the form

$$\begin{aligned}
&\sum_{p=0}^{m_{1,1}} \frac{\partial^{(p)}\mathbf{F}_1\left(\mathbf{u}_{1,r}^{e},\cdots,\mathbf{u}_{N,r}^{e}\right)}{\partial\mathbf{u}_1^{(p)}}\mathbf{u}_{1,r+1}^{e(p)} = R_1,\\
&\sum_{p=0}^{m_{2,2}} \frac{\partial^{(p)}\mathbf{F}_2\left(\mathbf{u}_{1,r+1}^{e},\mathbf{u}_{2,r}^{e},\cdots,\mathbf{u}_{N,r}^{e}\right)}{\partial\mathbf{u}_2^{(p)}}\mathbf{u}_{2,r+1}^{e(p)} = R_2,\\
&\vdots\\
&\sum_{p=0}^{m_{N,N}} \frac{\partial^{(p)}\mathbf{F}_N\left(\mathbf{u}_{1,r+1}^{e},\cdots,\mathbf{u}_{N-1,r+1}^{e},\mathbf{u}_{N,r}^{e}\right)}{\partial\mathbf{u}_N^{(p)}}\mathbf{u}_{N,r+1}^{e(p)} = R_N,
\end{aligned} \tag{1.13}$$

where $\mathbf{u}^{e}_{l,r+1}$ and $\mathbf{u}^{e}_{l,r}$, $l = 1,2,\ldots,N$ denote the solution to the system (1.13) at each sub-interval ρ_e. The multi-domain process involves starting with some initial condition in the first sub-interval and using it to obtain solutions throughout that particular sub-interval. The solution at the end of the first sub-interval becomes the initial solution for the subsequent sub-interval. The continuity condition defined by Agbaje et al. [50] as

$$\mathbf{u}^{(e)}\left(\zeta,\tau_{e-1}\right) = \mathbf{u}^{(e-1)}\left(\zeta,\tau_{e-1}\right),$$

is implemented over the interval $[\tau_{e-1},\tau_e]$. We note here that the implementation of the multi-domain approach is the same for the case of the paired quasilinearization method (PQLM). We also remark that the process of applying spectral methods to the system (1.12) is the same as on the system (1.13). For further description, we use the system (1.12).

Bivariate spectral collocation method

In this section, we describe the application of spectral methods in space and time on the system (1.12). To begin, the physical domains $\zeta \in [a,b]$ and $\tau \in [0,T]$ are transformed into $x \in [-1,1]$ and $y \in [-1,1]$, respectively. Obtaining solutions $u_{1,r}(x,y),\ldots,u_{N,r}(x,y)$ to the system (1.12) is achieved with the use of bivariate Lagrange interpolation polynomials that have the form

$$\begin{aligned} u_1(x,y) &\approx \sum_{i=0}^{Mx}\sum_{j=0}^{My} u_1\left(x_i,y_j\right)\mathbf{L}_i(x)\mathbf{L}_j(y), \\ &\vdots \\ u_N(x,y) &\approx \sum_{i=0}^{Mx}\sum_{j=0}^{My} u_N\left(x_i,y_j\right)\mathbf{L}_i(x)\mathbf{L}_j(y), \end{aligned} \tag{1.14}$$

where Mx and My are grid-points in space and time, respectively, $\mathbf{L}_i$ and $\mathbf{L}_j$ are Lagrange cardinal functions defined as

$$\begin{aligned} L_i(x) &= \prod_{i=0,i\neq k}^{M_x}\frac{x-x_k}{x_i-x_k}, \\ L_j(y) &= \prod_{j=0,j\neq k}^{M_y}\frac{y-y_k}{y_j-y_k}, \end{aligned} \tag{1.15}$$

where

$$L_i(x_k) = \delta_{ik} = \begin{cases} 0 \text{ if } i \neq k \\ 1 \text{ if } i = k \end{cases},$$

$$L_j(y_k) = \delta_{jk} = \begin{cases} 0 \text{ if } j \neq k \\ 1 \text{ if } j = k \end{cases}. \tag{1.16}$$

Gauss-Chebyshev-Lobatto points are chosen as grid-points x_i and y_j as they are known to smoothly convert continuous time and spatial derivatives into discrete derivatives and these points are obtained thus;

$$\begin{aligned} x_i &= \cos\frac{\pi i}{M_x}, \quad i = 0, 1, \ldots, M_x, \\ y_j &= \cos\frac{\pi j}{M_y}, \quad i = 0, 1, \ldots, M_t \end{aligned} \tag{1.17}$$

Following Trefethen [13], differentiation matrices (denoted D and d) are used to collocate and are applied in the form

$$\begin{aligned} \left.\frac{\partial u_1^{(p)}}{\partial x^{(p)}}\right|_{x_i,y_j} &= \mathbf{D}^{(p)} U_{1,i}, \quad \left.\frac{\partial u_1}{\partial t}\right|_{x_i,y_j} = \sum_{j=0}^{M_y} \mathbf{d}_{ij} U_{1,j}, \\ \left.\frac{\partial u_2^{(p)}}{\partial x^{(p)}}\right|_{x_i,y_j} &= \mathbf{D}^{(p)} U_{2,i}, \quad \left.\frac{\partial u_2}{\partial t}\right|_{x_i,y_j} = \sum_{j=0}^{M_y} \mathbf{d}_{ij} U_{2,j}, \\ &\vdots \\ \left.\frac{\partial u_N^{(p)}}{\partial x^{(p)}}\right|_{x_i,y_j} &= \mathbf{D}^{(p)} U_{N,i}, \quad \left.\frac{\partial u_N}{\partial t}\right|_{x_i,y_j} = \sum_{j=0}^{M_y} \mathbf{d}_{ij} U_{N,j}, \end{aligned} \tag{1.18}$$

where U_1, U_2, …, U_N are vectors of the form

$$\begin{aligned} U_1 &= \left[u_1(x_0, y_j), u_1(x_1, y_j), \ldots, u_1(x_{N_x}, y_j)\right]^T, \\ U_2 &= \left[u_2(x_0, y_j), u_2(x_1, y_j), \ldots, u_2(x_{N_x}, y_j)\right]^T, \\ &\vdots \\ U_N &= \left[u_N(x_0, y_j), u_N(x_1, y_j), \ldots, u_N(x_{N_x}, y_j)\right]^T. \end{aligned}$$

Applying the description (1.18) in (1.12), we obtain

$$\begin{aligned}
&\sum_{p=0}^{m_{1,1}} \mathbf{diag}\left[\frac{\partial^{(p)}\mathbf{F}_1\left(\mathbf{u}_{1,j,r},\ldots,\mathbf{u}_{N,j,r}\right)}{\partial\left(u_{1,j}\right)^{(p)}}\right]\left(\left(\mathbb{U}_{1,r+1}\right)^{(p)}\right)=\mathbf{R}_{1,j},\\
&\sum_{p=0}^{m_{2,2}} \mathbf{diag}\left[\frac{\partial^{(p)}\mathbf{F}_2\left(\mathbf{u}_{1,j,r+1},\mathbf{u}_{2,j,r},\ldots,\mathbf{u}_{N,j,r}\right)}{\partial\left(u_{2,j}\right)^{(p)}}\right]\left(\left(\mathbb{U}_{2,r+1}\right)^{(p)}\right)=\mathbf{R}_{2,j},\\
&\vdots\\
&\sum_{p=0}^{m_{N,N}} \mathbf{diag}\left[\frac{\partial^{(p)}\mathbf{F}_N\left(\mathbf{u}_{1,j,r+1},\ldots,\mathbf{u}_{N-1,j,r+1},\mathbf{u}_{N,j,r}\right)}{\partial\left(u_{N,j}\right)^{(p)}}\right]\left(\left(\mathbb{U}_{N,r+1}\right)^{(p)}\right)=\mathbf{R}_{N,j},
\end{aligned} \tag{1.19}$$

which is expressed compactly as

$$\begin{aligned}
&\mathbf{A}_1\mathbf{u}_{1,r+1}=\mathbf{R}_{1,j},\\
&\mathbf{A}_2\mathbf{u}_{2,r+1}=\mathbf{R}_{2,j},\\
&\vdots\\
&\mathbf{A}_N\mathbf{u}_{N,r+1}=\mathbf{R}_{N,j},
\end{aligned} \tag{1.20}$$

where the entries of $\mathbf{A}_l=\sum_{p=0}^{m_{l,l}}\mathbf{diag}\left[\frac{\partial^{(p)}\mathbf{F}_l\left(\mathbf{u}_{1,j,r},\ldots,\mathbf{u}_{N,j,r}\right)}{\partial\left(u_{l,j}\right)^{(p)}}\right]\mathbf{D}^{(p)}$ are matrices of size $N_y\left(N_x+1\right)\times N_y\left(N_x+1\right)$ and each entry of both $\mathbf{u}_l$ and $\mathbf{R}_l$ have $N_y\left(N_x+1\right)$ dimensions. To illustrate further, consider the first equation of the system (1.20)

$$\mathbf{A}_1\mathbf{u}_{1,r+1}=\mathbf{R}_{1,j}. \tag{1.21}$$

Equation (1.21) can be shown in matrix form as

$$\begin{bmatrix}
\mathbf{A}_{0,0} & \mathbf{A}_{0,1} & \cdots & \mathbf{A}_{0,Ny}\\
\mathbf{A}_{1,0} & \mathbf{A}_{1,1} & \cdots & \mathbf{A}_{1,Ny}\\
\vdots & \vdots & \ddots & \vdots\\
\mathbf{A}_{Ny,0} & \mathbf{A}_{Ny,1} & \cdots & \mathbf{A}_{Ny,Ny}
\end{bmatrix}\begin{bmatrix}\mathbf{u}_0\\ \mathbf{u}_1\\ \vdots\\ \mathbf{u}_{Ny}\end{bmatrix}=\begin{bmatrix}\mathbf{R}_0\\ \mathbf{R}_1\\ \vdots\\ \mathbf{R}_{N_y}\end{bmatrix}, \tag{1.22}$$

where

$$\begin{aligned}
\mathbf{A}_{j,j}&=\sum_{p=0}^{m_{1,1}}\mathbf{diag}\left[\frac{\partial^{(p)}F_1\left(\mathbf{u}_{1,j,r}\right)}{\partial u_j^{(p)}}\right]\mathbf{D}^{(p)}-d_{j,j}\mathbf{I},\quad \text{when } j=k,\\
\mathbf{A}_{j,k}&=-d_{j,k}\mathbf{I},\quad \text{when } j\neq k.
\end{aligned} \tag{1.23}$$

1.7.2 Paired Quasilinearization Method (PQLM)

In this section, the paired quasilinearization methods' numerical algorithm, introduced by Motsa and Animasaun [20], for the generalized system of PDEs (1.8) is presented. The PQLM is a numerical technique that seeks to decouple the system (1.8) into pairs. This is done by solving a pair from the set $\{\mathbf{u}_1, \mathbf{u}_2, \cdots, \mathbf{u}_N\}$ and their corresponding $\mathbf{F}_l^{th}$ equations and using the updated solutions in following pairs. For further illustration, consider the coupled general system (1.8)

$$\mathbf{F}_l\left(\mathbf{u}_1\left(\zeta,\tau\right), \mathbf{u}_2\left(\zeta,\tau\right), \cdots, \mathbf{u}_N\left(\zeta,\tau\right)\right) = 0, \;\; l = 1,2,\ldots,N. \tag{1.24}$$

To illustrate the PQLM for the general system (1.8), an ordered pairing will be performed, but pairing can be done using random combinations. We let $\mathbf{u}_1$ and $\mathbf{u}_2$ be the first pairing. Quasilinearization is applied to equations $\mathbf{F}_1\left(\mathbf{u}_1, \mathbf{u}_2, \cdots, \mathbf{u}_N\right)$ and $F_2\left(\mathbf{u}_1, \mathbf{u}_2, \cdots, \mathbf{u}_N\right)$. This process is continued for subsequent pairs using solutions from previous pairs to update subsequent pairs. In general, the pairing takes the form

$$\mathbf{F}_k\left(\zeta, \mathbf{u}_1, \cdots, \mathbf{u}_N\right) = 0, \;\; k = \{1,2\},\{3,4\},\ldots,\{N-1,N\}. \tag{1.25}$$

Quasilinearization is applied on each set of pairs in the system so as to linearize the system by application of Taylor series expansion. To do this, approximating points $(\mathbf{u}_1, \mathbf{u}_2, \cdots, \mathbf{u}_N)$ are chosen and expansion is performed such that

$$\mathbf{F}_k\left(\left(\mathbf{u}_{1,r},\ldots,\mathbf{u}_{N,r}\right)+\Delta\left(\mathbf{u}_1,\ldots,\mathbf{u}_N\right)\right) \approx \mathbf{F}_k\left(\mathbf{u}_{1,r},\ldots,\mathbf{u}_{N,r}\right)+\sum_{p=0}^{m_{k,k}} \frac{\partial^{(p)}\mathbf{F}_k\left(\mathbf{u}_{1,r},\ldots,\mathbf{u}_{N,r}\right)}{\partial u_k^{(p)}}\left(\Delta\mathbf{u}_k^{(p)}\right), \tag{1.26}$$

$$k = \{1,2\},\{3,4\},\ldots,\{N-1,N\}.$$

where $\Delta\mathbf{u}_k^{(p)} = \mathbf{u}_{k,r+1}^{(p)} - \mathbf{u}_{k,r}^{(p)}$ and each pair $\frac{\partial^{(p)}\mathbf{F}_k\left(\mathbf{u}_{q,r}\right)}{\partial\mathbf{u}_k^{(p)}}$ is a 2×2 Jacobian matrix.

The expansion in (1.26) is expressed fully as

$$\begin{aligned}\mathbf{F}_k\left(\left(\mathbf{u}_{1,r},\ldots,\mathbf{u}_{N,r}\right)+\Delta\left(\mathbf{u}_1,\ldots,\mathbf{u}_N\right)\right) &\approx \mathbf{F}_k\left(\mathbf{u}_{1,r},\ldots,\mathbf{u}_{N,r}\right)+\sum_{p=0}^{m_{k,k}} \frac{\partial^{(p)}\mathbf{F}_k\left(\mathbf{u}_{1,r},\ldots,\mathbf{u}_{N,r}\right)}{\partial u_k^{(p)}}\left(\mathbf{u}_{k,r+1}^{(p)}\right)\\ &-\sum_{p=0}^{m_{k,k}} \frac{\partial^{(p)}\mathbf{F}_k\left(\mathbf{u}_{1,r},\ldots,\mathbf{u}_{N,r}\right)}{\partial u_k^{(p)}}\left(\mathbf{u}_{k,r}^{(p)}\right),\end{aligned} \tag{1.27}$$

$$k = \{1,2\},\{3,4\},\ldots,\{N-1,N\}$$

The expansion given in (1.27) is substituted into the system (1.25) and we obtain

$$\sum_{p=0}^{m_{k,k}} \frac{\partial^{(p)}\mathbf{F}_k\left(\mathbf{u}_{1,r},\ldots,\mathbf{u}_{N,r}\right)}{\partial u_k^{(p)}}\left(\mathbf{u}_{k,r+1}^{(p)}\right) = R_k, \tag{1.28}$$

$$k = \{1,2\},\{3,4\},\ldots,\{N-1,N\}$$

where

$$R_k = \sum_{p=0}^{m_{k,k}} \frac{\partial^{(p)}\mathbf{F}_k\left(\mathbf{u}_{1,r},\ldots,\mathbf{u}_{N,r}\right)}{\partial u_k^{(p)}}\left(\mathbf{u}_{k,r}^{(p)}\right) - \mathbf{F}_k\left(\mathbf{u}_{1,r},\ldots,\mathbf{u}_{N,r}\right).$$

Bivariate spectral collocation method

The system (1.28) is solved using Chebyshev spectral collocation method in the form;

$$\sum_{p=0}^{m_{k,k}} \mathbf{diag}\left[\frac{\partial^{(p)}\mathbf{F}_k\left(\mathbf{u}_{1,j,r},\ldots,\mathbf{u}_{N,j,r}\right)}{\partial u_{k,j}^{(p)}}\right]\left(\mathbb{U}_{k,r+1}^{(p)}\right) = \mathbf{R}_{k,j}, \tag{1.29}$$

where

$$\mathbf{diag}\left[\frac{\partial^{(p)}\mathbf{F}_k\left(\mathbf{u}_{1,j,r},\ldots,\mathbf{u}_{N,j,r}\right)}{\partial u_{k,j}^{(p)}}\right] = \tag{1.30}$$

$$\begin{bmatrix} \frac{\partial^{(p)}\mathbf{F}_k\left(\mathbf{u}_{1,j,r}\left(x_0,y_j\right),\ldots,\mathbf{u}_{N,j,r}\left(x_0,y_j\right)\right)}{\partial u_{k,j}^{(p)}} & & & \\ & \frac{\partial^{(p)}\mathbf{F}_k\left(\mathbf{u}_{1,j,r}\left(x_1,y_j\right),\ldots,\mathbf{u}_{N,j,r}\left(x_1,y_j\right)\right)}{\partial u_{k,j}^{(p)}} & & \\ & & \ddots & \\ & & & \frac{\partial^{(p)}\mathbf{F}_k\left(\mathbf{u}_{1,j,r}\left(x_N,y_j\right),\ldots,\mathbf{u}_{N,j,r}\left(x_N,y_j\right)\right)}{\partial u_{k,j}^{(p)}} \end{bmatrix}$$

and

$$\mathbb{U}_{k,r+1}^{(p)} = \mathbf{D}^p\mathbf{u}_{k,r+1}. \tag{1.31}$$

The coupled linearized system (1.29) can be expressed in matrix form as

$$\begin{bmatrix} \mathbf{A}_{k,k} & A_{k,k+1} \\ \mathbf{A}_{k+1,k} & \mathbf{A}_{k+1,k+1} \end{bmatrix}\begin{bmatrix} \mathbf{u}_k \\ \mathbf{u}_{k+1} \end{bmatrix} = \begin{bmatrix} \mathbf{R}_{k,j} \\ \mathbf{R}_{k+1,j} \end{bmatrix}, \tag{1.32}$$

where each entry of $\mathbf{A}_{\{k,k+1\}}$ is a matrix of size $N_y\left(N_x+1\right)\times N_y\left(N_x+1\right)$ and each entry of both $\mathbf{U}_k$ and $\mathbf{R}_k$ have $N_y\left(N_x+1\right)$ dimensions.

1.8 Structure of Thesis

The relevant processes and methods introduced in this chapter will be used in the subsequent chapters, which are described below.

- Chapter 2 focuses on the problem of mixed convection in a gravity-driven nano-liquid film containing both nanoparticles and gyrotactic microorganisms, which is solved using the PQLM and SLLM. We investigate the effect of using different combinations of the PQLM on the convergence of the PQLM and observe whether there is a difference in the accuracy of the respective solutions. We also investigate the computational time for the methods to ascertain which method achieves convergent solutions faster.

- In Chapter 3, the unsteady MHD flow of a micropolar fluid over a stretching sheet with heat and mass transfer and an unsteady three-dimensional boundary layer flow due to a stretching surface in a viscous and incompressible micropolar fluid. The equations are solved using the paired quasilinearization method (PQLM) and the bivariate spectral local linearization method (BSLLM). We thus extend the paired quasilinearization method to partial differential equations to investigate the robustness of the method by observing the accuracy and convergence of the method. When convergence is confirmed, we investigate whether it improves the speed of convergence of the BSLLM. The versatility of the PQLM is shown in Chapters 4, 5 and 6.

- Chapter 4 focuses on investigating the combined influence of radiation, Hall and ion effects on a system of partial differential equations that model a magneto-hydrodynamic free convective heat generating flow past a semi-infinite vertical flat plate. These equations are solved using the PQLM.

- In Chapter 5, the PQLM is used to further investigate the effect of increasing thermophoresis, buoyancy ratio, Brownian motion and Dufour on the velocity, temperature, concentration and nanoparticle concentration profiles of a system of partial differential equations that model an

induced Darcy flow of an incompressible nano-fluid along an inclined isothermal surface embedded in porous medium.

- Chapter 6 details the study of double-diffusive mixed convection flow of a nanofluid near a vertical cone embedded in a porous medium with Soret and Dufour effects.

- In Chapter 7 we study the non-isothermal, magneto-hydrodynamic free convection boundary layer flow of a non-Newtonian tangential hyperbolic fluid past a vertical surface in a non-Darcy, isotropic, homogeneous porous medium in the presence of Hall and ion slip currents using the multidomain paired quasilinearization method (MD-PQLM) and the multi-domain spectral local linearization method (MD-SLLM).

- A general conclusion is given in Chapter 8. Here, we summarize the findings on the accuracy and convergence of the paired quasilinearization method for solving systems of ordinary and partial differential equations and highlight future research interests.

Chapter 2

Paired Quasilinearization Method for solving systems of ordinary differential equations

2.1 Introduction

Numerical methods have important applications and proven to be very effective in providing approximate solutions to nonlinear differential equations that model real world problems. The complex nature of these nonlinear differential equations has made them very difficult to solve analytically; hence the need to apply numerical techniques to provide approximate answers. The applicability of numerical techniques ranges from solving nonlinear differential equations that model optimal stochastic control problems [51, 52], weather prediction [53], and boundary layer theory [54], to mention a few scenarios. Over the years, a number of numerical techniques have been developed in order to provide approximate answers to these complex differential equations. Some such methods include the finite differences based approaches [55–58], finite element and volume methods, Runge-Kutta integration method [59, 60], homotopy based methods [61–64], Keller-Box method [65–68], linearization methods [38, 39, 42, 45, 47] and spectral methods [13, 17, 32].

The use of spectral methods to solve ordinary differential equations numerically was started by Lanczos [69], although they had been applied earlier in analytical research [31]. The idea behind spectral methods is using a truncated series of independent variable functions that are known to represent solutions to mathematical problems [24]. Gottlieb and Gottlieb [28], Hussaini and Zang

[70] and Fornberg [71] all described spectral methods to be global methods that process information from a full domain for computational purposes. An important property of spectral methods is their ability to converge exponentially [24, 32]. It has been noted by Fornberg [71] that when a problem is defined under domains or boundary conditions that are irregular, or there is the presence of strong shocks, or the theoretical aspect of the problem is incompletely understood, spectral methods might not perform properly. Nevertheless, spectral methods are very convenient to work with, as is shown by their extensive application and implementation [13, 14, 17].

Spectral methods have been successfully combined with linearization and relaxation techniques to come up with more robust methods in recent years, such as the spectral relaxation method [72–76], the spectral local linearization method [18, 77, 78] and the spectral quasilinearization method [18, 73]. The SRM uses the idea of the Gauss-Seidel relaxation approach in decoupling systems of nonlinear differential equations and spectral collocation is applied to discretize the resulting linear decoupled systems [72]. The SQLM employs the spectral collocation approach in solving coupled systems of differential equations that have been linearized using the quasilinearization method introduced by Bellman and Kalaba [38]. The SLLM implements the quasilinearization method in a sequential manner by linearizing one equation at a time in terms of one independent variable. This leads to a decoupled sequence of equations that can be solved independently in a sequential manner [18].

The SLLM and the SQLM were both introduced by Motsa [18] and were used to solve both the Blasius boundary layer problem and the problem of an unsteady free convective heat and mass transfer on a stretching surface in a porous medium in the presence of a chemical reaction that was modeled by a system of three differential equations. By observing the results, it was noted that the SLLM and the SQLM were efficient methods as they gave results that were consistent with those in published literature and also with MATLABs' in-built bvp4c routine. It was also observed that the SQLM converged much faster than the SLLM, even after applying the successive over-relaxation technique on the SLLM.

The SLLM was used by Motsa et al. [77] in solving a system of two differential equations that

modeled the problem of natural convection boundary layer flow with heat transfer. The accuracy of the method was shown to be good; results being consistent with those in the published literature, and the authors found the method easy to implement. However, once again, the successive over-relaxation technique was needed to improve the rate of convergence of the SLLM; highlighting the number of iterations it took to converge as indicating slightly weak point of the SLLM when compared to the SQLM.

In order to substantiate the earlier findings, an extensive study was carried out by Otegbeye [23] on the SRM, SLLM and SQLM. In the study, the methods were compared in terms of their convergence rates and accuracy of solutions obtained using the methods. It was confirmed that the SRM and SLLM could not converge as fast as the SQLM but they gave better accuracy. The rapid convergence of the SQLM was observed to be due to its quadratic convergence, while the SLLM had a linear convergence. The poor accuracy of the SQLM can be explained in part by its being derived from a first-order Taylor series, leading to the truncation error in the underlying Taylor series. In addition, the lower accuracy of the SQLM can be attributed to the coupled nature of the large matrix system that results from the discretization technique of the SQLM, unlike with the SLLM that breaks down the system into single equations. The latter results in the slower convergence of the SLLM because it solves equations independently at every iteration level.

Noting that each of the three methods has some drawbacks, the idea arose of developing a new technique that utilised the coupled aspect of the SQLM encapsulated within the decoupled method SLLM. This method is named the paired quasilinearization method.

The aim of this research is to fully examine the dynamics of the PQLM and to compare it with the SLLM so as to verify that it has achieved its purpose of successfully improving the convergence of the SLLM while maintaining its high accuracy. The SLLM and PQLM will be applied to a system of four differential equations to obtain solutions. The comparison will be made in terms of their speed of convergence, convergence error-norm, and residual-norm. Time taken to achieve convergence will also be measured to test for computational efficiency of the methods and in the case where linear convergence is obtained for the PQLM, the asymptotic error constants of the

PQLM and the SLLM will be obtained so as to determine which method converges faster.

2.2 Iteration Schemes

For the purposes of application of the PQLM and SLLM, consider a system of ordinary differential equations that models the problem of mixed convection in gravity-driven nano-liquid film containing nanoparticles and gyrotactic microorganisms, as previously studied by Raees et al. [79];

$$f''' + \frac{2}{3}\left(1 - f'^2\right) + ff'' + Gr\theta - Nr\phi + Rb\omega = 0, \tag{2.1}$$

$$\theta'' + Prf\theta' + Nb\theta'\phi' + Nt\theta'^2 = 0, \tag{2.2}$$

$$\phi'' + \frac{Nt}{Nb}\theta'' + Lef\phi' = 0, \tag{2.3}$$

$$\omega'' + Scf\omega' - Pe\omega'\phi' - Pe\omega\phi'' = 0, \tag{2.4}$$

with corresponding boundary conditions

$$\begin{aligned} &f(0) = 0,\ f'(0) = 0,\ f'(\infty) = 1,\ \theta'(0) - \gamma\theta(0) = -\gamma, \\ &\omega(0) = 1,\ \theta(\infty) = \phi(\infty) = \omega(\infty) = 0,\ \phi(0) = 1, \end{aligned} \tag{2.5}$$

where $f(\eta)$, $\theta(\eta)$, $\phi(\eta)$ and $\omega(\eta)$ denote, respectively, the dimensionless stream function, temperature, nano-particle volume fraction and density of motile microorganisms while Gr stands for the Grashof number, Rb and Pe the bioconvection Rayleigh and Peclet numbers, respectively, Pr the Prandtl number, Sc the Schmidt number, Le the Lewis number, γ is a constant dimensionless parameter, and Nr, Nt and Nb the bouyancy-ratio, thermophoresis and Brownian motion parameters, respectively. The system of equations $(2.1) - (2.4)$ is solved using three different combinations by applying the quasilinearization on a pair of equations thereby decoupling the original system and in the process using updated solutions from the previous pair in the next pair. Comparison will be made between the spectral local linearization method and the spectral quasi-linearization method.

2.3 Solution Techniques

In this section, the development of the iteration schemes for the PQLM, SLLM and SQLM are described for obtaining solutions to the system of equations (2.1) − (2.4).

The system of equations (2.1) − (2.4) can be paired in three different ways and all of these combinations are considered to investigate the effect of the different sets of pairing. The SLLM and all possible combinations of the PQLM will be presented as follows:

1. Case 1: ($\{f,\omega\}$ and $\{\theta,\phi\}$) which represents the pairings {(2.1),(2.4)} and {(2.2),(2.3)},
2. Case 2:($\{f,\theta\}$ and $\{\phi,\omega\}$) which represents the pairings {(2.1),(2.2)} and {(2.3),(2.4)},
3. Case 3: ($\{f,\phi\}$ and $\{\theta,\omega\}$) which represents the pairings {(2.1),(2.3)} and {(2.2),(2.4)},
4. SLLM.

2.3.1 Case 1:($\{f,\omega\}$ and $\{\theta,\phi\}$)

In the first pair of equations, nonlinear terms f'^2, ff'' and $f\omega'$ are linearized using the Taylor series expansion to first order to obtain the linearized pair

$$\begin{aligned} f'''_{r+1}+\frac{2}{3}-\frac{4}{3}f'_rf'_{r+1}+\frac{2}{3}f'^2_r+f_rf''_{r+1}+f''_rf_{r+1}-f_rf''_r \\ +Gr\theta_r-Nr\phi_r+Rb\omega_{r+1}=0, \\ \omega''_{r+1}+Scf_r\omega'_{r+1}+Sc\omega'_rf_{r+1}-Sc\omega'_rfr-Pe\phi'_r\omega'_{r+1}-Pe\phi''_r\omega_{r+1}=0. \end{aligned} \tag{2.6}$$

The pair of equations (2.6) is integrated using Chebyshev spectral collocation method in the form

$$\begin{aligned} \left[\mathbf{D}^3+[\mathbf{f}_r]\mathbf{D}^2-\left[\frac{4}{3}\mathbf{f}'_r\right]\mathbf{D}+\left[\mathbf{f}''_r\right]\right]\mathbf{F}_{r+1}+[Rb\mathbf{I}]\,\omega_{r+1}= \\ -\frac{2}{3}-\frac{2}{3}\mathbf{f}'^2_r+\mathbf{f}_r\mathbf{f}''_r-Gr\theta_r+Nr\phi_r, \\ \left[Sc\omega'_r\right]\mathbf{F}_{r+1}+\left[\mathbf{D}^2+\left[Sc\mathbf{f}_r-Pe\phi'_r\right]\mathbf{D}-\left[Pe\phi''_r\right]\right]\omega_{r+1}=Sc\mathbf{f}_r\omega'_r, \end{aligned} \tag{2.7}$$

where $[\cdots]$ denotes a diagonal matrix containing vectors and $\mathbf{I}$ is an identity matrix used to multiply scalar quantities.

Updated solutions for $\mathbf{f}$ and ω are used in the second pair of equations. In the second pair, the nonlinear terms are $\theta'\phi'$ and θ'^2 and the linearized pair is obtained as;

$$\begin{aligned} \theta''_{r+1}+Prf_r\theta'_{r+1}+Nb\theta'_r\phi'_{r+1}+Nb\phi'_r\theta'_{r+1}+2Nt\theta'_r\theta'_{r+1} &= Nb\theta'_r\phi'_r+Nt\theta'^2_r, \\ \phi''_{r+1}+\frac{Nt}{Nb}\theta''_{r+1}+Lef_r\phi'_{r+1} &= 0. \end{aligned} \tag{2.8}$$

The Chebyshev spectral collocation method is then applied on the pair of equations (2.8) to give

$$\begin{aligned} \left[\mathbf{D}^2+\left[Pr\mathbf{f}_r+Nb\phi'_r+2Nt\theta'_r\right]\mathbf{D}\right]\theta_{r+1}+\left[\left[Nb\theta'_r\right]\mathbf{D}\right]\phi_{r+1} & \\ = Nb\theta'_r\phi'_r+Nt\theta'^2_r, & \\ \left[\frac{Nt}{Nb}\mathbf{D}^2\right]\theta_{r+1}+\left[\mathbf{D}^2+[Le\mathbf{f}_r]\mathbf{D}\right]\phi_{r+1} &= 0. \end{aligned} \tag{2.9}$$

2.3.2 Case 2:({f,θ} and {ϕ,ω})

Nonlinear terms in the first pair of equations are f'^2, ff'', $f\theta'$ and θ'^2.The following linearized pair is obtained:

$$\begin{aligned} f'''_{r+1}-\frac{4}{3}f'_rf'_{r+1}+f_rf''_{r+1}+f''_rf_{r+1}+Gr\theta_{r+1} & \\ = Nr\phi_r-Rb\omega_r-\frac{2}{3}-\frac{2}{3}f'^2_r+f_rf''_r, & \\ \theta''_{r+1}+Prf_r\theta'_{r+1}+Pr\theta'_rf_{r+1}+Nb\phi'_r\theta'_{r+1}+2Nt\theta'_r\theta'_{r+1} &= Prf_r\theta_r+Nt\theta'^2_r. \end{aligned} \tag{2.10}$$

The spectral collocation technique is applied to the pair of equations (2.10) in the form;

$$\begin{aligned} \left[\mathbf{D}^3+[\mathbf{f}_r]\mathbf{D}^2-\left[\frac{4}{3}\mathbf{f}'_r\right]\mathbf{D}+\left[\mathbf{f}''_r\right]\right]\mathbf{F}_{r+1}+[Gr\mathbf{I}]\theta_{r+1} & \\ -\frac{2}{3}-\frac{2}{3}\mathbf{f}'^2_r+\mathbf{f}_r\mathbf{f}''_r+Nr\phi_r-Rb\omega_r, & \\ \left[Pr\theta'_r\right]\mathbf{F}_{r+1}+\left[\mathbf{D}^2+\left[Pr\mathbf{f}_r+Nb\phi'_r+2Nt\theta'_r\right]\mathbf{D}\right]\theta_{r+1} & \\ = Pr\mathbf{f}_r\theta'_r+Nt\theta'^2_r. & \end{aligned} \tag{2.11}$$

The updated solution of $\mathbf{f}$ and θ from the pair (2.11) is inserted into the second pair of equations, whose nonlinear terms $\omega^{'}\phi^{'}$ and $\omega\phi^{''}$ are linearized to obtain the pair

$$\begin{aligned}\phi^{''}_{r+1}+Lef_r\phi^{'}_{r+1}&=-\frac{Nt}{Nb}\theta^{''}_r,\\ \omega^{''}_{r+1}+Scf_r\omega^{'}_{r+1}-Pe\omega^{'}_r\phi^{'}_{r+1}-Pe\phi^{'}_r\omega^{'}_{r+1}-Pe\omega_r\phi^{''}_{r+1}&\\ -Pe\phi^{''}_r\omega_{r+1}&=-Pe\omega^{'}_r\phi^{'}_r--+Pe\phi^{''}_r\omega_r.\end{aligned}\tag{2.12}$$

The Chebyshev spectral collocation method is applied to integrate the pair (2.12) in the form;

$$\begin{aligned}\left[\mathbf{D}^2+[Le\mathbf{f}_r]\,\mathbf{D}\right]\phi_{r+1}+[\mathbf{0}]\,\omega_{r+1}&=-\frac{Nt}{Nb}\theta^{''}_r,\\ \left[[-Pe\omega_r]\,\mathbf{D}^2-\left[Pe\omega^{'}_r\right]\mathbf{D}\right]\phi_{r+1}+\left[\mathbf{D}^2+\left[Sc\mathbf{f}_r-Pe\phi^{'}_r\right]\mathbf{D}-\left[Pe\phi^{''}_r\right]\right]\omega_{r+1}&\\ =-Pe\omega^{'}_r\phi^{'}_r-Pe\phi^{''}_r\omega_r.&\end{aligned}\tag{2.13}$$

2.3.3 Case 3:({f,ϕ} and {θ,ω})

The nonlinear terms in the first pair of equations are $f^{'2}$, $ff^{''}$ and $f\phi$. The following linearized pair is obtained:

$$\begin{aligned}f^{'''}_{r+1}-\frac{4}{3}f^{'}_rf^{'}_{r+1}+f_rf^{''}_{r+1}+f^{''}_rf_{r+1}-Nr\phi_{r+1}&=\\ -\frac{2}{3}-\frac{2}{3}f^{'2}_r+f_rf^{''}_r-Gr\theta_r-Rb\omega_r,&\\ \phi^{''}_{r+1}+Lef_r\phi^{'}_{r+1}+Le\phi^{'}_rf_{r+1}=Lef_r\phi^{'}_r-\frac{Nt}{Nb}\theta^{''}_r.&\end{aligned}\tag{2.14}$$

The Chebyshev spectral collocation method is applied on the pair (2.14) to obtain;

$$\begin{aligned}\left[\mathbf{D}^3+[\mathbf{f}_r]\,\mathbf{D}^2-\left[\frac{4}{3}\mathbf{f}^{'}_r\right]\mathbf{D}+\left[\mathbf{f}^{''}_r\right]\right]\mathbf{F}_{r+1}+[-Nr\mathbf{I}]\,\phi_{r+1}&\\ =-\frac{2}{3}-\frac{2}{3}\mathbf{f}^{'2}_r+\mathbf{f}_r\mathbf{f}^{''}_r-Gr\theta_r-Rb\omega_r,&\\ \left[Le\phi^{'}_r\right]\mathbf{F}_{r+1}+\left[\mathbf{D}^2+[Le\mathbf{f}_r]\,\mathbf{D}\right]\phi_{r+1}=-\frac{Nt}{Nb}\theta^{''}_r+Le\mathbf{f}_r\phi^{'}_r.&\end{aligned}\tag{2.15}$$

Updated solutions for $\mathbf{f}$ and ϕ from the pair (2.15) are applied in the second pair of equations. The nonlinear term θ^2 is linearized to obtain the linearized pair

$$\begin{aligned}\theta^{''}_{r+1}+Prf_r\theta^{'}_{r+1}+Nb\phi^{'}_r\theta^{'}_{r+1}+2Nt\theta^{'}_r\theta^{'}_{r+1}&=Nt\theta^{'2}_r,\\ \omega^{''}_{r+1}+Scf_r\omega^{'}_{r+1}-Pe\phi^{'}_r\omega^{'}_{r+1}-Pe\phi^{''}_r\omega_{r+1}&=0.\end{aligned}\tag{2.16}$$

The Chebyshev spectral collocation technique is applied on the pair (2.16) in the form

$$\begin{aligned}\left[\mathbf{D}^2+\left[Pr\mathbf{f}_r+Nb\phi_r^{'}+2Nt\theta_r^{'}\right]\mathbf{D}\right]\theta_{r+1}+[\mathbf{0}]\,\omega_{r+1}&=Nt\theta_r^{'2},\\ [\mathbf{0}]\,\theta_{r+1}+\left[\mathbf{D}^2+\left[Sc\mathbf{f}_r-Pe\phi_r^{'}\right]\mathbf{D}-\left[Pe\phi_r^{''}\right]\right]\omega_{r+1}&=0.\end{aligned}\tag{2.17}$$

2.3.4 Case 4: SLLM

In this method, linearization is applied on a nonlinear function and its derivatives in equation (2.1) and its updated solution is used in equations (2.2) − (2.4). This process is continued for other functions in subsequent equations. Nonlinear terms are identified as terms that involve only a particular function and its derivatives in each equation and linearization is performed using the Taylor series expansion to first order before application of the Chebyshev spectral collocation method in order to integrate the linearized system. Nonlinear terms in the system (2.1) − (2.4) are $f^{'2}$, $ff^{''}$ and $\theta^{'2}$ and they are all linearized to give the linearized decoupled system;

$$\begin{aligned}f_{r+1}^{'''}-\frac{4}{3}f_r^{'}f_{r+1}^{'}+f_rf_{r+1}^{''}+f_r^{''}f_{r+1}&=-\frac{2}{3}-\frac{2}{3}f_r^{'2}\\ &\quad+f_rf_r^{''}-Gr\theta_r+Nr\phi_r-Rb\omega_r,\\ \theta_{r+1}^{''}+Prf_r\theta_{r+1}^{'}+Nb\phi_r^{'}\theta_r^{'}+2Nt\theta_r^{'}\theta_{r+1}^{'}-Nt\theta_r^{'2}&=0,\\ \phi_{r+1}^{''}+Lef_r\phi_{r+1}^{'}+\frac{Nt}{Nb}\theta_r^{''}&=0,\\ \omega_{r+1}^{''}+Scf_r\omega_{r+1}^{'}-Pe\phi_r^{'}\omega_{r+1}^{'}-Pe\phi_r^{''}\omega_{r+1}&=0.\end{aligned}\tag{2.18}$$

The Chebyshev Spectral collocation method is then applied to the decoupled linearized system (2.18) in the form

$$\begin{aligned}\left[\mathbf{D}^3+[\mathbf{f}_r]\mathbf{D}^2-\left[\frac{4}{3}\mathbf{f}_r^{'}\right]+\left[\mathbf{f}_r^{''}\right]\right]\mathbf{F}_{r+1}&\\ =-\frac{2}{3}-\frac{2}{3}\mathbf{f}_r^{'2}+\mathbf{f}_r\mathbf{f}_r^{''}-Gr\theta_r+Nr\phi_r-Rb\omega_r,&\\ \left[\mathbf{D}^2+\left[Pr\mathbf{f}_r+Nb\phi_r^{'}+2Nt\theta_r^{'}\right]\mathbf{D}\right]\theta_{r+1}=Nt\theta_r^{'2},&\\ \left[\mathbf{D}^2+[Le\mathbf{f}_r]\mathbf{D}\right]\phi_{r+1}=-\frac{Nt}{Nb}\theta_r^{''},&\\ \left[\mathbf{D}^2+\left[Sc\mathbf{f}_r-Pe\phi_r^{'}\right]\mathbf{D}-\left[Pe\phi_r^{''}\right]\right]\omega_{r+1}=0.&\end{aligned}\tag{2.19}$$

2.4 Results and Discussion

In this section, solutions generated using the PQLM and the SLLM are presented and comparison is made for the speed of convergence of the methods, in terms of number of iterations taken to converge and also the time taken for convergence. Residual analysis and solution error analysis are also performed to further compare the accuracy of the PQLM used in the three cases with that of the SLLM. As noted by Hull et al. [80], in order to make a meaningful comparison, it is essential to select a well posed problem, compare methods that are used to solve similar type of problems and define the right criteria for which conclusive evidence can be obtained. In conducting this study, all of the conditions were considered. The parameters in the system of ordinary differential equations (2.1) − (2.4) were assigned specific values except where stated otherwise. The value of the Prandtl number used is that assigned to water, which is $Pr = 1$. The Schmidt number chosen is $Sc = 1$, which is close to the value assigned to Carbon dioxide (Sc=0.94). The Lewis number Le, the bioconvection Rayleigh number Rb, the reduced heat transfer parameter γ and the constant λ, are all set to be 1. The thermophoresis parameter Nt is set to be 0.3 while the Brownian motion parameter Nb and the bouyancy ratio parameter Nr are both set at 0.1. The Grashof number is $Gr = 1$. The number of grid points used to generate convergent solutions were 100 and the domain was scaled at $L = 20$. These values were used to obtain all results presented in Tables 2.1 to 2.9 and in graphical form in Figures 2.1 to 2.8.

The four cases generated solutions starting with an initial approximation. The initial approximation was chosen as a function that satisfied all the given boundary conditions (2.5). This approximation is referred to as an initial guess. The initial guess was used to generate the next iteration and the process carried on iteratively. The initial approximations that satisfied all the boundary conditions (2.5) are

$$f_0 = \eta - \frac{1}{\lambda}\left(\exp^{-\lambda\eta} - \exp^{-2\lambda\eta}\right), \tag{2.20}$$

$$\theta_0 = \exp^{-\lambda\eta} - \left(\frac{\lambda}{\gamma+2\lambda}\right)\exp^{-2\lambda\eta}, \;\; \omega_0 = \phi_0 = \exp^{-\lambda\eta}. \tag{2.21}$$

Table 2.1: Convergence of solutions obtained using the PQLM (Cases 1, 2 and 3) and SLLM for the local skin friction $-f''(0)$ and time taken to achieve convergence

	PQLM 1	PQLM 2	PQLM 3	SLLM
iterations	$-f''(0)$	$-f''(0)$	$-f''(0)$	$-f''(0)$
1	1.8334931700	1.8743037190	1.8868124760	1.9050029200
2	1.8307803870	1.8283504230	1.8219057760	1.8247166930
3	1.8332432550	1.8333121990	1.8360615200	1.8343419660
4	1.8330958970	1.8330957750	1.8324447310	1.8329398690
5	1.8331051780	1.8331050630	1.8332541230	1.8331270720
6	1.8331045940	1.8331046070	1.8330708110	1.8331015720
7	1.8331046310	1.8331046300	1.8331122710	1.8331050450
8	1.8331046280	1.8331046280	1.8331029000	1.8331045720
9	1.8331046280	1.8331046290	1.8331050190	1.8331046360
10	1.8331046290	1.8331046290	1.8331045400	1.8331046280
11	1.8331046290	1.8331046290	1.8331046480	1.8331046280
12	1.8331046290	1.8331046290	1.8331046240	1.8331046290
13	1.8331046290	1.8331046290	1.8331046290	1.8331046290
⋮				⋮
30	1.8331046290	1.8331046290	1.8331046290	1.8331046290
Time (secs)	2.87	3.00	3.65	3.10

Table 2.2: Convergence of solutions obtained using the PQLM (Cases 1, 2 and 3) and SLLM for the local Nusselt number $-\theta^{'}(0)$ and time taken to achieve convergence

	PQLM 1	PQLM 2	PQLM 3	SLLM
iterations	$-\theta^{'}(0)$	$-\theta^{'}(0)$	$-\theta^{'}(0)$	$-\theta^{'}(0)$
1	0.3575368484	0.3534512412	0.3599893987	0.3552595759
2	0.3560754788	0.3558119605	0.3556049868	0.3554794226
3	0.3561932566	0.3562091465	0.3563218573	0.3562678885
4	0.3561859693	0.3561855505	0.3561558052	0.3561752615
5	0.3561864279	0.3561864385	0.3561933086	0.3561879167
6	0.3561863991	0.3561863989	0.3561848380	0.3561861942
7	0.3561864009	0.3561864009	0.3561867540	0.3561864289
8	0.3561864008	0.3561864008	0.3561863209	0.3561863969
9	0.3561864008	0.3561864008	0.3561864188	0.3561864013
10	0.3561864008	0.3561864008	0.3561863967	0.3561864007
11	0.3561864008	0.3561864008	0.3561864017	0.3561864008
12	0.3561864008	0.3561864008	0.3561864006	0.3561864008
13	0.3561864008	0.3561864008	0.3561864008	0.3561864008
⋮				⋮
30	0.3561864008	0.3561864008	0.3561864008	0.3561864008
Time (secs)	2.56	2.64	3.63	2.69

Table 2.3: Convergence of solutions obtained using the PQLM (Cases 1, 2 and 3) and SLLM for the local wall mass flux $-\phi^{'}(0)$ and time taken to achieve convergence

	PQLM 1	PQLM 2	PQLM 3	SLLM
iterations	$-\phi^{'}(0)$	$-\phi^{'}(0)$	$-\phi^{'}(0)$	$-\phi^{'}(0)$
1	0.2528181611	0.2767272338	0.3203705008	0.2830716427
2	0.2477337923	0.2480429023	0.2389700963	0.2482071888
3	0.2478471957	0.2478255602	0.2496528293	0.2478757930
4	0.2478384221	0.2478387692	0.2474221338	0.2478342898
5	0.2478389744	0.24783895211	0.2479334473	0.2478395823
6	0.2478389396	0.2478389416	0.2478176191	0.2478388549
7	0.2478389418	0.2478389417	0.2478437664	0.2478389535
8	0.2478389417	0.2478389417	0.2478378513	0.2478389401
9	0.2478389417	0.2478389417	0.2478391882	0.2478389419
10	0.2478389417	0.2478389417	0.2478388860	0.2478389417
11	0.2478389417	0.2478389417	0.2478389543	0.2478389417
12	0.2478389417	0.2478389417	0.2478389388	0.2478389417
13	0.2478389417	0.2478389417	0.2478389423	0.2478389417
14	0.2478389417	0.2478389417	0.2478389415	0.2478389417
15	0.2478389417	0.2478389417	0.2478389417	0.2478389417
⋮				⋮
30	0.2478389417	0.2478389417	0.2478389417	0.2478389417
Time (secs)	2.62	2.43	4.08	2.50

Table 2.4: Convergence of solutions obtained using the PQLM (Cases 1, 2 and 3) and SLLM for the local wall motile microorganisms flux $-\omega'(0)$ and time taken to achieve convergence

	PQLM 1	PQLM 2	PQLM 3	SLLM
iterations	-$\omega'(0)$	-$\omega'(0)$	-$\omega'(0)$	-$\omega'(0)$
1	1.4037974500	0.8073354409	0.8528074166	0.8256976704
2	0.7850167022	0.7805901770	0.7726468799	0.7802153695
3	0.780894543	0.7809594987	0.7826111815	0.7811291749
4	0.7809436955	0.7809383156	0.7805537661	0.7809147461
5	0.7809397235	0.7809400340	0.7810273966	0.7809433983
6	0.7809399736	0.7809399555	0.7809202214	0.7809394908
7	0.7809399579	0.7809399590	0.7809444242	0.7809400225
8	0.7809399589	0.7809399588	0.7809389496	0.7809399501
9	0.7809399588	0.7809399588	0.7809401870	0.7809399600
10	0.7809399588	0.7809399588	0.7809399072	0.7809399586
11	0.7809399588	0.7809399588	0.7809399705	0.7809399588
12	0.7809399588	0.7809399588	0.7809399562	0.7809399588
13	0.7809399588	0.7809399588	0.7809399594	0.7809399588
14	0.7809399588	0.7809399588	0.7809399587	0.7809399588
15	0.7809399588	0.7809399588	0.7809399588	0.7809399588
⋮				⋮
30	0.7809399588	0.7809399588	0.7809399588	0.7809399588
Time (secs)	2.91	2.79	4.05	2.75

Tables 2.1 to 2.4 display the convergence speed and the time taken to obtain convergence using the PQLM cases 1-3 and the SLLM. It is observed that as the number of iterations increase, the solutions tend towards convergence. It is shown in Tables 2.1 to 2.4 that the PQLM cases 1 and 2 converge the fastest, with the SLLM converging later. The PQLM case 3 is shown to be the slowest to converge. Despite these differences, with respect to the time taken to attain convergence, it is observed that the methods all converge in a very short period, that is within 4 seconds.

Tables 2.5 to 2.8 display the convergence rate of the SLLM and the PQLM cases 1, 2 and 3 using

the norm of the error between successive iterations. This is calculated using the formula

$$p_f = \frac{\ln(||Error(f)||_\infty(n+2)/||Error(f)||_\infty(n+1))}{\ln(||Error(f)||_\infty(n+1)/||Error(f)||_\infty(n))},$$
$$p_\theta = \frac{\ln(||Error(\theta)||_\infty(n+2)/||Error(\theta)||_\infty(n+1))}{Ln(||Error(\theta)||_\infty(n+1)/||Error(\theta)||_\infty(n))},$$
$$p_\phi = \frac{\ln(||Error(\phi)||_\infty(n+2)/||Error(\phi)||_\infty(n+1))}{\ln(||Error(\phi)||_\infty(n+1)/||Error(\phi)||_\infty(n))},$$
$$p_\omega = \frac{\ln(||Error(\omega)||_\infty(n+2)/||Error(\omega)||_\infty(n+1))}{\ln(||Error(\omega)||_\infty(n+1)/||Error(\omega)||_\infty(n))},$$

where n is the iteration level and p the convergence rate.

Table 2.5: Convergence rate $||Error(f)||_\infty$ after each iteration using the PQLM cases 1, 2 and 3 and the SLLM

Iterations	PQLM 1	PQLM 2	PQLM 3	SLLM
1				
2				
3	2.68	3.30	6.50	13.00
4	0.68	0.98	0.58	0.59
5	1.06	1.01	1.00	1.10
6	1.00	1.00	1.00	1.00
7	1.00	1.00	1.00	1.00
8	1.00	1.00	1.00	1.00
9	1.00	1.00	1.00	1.00

Table 2.6: Convergence rate $||Error(\theta)||_\infty$ after each iteration using the PQLM cases 1, 2 and 3 and the SLLM

Iterations	PQLM 1	PQLM 2	PQLM 3	SLLM
1				
2				
3	0.89	0.75	0.84	1.00
4	1.02	1.00	0.84	0.95
5	1.00	1.00	1.00	1.00
6	1.00	1.00	1.00	1.00
7	1.00	1.00	1.00	1.00
8	1.00	1.00	1.00	1.00
9	1.00	1.00	1.00	1.00

Table 2.7: Convergence rate $||Error(\phi)||_\infty$ after each iteration using the PQLM cases 1, 2 and 3 and the SLLM

Iterations	PQLM 1	PQLM 2	PQLM 3	SLLM
1				
2				
3	0.82	0.88	2.00	0.85
4	0.87	1.10	0.60	0.80
5	1.02	1.00	1.10	1.00
6	1.00	1.00	0.98	1.00
7	1.00	1.00	1.00	1.00
8	1.00	1.00	1.00	1.00
9	1.00	1.00	1.00	1.00

Table 2.8: Convergence rate $||Error(\omega)||_\infty$ after each iteration using the PQLM cases 1, 2 and 3 and the SLLM

Iterations	PQLM 1	PQLM 2	PQLM 3	SLLM
1				
2				
3	-25.77	1.30	1.20	1.30
4	0.92	1.10	0.90	0.79
5	0.65	1.00	1.00	1.00
6	1.00	1.00	1.00	1.00
7	1.00	1.00	1.00	1.00
8	1.00	1.00	1.00	1.00
9	1.00	1.00	1.00	1.00

It is observed from the data in Tables 2.5 - 2.8 that the SLLM and the PQLM cases 1, 2 and 3 all converge linearly; that is, they have a convergence rate of 1.

The data in Tables 2.5 to 2.8 showing the linear convergence of all four methods, PQLM cases $1-3$ and SLLM, prompts further analysis to test which of the methods converge faster; hence the introduction of the asymptotic error constant. The asymptotic error constant, as described by Babajee and Dauhoo [81] and Traub [82], is obtained using the formula

$$\lim_{k\to\infty} \frac{||x_{k+1}-x^*||}{||x_k-x^*||^l} = C, \tag{2.22}$$

where l is the rate of convergence and is linear in all four methods, k is the iteration number, x^* the converged solution, x_{k+1} and x_k are the solutions at current and previous iteration levels, respectively and C is the asymptotic error constant. Babajee and Dauhoo [81] used the asymptotic error constant when comparing various convergence rates for different numerical methods. The smaller the value of the asymptotic error constant C, the faster the convergence of solutions obtained using the methods.

Table 2.9 displays the asymptotic error constants in the PQLM cases $1-3$ and the SLLM.

Table 2.9: Asymptotic error constant of $-f''(0)$ after each iteration using the PQLM cases 1, 2 and 3 and the SLLM

Iterations	PQLM 1	PQLM 2	PQLM 3	SLLM
3	0.060	0.044	0.055	0.148
4	0.063	0.043	0.227	0.133
5	0.063	0.049	0.227	0.136
6	0.064	0.046	0.226	0.136

The results in Table 2.9 show that the PQLM case 2 has the smallest asymptotic error constant with the PQLM case 1 slightly larger but nevertheless smaller than the SLLM, while the PQLM case 3 has the largest error constant. The constants displayed indicate that the PQLM cases 1 and 2 both converge much faster than the SLLM while the PQLM case 3 converges the slowest.

Figures 2.1 to 2.8 below show the norm of the error between previous and current iterations and the norm of the residual error. Accuracy here is determined using the error between successive iterations and the infinity norm of the residual error. The error is calculated by subtracting the previous iteration from the current iteration as the number of iterations increase. The residual error is an error that is calculated by inserting an approximate solution obtained back into the original system of equations $(2.1)-(2.3)$. The residual error is given by

$$\begin{aligned} Res(\mathbf{f}) &= \mathbf{f}''' + \frac{2}{3}\left(1-\mathbf{f}'^2\right) + \mathbf{f}\mathbf{f}'' + Gr\theta - Nr\phi + Rb\omega, \\ Res(\theta) &= \theta'' + Pr\mathbf{f}\theta + Nb\theta'\phi' + Nt\theta'^2, \\ Res(\phi) &= \phi'' + \frac{Nt}{Nb}\theta'' + Le\mathbf{f}\phi', \\ Res(\omega) &= \omega'' + Sc\mathbf{f}\omega' - Pe\omega'\phi' - Pe\omega\phi'', \end{aligned} \tag{2.23}$$

where the system of equations (2.23) is made up of approximate solutions obtained using the PQLM case 1, PQLM case 2, PQLM case 3 and the SLLM. The infinity norms of (2.23) defined

as

$$
\begin{aligned}
IN_r(f) &= ||Res(\mathbf{f})||_\infty, \\
IN_r(\theta) &= ||Res(\theta)||_\infty, \\
IN_r(\phi) &= ||Res(\phi)||_\infty, \\
IN_r(\omega) &= ||Res(\omega)||_\infty,
\end{aligned}
$$

were used to identify the extent of deviation of the approximate solution from the true solution for the system $(2.1) - (2.4)$. At the minimum point, where the residual error can no longer improve, *optimal residual* is said to be attained and that is the point used in this study in determining the convergence and accuracy of the solutions obtained with the PQLM case 1, PQLM case 2, PQLM case 3 and SLLM.

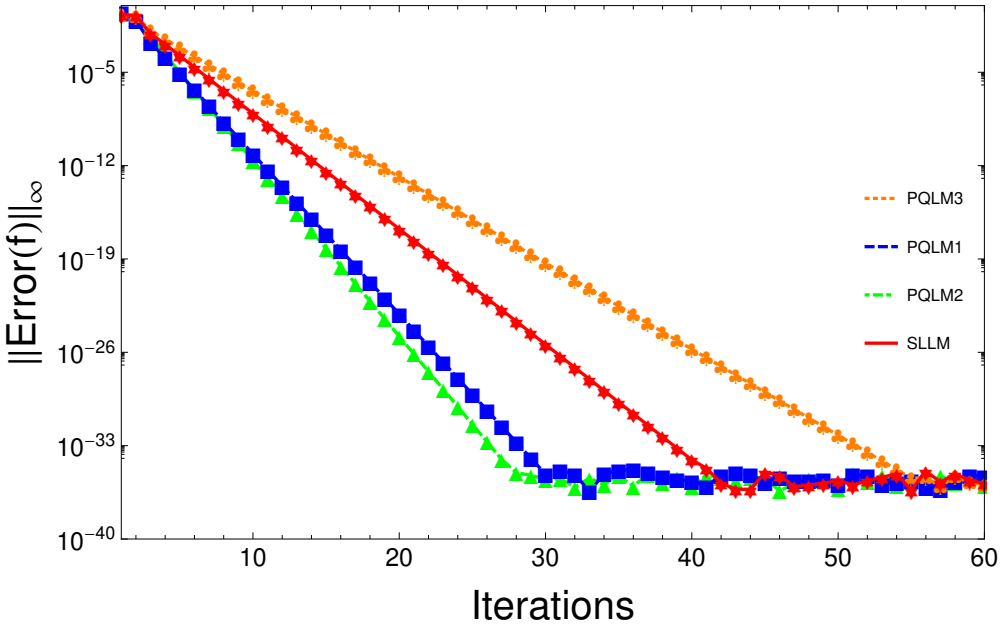

Figure 2.1: Error obtained between successive iterations in f

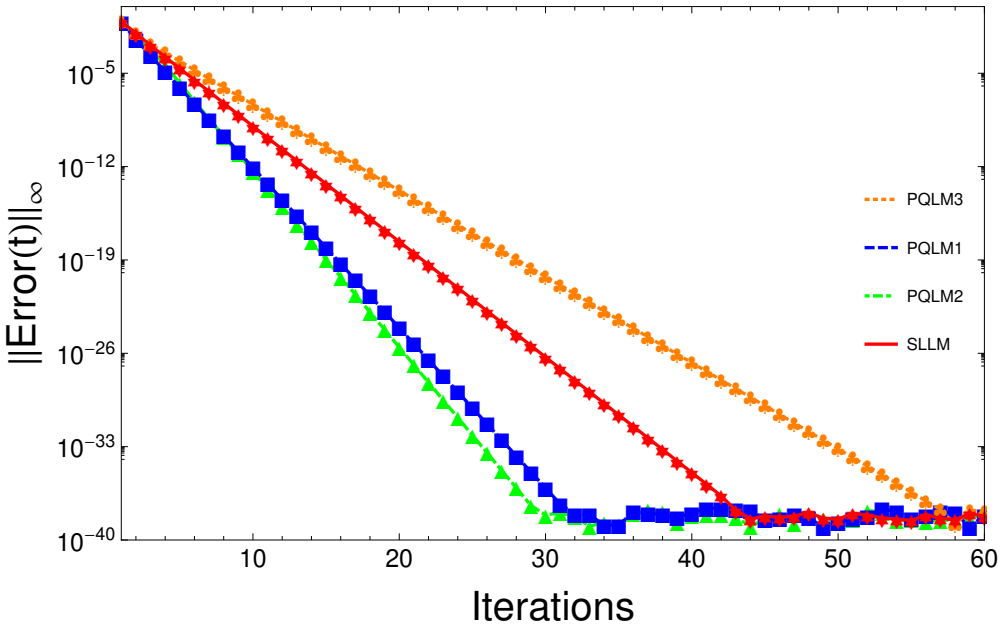

Figure 2.2: Error obtained between successive iterations in θ

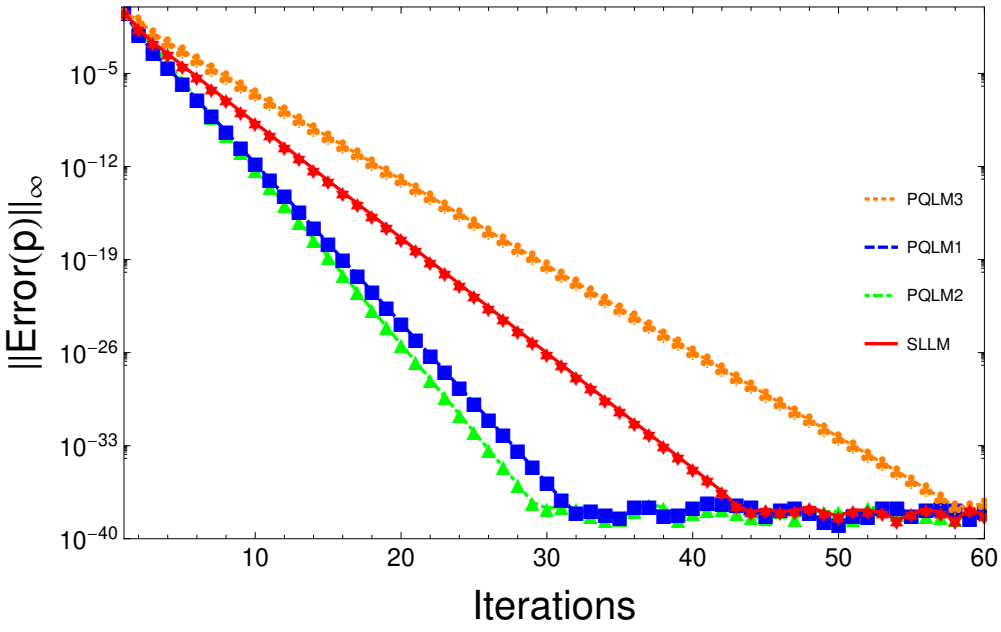

Figure 2.3: Error obtained between successive iterations in ϕ

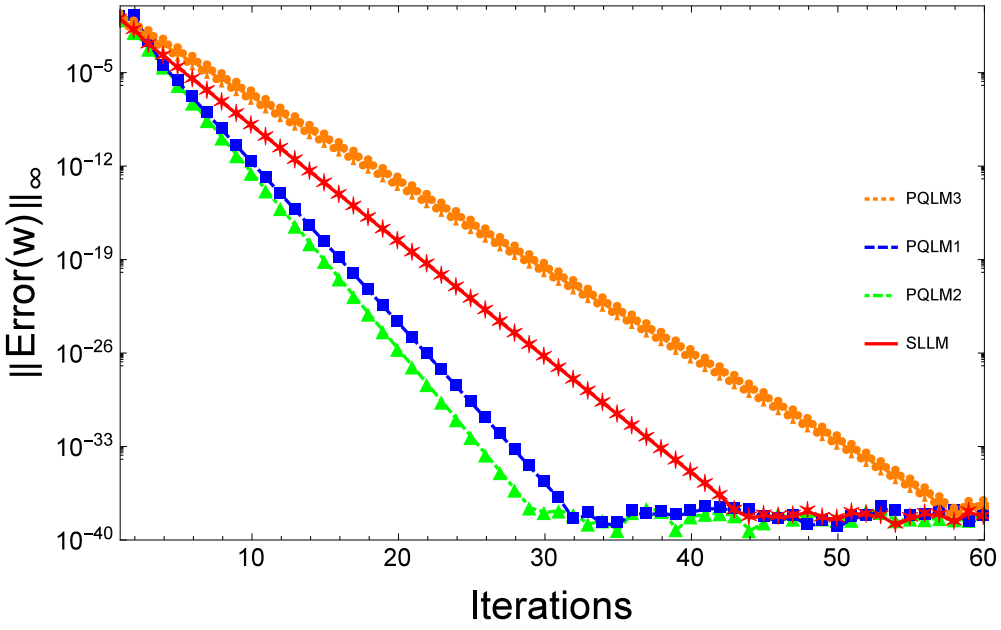

Figure 2.4: Effect of iterations on the error obtained in ω

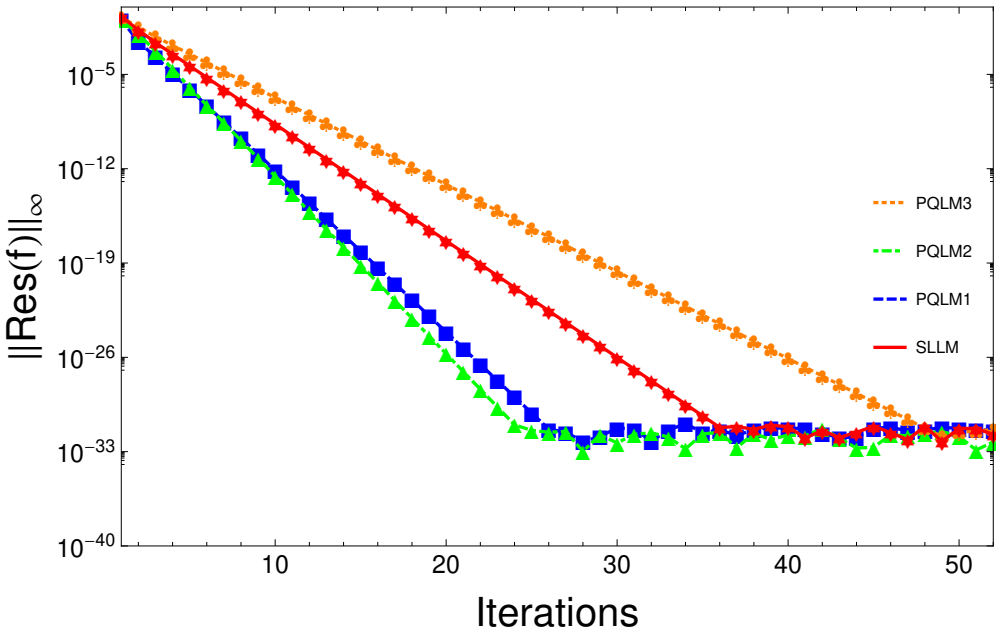

Figure 2.5: Effect of iterations on $||f||_\infty$

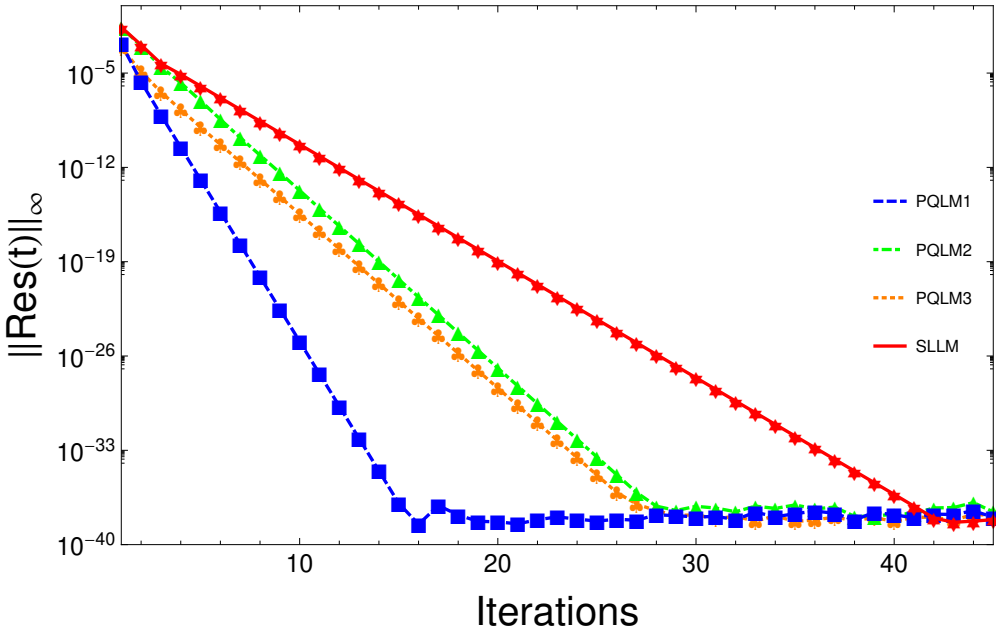

Figure 2.6: Effect of iterations on $||\theta||_\infty$

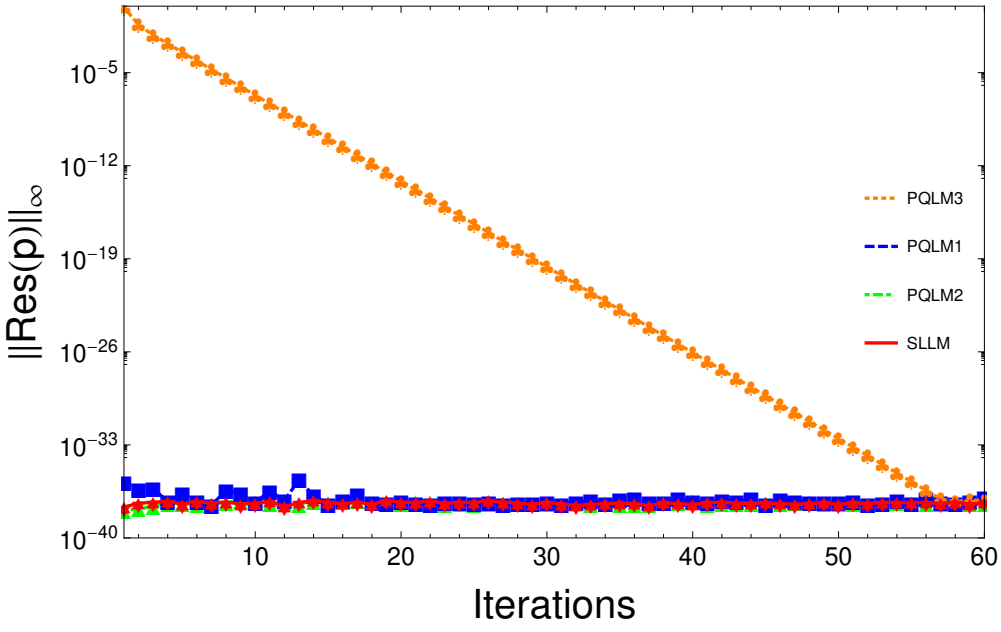

Figure 2.7: Effect of iterations on $||\phi||_\infty$

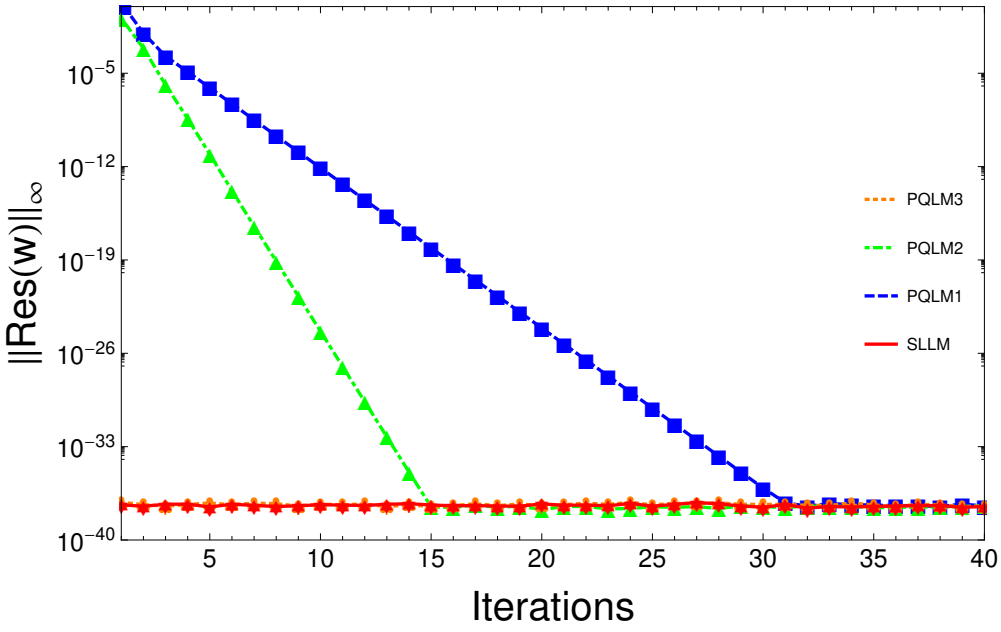

Figure 2.8: Effect of iterations on $||\omega||_\infty$

In Figures 2.1 to 2.8, it is observed that an increase in the number of iterations has a significant effect on both the error between successive iterations and the residual norm.

The first four graphs, Figures 2.1 to 2.4 display the manner in which the error after each iteration decreases until the point when the difference between successive iterations become negligible or nonexistent. As shown in Figures 2.1 to 2.4, the PQLM case 2 converges fastest after the 28^{th} iteration. As was earlier discussed, the SLLM and the PQLM cases 1, 2 and 3 all converge linearly but the steep nature of their respective slopes can also validate the observation made using their respective asymptotic error constants. From Figures 2.1 to 2.4, it can be seen that the PQLM case 2 has a slightly steeper slope than the PQLM case 1 and the PQLM case 3 has the least incline. This implies that the PQLM cases 1 and 2 both converge faster than the SLLM as was observed in Table 2.9.

The next four graphs, Figures 2.5 to 2.8 display the effect of iterations on the residual norm. It can be seen that all four methods have high accuracy levels. It is observed in Figure 2.5 that all the methods converge to an accuracy of 10^{-33}. It is also observed from Figures 2.5 and 2.6 that the

PQLM cases 1 and 2 converge much faster than the SLLM and again they all converge to the same accuracy. As shown in Figure 2.8, the accuracies of all the methods are comparable at 10^{-38}.

2.5 Summary

This study successfully introduced the paired quasilinearization method (PQLM) by using it to solve a system of ordinary differential equations in three different combinations. Results obtained from the different combinations were compared to those from the SLLM and some observations were made. It was observed that two of the PQLM cases converged quicker than the SLLM and matched the high level of accuracy of the SLLM. The PQLM cases 1 and 2 were shown to exhibit both properties of quick convergence and high accuracy in all four equations. It is important to note that both PQLM cases 1 and 2 contained more nonlinear terms than in case 3, thereby contributing to their quicker convergence, as the quasilinearization technique was employed more often in the first two cases. The computational efficiency of the PQLM was also observed. It took less than five seconds for all three cases to obtain converged solutions. It was also noted from the residual norm graphs that some of the PQLM cases had residual norms comparable to those from the SLLM, implying that the PQLM cases gave solutions as close to an exact solution as would be the case with the SLLM. The slope of the error norm graphs also gave an indication as to why the PQLM cases 1 and 2 converged faster than the SLLM as it was observed that they both showed steeper slopes than obtained with the SLLM. This study has been able to add an innovative method that improves the convergence speed of the SLLM but also maintains the high accuracy of the SLLM especially when the combination of the PQLM with the most number of nonlinearities is chosen. The strategy for choosing this combination will be to verify the number of nonlinear functions that will be attained using all possible combinations and applying quasilinearization on those pairs.

In the next chapter, the PQLM will be extended to solve a system of partial differential equations and to examine if we are able to replicate the same findings as obtained here.

Chapter 3

Paired Quasilinearization Method for solving systems of partial differential equations

3.1 Introduction

The complex nature of some highly nonlinear differential equations (Navier-Stokes equation, Maxwell's equations, Schrödinger's equation, Fourier equations, to mention a few) that model real life problems that cannot be solved analytically necessitates developing numerical strategies in an attempt to provide answers to these problems. Various numerical techniques have been introduced over the years. Numerical techniques are founded on the idea of proposing an *approximation* that approaches the limit of the true continuum solution as the number of discrete variables increases so as to overcome the inflexible nature of realistic types of continuous problems [83]. As numerical techniques are not renowned for providing exact solutions, the idea has always been to refine existing numerical techniques or develop new algorithms for the purpose of reducing errors. Numerical techniques that have been proven to be reliable include the finite element method [84], the finite volume method [85, 86], the finite difference method [87] and the spectral collocation method [13, 16, 17].

According to Ben-Yu [88], the idea of spectral methods arises from Fourier analysis. Spectral methods approximate functions using orthogonal polynomials [14] or, expressed differently, they commonly use different orthogonal systems of infinitely differentiable global functions as the trial

functions [88]. The type of spectral approximation used is highly dependent on the trial function, as is observed in the application of Hermite polynomials and sinc functions to approximate on the real line, and Laguerre polynomials to approximate on the half-line. Spectral methods are frequently known to provide highly accurate solutions, even with very few iterations [89]. To apply numerical techniques on nonlinear differential equations, linearization techniques are sometimes used to linearize the differential equations before solving them. The global properties of spectral methods also makes them easy to apply to nonlinear problems, as observed by Boyd [16] and this has led to the formulation of algorithms that have been shown to be efficient such as the spectral quasilinearization method [18, 73] and the spectral local linearization method [18, 77, 90] to mention two examples.

The spectral quasilinearization method and the spectral local linearization method were introduced by Motsa [18] for solving systems of ordinary differential equations (ODEs). The SQLM uses quasilinearization, introduced by Bellman and Kalaba [38], in linearizing a nonlinear system of ODEs, interpolating using Lagrange polynomials and collocating with Chebyshev spectral methods. Quasilinearization involves linearizing a system of equations at once thereby rendering the linearized system coupled. Motsa et al. [19] extended the applicability of the SQLM to systems of partial differential equations by introducing bivariate Lagrange interpolation polynomials both in space and time and named it the bivariate spectral quasilinearization method (BSQLM). It was ascertained that the quasilinearization based methods are computationally efficient methods as they were seen to attain accurate solutions in a short space of time. It was also observed that the methods converge to consistent solutions after very few iterations.

The SLLM, on the other hand, breaks down a coupled system of differential equations into single equations that are then solved sequentially [18]. To develop the numerical scheme for the SLLM, linearization is performed on a single function and its derivatives in a particular equation, while assuming that the other functions are known from the initial solution. The process is repeated in subsequent equations. This process is performed using the idea of the well known Gauss-Seidel relaxation method. The linearized decoupled system of equations is then solved with Chebyshev

spectral collocation methods. The ease of implementation of the SLLM was established by Motsa et al. [77] where it was shown that the method gave accurate solutions and had good convergence rates. When the SQLM and SLLM were compared by Motsa [18], he observed that the SQLM converged to consistent solutions with fewer iterations than it took the SLLM to converge to the same set of solutions. It was also noted that the SLLM needed fewer collocation points than the SQLM in generating accurate solutions. This is as a result of the smaller size of the matrices being inverted in the SLLM. The process of decoupling the system of equations in the SLLM implies that the matrices are inverted individually while the coupling process of the SQLM means the size of the matrices is dependent on the number of equations in the system. In order to mitigate the loss of accuracy due to larger number of collocation points, it is possible to decouple a large system into pairs of equations such that quasilinearization still occurs and the process of solving the equations involves smaller matrices being inverted when compared against the SQLM. This numerical method, the paired quasilinearization method (PQLM), was successfully introduced by Motsa and Animasaun [20] on a system of PDEs; their results showed that the method was very accurate and converged after few iterations. Their idea involved decoupling a system of four PDEs into coupled pairs of equations and the application of spectral collocation method both in space and time to discretize the linearized pairs. In developing the PQLM however, the focus of the Motsa and Animasaun[20] study was on the problem being solved, which required only a single case of pairing to be considered.

One of the aims of this study is to extend the study of the PQLM previously conducted in chapter 1 to systems of partial differential equations and to thoroughly examine the PQLM in terms of the effect of applying different possible combinations. We also compare the PQLM to the SLLM. To perform this comparison, solution error and residual norm analysis will be carried out. The solution error will be used to test the rate of convergence of the different combinations while the residual norm will be used to compare the respective accuracies of the numerical schemes of the different pairing combinations in the PQLM. The objective is to observe whether different combinations give different nonlinearities and if so, how the number of nonlinear terms in each combination affects both the rate of convergence and the accuracy. The SLLM is also compared against the

PQLM to observe if the PQLM converges faster than the SLLM. We begin by performing numerical experiments on two systems of 4 PDEs.

3.2 Example 1

In this section, the iteration schemes of the PQLM and SLLM for a system of partial differential equations that models an unsteady MHD flow of a micropolar fluid over a stretching sheet with heat and mass transfer are presented. This model was previously studied by Hayat and Qasim [91] using the homotopy analysis method, as introduced by Liao [2], to obtain series solutions. The equations representing the model are given as

$$(1+K)f'''+(1-\xi)\left(\frac{\eta}{2}f''-\xi\frac{\partial f'}{\partial\xi}\right)+\xi\left(ff''-\left(f'\right)^2-M^2f'\right)+Kg'=0, \tag{3.1}$$

$$\left(1+\frac{K}{2}\right)g''+(1-\xi)\left(\frac{1}{2}g+\frac{\eta}{2}g'-\xi\frac{\partial g}{\partial\xi}\right)+\xi\left(fg'-f'g-2Kg-Kf''\right)=0, \tag{3.2}$$

$$(1+N_R)\theta''+Pr(1-\xi)\left(\frac{\eta}{2}\theta'-\xi\frac{\partial\theta}{\partial\xi}\right)+Pr\xi f\theta'=0, \tag{3.3}$$

$$\phi''+Sc(1-\xi)\left(\frac{\eta}{2}\phi'-\xi\frac{\partial\phi}{\partial\xi}\right)+Sc\xi f\phi'-\gamma Sc\xi\phi=0, \tag{3.4}$$

with corresponding boundary conditions

$$\begin{aligned} &f(\xi,0)=0,\ f'(\xi,0)=\theta(\xi,0)=\phi(\xi,0)=1,\ g(\xi,0)=-m_0f''(\xi,0),\\ &f'(\xi,\infty)=g(\xi,\infty)=\theta(\xi,\infty)=\phi(\xi,\infty)=0, \end{aligned} \tag{3.5}$$

where K is the material parameter, M is the Hartman number, Pr the Prandtl number, N_R the radiation parameter, Sc the Schmidt number and γ is the chemical reaction parameter while the prime denotes differentiation with respect to η.

3.2.1 Solution Techniques

In this section, the iteration schemes of the PQLM and SLLM for the system (3.1) - (3.4) are elucidated. The pairing of equations in the system (3.1) - (3.4) is performed using different combinations.

1. PQLM Case I: ($\{f,g\}$ and $\{\theta,\phi\}$) which represents the pairings {(3.1) and (3.2)} and {(3.3) and (3.4)},

2. PQLM Case II:($\{f,\theta\}$ and $\{\phi,g\}$) which represents the pairings {(3.1) and (3.3)} and {(3.4) and (3.2)},

3. PQLM Case III: ($\{f,\phi\}$ and $\{\theta,g\}$) which represents the pairings {(3.1) and (3.4)} and {(3.3) and (3.2)},

4. Case 4: SLLM,

Spectral local linearization method (SLLM)

In this section, the SLLM scheme is presented. It is important to remember that the SLLM linearizes and decouples large systems of equations into individual equations. In that regard, let equation (3.1) be considered initially with the nonlinear terms $ff^{''}$ and $f^{'2}$. The nonlinear terms are linearized with the Taylor series expansion to first order and the following linearized decoupled equation is obtained.

$$\begin{aligned}&(1+K)f^{'''}_{r+1}+(1-\xi)\frac{\eta}{2}f^{''}_{r+1}+\xi f_r f^{''}_{r+1}+\xi f^{''}_r f_{r+1}-2\xi f^{'}_r f^{'}_{r+1}-\xi M^2 f^{'}_{r+1}\\&-\xi(1-\xi)\frac{\partial f^{'}_{r+1}}{\partial\xi}=\xi f_r f^{''}_r-\xi f^{'2}_r-Kg^{'}_r,\end{aligned} \tag{3.6}$$

where terms containing r subscripts are at the previous iteration level while terms containing subscripts $r+1$ are at the current iteration level. It can be noted from the earlier description of the SLLM that the solution of f will be known from equation (3.6) hence it will be applied at the

current iteration level in the subsequent equations and the same procedure will occur for g and θ. Equations (3.2), (3.3) and (3.4) do not contain nonlinear terms so they are expressed thus:

$$\left(1+\frac{K}{2}\right)g''_{r+1}+\frac{1}{2}(1-\xi)g_{r+1}+\frac{\eta}{2}(1-\xi)g'_{r+1}+\xi f_{r+1}g'_{r+1}-\xi f'_{r+1}g_{r+1}-2\xi K g_{r+1} \\ -\xi(1-\xi)\frac{\partial g_{r+1}}{\partial \xi}=\xi K f''_{r+1}, \tag{3.7}$$

$$(1+N_R)\,\theta''_{r+1}+Pr\frac{\eta}{2}(1-\xi)\theta'_{r+1}+Pr\xi f_{r+1}\theta'_{r+1}-Pr\xi(1-\xi)\frac{\partial \theta_{r+1}}{\partial \xi}=0, \tag{3.8}$$

$$\phi''_{r+1}+Sc\frac{\eta}{2}(1-\xi)\phi'_{r+1}+Sc\xi f_{r+1}\phi'_{r+1}-\gamma Sc\xi\phi_{r+1}-\xi(1-\xi)\frac{\partial \phi_{r+1}}{\partial \xi}=0. \tag{3.9}$$

Rewriting equations (3.6), (3.7), (3.8) and (3.9) in a compact form, we obtain

$$(a_1)\,f'''_{r+1}+[a_2]\,f''_{r+1}-[a_3]\,f'_{r+1}+[a_4]\,f_{r+1}-\xi(1-\xi)\frac{\partial f'_{r+1}}{\partial \xi} \;=\; a_5, \tag{3.10}$$

$$(b_1)\,g''_{r+1}+[b_2]\,g'_{r+1}+[b_3]\,g_{r+1}-\xi(1-\xi)\frac{\partial g_{r+1}}{\partial \xi} \;=\; b_4, \tag{3.11}$$

$$(c_1)\,\theta''_{r+1}+[c_2]\,\theta'_{r+1}-Pr\xi(1-\xi)\frac{\partial \theta_{r+1}}{\partial \xi} \;=\; 0, \tag{3.12}$$

$$\theta''_{r+1}+[e_1]\,\theta'_{r+1}-(e_2)\,\theta_{r+1}-Sc\xi(1-\xi)\frac{\partial \phi_{r+1}}{\partial \xi} \;=\; 0, \tag{3.13}$$

where terms in $(\cdots)$ and $[\cdots]$ are scalar and vector quantities, respectively, and

$$a_1=1+K,\;\; a_2=\frac{\eta}{2}(1-\xi)+f_r,\;\; a_3=2\xi f'_r+\xi M^2, \\ a_4=\xi f''_r,\; a_5=\xi f_r f''_r-\xi f'^2_r-K g'_r,\;\; b_1=1+\frac{K}{2}, \\ b_2=\frac{\eta}{2}(1-\xi)+\xi f_{r+1},\; b_3=\frac{1}{2}(1-\xi)-\xi f'_{r+1}-2\xi K,\; b_4=\xi K f''_{r+1}, \\ c_1=1+N_R,\;\; c_2=Pr\frac{\eta}{2}(1-\xi)+Pr\xi f_r,\; e_1=Sc\frac{\eta}{2}(1-\xi)+Sc\xi f_r,\;\; e_2=\gamma Sc\xi.$$

The system (3.10) $-$ (3.13) represents a linearized decoupled system of partial differential equations that can be solved using various numerical techniques. In this section the SLLM and the spectral collocation technique is used in solving the system. The Chebyshev spectral collocation

method is applied on the decoupled system (3.10) − (3.13) in the form

$$\begin{aligned}
&\left[(a_1)\,\mathbf{D}^3+[\mathbf{a}_2]\,\mathbf{D}^2-[\mathbf{a}_3]\,\mathbf{D}+[\mathbf{a}_4]\right]\mathbf{F}_{r+1,j}-\xi(1-\xi)\sum_{k=0}^{N_y-1}\mathbf{d}_{jk}\mathbf{D}\mathbf{F}_{r+1,k}=\mathbf{a}_{5,j},\\
&\left[(b_1)\,\mathbf{D}^2+[\mathbf{b}_2]\,\mathbf{D}+[\mathbf{b}_3]\right]\mathbf{G}_{r+1,j}-\xi(1-\xi)\sum_{k=0}^{N_y-1}\mathbf{d}_{jk}\mathbf{G}_{r+1,k}=\mathbf{b}_{4,j},\\
&\left[(c_1)\,\mathbf{D}^2+[\mathbf{c}_2]\,\mathbf{D}\right]\theta_{r+1,j}-Pr\xi(1-\xi)\sum_{k=0}^{N_y-1}\mathbf{d}_{jk}\theta_{r+1,k}=0,\\
&\left[\mathbf{D}^2+[\mathbf{e}_1]\,\mathbf{D}-(e_2)\,\mathbf{I}\right]\phi_{r+1,j}-Sc\xi(1-\xi)\sum_{k=0}^{N_y-1}\mathbf{d}_{jk}\phi_{r+1,k}=0,
\end{aligned}\tag{3.14}$$

where $\mathbf{D}=\frac{2}{L}D$, $[\ldots]$ denotes a diagonal matrix and $\mathbf{I}$ an identity matrix. The decoupled system of linear equations (3.14) can be expressed compactly as

$$\begin{aligned}
\mathbf{A}1\mathbf{F}_{r+1,j}&=\mathbf{R}_{1,j},\\
\mathbf{A}2\mathbf{G}_{r+1,j}&=\mathbf{R}_{2,j},\\
\mathbf{A}3\Theta_{r+1,j}&=\mathbf{R}_{3,j},\\
\mathbf{A}4\Phi_{r+1,j}&=\mathbf{R}_{4,j},
\end{aligned}\tag{3.15}$$

where the main and off-diagonal entries of $\mathbf{A}1,\ldots,\mathbf{A}4$ are given as

$$\begin{aligned}
\mathbf{A}1_{j,j}&=(a_1)\,\mathbf{D}^3+[\mathbf{a}_2]\,\mathbf{D}^2-[\mathbf{a}_3]\,\mathbf{D}+[\mathbf{a}_4]-\xi_j\left(1-\xi_j\right)\mathbf{d}_{j,j}\mathbf{D},\\
\mathbf{A}1_{j,k}&=-\xi(1-\xi)\mathbf{d}_{j,k}\mathbf{D},\\
\mathbf{A}2_{j,j}&=(b_1)\,\mathbf{D}^2+[\mathbf{b}]\,\mathbf{D}+[\mathbf{b}_3]-\xi_j\left(1-\xi_j\right)\mathbf{d}_{j,j}\mathbf{I},\\
\mathbf{A}2_{j,k}&=-\xi(1-\xi)\mathbf{d}_{j,k}\mathbf{I},\\
\mathbf{A}3_{j,j}&=(c_1)\,\mathbf{D}^2+[\mathbf{c}_2]\,\mathbf{D}-Pr\xi_j\left(1-\xi_j\right)\mathbf{d}_{j,j}\mathbf{I},\\
\mathbf{A}3_{j,k}&=-Pr\xi(1-\xi)\mathbf{d}_{j,k}\mathbf{I},\\
\mathbf{A}4_{j,j}&=\mathbf{D}^2+[\mathbf{e}_1]\,\mathbf{D}-(e_2)\,\mathbf{I}-Sc\xi_j\left(1-\xi_j\right)\mathbf{d}_{j,j}\mathbf{I},\\
\mathbf{A}4_{j,k}&=-Sc\xi(1-\xi)\mathbf{d}_{j,k}\mathbf{I},
\end{aligned}\tag{3.16}$$

and

$$\begin{aligned}
\mathbf{R}_{1,r,j} &= \xi_j\left(1-\xi_j\right)\mathbf{d}_{jN_y}\mathbf{DF}_{N_y,r}+\mathbf{a}_{5,j},\\
\mathbf{R}_{2,r,j} &= \xi_j\left(1-\xi_j\right)\mathbf{d}_{jN_y}\mathbf{G}_{N_y,r}+\mathbf{b}_{4,j},\\
\mathbf{R}_{3,r,j} &= Pr\xi_j\left(1-\xi_j\right)\mathbf{d}_{jN_y}\Theta_{N_y,r},\\
\mathbf{R}_{4,r,j} &= \xi_j\left(1-\xi_j\right)\mathbf{d}_{jN_y}\Phi_{N_y,r}.
\end{aligned} \tag{3.17}$$

PQLM Case I: ({f,g} and {θ,ϕ}) which represents the pairings {(3.1) **and** (3.2)**} and {**(3.3) **and** (3.4)**}**

In this section, the algorithm for the PQLM case I is presented. As was indicated in the previous section for the general case, the PQLM involves the application of quasilinearization on a pair of equations in the system (3.1) − (3.4) and in the process decoupling the system and also using updated solutions from the previous pair in the following pair of equations. In this first case, we linearize nonlinear terms that involves f,g and their corresponding derivatives in equations (3.1) and (3.2). Nonlinear terms identified here are $ff^{''}$, $f^{'2}$, $fg^{'}$ and $f^{'}g$. These terms are linearized using the Taylor series expansion to first order and we obtain

$$\begin{aligned}
&(a_1)\,f^{'''}_{r+1}+[a_2]\,f^{''}_{r+1}+[a_3]\,f^{'}_{r+1}+[a_4]\,f_{r+1}-\xi(1-\xi)\frac{\partial f^{'}_{r+1}}{\partial\xi}+Kg^{'}_{r+1}=a_5,\\
&(b_1)\,f^{''}_{r+1}+[b_2]\,f^{'}_{r+1}+[b_3]\,f_{r+1}+(b_4)\,g^{''}_{r+1}+[b_5]\,g^{'}_{r+1}\\
&+[b_6]\,g_{r+1}-\xi(1-\xi)\frac{\partial g_{r+1}}{\partial\xi}=b_7,
\end{aligned} \tag{3.18}$$

which represents a linear coupled pair of equations where $(\cdots)$ are scalars and $[\cdots]$ are vectors and

$$\begin{aligned}
&a_1=1+K,\;\; a_2=(1-\xi)\frac{\eta}{2}+\xi f_r,\;\; a_3=-2\xi f^{'}_r-\xi M^2,\\
&a_4=\xi f^{''}_r,\;\; a_5=\xi f_r f^{''}_r-\xi f^{'2}_r,\;\; b_1=-\xi K,\\
&b_2=-\xi g_r,\;\; b_3=\xi g^{'}_r,\;\; b_4=1+\frac{K}{2},\\
&b_5=\frac{\eta}{2}(1-\xi)+\xi f_r,\;\; b_6=\frac{1}{2}(1-\xi)-\xi\left(f^{'}_r+2K\right),\\
&b_7=\xi\left(f_r g^{'}_r-f^{'}_r g_r\right).
\end{aligned} \tag{3.19}$$

Applying quasilinearization on f and g in equations (3.1) and (3.2) has effectively decoupled the full system of equations (3.1) $-$ (3.4) into two pairs of equations. It can be observed that equations (3.3) and (3.4) are both linear and can thus be written as

$$\begin{aligned}(c_1)\,\theta''_{r+1}+[c_2]\,\theta'_{r+1}-Pr\xi(1-\xi)\frac{\partial\theta_{r+1}}{\partial\xi}=0,\\ \phi''_{r+1}+[e_1]\,\phi'_{r+1}-(e_2)\,\phi_{r+1}-Sc\xi(1-\xi)\frac{\partial\phi_{r+1}}{\partial\xi}=0,\end{aligned} \tag{3.20}$$

where

$$\begin{aligned}c_1=1+N_R,\;\; c_2=Pr(1-\xi)\frac{\eta}{2}+Pr\xi f_{r+1},\\ e_1=Sc(1-\xi)\frac{\eta}{2}+Sc\xi f_{r+1},\;\; e_2=\gamma Sc\xi.\end{aligned} \tag{3.21}$$

The Chebyshev spectral collocation method is applied as described in the previous section on the decoupled system of linear pairs (3.18) and (3.20) in the forms

$$\begin{aligned}&\left[(a_1)\,\mathbf{D}^3+[a_2]\,\mathbf{D}^2+[a_3]\,\mathbf{D}+[a_4]\right]\mathbf{F}_{r+1,i}\\ &-\xi_i(1-\xi_i)\sum_{j=0}^{N_y-1}\mathbf{d}_{ij}\mathbf{D}\mathbf{F}_{r+1,j}+[K\mathbf{D}]\,\mathbf{G}_{r+1,i}=\mathbf{R}_{1,r,i},\\ &\left[(b_1)\,\mathbf{D}^2+[b_2]\,\mathbf{D}+[b_3]\right]\mathbf{F}_{r+1}+\left[(b_4)\,\mathbf{D}^2+[b_5]\,\mathbf{D}+[b_6]\right]\mathbf{G}_{r+1}\\ &-\xi_i(1-\xi_i)\sum_{j=0}^{N_y-1}\mathbf{d}_{ij}\mathbf{I}\mathbf{G}_{r+1,j}=\mathbf{R}_{2,r,i},\end{aligned} \tag{3.22}$$

and

$$\begin{aligned}&\left[(c_1)\,\mathbf{D}^2+[c_2]\,\mathbf{D}\right]\Theta_{r+1}-Pr\xi_i(1-\xi_i)\sum_{j=0}^{N_y-1}\mathbf{d}_{ij}\mathbf{I}\Theta_{r+1,j}=\mathbf{R}_{3,r,i}\\ &\left[\mathbf{D}^2+[e_1]\,\mathbf{D}-(e_2)\right]\Phi_{r+1}-Sc\xi_i(1-\xi_i)\sum_{j=0}^{N_y-1}\mathbf{d}_{ij}\mathbf{I}\Phi_{r+1,j}=\mathbf{R}_{4,r,i},\end{aligned} \tag{3.23}$$

where

$$\begin{aligned}\mathbf{R}_{1,r,j}&=\xi(1-\xi)\mathbf{d}_{jN_y}\mathbf{D}\mathbf{F}_{N_y,r}+a_5,\\ \mathbf{R}_{2,r,j}&=\xi(1-\xi)\mathbf{d}_{jN_y}\mathbf{G}_{N_y,r}+b_7,\\ \mathbf{R}_{3,r,j}&=Pr\xi(1-\xi)\mathbf{d}_{jN_y}\Theta_{N_y,r},\\ \mathbf{R}_{4,r,j}&=Sc\xi(1-\xi)\mathbf{d}_{jN_y}\Phi_{N_y,r}.\end{aligned} \tag{3.24}$$

The decoupled pairs (3.22) and (3.23) can be expressed in matrix form as

$$\begin{bmatrix} A_{1,1}\{j,j\} & A_{1,2}\{j,j\} \\ A_{2,1}\{j,j\} & A_{2,2}\{j,j\} \end{bmatrix} \times \begin{bmatrix} \mathbf{F}_{r+1,j} \\ \mathbf{G}_{r+1,j} \end{bmatrix} = \begin{bmatrix} \mathbf{R}_{1,r,j} \\ \mathbf{R}_{2,r,j} \end{bmatrix}, \tag{3.25}$$

and

$$\begin{bmatrix} B_{1,1}\{j,j\} & B_{1,2}\{j,j\} \\ B_{2,1}\{j,j\} & B_{2,2}\{j,j\} \end{bmatrix} \times \begin{bmatrix} \Theta_{r+1,j} \\ \Phi_{r+1,j} \end{bmatrix} = \begin{bmatrix} \mathbf{R}_{3,r,j} \\ \mathbf{R}_{4,r,j} \end{bmatrix}, \tag{3.26}$$

where

$$\begin{aligned}
A_{1,1}\{j,j\} &= (a_1)\,\mathbf{D}^3+[a_2]\,\mathbf{D}^2+[a_3]\,\mathbf{D}+[a_4]-\xi_j(1-\xi_j)\mathbf{d}_{jj}\mathbf{D}, \\
A_{1,2}\{j,j\} &= K\mathbf{D}, \\
A_{2,1}\{j,j\} &= (b_1)\,\mathbf{D}^2+[b_2]\,\mathbf{D}+[b_3]\,, \\
A_{2,2}\{j,j\} &= (b_4)\,\mathbf{D}^2+[b_5]\,\mathbf{D}+[b_6]-\xi_j(1-\xi_j)\mathbf{d}_{jj}\mathbf{I}, \\
B_{1,1}\{j,j\} &= (c_1)\,\mathbf{D}^2+[c_2]\,\mathbf{D}-Pr\xi_j(1-\xi_j)\mathbf{d}_{jj}\mathbf{I}, \\
B_{1,2}\{j,j\} &= 0,\;\; B_{2,1}\{j,j\} = 0, \\
B_{2,2}\{j,j\} &= \mathbf{D}^2+[e_1]\,\mathbf{D}-(e_2)-Sc\xi_j(1-\xi_j)\mathbf{d}_{jj}\mathbf{I},
\end{aligned} \tag{3.27}$$

with off-diagonal entries

$$\begin{aligned}
A_{1,1}\{j,k\} &= -\xi_k\,(1-\xi_k)\,\mathbf{d}_{jk}\mathbf{D}, \\
A_{2,2}\{j,k\} &= -\xi_k\,(1-\xi_k)\,\mathbf{d}_{jk}\mathbf{I}, \\
B_{1,1}\{j,k\} &= -Pr\xi_k\,(1-\xi_k)\,\mathbf{d}_{jk}\mathbf{I}, \\
B_{2,2}\{j,k\} &= -Sc\xi_k\,(1-\xi_k)\,\mathbf{d}_{jk}\mathbf{I},
\end{aligned} \tag{3.28}$$

where $\mathbf{I}$ is an $(N_x+1)\times(N_x+1)$ identity matrix.

PQLM Case II: ({f,θ} and {g,ϕ}) which represents the pairings {(3.1) **and** (3.3)**} and {**(3.2) **and** (3.4)**}**

The PQLM case II iterative scheme is presented in this section. In contrast to the first case, non-linear terms that involve f,θ and their corresponding derivatives in equations (3.1) and (3.3) are

linearized. The nonlinear terms in both equations are $ff^{''}$, $f^{'2}$ and $f\theta^{'}$ and they are linearized with the use of Taylor series expansion to first order and we obtain

$$\begin{aligned}
&(a_1)\, f^{'''}_{r+1}+[a_2]\, f^{''}_{r+1}+[a_3]\, f^{'}_{r+1}+[a_4]\, f_{r+1}-\xi(1-\xi)\frac{\partial f^{'}_{r+1}}{\partial \xi}=a_5,\\
&[b_1]\, f_{r+1}+(b_2)\,\theta^{''}_{r+1}+[b_3]\,\theta^{'}_{r+1}-Pr\xi(1-\xi)\frac{\partial \theta_{r+1}}{\partial \xi}=b_4,
\end{aligned} \tag{3.29}$$

where

$$\begin{aligned}
&a_1=1+K,\;\; a_2=(1-\xi)\frac{\eta}{2}+\xi f_r,\;\; a_3=-2\xi f^{'}_r-\xi M^2,\\
&a_4=\xi f^{''}_r,\;\; a_5=\xi f_r f^{''}_r-\xi f^{'2}_r-Kg^{'}_r,\;\; b_1=Pr\xi\theta^{'}_r,\\
&b_2=1+\frac{K}{2},\;\; b_3=Pr\left((1-\xi)\frac{\eta}{2}+\xi f_r\right),\;\; b_4=Pr\xi f_r\theta^{'}_r.
\end{aligned} \tag{3.30}$$

The pair (3.29) represents a linear coupled pair of equations where $(\ldots)$ are scalars and $[\ldots]$ are vectors. The second pair of equations (3.2) and (3.4) are linear and can be expressed as

$$\begin{aligned}
&(c_1)\, g^{''}_{r+1}+[c_2]\, g^{'}_{r+1}+[c_3]\, g_{r+1}-\xi(1-\xi)\frac{\partial g_{r+1}}{\partial \xi}=c_4,\\
&\phi^{''}_{r+1}+[e_1]\,\phi^{'}_{r+1}-(e_2)\,\phi_{r+1}-Sc\xi(1-\xi)\frac{\partial \phi_{r+1}}{\partial \xi}=0,
\end{aligned} \tag{3.31}$$

where

$$\begin{aligned}
&c_1=1+\frac{K}{2},\;\; c_2=(1-\xi)\frac{\eta}{2}+\xi f_r,\;\; c_3=(1-\xi)\frac{1}{2}-\xi f^{'}_r-2\xi K,\\
&c_4=\xi K f^{''}_r,\;\; e_1=Sc\left((1-\xi)\frac{\eta}{2}+\xi f_r\right),\;\; e_2=\gamma Sc\xi.
\end{aligned} \tag{3.32}$$

We apply the Chebyshev spectral collocation technique to the decoupled linearized pairs (3.29) and (3.31) in the form

$$\begin{aligned}
&\left[(a_1)\,\mathbf{D}^3+[\mathbf{a}_2]\,\mathbf{D}^2+[\mathbf{a}_3]\,\mathbf{D}+[\mathbf{a}_4]\right]\mathbf{F}_{r+1,j}\\
&-\xi_j\left(1-\xi_j\right)\sum_{k=0}^{N_y-1}\mathbf{d}_{jk}\mathbf{D}\mathbf{F}_{r+1,k}=\mathbf{R}_{1,r,j},\\
&[[\mathbf{b}_1]]\,\mathbf{F}_{r+1,j}+\left[(b_1)\,\mathbf{D}^2+[\mathbf{b}_3]\,\mathbf{D}\right]\Theta_{r+1,j}-\\
&Pr\xi_j\left(1-\xi_j\right)\sum_{k=0}^{N_y-1}\mathbf{d}_{jk}\Theta_{r+1,k}=\mathbf{R}_{2,r,j},
\end{aligned} \tag{3.33}$$

$$
\begin{aligned}
&\left[(c_1)\,\mathbf{D}^2+[\mathbf{c}_2]\,\mathbf{D}+[\mathbf{c}_3]\right]\mathbf{G}_{r+1,j}-\\
&\xi_j\left(1-\xi_j\right)\sum_{k=0}^{N_y-1}\mathbf{d}_{jk}\mathbf{G}_{r+1,k}=\mathbf{R}_{3,r,j},\\
&\left[\mathbf{D}^2+[\mathbf{e}_1]\,\mathbf{D}+(e_2)\,\mathbf{I}\right]\Phi_{r+1,j}-\\
&Sc\xi_j\left(1-\xi_j\right)\sum_{k=0}^{N_y-1}\mathbf{d}_{jk}\Phi_{r+1,k}=\mathbf{R}_{4,r,j},
\end{aligned}
\tag{3.34}
$$

where

$$
\begin{aligned}
&\mathbf{R}_{1,r,j}=\xi_j\left(1-\xi_j\right)\mathbf{d}_{jN_y}\mathbf{D}\mathbf{F}_{N_y,r}+\mathbf{a}_5,\\
&\mathbf{R}_{2,r,j}=Pr\xi_j\left(1-\xi_j\right)\mathbf{d}_{jN_y}\Theta_{N_y,r}+\mathbf{b}_4,\\
&\mathbf{R}_{3,r,j}=\xi_j\left(1-\xi_j\right)\mathbf{d}_{jN_y}\mathbf{G}_{N_y,r}+\mathbf{c}_4,\\
&\mathbf{R}_{4,r,j}=Sc\xi_j\left(1-\xi_j\right)\mathbf{d}_{jN_y}\Phi_{N_y,r}.
\end{aligned}
\tag{3.35}
$$

PQLM Case III: ({f,ϕ} and {g,θ}) which represents the pairings {(3.1) **and** (3.4)**} and {**(3.2) **and** (3.3)**}**

In this section, the PQLM numerical scheme for case III is presented. The first pair is selected such that nonlinear terms $ff^{''}$, $f^{'2}$ and $f\theta^{'}$ in equations (3.1) and (3.4) are linearized and we obtain

$$
\begin{aligned}
&(a_1)\,f_{r+1}^{'''}+[a_2]\,f_{r+1}^{''}+[a_3]\,f_{r+1}^{'}+[a_4]\,f_{r+1}-\xi(1-\xi)\frac{\partial f_{r+1}^{'}}{\partial\xi}=a_5,\\
&[b_1]\,f_{r+1}+\phi_{r+1}^{''}+[b_2]\,\phi_{r+1}^{'}\,(b_3)\,\phi_{r+1}-Sc\xi(1-\xi)\frac{\partial\phi_{r+1}}{\partial\xi}=b_4,
\end{aligned}
\tag{3.36}
$$

where

$$
\begin{aligned}
&a_1=1+K,\;\; a_2=(1-\xi)\frac{\eta}{2}+\xi f_r,\;\; a_3=-2\xi f_r^{'}-\xi M^2,\\
&a_4=\xi f_r^{''},\;\; a_5=\xi f_r f_r^{''}-\xi f_r^{'2}-Kg_r^{'},\;\; b_1=Sc\xi\phi_r^{'},\\
&b_2=Sc\left((1-\xi)\frac{\eta}{2}+\xi f_r\right),\;\; b_3=-\gamma Sc\xi,\;\; b_4=Sc\xi f_r\phi_r^{'}.
\end{aligned}
\tag{3.37}
$$

The pair given by (3.36) represents a linear coupled pair of equations where terms contained in $(\cdots)$ and $[\cdots]$ are, respectively, scalars and vectors. The second pair of equations (3.2) and (3.3)

are linear and can be expressed as

$$
\begin{aligned}
&(c_1)\, g''_{r+1} + [c_2]\, g'_{r+1} + [c_3]\, g_{r+1} - \xi(1-\xi)\frac{\partial g_{r+1}}{\partial \xi} = c_4, \\
&(e_1)\, \theta''_{r+1} + [e_2]\, \theta'_{r+1} - Pr\xi(1-\xi)\frac{\partial \theta_{r+1}}{\partial \xi} = 0,
\end{aligned}
\tag{3.38}
$$

where

$$
\begin{aligned}
&c_1 = 1+\frac{K}{2},\ \ c_2 = (1-\xi)\frac{\eta}{2}+\xi f_r,\ \ c_3 = (1-\xi)\frac{1}{2}-\xi f'_r-2\xi K, \\
&c_4 = \xi K f''_r,\ \ e_1 = 1+N_R,\ \ e_2 = Pr\left(\frac{\eta}{2}(1-\xi)+\xi f_r\right).
\end{aligned}
\tag{3.39}
$$

The Chebyshev spectral collocation method is applied to solve the decoupled linearized pairs (3.36) and (3.38) in the form

$$
\begin{aligned}
&\left[(a_1)\mathbf{D}^3+[\mathbf{a}_2]\mathbf{D}^2+[\mathbf{a}_3]\mathbf{D}+[\mathbf{a}_4]\right]\mathbf{F}_{r+1,j} \\
&-\xi_j\left(1-\xi_j\right)\sum_{k=0}^{N_y-1}\mathbf{d}_{jk}\mathbf{D}\mathbf{F}_{r+1,k} = \mathbf{R}_{1,r,j}, \\
&[\mathbf{b}_1]\mathbf{F}_{r+1,j}+\left[\mathbf{D}^2+[\mathbf{b}_2]\mathbf{D}+(b_3)\mathbf{I}\right]\Phi_{r+1,j}- \\
&Sc\xi_j\left(1-\xi_j\right)\sum_{k=0}^{N_y-1}\mathbf{d}_{jk}\Phi_{r+1,k} = \mathbf{R}_{2,r,j},
\end{aligned}
\tag{3.40}
$$

$$
\begin{aligned}
&\left[(c_1)\mathbf{D}^2+[\mathbf{c}_2]\mathbf{D}+[\mathbf{c}_3]\right]\mathbf{G}_{r+1,j} \\
&-\xi_j\left(1-\xi_j\right)\sum_{k=0}^{N_y-1}\mathbf{d}_{jk}\mathbf{G}_{r+1,k} = \mathbf{R}_{3,r,j}, \\
&\left[(e_1)\mathbf{D}^2+[\mathbf{e}_2]\mathbf{D}\right]\Theta_{r+1,j}- \\
&Pr\xi_j\left(1-\xi_j\right)\sum_{k=0}^{N_y-1}\mathbf{d}_{jk}\Theta_{r+1,k} = \mathbf{R}_{4,r,j},
\end{aligned}
\tag{3.41}
$$

where

$$
\begin{aligned}
&\mathbf{R}_{1,r,j} = \xi_j\left(1-\xi_j\right)\mathbf{d}_{jN_y}\mathbf{D}\mathbf{F}_{N_y,r}+\mathbf{a}_5, \\
&\mathbf{R}_{2,r,j} = Sc\xi_j\left(1-\xi_j\right)\mathbf{d}_{jN_y}\Phi_{N_y,r}+\mathbf{b}_4, \\
&\mathbf{R}_{3,r,j} = \xi_j\left(1-\xi_j\right)\mathbf{d}_{jN_y}\mathbf{G}_{N_y,r}+\mathbf{c}_4, \\
&\mathbf{R}_{4,r,j} = Pr\xi_j\left(1-\xi_j\right)\mathbf{d}_{jN_y}\Theta_{N_y,r}.
\end{aligned}
\tag{3.42}
$$

3.3 Example 2

In this section, the PQLM and SLLM iteration schemes are presented for the system of partial differential equations that model an unsteady three-dimensional boundary layer flow due to a stretching surface in a viscous and incompressible micropolar fluid, as previously solved by Ahmad et al. [92] using the Keller-box method. The equations are

$$(1+K)f''' + \frac{\eta}{2}(1-\xi)f'' + \xi(f+g)f'' - \xi f'^2 + K\theta' = \xi(1-\xi)\frac{\partial f'}{\partial \xi}, \tag{3.43}$$

$$(1+K)g''' + \frac{\eta}{2}(1-\xi)g'' + \xi(f+g)g'' - \xi g'^2 - K\phi' = \xi(1-\xi)\frac{\partial g'}{\partial \xi}, \tag{3.44}$$

$$\begin{aligned}\left(1+\frac{K}{2}\right)\theta'' + \frac{\eta}{2}(1-\xi)\theta' + \frac{1}{2}(1-\xi)\theta + \xi(f+g)\theta' \\ -\xi f'\theta - 2\xi K\theta - \xi K f'' = \xi(1-\xi)\frac{\partial \theta}{\partial \xi},\end{aligned} \tag{3.45}$$

$$\begin{aligned}\left(1+\frac{K}{2}\right)\phi'' + \frac{\eta}{2}(1-\xi)\phi' + \frac{1}{2}(1-\xi)\phi + \xi(f+g)\phi' \\ -\xi g'\phi - 2\xi K\phi + \xi K g'' = \xi(1-\xi)\frac{\partial \phi}{\partial \xi},\end{aligned} \tag{3.46}$$

with corresponding boundary conditions

$$\begin{aligned}&f(\xi,0) = g(\xi,0) = 0,\ f'(\xi,\infty) = g'(\xi,\infty) = \theta(\xi,\infty) = \phi(\xi,\infty) = 0,\\ &f'(\xi,0) = 1,\ g'(\xi,0) = c,\ \theta(\xi,0) = -nf''(\xi,0),\ \phi(\xi,\infty) = ng''(\xi,0),\end{aligned} \tag{3.47}$$

where K is the material parameter and prime ($'$) denotes differentiation with respect to η.

3.3.1 Solution Techniques

The PQLM and SLLM numerical schemes for the system (3.43) - (3.46) are displayed in this section.

The given pairing of equations in the system (3.43) - (3.46) is performed using different combinations.

1. PQLM Case 1: ($\{f,g\}$ and $\{\theta,\phi\}$) which represents the pairings {(3.43) and (3.44)} and {(3.45) and (3.46)},

2. PQLM Case 2:($\{f,\theta\}$ and $\{\phi,g\}$) which represents the pairings {(3.43) and (3.45)} and {(3.46) and (3.44)},

3. PQLM Case 3: ($\{f,\phi\}$ and $\{\theta,g\}$) which represents the pairings {(3.43) and (3.46)} and {(3.45) and (3.44)},

4. SLLM,

Spectral local linearization method (SLLM)

Following the description of the SLLM in Chapter 1, the discretized decoupled system of linearized equations is of the form;

$$\begin{aligned}
\mathbf{A}1\mathbf{F}_{r+1} &= \mathbf{R}_1,\\
\mathbf{A}2\mathbf{G}_{r+1} &= \mathbf{R}_2,\\
\mathbf{A}3\Theta_{r+1} &= \mathbf{R}_3,\\
\mathbf{A}4\Phi_{r+1} &= \mathbf{R}_4,
\end{aligned} \tag{3.48}$$

where the main and off-diagonal entries of $\mathbf{A}1, \mathbf{A}2,\ \mathbf{A}3$ and $\mathbf{A}4$ are defined as

$$\begin{aligned}
\mathbf{A}1_{j,j} &= (1+K)\mathbf{D}^3+\mathbf{diag}\,[\mathbf{a}_1]\,\mathbf{D}^2+\mathbf{diag}\,[\mathbf{a}_2]\,\mathbf{D}+\mathbf{diag}\,[\mathbf{a}_3]-\xi(1-\xi)\mathbf{d}_{j,j}\mathbf{D}, \quad \text{when } j=k,\\
\mathbf{A}1_{j,k} &= -\xi(1-\xi)\mathbf{d}_{j,k}\mathbf{D}, \quad \text{when } j\neq k,\\
\mathbf{A}2_{j,j} &= (1+K)\mathbf{D}^3+\mathbf{diag}\,[\mathbf{b}_1]\,\mathbf{D}^2+\mathbf{diag}\,[\mathbf{b}_2]\,\mathbf{D}+\mathbf{diag}\,[\mathbf{b}_3]-\xi(1-\xi)\mathbf{d}_{j,j}\mathbf{D}, \quad \text{when } j=k,\\
\mathbf{A}2_{j,k} &= -\xi 2(1-\xi)\mathbf{d}_{j,k}\mathbf{D}, \quad \text{when } j\neq k,\\
\mathbf{A}3_{j,j} &= \left(1+\frac{K}{2}\right)\mathbf{D}^2+\mathbf{diag}\,[\mathbf{c}_1]\,\mathbf{D}+[\mathbf{c}_2]-\xi(1-\xi)\mathbf{d}_{j,j}\mathbf{I}, \quad \text{when } j=k,\\
\mathbf{A}3_{j,k} &= -\xi(1-\xi)\mathbf{d}_{j,k}\mathbf{I}, \quad \text{when } j\neq k,\\
\mathbf{A}4_{j,j} &= \left(1+\frac{K}{2}\right)\mathbf{D}^2+\mathbf{diag}\,[\mathbf{e}_1]\,\mathbf{D}+[\mathbf{e}_2]-\xi(1-\xi)\mathbf{d}_{j,j}\mathbf{I}, \quad \text{when } j=k,\\
\mathbf{A}4_{j,k} &= -\xi(1-\xi)\mathbf{d}_{j,k}\mathbf{I}, \quad \text{when } j\neq k,
\end{aligned} \tag{3.49}$$

and

$$
\begin{aligned}
&\mathbf{R}_1 = \xi(1-\xi)\mathbf{d}_1(j,N_t+1)\,\mathbf{DF}+\mathbf{a}_4,\\
&\mathbf{R}_2 = \xi(1-\xi)\mathbf{d}_1(j,N_t+1)\,\mathbf{DG}+\mathbf{b}_4,\\
&\mathbf{R}_3 = \xi(1-\xi)\mathbf{d}_1(j,N_t+1)\,\Theta+\mathbf{c}_3,\\
&\mathbf{R}_4 = \xi(1-\xi)\mathbf{d}_1(j,N_t+1)\,\Phi+\mathbf{e}_3,\\
&\mathbf{a}_1 = \frac{\eta}{2}(1-\xi)+\xi(\mathbf{f}_r+\mathbf{g}_r),\ \ \mathbf{a}_2 = -2\xi\mathbf{f}_r^{'},\\
&\mathbf{a}_3 = \xi\mathbf{f}_r^{''},\ \ \mathbf{a}_4 = \xi\mathbf{f}_r\mathbf{f}_r^{''}-\xi\mathbf{f}_r^{'2}-K\theta_r^{'},\\
&\mathbf{b}_1 = \frac{\eta}{2}(1-\xi)+\xi(\mathbf{f}_{r+1}+\mathbf{g}_r),\ \ \mathbf{b}_2 = -2\xi\mathbf{g}_r^{'},\\
&\mathbf{b}_3 = \xi\mathbf{g}_r^{''},\ \ \mathbf{b}_4 = \xi\mathbf{g}_r\mathbf{g}_r^{''}-\xi\mathbf{g}_r^{'2}+K\phi_r^{'},\\
&\mathbf{c}_1 = \frac{\eta}{2}(1-\xi)+\xi(\mathbf{f}_{r+1}+\mathbf{g}_{r+1}),\ \ \mathbf{c}_2 = \frac{1}{2}(1-\xi)-\xi\left(\mathbf{f}_{r+1}^{'}+2K\right),\ \ \mathbf{c}_3 = \xi K\mathbf{f}_{r+1}^{''},\\
&\mathbf{e}_1 = \frac{\eta}{2}(1-\xi)+\xi(\mathbf{f}_{r+1}+\mathbf{g}_{r+1}),\ \ \mathbf{e}_2 = \frac{1}{2}(1-\xi)-\xi\left(\mathbf{g}_{r+1}^{'}+2K\right),\ \ \mathbf{e}_3 = -\xi K\mathbf{g}_{r+1}^{''}.
\end{aligned}
\tag{3.50}
$$

PQLM Case I: ({f,g} and {θ,ϕ}) which represents the pairings {(3.43) **and** (3.44)**} and {**(3.45) **and** (3.46)**}**

The PQLM, as described in Chapter 1, is applied to the nonlinear system (3.43) − (3.46) and we obtain the discretized decoupled system of linear pairs

$$
\begin{aligned}
\mathbf{A}11\mathbf{F}_{r+1}+\mathbf{A}12\mathbf{G}_{r+1} &= \mathbf{R}_1,\\
\mathbf{A}21\mathbf{F}_{r+1}+\mathbf{A}22\mathbf{G}_{r+1} &= \mathbf{R}_2,
\end{aligned}
\tag{3.51}
$$

and

$$
\begin{aligned}
\mathbf{A}31\Theta_{r+1}+\mathbf{A}32\Phi_{r+1} &= \mathbf{R}_3,\\
\mathbf{A}41\Theta_{r+1}+\mathbf{A}42\Phi_{r+1} &= \mathbf{R}_4,
\end{aligned}
\tag{3.52}
$$

where

$$
\begin{aligned}
&\mathbf{A}11_{j,j} = (1+K)\mathbf{D}^3 + \mathbf{diag}\left[\mathbf{a}_1\right]\mathbf{D}^2 + \mathbf{diag}\left[\mathbf{a}_2\right]\mathbf{D} + \mathbf{diag}\left[\mathbf{a}_3\right] - \xi(1-\xi)\mathbf{d}_{j,j}\mathbf{D},\\
&\mathbf{A}11_{j,k} = -\xi(1-\xi)\mathbf{d}_{j,k}\mathbf{D},\\
&\mathbf{A}12_{j,j} = \mathbf{diag}\left[\mathbf{a}_4\right],\ \ \mathbf{A}_{21} = \mathbf{diag}\left[\mathbf{b}_1\right],\\
&\mathbf{A}22_{j,j} = (1+K)\mathbf{D}^3 + \mathbf{diag}\left[\mathbf{b}_2\right]\mathbf{D}^2 + \mathbf{diag}\left[\mathbf{b}_3\right]\mathbf{D} + \mathbf{diag}\left[\mathbf{b}_4\right] - \xi(1-\xi)\mathbf{d}_{j,j}\mathbf{D},\\
&\mathbf{A}22_{j,k} = -\xi(1-\xi)\mathbf{d}_{j,k}\mathbf{I},\\
&\mathbf{A}31_{j,j} = \left(1+\frac{K}{2}\right)\mathbf{D}^2 + \mathbf{diag}\left[\mathbf{c}_1\right]\mathbf{D} + \mathbf{diag}\left[\mathbf{c}_2\right] - \xi(1-\xi)\mathbf{d}_{j,j}\mathbf{I},\\
&\mathbf{A}31_{j,k} = -\xi(1-\xi)\mathbf{d}_{j,k}\mathbf{I},\ \ \mathbf{A}32_{j,j} = \mathbf{A}41_{j,j} = 0,\\
&\mathbf{A}42_{j,j} = \left(1+\frac{K}{2}\right)\mathbf{D}^2 + \mathbf{diag}\left[\mathbf{e}_1\right]\mathbf{D} + \mathbf{diag}\left[\mathbf{e}_2\right] - \xi(1-\xi)\mathbf{d}_{j,j}\mathbf{I},\\
&\mathbf{A}42_{j,k} = -\xi(1-\xi)\mathbf{d}_{j,k}\mathbf{I},
\end{aligned}
\tag{3.53}
$$

and

$$
\begin{aligned}
&\mathbf{R}_1 = \xi(1-\xi)\mathbf{d}_1\left(j, N_t+1\right)\mathbf{DF} + \mathbf{a}_5,\\
&\mathbf{R}_2 = \xi(1-\xi)\mathbf{d}_1\left(j, N_t+1\right)\mathbf{DG} + \mathbf{b}_5,\\
&\mathbf{R}_3 = \xi(1-\xi)\mathbf{d}_1\left(j, N_t+1\right)\Theta + \mathbf{c}_3,\\
&\mathbf{R}_4 = \xi(1-\xi)\mathbf{d}_1\left(j, N_t+1\right)\Phi + \mathbf{e}_3,\\
&\mathbf{a}_1 = \xi\left(\mathbf{f}_r + \mathbf{g}_r\right) + \frac{\eta}{2}(1-\xi),\ \ \mathbf{a}_2 = -2\xi\mathbf{f}_r^{'},\\
&\mathbf{a}_3 = \xi\mathbf{f}_r^{''},\ \ \mathbf{a}_4 = \xi\mathbf{f}_r^{''},\\
&\mathbf{a}_5 = \xi\left(\mathbf{f}_r + \mathbf{g}_r\right)\mathbf{f}_r^{''} - \xi\mathbf{f}_r^{'2} - K\theta_r^{'},\\
&\mathbf{b}_2 = \xi\left(\mathbf{f}_r + \mathbf{g}_r\right) + \frac{\eta}{2}(1-\xi),\ \ \mathbf{b}_2 = -2\xi\mathbf{g}_r^{'},\\
&\mathbf{b}_1 = \xi\mathbf{g}_r^{''},\ \ \mathbf{b}_4 = \xi\mathbf{g}_r^{''},\\
&\mathbf{b}_5 = \xi\left(\mathbf{f}_r + \mathbf{g}_r\right)\mathbf{g}_r^{''} - \xi\mathbf{g}_r^{'2} + K\phi_r^{'},\ \ \mathbf{c}_1 = \frac{\eta}{2}(1-\xi) + \xi\left(\mathbf{f}_{r+1} + \mathbf{g}_{r+1}\right),\\
&\mathbf{c}_2 = \frac{1}{2}(1-\xi) - \xi\left(\mathbf{f}_{r+1}^{'} + 2K\right),\ \ \mathbf{c}_3 = \xi K\mathbf{f}_{r+1}^{''},\ \ \mathbf{e}_1 = \frac{\eta}{2}(1-\xi) + \xi\left(\mathbf{f}_{r+1} + \mathbf{g}_{r+1}\right),\\
&\mathbf{e}_2 = \frac{1}{2}(1-\xi) - \xi\left(\mathbf{g}_{r+1}^{'} + 2K\right),\ \ \mathbf{e}_3 = -\xi K\mathbf{g}_{r+1}^{''}.
\end{aligned}
\tag{3.54}
$$

PQLM Case II:({f,θ} and {ϕ,g}) which represents the pairings {(3.43) **and** (3.45)**} and {**(3.46) **and** (3.44)**}**

Following description of the PQLM in Chapter 1,;

$$\begin{aligned}\mathbf{A}11\mathbf{F}_{r+1}+\mathbf{A}12\Theta_{r+1}&=\mathbf{R}_1,\\ \mathbf{A}21\mathbf{F}_{r+1}+\mathbf{A}22\Theta_{r+1}&=\mathbf{R}_2,\end{aligned}\tag{3.55}$$

and

$$\begin{aligned}\mathbf{A}31\mathbf{G}_{r+1}+\mathbf{A}32\Phi_{r+1}&=\mathbf{R}_3,\\ \mathbf{A}41\mathbf{G}_{r+1}+\mathbf{A}42\Phi_{r+1}&=\mathbf{R}_4,\end{aligned}\tag{3.56}$$

where

$$\begin{aligned}
\mathbf{A}11_{j,j}&=(1+K)\mathbf{D}^3+\mathbf{diag}\left[\mathbf{a}_1\right]\mathbf{D}^2+\mathbf{diag}\left[\mathbf{a}_2\right]\mathbf{D}+\mathbf{diag}\left[\mathbf{a}_3\right]-\xi(1-\xi)\mathbf{d}_{j,j}\mathbf{D},\\
\mathbf{A}11_{j,k}&=-\xi(1-\xi)\mathbf{d}_{j,k}\mathbf{D},\\
\mathbf{A}12_{j,j}&=K\mathbf{D},\ \ \mathbf{A}21_{j,j}=\mathbf{diag}\left[\mathbf{b}_1\right]\mathbf{D}^2+\mathbf{diag}\left[\mathbf{b}_2\right]\mathbf{D}+\mathbf{diag}\left[\mathbf{b}_3\right],\\
\mathbf{A}22_{j,j}&=\left(1+\frac{K}{2}\right)\mathbf{D}^2+\mathbf{diag}\left[\mathbf{b}_4\right]\mathbf{D}+\mathbf{diag}\left[\mathbf{b}_5\right]-\xi(1-\xi)\mathbf{d}_{j,j}\mathbf{I},\\
\mathbf{A}22_{j,k}&=-\xi(1-\xi)\mathbf{d}_{j,k}\mathbf{I},\\
\mathbf{A}31_{j,j}&=(1+K)\mathbf{D}^3+\mathbf{diag}\left[\mathbf{c}_1\right]\mathbf{D}^2+\mathbf{diag}\left[\mathbf{c}_2\right]\mathbf{D}+\mathbf{diag}\left[\mathbf{c}_3\right]-\xi(1-\xi)\mathbf{d}_{j,j}\mathbf{D},\\
\mathbf{A}31_{j,k}&=-\xi(1-\xi)\mathbf{d}_{j,k}\mathbf{D},\ \ \mathbf{A}32_{j,j}=-K\mathbf{D},\\
\mathbf{A}41_{j,j}&=\mathbf{diag}\left[\mathbf{e}_1\right]\mathbf{D}^2+\mathbf{diag}\left[\mathbf{e}_2\right]\mathbf{D}+\mathbf{diag}\left[\mathbf{e}_3\right],\\
\mathbf{A}42_{j,j}&=\left(1+\frac{K}{2}\right)\mathbf{D}^2+\mathbf{diag}\left[\mathbf{e}_4\right]\mathbf{D}+\mathbf{diag}\left[\mathbf{e}_5\right]-\xi(1-\xi)\mathbf{d}_{j,j}\mathbf{I},\\
\mathbf{A}42_{j,k}&=-\xi(1-\xi)\mathbf{d}_{j,j}\mathbf{I},
\end{aligned}\tag{3.57}$$

and

$$
\begin{aligned}
&\mathbf{R}_1 = \xi(1-\xi)\mathbf{d}_1\left(j, N_t+1\right)\mathbf{DF}+\mathbf{a}_4,\\
&\mathbf{R}_2 = \xi(1-\xi)\mathbf{d}_1\left(j, N_t+1\right)\Theta+\mathbf{b}_6,\\
&\mathbf{R}_3 = \xi(1-\xi)\mathbf{d}_1\left(j, N_t+1\right)\mathbf{DG}+\mathbf{c}_4,\\
&\mathbf{R}_4 = \xi(1-\xi)\mathbf{d}_1\left(j, N_t+1\right)\Phi+\mathbf{e}_6,\\
&\mathbf{a}_1 = \xi\left(\mathbf{f}_r+\mathbf{g}_r\right)+\frac{\eta}{2}(1-\xi),\ \ \mathbf{a}_2 = -2\xi\mathbf{f}_r^{'},\\
&\mathbf{a}_3 = \xi\mathbf{f}_r^{''},\ \ \mathbf{a}_4 = \xi\mathbf{f}_r\mathbf{f}_r^{''}-\xi\mathbf{f}_r^{'2},\\
&\mathbf{b}_1 = -\xi K,\ \ \mathbf{b}_2 = -\xi\theta_r,\ \ \mathbf{b}_3 = \xi\theta_r^{'},\\
&\mathbf{b}_4 = \frac{\eta}{2}(1-\xi)+\xi\left(\mathbf{f}_r+\mathbf{g}_r\right),\ \ \mathbf{b}_5 = \frac{1}{2}(1-\xi)-\xi\left(\mathbf{f}_r^{'}+2\xi K\right),\\
&\mathbf{b}_6 = \xi\left(\mathbf{f}_r\theta_r^{'}-\mathbf{f}_r^{'}\theta_r\right),\\
&\mathbf{c}_1 = \xi\left(\mathbf{f}_{r+1}+\mathbf{g}_r\right)+\frac{\eta}{2}(1-\xi),\ \ \mathbf{c}_2 = -2\xi\mathbf{g}_r^{'},\\
&\mathbf{c}_3 = \xi\mathbf{g}_r^{''},\ \ \mathbf{c}_4 = \xi\mathbf{g}_r\mathbf{g}_r^{''}-\xi\mathbf{g}_r^{'2},\\
&\mathbf{e}_1 = \xi K,\ \ \mathbf{e}_2 = -\xi\phi_r,\ \ \mathbf{e}_3 = \xi\phi_r^{'},\\
&\mathbf{e}_4 = \frac{\eta}{2}(1-\xi)+\xi\left(\mathbf{f}_{r+1}+\mathbf{g}_r\right),\ \ \mathbf{e}_5 = \frac{1}{2}(1-\xi)-\xi\left(\mathbf{g}_r^{'}+2\xi K\right),\\
&\mathbf{e}_6 = \xi\left(\mathbf{g}_r\phi_r^{'}-\mathbf{g}_r^{'}\phi_r\right).
\end{aligned}
\tag{3.58}
$$

PQLM Case III:({f,ϕ} and {θ,g}) which represents the pairings {(3.43) **and** (3.46)**} and {**(3.45) **and** (3.44)**}**

The pairings are of the form

$$
\begin{aligned}
&\mathbf{A}11\mathbf{F}_{r+1}+\mathbf{A}12\Phi_{r+1} = \mathbf{R}_1,\\
&\mathbf{A}21\mathbf{F}_{r+1}+\mathbf{A}22\Phi_{r+1} = \mathbf{R}_2,
\end{aligned}
\tag{3.59}
$$

and

$$
\begin{aligned}
&\mathbf{A}31\mathbf{G}_{r+1}+\mathbf{A}32\Theta_{r+1} = \mathbf{R}_3,\\
&\mathbf{A}41\mathbf{G}_{r+1}+\mathbf{A}42\Theta_{r+1} = \mathbf{R}_4,
\end{aligned}
\tag{3.60}
$$

where

$$\mathbf{A}11_{j,j} = (1+K)\mathbf{D}^3 + \mathbf{diag}\left[\mathbf{a}_1\right]\mathbf{D}^2 + \mathbf{diag}\left[\mathbf{a}_2\right]\mathbf{D} + \mathbf{diag}\left[\mathbf{a}_3\right] - \xi(1-\xi)\mathbf{d}_{j,j}\mathbf{D},$$

$$\mathbf{A}11_{j,k} = -\xi(1-\xi)\mathbf{d}_{j,k}\mathbf{D},$$

$$\mathbf{A}12_{j,j} = 0, \;\; \mathbf{A}21_{j,j} = \mathbf{diag}\left[\mathbf{b}_1\right],$$

$$\mathbf{A}22_{j,j} = \left(1+\frac{K}{2}\right)\mathbf{D}^2 + \mathbf{diag}\left[\mathbf{b}_2\right]\mathbf{D} + \mathbf{diag}\left[\mathbf{b}_3\right] - \xi(1-\xi)\mathbf{d}_{j,j}\mathbf{I},$$

$$\mathbf{A}22_{j,k} = -\xi(1-\xi)\mathbf{d}_{j,k}\mathbf{I},$$

$$\mathbf{A}31_{j,j} = (1+K)\mathbf{D}^3 + \mathbf{diag}\left[\mathbf{c}_1\right]\mathbf{D}^2 + \mathbf{diag}\left[\mathbf{c}_2\right]\mathbf{D} + \mathbf{diag}\left[\mathbf{c}_3\right] - \xi(1-\xi)\mathbf{d}_{j,j}\mathbf{D},$$

$$\mathbf{A}31_{j,k} = -\xi(1-\xi)\mathbf{d}_{j,k}\mathbf{D}, \;\; \mathbf{A}32_{j,j} = 0,$$

$$\mathbf{A}41_{j,j} = \mathbf{diag}\left[\mathbf{e}_1\right],$$

$$\mathbf{A}42_{j,j} = \left(1+\frac{K}{2}\right)\mathbf{D}^2 + \mathbf{diag}\left[\mathbf{e}_2\right]\mathbf{D} + \mathbf{diag}\left[\mathbf{e}_3\right] - \xi(1-\xi)\mathbf{d}_{j,j}\mathbf{I},$$

$$\mathbf{A}42_{j,k} = -\xi(1-\xi)\mathbf{d}_{j,k}\mathbf{I},$$

$$\mathbf{R}_1 = \xi(1-\xi)\mathbf{d}_1\left(j, N_t+1\right)\mathbf{DF} + \mathbf{a}_4,$$

$$\mathbf{R}_2 = \xi(1-\xi)\mathbf{d}_1\left(j, N_t+1\right)\Phi + \mathbf{b}_4,$$

$$\mathbf{R}_3 = \xi(1-\xi)\mathbf{d}_1\left(j, N_t+1\right)\mathbf{DG} + \mathbf{c}_4,$$

$$\mathbf{R}_4 = \xi(1-\xi)\mathbf{d}_1\left(j, N_t+1\right)\Theta + \mathbf{e}_4,$$

and

$$\mathbf{a}_1 = \xi(\mathbf{f}_r+\mathbf{g}_r)+\frac{\eta}{2}(1-\xi),\ \ \mathbf{a}_2 = -2\xi\mathbf{f}_r^{'},$$
$$\mathbf{a}_3 = \xi\mathbf{f}_r^{''},\ \ \mathbf{a}_4 = \xi\mathbf{f}_r\mathbf{f}_r^{''}-\xi\mathbf{f}_r^{'2}-K\theta_r^{'},$$
$$\mathbf{b}_1 = \xi\phi_r^{'},$$
$$\mathbf{b}_2 = \frac{\eta}{2}(1-\xi)+\xi(\mathbf{f}_r+\mathbf{g}_r),\ \ \mathbf{b}_3 = \frac{1}{2}(1-\xi)-\xi\left(\mathbf{g}_r^{'}+2\xi K\right),$$
$$\mathbf{b}_4 = \xi\left(\mathbf{f}_r\phi_r^{'}-\xi K\mathbf{g}_r^{''}\right),$$
$$\mathbf{c}_1 = \xi(\mathbf{f}_{r+1}+\mathbf{g}_r)+\frac{\eta}{2}(1-\xi),\ \ \mathbf{c}_2 = -2\xi\mathbf{g}_r^{'},$$
$$\mathbf{c}_3 = \xi\mathbf{g}_r^{''},\ \ \mathbf{c}_4 = \xi\mathbf{g}_r\mathbf{g}_r^{''}-\xi\mathbf{g}_r^{'2}+K\phi_r^{'},$$
$$\mathbf{e}_1 = \xi\theta_r^{'},$$
$$\mathbf{e}_2 = \frac{\eta}{2}(1-\xi)+\xi(\mathbf{f}_{r+1}+\mathbf{g}_r),\ \ \mathbf{e}_3 = \frac{1}{2}(1-\xi)-\xi\left(\mathbf{f}_r^{'}+2\xi K\right),$$
$$\mathbf{e}_4 = \xi\left(\mathbf{g}_r\theta_r^{'}+K\mathbf{f}_r^{''}\right).$$

3.4 Results and Discussion

In this section, the approximate numerical solutions to the systems of partial differential equations (3.1) − (3.4) and (3.43) − (3.46) using the PQLM and SLLM are presented. To generate these results, the number of grid points used in space was 50 while 20 grid points were used in time. The number of grid points was chosen such that further increase yielded the same solutions consistent to 6 decimal places. Comparison of the performance of the PQLM in three different combinations and the BSLLM was carried out by observing the convergence and accuracy of the methods.

3.4.1 Example 1

We present the numerical solutions of the system (3.1) − (3.4) using the PQLM and SLLM. To generate solutions for comparison, all computations performed were for the set values of parameters $Pr = 0.7$, $Sc = 0.7$, $\gamma = 1$, $m_0 = 0.5$, $M = 0.5$ and $Nr = 0.5$. To compare convergence of the PQLM cases and the SLLM, we consider the norm of the difference between successive iterations

using each method set to within a tolerance level of 10^{-6}. To show that our numerical schemes converge, the solution error is expected to get smaller as the number of iterations increase. This trend should continue to a point where the error does not change with further iterations. It is important to note that different norms can be used, but we elect to investigate the maximum error which is defined for each function F, G, Θ and Φ as

$$||\Omega||_\infty = \max_{0\leq i\leq N_y} ||\Omega_{r+1,i} - \Omega_{r,i}||_\infty, \tag{3.61}$$

where Ω represents F, G, Θ and Φ.

Figures 3.1−3.4 show the effect of iterations on $||\mathbf{F}||_\infty$, $||\mathbf{G}||_\infty$, $||\Theta||_\infty$ and $||\Phi||_\infty$.

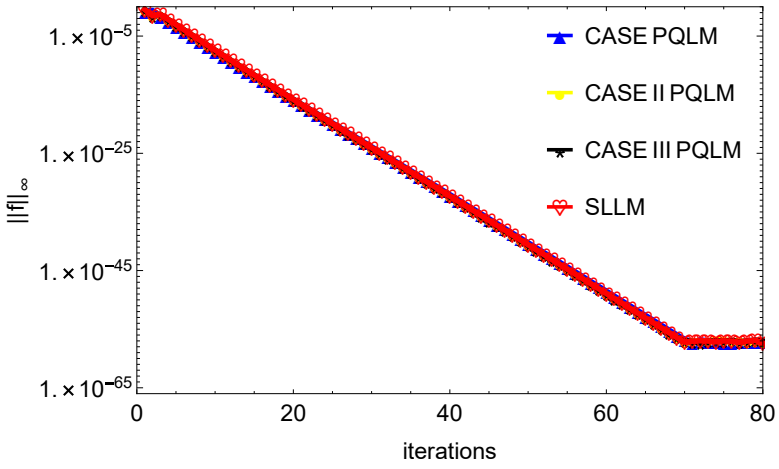

Figure 3.1: Effect of iterations on the maximum solution error for F

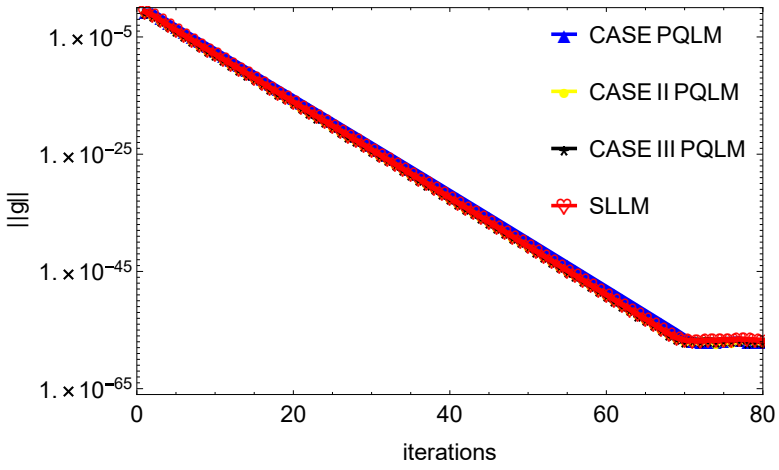

Figure 3.2: Effect of iterations on the maximum solution error for G

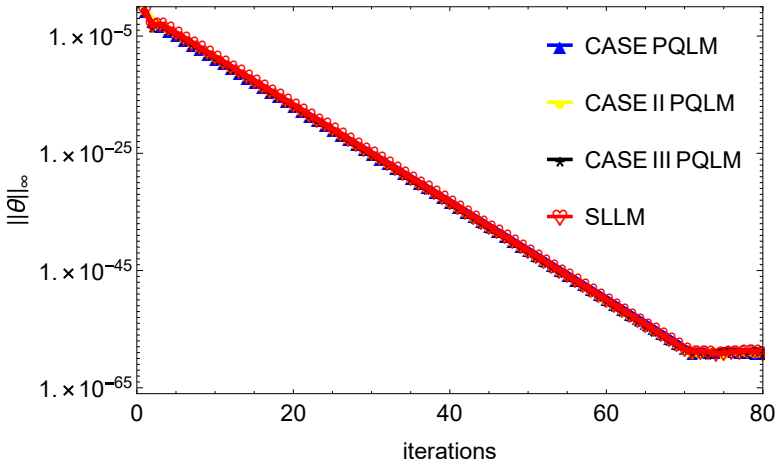

Figure 3.3: Effect of iterations on the maximum solution error for Θ

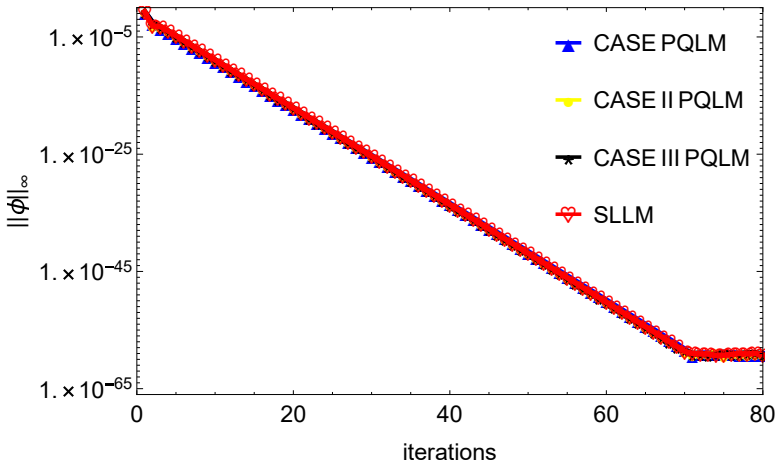

Figure 3.4: Effect of iterations on the maximum solution error for Φ

It is observed from Figures 3.1 to 3.4 that as the number of iterations increases, the respective solution errors for the three PQLM cases and SLLM reduce significantly until they all become consistent at 10^{-60}. It is also observed that, for all the methods, it takes 70 iterations to attain convergence to this level. For the level of accuracy attained with this system of highly nonlinear partial differential equations, such convergence is quite fast. We observe that the convergence speed for all the PQLM cases is comparable with each other and the SLLM. We further investigate their accuracy and the speed at which convergence is attained.

The accuracy of the PQLM and SLLM can be determined by calculating the residual errors. The residual error is used to determine how close the approximate solution is to the true solution of a differential equation. We consider the maximum residual error, hence the choice of the infinity norm when calculating the residual error. For the system (3.1) $-$ (3.4), the residual error are

defined as

$$\mathbf{Res}(\mathbf{F}) = \max_{0\le i\le N_y} \left|\left|(1+K)\mathbf{f}_i''' + (1-\xi)\left(\frac{\eta}{2}\mathbf{f}_i'' - \xi\frac{\partial \mathbf{f}_i'}{\partial \xi}\right) + \xi\left(\mathbf{f}_i\mathbf{f}_i'' - \left(\mathbf{f}_i'\right)^2 - M^2\mathbf{f}_i'\right) + K\mathbf{g}_i'\right|\right|_\infty, \quad (3.62)$$

$$\mathbf{Res}(\mathbf{G}) = \max_{0\le i\le N_y} \left|\left|\left(1+\frac{K}{2}\right)\mathbf{g}_i'' + (1-\xi)\left(\frac{1}{2}\mathbf{g}_i + \frac{\eta}{2}\mathbf{g}_i' - \xi\frac{\partial \mathbf{g}_i}{\partial \xi}\right) + \xi\left(\mathbf{f}\mathbf{g}_i' - \mathbf{f}_i'\mathbf{g}_i - 2K\mathbf{g}_i - K\mathbf{f}_i''\right)\right|\right|_\infty, \quad (3.63)$$

$$\mathbf{Res}(\Theta) = \max_{0\le i\le N_y} \left|\left|(1+N_R)\theta_i'' + Pr(1-\xi)\left(\frac{\eta}{2}\theta_i' - \xi\frac{\partial \theta_i}{\partial \xi}\right) + Pr\xi\mathbf{f}_i\theta_i'\right|\right|_\infty, \quad (3.64)$$

$$\mathbf{Res}(\Phi) = \max_{0\le i\le N_y} \left|\left|\phi_i'' + Sc(1-\xi)\left(\frac{\eta}{2}\phi_i' - \xi\frac{\partial \phi_i}{\partial \xi}\right) + Sc\xi\mathbf{f}_i\phi_i' - \gamma Sc\xi\phi_i\right|\right|_\infty, \quad (3.65)$$

Figures 3.5 to 3.8 compare the accuracy of all PQLM cases and the SLLM, which indicates how the methods behave when iterations increase. The figures show the accuracy when $\xi = 0.8$.

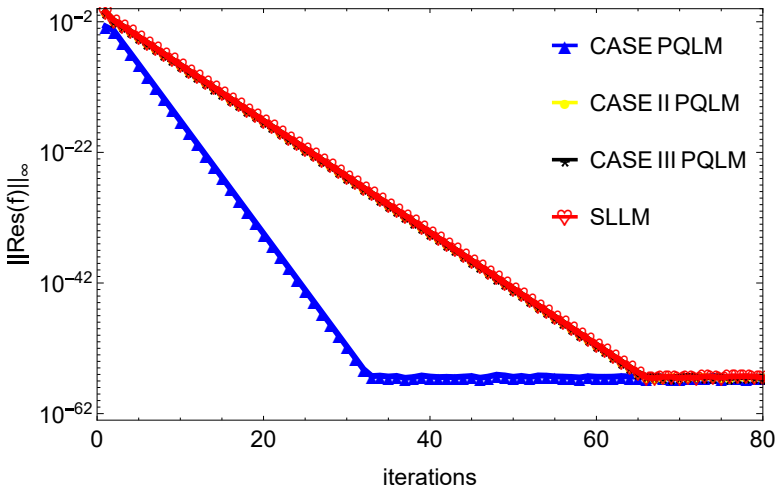

Figure 3.5: Effect of iterations on the residual error norm for F

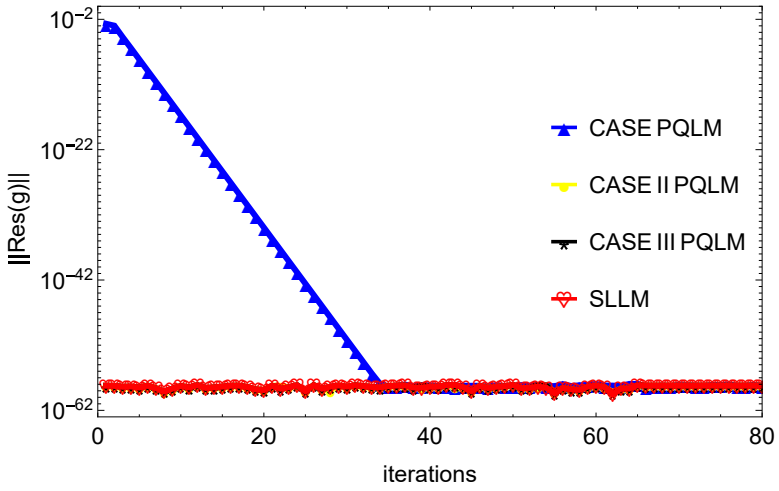

Figure 3.6: Effect of iterations on the residual error norm for G

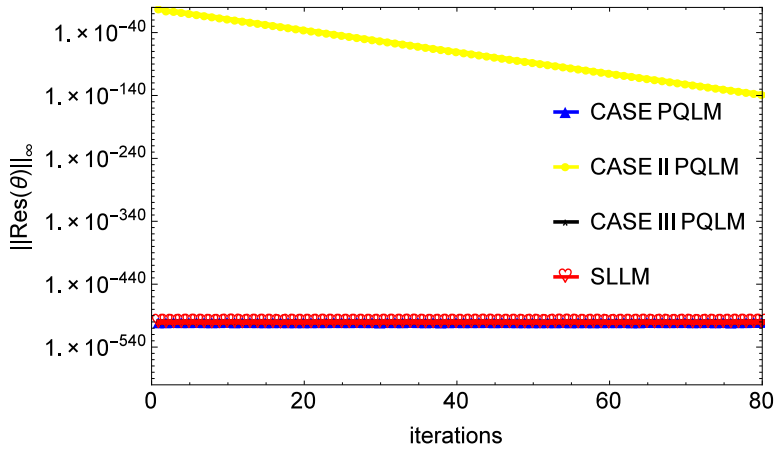

Figure 3.7: Effect of iterations on the residual error norm for θ

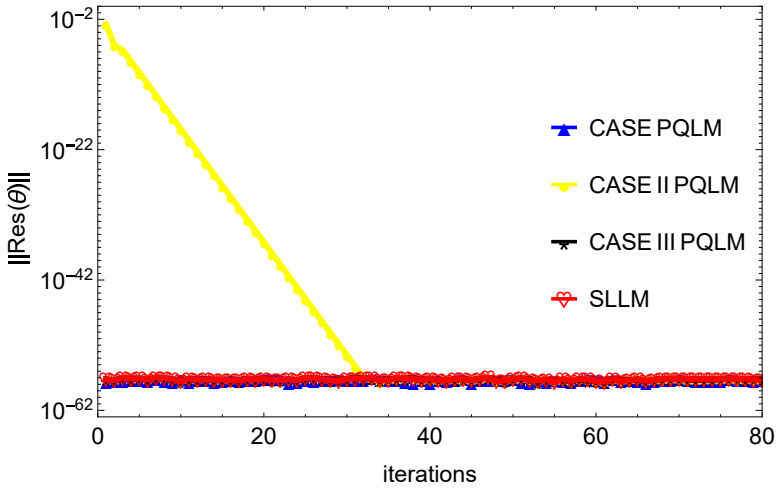

Figure 3.8: Effect of iterations on the residual error norm for Φ

It can be seen in Figures 3.5 to 3.8 that increasing the number of iterations leads to a decrease in the residual error. This indicates that, with further iterations, the accuracy of the methods improve. It is observed that the PQLM and SLLM are accurate methods as it is seen that the residual errors reduce rapidly with further iterations. To compare the methods, we consider the residual error norms at 50 iterations on all four figures. It is observed from Figure 3.5 that PQLM case I converges fastest to the same accuracy as the rest of the methods after 30 iterations while the rest of the cases and SLLM converge at the same rate. It is seen from Figure 3.6 that the PQLM cases and the SLLM all have the same accuracy level. It is observed in Figures 3.7 that the PQLM case II converges to a bigger residual norm (10^{-140}) than the rest of the PQLM cases and SLLM which all converge to 10^{-500}. We observe from Figure 3.8 that the PQLM cases 1, 2, and 3 all have the same accuracy as the SLLM at 10^{-500}. We see that the PQLM cases give very accurate solutions as they are shown to match the high accuracy of the SLLM.

In order to investigate the effect of time on the accuracy of numerical solutions generated by the various methods, we compute the residual error for $0 \leq \xi \leq 1$ using a time-step of 0.1. This is done to examine the points where solutions obtained using the PQLM and SLLM are most accurate. Results generated at the 50^{th} iteration are shown in Figures 3.9 to 3.12.

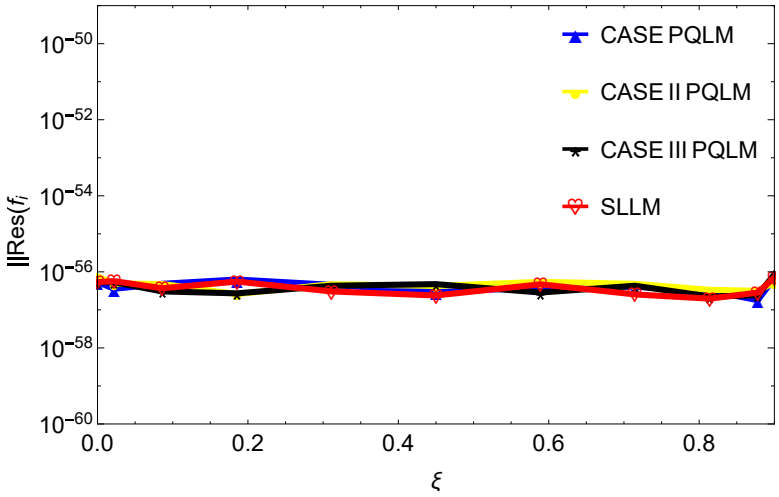

Figure 3.9: Effect of time on the residual error norm for F

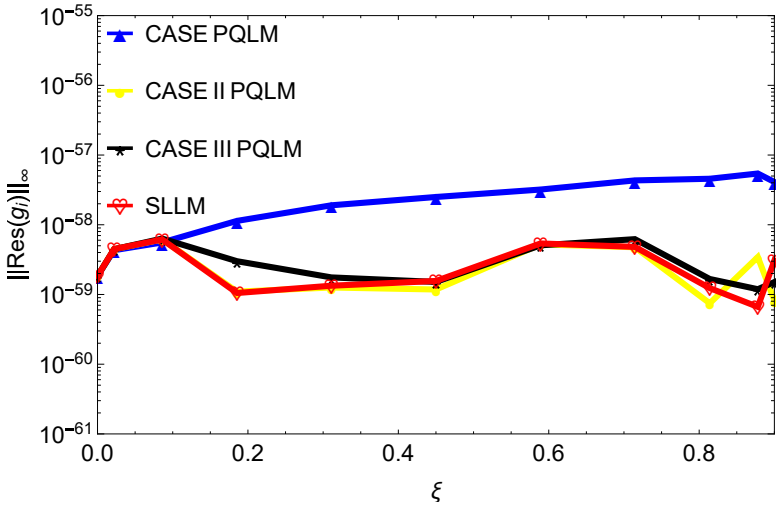

Figure 3.10: Effect of time on the residual error norm for G

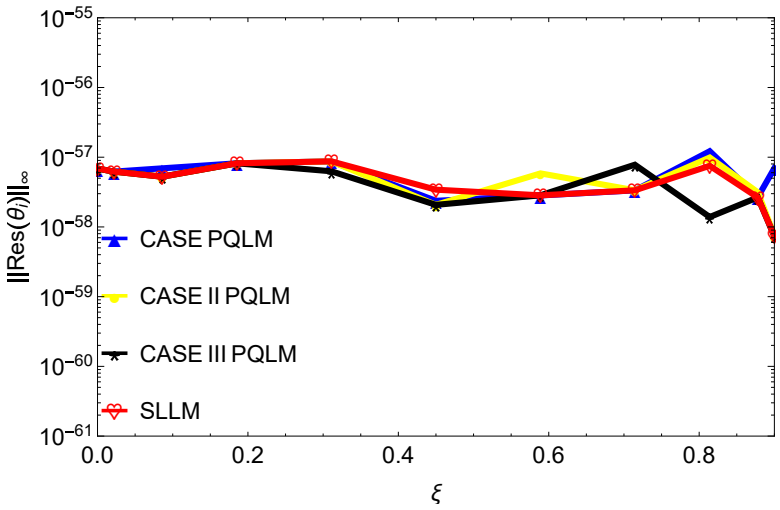

Figure 3.11: Effect of time on the residual error norm for Θ

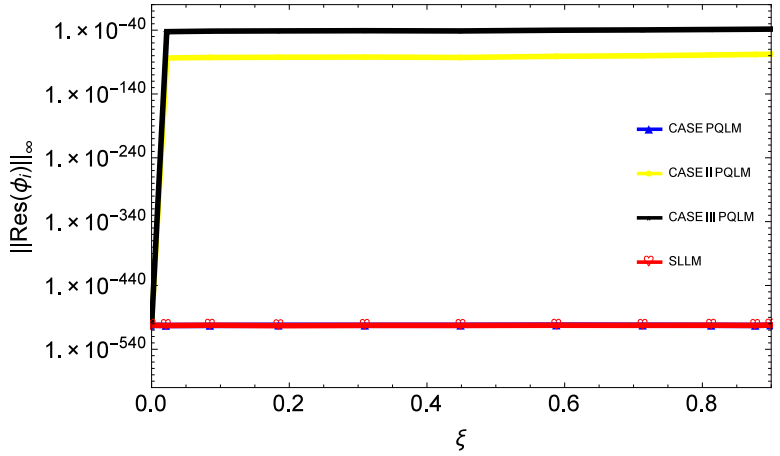

Figure 3.12: Effect of time on the residual error norm for Φ

It can be seen from Figures 3.9 to 3.12 that, within the time interval $0 \leq \xi \leq 1$, all the methods maintain very high accuracy. We also observe that the accuracy of the solutions obtained using all the methods are independent of time. We see that the methods are all highly accurate and the PQLM is seen to be a suitable alternative for solving problems of a similar nature.

3.4.2 Example 2

In this section, we present the numerical solutions of the system (3.43) − (3.46) obtained using the PQLM and SLLM. In order to generate solutions for comparison, all computations performed were under the pre-chosen values of parameters at $K = 1$, $n = 0.5$ and $Nr = 0.5$. We investigate the convergence of the methods by comparing the norm of their respective solution errors between successive iterations. The methods are said to be convergent if the error reduces with each further iteration, to a point where further iterations gives the same error. We define the solution errors of the system (3.43) − (3.46) as given in equation (7.97)

Figures 3.13 to 3.16 display the number of iterations taken to converge for each method.

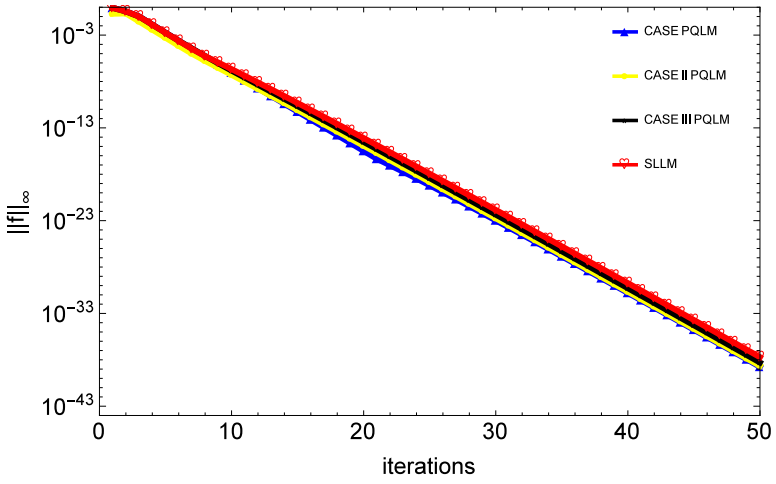

Figure 3.13: Effect of iterations on the solution error for F

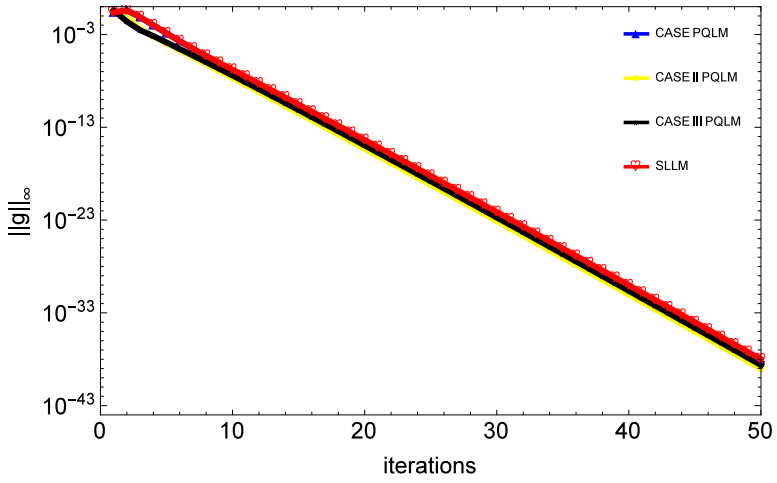

Figure 3.14: Effect of iterations on the solution error for G

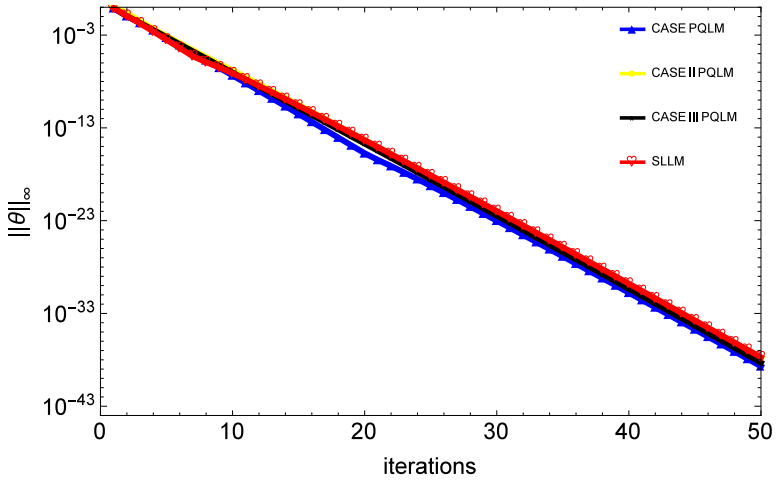

Figure 3.15: Effect of iterations on the solution error for Θ

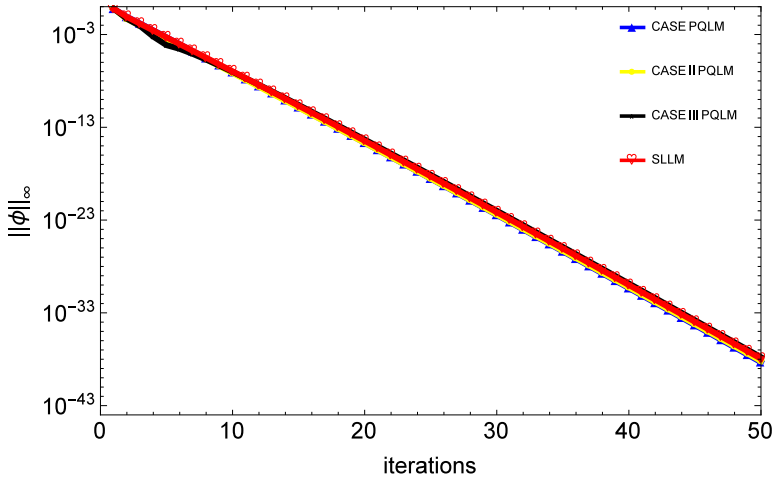

Figure 3.16: Effect of iterations on the solution error for Φ

It is observed from Figures 3.13 to 3.16 that the solution errors reduce significantly with increasing iterations. We can also observe that for each figure, there are similar gradients for all four methods. This indicates that the rate of convergence for all four methods is similar.

We also investigate the accuracies of the three PQLM cases and the SLLM. The investigation is carried out using the residual error of the methods. The residual error measures the extent to which the approximate solution to a differential equation approaches the true solution. We define the residual error of the system (3.43) − (3.46) as

$$\begin{aligned}
\mathbf{Res}(\mathbf{F}) &= \max_{0\le i\le N_y}\left\|(1+K)\mathbf{f}_i'''+\frac{\eta}{2}(1-\xi)\mathbf{f}_i''+\xi(\mathbf{f}_i+\mathbf{g}_i)\mathbf{f}_i''-\xi\mathbf{f}_i'^2+K\theta_i'-\xi(1-\xi)\frac{\partial\mathbf{f}_i'}{\partial\xi}\right\|_\infty,\\
\mathbf{Res}(\mathbf{G}) &= \max_{0\le i\le N_y}\left\|(1+K)\mathbf{g}_i'''+\frac{\eta}{2}(1-\xi)\mathbf{g}_i''+\xi(\mathbf{f}_i+\mathbf{g}_i)\mathbf{g}_i''-\xi\mathbf{g}_i'^2-K\phi_i'-\xi(1-\xi)\frac{\partial\mathbf{g}_i'}{\partial\xi}\right\|_\infty,\\
\mathbf{Res}(\Theta) &= \max_{0\le i\le N_y}\left\|\left(1+\frac{K}{2}\right)\theta_i''+\mathbf{h}_1\theta_i'-\xi(1-\xi)\frac{\partial\theta_i}{\partial\xi}+\mathbf{h}_2\theta_i-\xi K\mathbf{f}_i''\right\|_\infty,\\
\mathbf{Res}(\Phi) &= \max_{0\le i\le N_y}\left\|\left(1+\frac{K}{2}\right)\phi_i''+\mathbf{h}_1\phi_i'-\xi(1-\xi)\frac{\partial\phi_i}{\partial\xi}+\mathbf{h}_2\phi_i+\xi K\mathbf{g}_i''\right\|_\infty,
\end{aligned} \tag{3.66}$$

where

$$\mathbf{h}_1=\left((1-\xi)\frac{\eta}{2}\xi(\mathbf{f}_i+\mathbf{g}_i)\right),\ \ \mathbf{h}_2=\left(\frac{1}{2}(1-\xi)-\xi\mathbf{f}_i'-2\xi K\right). \tag{3.67}$$

Figures 3.17 to 3.20 display the effect of iterations on the residual error of the PQLM cases and the SLLM. We set the value of ξ to 0.8 for all the graphs.

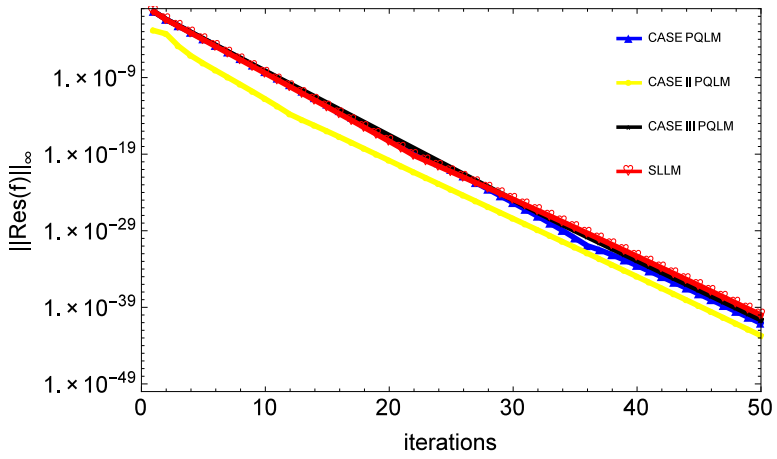

Figure 3.17: Effect of iterations on the residual error norm for F

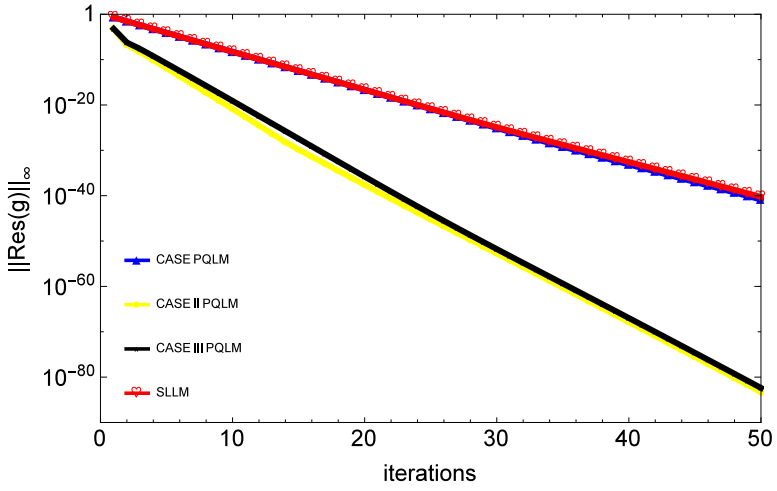

Figure 3.18: Effect of iterations on the residual error norm for G

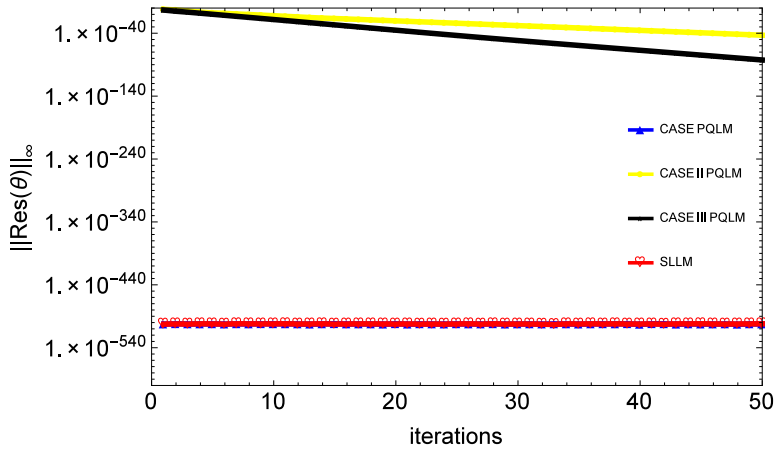

Figure 3.19: Effect of iterations on the residual error norm for θ

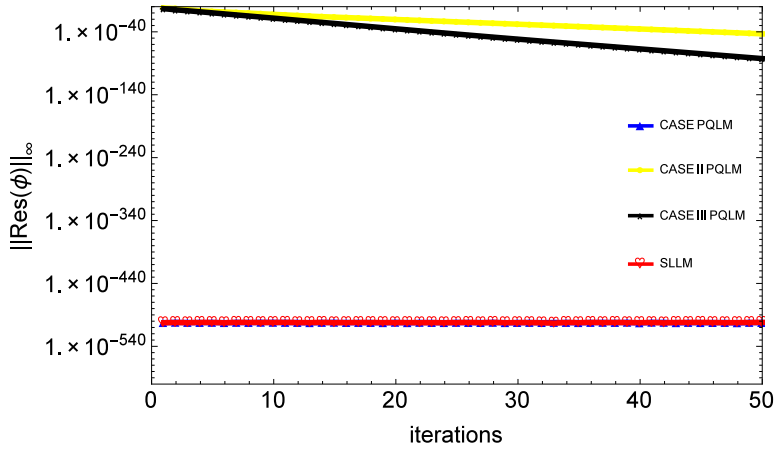

Figure 3.20: Effect of iterations on the residual error norm for Φ

From Figures 3.17 to 3.20, it is observed that increasing the number of iterations improves the accuracy of all the methods. As shown in Figure 3.17, the accuracy of the methods is comparable and after 50 iterations the residual error is 10^{-40}. In particular we note that in Figures 3.19 and 3.20 the PQLM case I and SLLM give a consistent error as small as 10^{-500}, while the accuracy of the other two methods are comparable.

Figures 3.21 to 3.24 given below display the residual errors of the three PQLM cases and the SLLM for various time levels ξ at the 50^{th} iteration point; where the convergence of the solution

to a certain tolerance level has been attained.

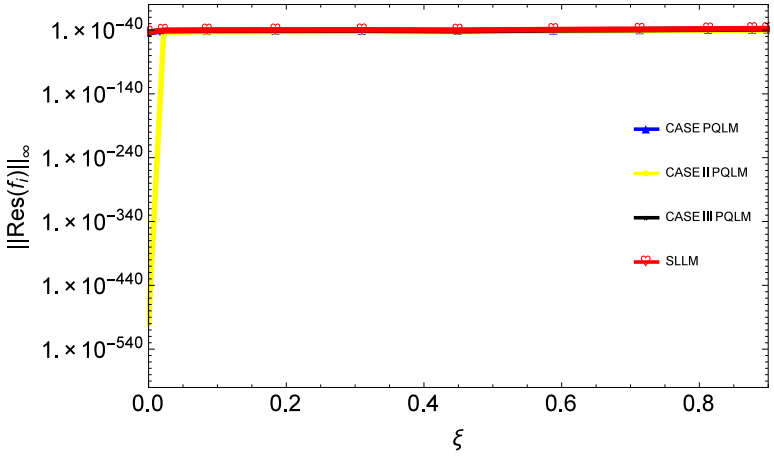

Figure 3.21: Effect of time on the residual error norm for F

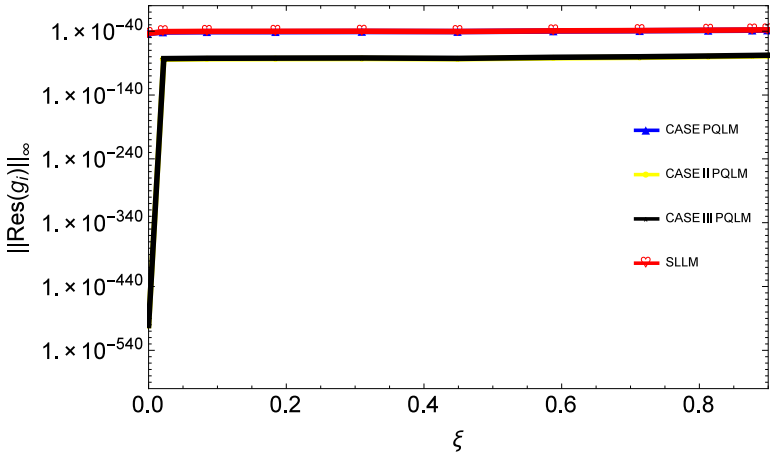

Figure 3.22: Effect of time on the residual error norm for G

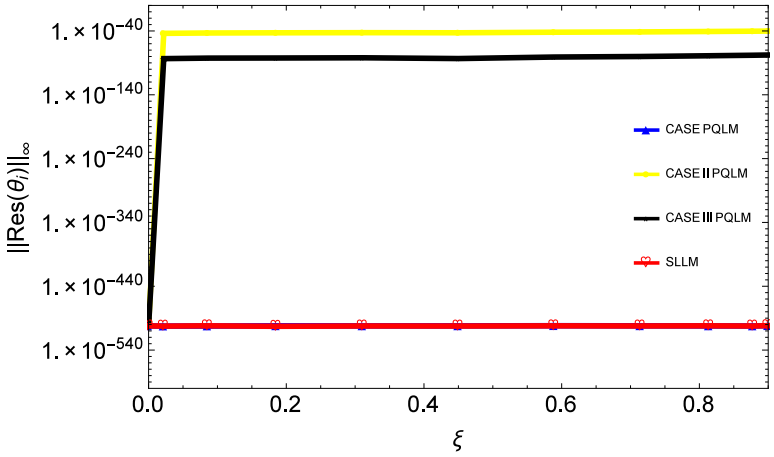

Figure 3.23: Effect of time on the residual error norm for Θ

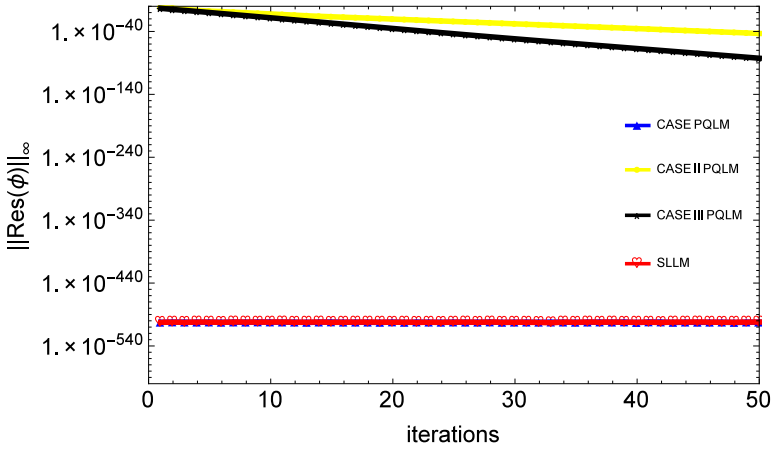

Figure 3.24: Effect of time on the residual error norm for Φ

It can be observed from Figures 3.21−3.24 that the residual errors at different times remain very small and comparable indicating that the methods are highly accurate over the chosen time interval.

3.5 Summary

This chapter set out to describe the paired quasilinearization method for a general system of partial differential equations and to determine the best choice of pairing. The study in this chapter compared the results obtained using three PQLM cases against those from the SLLM. It was observed

that the PQLM compared favorably to the SLLM. It was also observed that the PQLM converged faster than the SLLM. The accuracy of the PQLM was also shown to be the same as the SLLM. In determining the best pairing, we observed that the combination which had the most number of nonlinear terms had a better convergence rate than other cases. This shows that the use of quasi-linearization on more nonlinear terms reduces the number of iterations needed to achieve accurate solutions. In general, we conclude that using the PQLM in any combination yields very good and accurate results with few iterations, but the method is fully optimized by choosing the combination with the highest number of nonlinearities.

The findings in this chapter replicates what was ascertained in chapter 2 indicating that the higher the nonlinearity of the paired system, the faster the convergence of solutions. In chapter 4, chapter 5 and chapter 6, the PQLM is used to study the effects of various parameters on the flow profiles of different models.

Chapter 4

Combined influence of radiation and Hall and ion effects on MHD free convective heat generating flow past semi-infinite vertical flat plate

4.1 Introduction

Heat transfer phenomena frequently involving thermal convection along a vertical channel plate have received increased attention because of their importance in engineering. Their applications include technological processes such as early stages of melting and transient heating of insulating air gaps by heat input at the start-up of furnaces.

The increasing number of technical applications using magnetohydrodynamic (MHD) effects has driven the extension of many of the available hydrodynamic solutions to include the effect of magnetic fields, as applicable for those cases when the fluid is electrically conducting. Electrically conducting fluids have many applications in engineering problems such as MHD generators, plasma studies, nuclear reactors, geothermal energy extraction, and the boundary layer control in the field of aerodynamics. The effect of the magnetic field on free convection flows is important in liquid metals, electrolytes, and ionized gases. Many cross-galvano and thermo-magnetic effects occur in the boundary zone between hydraulics and thermal physics, and they are relevant in the

study of semi-conductor materials. For the case of a strong magnetic field, where the electron cyclotron frequency is much greater than the electron collision frequency, Hall effects become significant. Hall currents are important and they have a marked effect on the magnitude and direction of the current density and consequently on the magnetic force term. The effects of Hall and ion-slip in different geometries have been reported by several researchers such as Ghosh and Pop [93] and Abo-Eldahab and Salem [94]. The effect of radiation on MHD flow and heat transfer must be considered when high temperatures are reached. Many processes in engineering areas occur at high temperatures, and knowledge of radiative heat transfer becomes very important for the design of equipment. Free convection on a vertical plate with radiation effects with or without MHD has been studied by Shit [95] and Seddeek [96]. The unsteady free convection flow of a viscous fluid, considering the buoyancy, radiation, and Hall currents acting simultaneously, was investigated numerically by Mohamed *et al.* [97] using shooting method. Rao and Babu [98] analyzed the radiation and mass transfer effects on an unsteady two-dimensional laminar convective boundary layer flow of a viscous, incompressible, chemically reacting fluid along a semi-infinite vertical plate with suction by taking into account the effects of viscous dissipation. Radiation effects on free convection flow past a semi-infinite vertical plate, were studied by Soundalgekar and Takhar [99] and by Chamkha [100] who also included mass transfer effects.

Most of the studies mentioned above focused on the flow of Newtonian fluids. However, in reality, most liquids used in industrial applications such as molten plastics, food-stuffs or slurries, particularly in polymer processing applications, display non-Newtonian behavior. There exist several approaches to study the mechanics of fluids with sub-structure. Ericksen [101, 102] derived field equations that account for the presence of sub-structures in the fluid. It had been experimentally demonstrated by Hoyt [103] that fluids containing a small number of polymeric additives display a reduction in skin friction. Eringen [104] first formulated the theory of micropolar fluids, which display the effects of local rotary inertia and couple stresses. This theory can be used to explain the flow of colloidal fluids, liquid crystal, animal blood, etc. Eringen [105] extended the micropolar fluid theory and developed the theory of thermo-micropolar fluids. Physically, micropolar fluids may be described as non-Newtonian fluids consisting of dumb-bell shaped molecules or those

with a short rigid cylindrical element, as found in polymer fluids, fluid suspension, etc. The presence of dust or smoke, particularly in a gas, may also be modeled using micropolar fluid dynamics.

The main focus of the present study is to investigate the effects of radiation, Hall current, ion-slip and a heat/sink source on the free convection flow past a semi-infinite vertical flat plate. To carry out this investigation, we solve the highly nonlinear governing equations numerically, using the paired quasilinearization method (PQLM) introduced by Motsa and Animasaun [20]. The PQLM is applied to a large system of equations such that a pair of non-linear functions and their corresponding derivatives are linearized with the aid of quasilinearization [38] from a pair of equations. This implies that updated solutions for the first pair of functions are used in subsequent pairs of equations, thereby effectively decoupling the large system of equations into linear coupled pairs. To generate solutions, the Chebyshev spectral collocation method is applied to discretize the decoupled system. To test the convergence and accuracy of the PQLM, we conduct solution error tests and residual error tests, respectively. We graphically display the results and discuss the influence of important parameters on the fluid flow properties.

4.2 Mathematical formulation of the problem

Consider the steady free convection flow of an electrically conducting micropolar fluid up a heated semi-infinite vertical plate extending upwards in the x direction. The y axis is taken to be perpendicular to the plate, which is held at a constant temperature T_w. It is assumed that

- Boussinesq's approximation is valid.
- A uniform magnetic field is applied in the direction perpendicular to the plate $(0, B_0, 0)$ and the induced magnetic field is negligible in comparison with the applied one, which corresponds to a very small magnetic Reynolds number.
- The effect of viscous and Joule dissipation is negligible in the energy equation.

- The current trend for the application of magnetohydrodynamics is towards a strong magnetic field so that the influence of electromagnetic force is noticeable (Hall effects is retained).

The effect of Hall current gives rise to force in the z-direction, which induces a cross-flow in that direction and hence the flow becomes three-dimensional. To simplify the problem, we assume that there is no variation of flow or heat transfer quantities in z-direction. The equation for conservation of electric charges, $\nabla J = 0$, gives constant, where $J = (J_x, J_y, J_z)$ since the plate is electrically non-conductive, this constant is zero and $J_y = 0$ everywhere in the flow.

The generalized Ohm's law which retains Hall and ion-slip terms under the assumptions for this problem, is given by

$$J = \sigma \{\overrightarrow{q} X \overrightarrow{B} - \eta_1 (\overrightarrow{J} X \overrightarrow{B}) + \frac{\eta_1 \beta_i}{B_0} (\overrightarrow{J} X \overrightarrow{B}) X \overrightarrow{B}\}, \tag{4.1}$$

where $\overrightarrow{q}$ is velocity, $\overrightarrow{B}$ is magnetic induction vector, B_0 is the magnetic field of constant strength, σ is the electrical conductivity of the fluid, β_i is ion-slip parameter and η_1 is Hall factor.

Under these conditions, the problem is governed by the following system of equations:

$$\frac{\partial u}{\partial x} + \frac{\partial v}{\partial y} = 0, \tag{4.2}$$

$$\begin{aligned} u\frac{\partial u}{\partial x} + v\frac{\partial u}{\partial y} = \frac{\kappa}{\rho}\frac{\partial \Gamma}{\partial y} + \frac{\mu+\kappa}{\rho}\frac{\partial^2 u}{\partial y^2} + g^* \beta_T (T - T_0) \\ - \frac{\sigma B_0^2}{\rho[\beta_h^2 + \beta_e^2]}[\beta_h u + \beta_e w], \end{aligned} \tag{4.3}$$

$$u\frac{\partial w}{\partial x} + v\frac{\partial w}{\partial y} = \frac{(\mu+\kappa)}{\rho}\frac{\partial^2 w}{\partial y^2} + \frac{\sigma B_0^2}{\rho[\beta_h^2 + \beta_e^2]}[\beta_e u - \beta_h w], \tag{4.4}$$

$$u\frac{\partial \Gamma}{\partial x} + v\frac{\partial \Gamma}{\partial y} = -2\frac{\kappa}{\rho j}\Gamma + \frac{\kappa}{\rho j}\frac{\partial u}{\partial y} + \frac{\gamma}{\rho j}\frac{\partial^2 \Gamma}{\partial y^2}, \tag{4.5}$$

$$u\frac{\partial T}{\partial x} + v\frac{\partial T}{\partial y} = \alpha\frac{\partial^2 T}{\partial y^2} + \frac{Q_1(T - T_\infty)}{\rho C_p} - \frac{1}{\rho C_p} 4I(T - T_w), \tag{4.6}$$

where (u,v,w) are velocities associated with the direction of increasing coordinates (x,y,z), Γ is microrotation, j is the micro-inertia density, ρ is the fluid density, μ, κ and γ are the material constants (viscosity coefficients), $g*$ is the acceleration due to gravity, β_T is the coefficient of thermal expansion, B_0 is the magnetic field intensity, σ is the electrical conductivity, $\beta_h = 1+\beta_i\beta_h$ and β_i is the ion-slip parameter, $\beta_e = \sigma B_0\eta_1$ is a Hall parameter and α is the thermal diffusivity. The equation that describes the radiative heat flux term is [106]

$$\frac{\partial q_r}{\partial y} = 4(T-T_w)I, \tag{4.7}$$

$$I = \int_0^\infty P_{\lambda\omega}\left(\frac{\partial e_{b\lambda}}{\partial T}\right)_\omega d\lambda, \tag{4.8}$$

where T is the temperature of the fluid in the boundary layer, $P_{\lambda\omega}$ is the mean absorption coefficient, $e_{b\lambda}$ is Plan's function.

The boundary conditions are given by

$$u = 0, \quad v = 0, \quad w = 0, \quad \Gamma = 0, \quad T = T_w(x) \quad at \quad y = 0, \tag{4.9a}$$

$$u = 0, \quad w = 0, \quad \Gamma = 0, \quad T \to T_\infty \quad \text{as} \quad y \to \infty. \tag{4.9b}$$

Introducing the following similarity variables

$$\begin{gathered}
\zeta = x^{1/2}L^{-1/2}, \quad \eta = Cyx^{-1/4}, \quad C = \left(\frac{g^*\beta(T_w-T_\infty)}{4\nu^2}\right)^{1/4}, \quad M = \frac{\sigma B_0^2 L^2}{\rho\nu Gr^{1/2}}, \\
Pr = \frac{\nu\rho C_p}{\alpha} \quad \theta = \frac{T-T_\infty}{T_w-T_\infty}, \quad Q = \frac{Q_1 L^2}{\rho C_p \nu Gr^{1/2}}, \quad Gr = \frac{g^*\beta L^3(T_w-T_\infty)}{\nu^2}, \\
J = \frac{j}{L^2}, \quad K = \frac{\kappa}{\rho j}, R_d = \frac{4I}{\rho C_p \nu Gr^{1/2}} \\
\Psi = 4\nu C x^{3/4} f(\zeta,\eta), \quad w = 4\nu C^2 x^{1/2} g(\zeta,\eta), \quad \Gamma = 4\nu C^3 x^{1/4}\omega(\zeta,\eta).
\end{gathered} \tag{4.10}$$

Here, ζ and η are pseudo-similarity variables, Ψ is a stream function, Pr is the Prandtl number, M is the magnetic field parameter, Q is the heat source/sink parameter, J is the micro-inertia density, N is

the coupling number, m is the micropolar parameter, θ, g, and ω are respectively, the dimensionless temperature, η-component velocity and microrotation where Ψ satisfies

$$u = \frac{\partial \Psi}{\partial y}, \qquad v = -\frac{\partial \Psi}{\partial x}. \tag{4.11}$$

In terms of the new variables, the velocity components can be expressed as

$$u = 4\nu C^2 x^{1/2} f'(\zeta,\eta), \quad v = -\nu C x^{-1/2}(3f + 2\zeta\frac{\partial f}{\partial \zeta} - \eta f') \tag{4.12}$$

Applying the transformations on equations (4.3)-(4.6) we have

$$\frac{1}{1-N}f''' + \frac{N}{1-N}\omega' - 2f'^2 + 3ff'' + 2\zeta\left(f''\frac{\partial f}{\partial \zeta} - f'\frac{\partial f'}{\partial \zeta}\right) + \theta - \frac{2M\zeta}{\beta_h^2+\beta_e^2}\left[\beta_h f' + \beta_e g\right] = 0, \tag{4.13}$$

$$\frac{1}{1-N}g'' - 2f'g + 3fg' + 2\zeta\left(g'\frac{\partial f}{\partial \zeta} - f'\frac{\partial g}{\partial \zeta}\right) - \frac{2M\zeta}{\beta_h^2+\beta_e^2}[\beta_h g - \beta_e f'] = 0, \tag{4.14}$$

$$\frac{N}{1-N}\frac{2-N}{m^2}\omega'' + \frac{2NGr^{-1/2}}{1-N}\zeta(2\omega - f'') + aj\left(-f'\omega' + 3f\omega' + 2\zeta\left(\omega'\frac{\partial f}{\partial \zeta} - f'\frac{\partial \omega}{\partial \zeta}\right)\right) = 0, \tag{4.15}$$

$$\theta'' + 2Pr\zeta[(Q - R_d)\theta + R_d] + 3Prf\theta' + 2Pr\zeta\left(\theta'\frac{\partial f}{\partial \zeta} - f'\frac{\partial \theta}{\partial \zeta}\right) = 0, \tag{4.16}$$

where $\beta_e = \sigma\beta B_0$ is the Hall parameter , and $\beta_h = 1 + \beta_i\beta_e$.

The corresponding boundary conditions are

$$f'(\zeta,0) = 0, \quad 3f(\zeta,0) + 2\zeta\frac{\partial f(\zeta,0)}{\partial \zeta} = 0, \quad g(\zeta,0) = 0, \quad \omega(\zeta,0) = 0, \quad \theta(\zeta,0) = 1, \tag{4.17a}$$

$$f'(\zeta,\infty) = 0, \quad g(\zeta,\infty) = 0, \quad \omega(\zeta,\infty) = 0, \quad \theta(\zeta,\infty) = 0, \tag{4.17b}$$

4.3 Method of solution

In this section, we discuss the implementation of the PQLM as described by Motsa and Animasaun [20] on the system of PDEs (4.13) − (4.16). Obtaining numerical solutions by means of the PQLM involves using the quasilinearization method to linearize functions and derivatives in pairs of equations from the system (4.13) − (4.16). Solutions from the first pair of equations are used in the subsequent pair, thereby reducing the system of equations into decoupled pairs. To discretize the decoupled system of coupled pairs in order obtain solutions, we then apply the bivariate Chebyshev spectral collocation method.

We first apply the quasilinearization method to nonlinear functions f'^2, $3ff'$, $f''\frac{\partial f}{\partial\zeta}$, $f'\frac{\partial f'}{\partial\zeta}$, $f\theta'$, $\theta'\frac{\partial f}{\partial\zeta}$ and $f'\frac{\partial\theta}{\partial\zeta}$ in equations (4.13) and (4.16) by using a one-step Taylor series expansion to obtain the linearized pair

$$\begin{aligned}
&\frac{1}{1-N}f'''_{r+1}-4f'_rf'_{r+1}+2f'^2_r+3f_rf''_{r+1}+3f''_rf_{r+1}\\
&-3f_rf''_r+2\zeta f''_r\frac{\partial f_{r+1}}{\partial\zeta}+2\zeta\frac{\partial f_r}{\partial\zeta}f''_{r+1}-2\zeta f''_r\frac{\partial f_r}{\partial\zeta}-2\zeta f'_r\frac{\partial f'_{r+1}}{\partial\zeta}\\
&-2\zeta\frac{\partial f'_r}{\partial\zeta}f'_{r+1}+2\zeta f'_r\frac{\partial f'_r}{\partial\zeta}+\theta_{r+1}+\frac{N}{1-N}\omega'_r-\frac{2M\zeta}{\beta_h^2+\beta_e^2}\zeta\beta_hf'_{r+1}-\frac{2M\zeta}{\beta_h^2+\beta_e^2}\zeta\beta_eg_r=0,
\end{aligned}\tag{4.18}$$

$$\begin{aligned}
&\frac{1}{Pr}\theta''_{r+1}+2\zeta\left[(Q-R_d)\,\theta_{r+1}+R_d\right]+3f_r\theta'_{r+1}+3\theta'_{r+1}f_{r+1}-3f_r\theta'_r+2\zeta\theta'_r\frac{\partial f_{r+1}}{\partial\zeta},\\
&+2\zeta\frac{\partial f_r}{\partial\zeta}\theta'_{r+1}-2\zeta\theta'_r\frac{\partial f_r}{\partial\zeta}-2\zeta f'_r\frac{\partial\theta_{r+1}}{\partial\zeta}-2\zeta\frac{\partial\theta_{r+1}}{\partial\zeta}f'_{r+1}+2\zeta f'_r\frac{\partial\theta_{r+1}}{\partial\zeta},
\end{aligned}\tag{4.19}$$

where terms containing the subscripts r and $r+1$ denote previous and current iteration levels, respectively. The pair (4.18) and (4.19) is expressed compactly as

$$\frac{1}{1-N}f'''_{r+1}+[a_1]\,f''_{r+1}+[a_2]\,f'_{r+1}+[a_3]\,f_{r+1}+\theta_{r+1}=[a_4]\,\frac{\partial f'_{r+1}}{\partial\zeta}+[a_5]\,\frac{\partial f_{r+1}}{\partial\zeta}+a_6,\tag{4.20}$$

$$[b_1]\,f'_{r+1}+[b_2]\,f_{r+1}+\frac{1}{Pr}\theta''_{r+1}+[b_3]\,\theta'_{r+1}+(b_4)\,\theta_{r+1}=[b_5]\,\frac{\partial f_{r+1}}{\partial\zeta}+[b_6]\,\frac{\partial\theta_{r+1}}{\partial\zeta}+b_7\tag{4.21}$$

where

$$\alpha_1 = \frac{2M}{\beta_h^2+\beta_e^2},\ \ a_1 = 3f_r+2\zeta\frac{\partial f_r}{\partial\zeta},\ \ a_2 = -4f_r^{'}-2\zeta\frac{\partial f_r^{'}}{\partial\zeta}-\alpha_1\zeta\beta_h,$$

$$a_3 = 3f_r^{''},\ \ a_4 = 2\zeta f_r^{'},\ \ a_5-2\zeta f_r^{''},$$

$$a_6 = -2f_r^{'2}-\frac{N}{1-N}\omega_r^{'}+3f_rf_r^{''}+2\zeta f_r^{''}\frac{\partial f_r}{\partial\zeta}-2\zeta f_r^{'}\frac{\partial f_r^{'}}{\partial\zeta}+\alpha_1\zeta\beta_e g_r,$$

$$b_1 = -2\zeta\frac{\partial\theta_r}{\partial\zeta},\ \ b_2 = 3\theta_r^{'},\ \ b_3 = 3f_r+2\zeta\frac{\partial f_r}{\partial\zeta},$$

$$b_4 = 2\zeta\left(Q-R_d\right),\ \ b_5 = -2\zeta\theta_r^{'},\ \ b_6 = 2\zeta f_r^{'},$$

$$b_7 = -2\zeta R_d+3f_r\theta_r^{'}+2\zeta\theta_r^{'}\frac{\partial f_r}{\partial\zeta}-2\zeta f_r^{'}\frac{\partial\theta_r}{\partial\zeta}$$

Solutions for $f,\ \theta$ and their corresponding derivatives are updated in the second pair of equations (4.14) and (4.15) that are observed to be linear and we obtain

$$\frac{1}{1-N}g_{r+1}^{''}+[c_1]\,g_{r+1}^{'}+[c_2]\,g_{r+1} = [c_3]\,\frac{\partial g_{r+1}}{\partial\zeta}+c_4, \tag{4.22}$$

$$\frac{N}{1-N}\frac{2-N}{m^2}\omega_{r+1}^{''}+[e_1]\,\omega_{r+1}^{'}+[e_2]\,\omega_{r+1} = [e_3]\,\frac{\partial\omega_{r+1}}{\partial\zeta}+e_4, \tag{4.23}$$

where

$$\alpha_2 = \frac{2NG_r^{-1/2}}{1-N},\ \ c_1 = 3f_{r+1}+2\zeta\frac{\partial f_{r+1}}{\partial\zeta},\ \ c_2 = -2f_{r+1}^{'}-\alpha_1\zeta\beta_h,$$

$$c_3 = 2\zeta f_{r+1}^{'}, c_4 = -\alpha_1\zeta\beta_e f_{r+1}^{'},\ \ e_1 = -a_j f_{r+1}^{'}+3a_j f_{r+1}+2\zeta\frac{\partial f_{r+1}}{\partial\zeta},$$

$$e_2 = 2\alpha_2\zeta,\ \ e_3 = 2a_j\zeta f_{r+1}^{'},\ \ e_4 = \alpha_2\zeta f_{r+1}^{''}.$$

The linear boundary conditions of pairs {(4.20) & (4.21)} and {(4.22) & (4.23)} are, respectively,

$$f_{r+1}^{'}(\zeta,0) = 0,\quad 3f_{r+1}(\zeta,0)+2\zeta\frac{\partial f_{r+1}(\zeta,0)}{\partial\zeta} = 0,$$

$$f_{r+1}^{'}(\zeta,\infty) = 0,\quad \theta_{r+1}(\zeta,0) = 1,\quad \theta_{r+1}(\zeta,\infty) = 0, \tag{4.24}$$

and

$$g_{r+1}(\zeta,0) = 0,\quad g_{r+1}(\zeta,\infty) = 0,\quad \omega_{r+1}(\zeta,0) = 0,\quad \omega_{r+1}(\zeta,\infty) = 0. \tag{4.25}$$

We note that the linearized system can be solved using a variety of numerical methods, but the PQLM involves Chebyshev spectral method for discretization. An in-depth description of Chebyshev spectral method is given by Boyd [16]. To solve the pairs {(4.20) & (4.21)} and {(4.22) & (4.23)}, we transform the physical domains of $\eta \in [0,\infty)$ and $\zeta \in [0,\infty)$ to $x \in [-1,1]$ and $t \in [-1,1]$, respectively. We approximate the solutions of $f(x,t)$, $g(x,t)$, $\omega(x,t)$ and $\theta(x,t)$ using the Lagrange interpolating polynomials of the form

$$\begin{aligned} f(x,t) &= \sum_{i=0}^{Mx}\sum_{j=0}^{Mt} f\left(x_i,t_j\right) L_i(x)L_j(t), \\ g(x,t) &= \sum_{i=0}^{Mx}\sum_{j=0}^{Mt} g\left(x_i,t_j\right) L_i(x)L_j(t), \\ \omega(x,t) &= \sum_{i=0}^{Mx}\sum_{j=0}^{Mt} \omega\left(x_i,t_j\right) L_i(x)L_j(t), \\ \theta(x,t) &= \sum_{i=0}^{Mx}\sum_{j=0}^{Mt} \theta\left(x_i,t_j\right) L_i(x)L_j(t), \end{aligned} \tag{4.26}$$

where L_i and L_j are Lagrange cardinal functions defined as

$$\begin{aligned} L_i(x) &= \prod_{i=0,i\neq k}^{M_x} \frac{x-x_k}{x_i-x_k}, \\ L_j(t) &= \prod_{j=0,j\neq k}^{M_t} \frac{t-t_k}{t_j-t_k}, \end{aligned} \tag{4.27}$$

where

$$\begin{aligned} L_i\left(x_k\right) = \delta_{ik} &= \begin{cases} 0 \text{ if } i \neq k \\ 1 \text{ if } i = k \end{cases}, \\ L_j\left(t_k\right) = \delta_{jk} &= \begin{cases} 0 \text{ if } j \neq k \\ 1 \text{ if } j = k \end{cases}. \end{aligned} \tag{4.28}$$

We choose Gauss-Chebyshev-Lobatto points as grid points x_i and t_j because they smoothly covert continuous time and spacial derivatives into discrete derivatives and we obtain these points from

$$\begin{aligned} x_i &= \cos\frac{\pi i}{M_x}, \quad i = 0,1,\ldots,M_x, \\ t_j &= \cos\frac{\pi j}{M_t}, \quad i = 0,1,\ldots,M_t. \end{aligned} \tag{4.29}$$

Differentiation matrices (denoted D and d) are used to collocate and are applied in the form

$$\begin{aligned}
\left.\frac{\partial f^{(p)}}{\partial x^{(p)}}\right|_{x_i,t_j} &= \mathbf{D}^{(p)}F_i, \quad \left.\frac{\partial f}{\partial t}\right|_{x_i,t_j} = \sum_{j=0}^{M_t}\mathbf{d}_{ij}F_j, \\
\left.\frac{\partial^{(p)} g}{\partial x^{(p)}}\right|_{x_i,t_j} &= \mathbf{D}^{(p)}G_i, \quad \left.\frac{\partial g}{\partial t}\right|_{x_i,t_j} = \sum_{j=0}^{M_t}\mathbf{d}_{ij}G_j, \\
\left.\frac{\partial^{(p)}\omega}{\partial x^{(p)}}\right|_{x_i,t_j} &= \mathbf{D}^{(p)}\Omega_i, \quad \left.\frac{\partial \omega}{\partial t}\right|_{x_i,t_j} = \sum_{j=0}^{M_t}\mathbf{d}_{ij}\Omega_j, \\
\left.\frac{\partial^{(p)}\theta}{\partial x^{(p)}}\right|_{x_i,t_j} &= \mathbf{D}^{(p)}\Theta_i, \quad \left.\frac{\partial \theta}{\partial t}\right|_{x_i,t_j} = \sum_{j=0}^{M_t}\mathbf{d}_{ij}\Theta_j,
\end{aligned} \tag{4.30}$$

where F, G, Ω and Θ are vectors of the form

$$\begin{aligned}
F &= \left[f\left(x_0,t_j\right), f\left(x_1,t_j\right), \ldots, f\left(x_{N_x},t_j\right)\right]^T, \\
G &= \left[g\left(x_0,t_j\right), g\left(x_1,t_j\right), \ldots, g\left(x_{N_x},t_j\right)\right]^T, \\
\Omega &= \left[\omega\left(x_0,t_j\right), \omega\left(x_1,t_j\right), \ldots, \omega\left(x_{N_x},t_j\right)\right]^T, \\
\Theta &= \left[\theta\left(x_0,t_j\right), \theta\left(x_1,t_j\right), \ldots, \theta\left(x_{N_x},t_j\right)\right]^T.
\end{aligned}$$

Substituting the representation given by equation (4.30) in the decoupled system of paired PDEs,we obtain

$$\begin{aligned}
A^i_{11}F_{r+1,i} - \left[\mathbf{a}^i_4\right]\sum_{j=0}^{M_t}\mathbf{d}_{i,j}\mathbf{D}F_{r+1,j} - \left[\mathbf{a}^i_5\right]\sum_{j=0}^{M_t}\mathbf{d}_{i,j}F_{r+1,j} + A^i_{12}\Theta_{r+1,i} &= \mathbf{R}_{1,i}, \\
A^i_{21}F_{r+1,i} - \left[\mathbf{b}^i_5\right]\sum_{j=0}^{M_t}\mathbf{d}_{i,j}F_{r+1,j} + A^i_{22}\Theta_{r+1,i} - \left[\mathbf{b}^i_6\right]\sum_{j=0}^{M_t}\mathbf{d}_{i,j}\Theta_{r+1,j} &= \mathbf{R}_{2,i},
\end{aligned} \tag{4.31}$$

and

$$\begin{aligned}
A^i_{31}G_{r+1,i} - \left[\mathbf{c}^i_3\right]\sum_{j=0}^{M_t}\mathbf{d}_{i,j}G_{r+1,j} + A^i_{32}\Omega_{r+1,i} &= \mathbf{R}_{3,i}, \\
A^i_{41}G_{r+1,i} + A^i_{42}\Omega_{r+1,i} - \left[\mathbf{e}^i_3\right]\sum_{j=0}^{M_t}\mathbf{d}_{i,j}\Omega_{r+1,j} &= \mathbf{R}_{4,i},
\end{aligned} \tag{4.32}$$

where each A^i are matrices of size $(M_{x+1})\times(M_{x+1})$, and $F_{r+1,i}$, $G_{r+1,i}$, $\Omega_{r+1,i}$, $\Theta_{r+1,i}$ and $\mathbf{R}_i$ are column matrices of size $(M_x+1)\times(1)$.

4.4 Results and discussion

In this section, we present the solution to the system of equations (4.13) − (4.16) generated using the PQLM. We also investigate the influence of radiation, heat source/sink, the Hall and ion effects on the respective profiles for velocity, temperature and microrotation.

To carry out an effective study, we conduct a grid-independence test to ensure an adequate number of grid points in space and time are used to generate convergent solutions to a tolerance level that is set to 9 decimal places. The results are shown below in Tables 4.1 and 4.2. Results in both tables were obtained using the values $N = 0.5,\ Pr = 0.71,\ Gr = 1,\ M = 3,\ m = 0.1,\ \beta_e = 1,\ \beta_i = 5,\ a_j = 1,\ Q = 0.002$ and $R_d = 0.001$.

Table 4.1: Spatial grid-independence test

M_x \ $M_t = 10$	$f''(\eta,0)$	$g'(\eta,0)$	$\theta'(\eta,0)$	$\omega'(\eta,0)$
20	0.380475520	0.011198327	-0.406938130	0.000442803
30	0.379850320	0.011196845	-0.40692110	0.000442760
40	0.379849990	0.011196844	-0.406921070	0.000442760
50	0.379849990	0.011196844	-0.406921070	0.000442760

Table 4.2: Time grid-independence test

M_t \ $M_x = 40$	$f''(\eta,0)$	$g'(\eta,0)$	$\theta'(\eta,0)$	$\omega'(\eta,0)$
5	0.379850000	0.011196781	-0.4069321210	0.000442871
10	0.379849990	0.011196844	-0.406921070	0.000442760
15	0.379849990	0.011196844	-0.406921070	0.000442760

It is observed from Tables 4.1 and 4.2 that to generate converged solutions to 9 decimal places, 40 grid points in space and 10 grid points in time are needed. These points are used in obtaining the

rest of the results displayed and we represent the semi-infinite domain $[0,\infty)$ with $[0,L=15]$.

4.4.1 Verification of results

In this section, we compare results obtained using the PQLM against those obtained with the bivariate spectral quasilinearization method (BSQLM), introduced by Motsa et al. [19]. The BSQLM involves quasilinearization of the nonlinear functions and their corresponding derivatives and solving the linearized system at the same time. Results were generated with values chosen as $N=0,\ Pr=0.72,\ Gr=1,\ m=0.1,\ M=0.6,\ \beta_e=1,\ \beta_i=0.1,\ a_j=0.01,\ Q=0.1$ and $R_d=0$.

Table 4.3: Comparison of skin friction $-f''(\xi=0,\zeta=0)$ generated using the PQLM and BSQLM.

PQLM	BSQLM
0.649147930	0.649147930

It is observed from the data in Table 4.3 that the solution obtained using the PQLM is consistent with that of the BSQLM. This shows the PQLM gives numerical solution results that are equally as accurate and precise as those from the BSQLM.

We also compare our result for $-\theta'(0)$ for two Prandtl numbers with those obtained by Abo-Eldahab and El Aziz [107] in Table 4.4 below. The values chosen were $N=0,\ Gr=1,\ m=0.1,\ M=0,\ \beta_e=0,\ \beta_i=0,\ a_j=0,\ Q=0$ and $R_d=0$.

Table 4.4: Comparison of $-\theta'(0)$ for an isothermal vertical plate with Prandtl numbers.

Pr	Abo-Eldahab and El Aziz [107]	PQLM
0.9	0.546501	0.546536130
0.5	0.441191	0.441166860

It is observed from Table 4.4 that the results generated using the PQLM is in good agreement with those obtained by Abo-Eldahab and El Aziz [107].

4.4.2 Convergence

To test convergence, we perform a solution error analysis. This is done by calculating the error between successive solutions as the number of iterations increases. The solution errors of Equations (4.13) − (4.16) are displayed in Figures 4.2 to 4.5 below. They were obtained from

$$||\Gamma||_\infty = \max_{0\leq i\leq N_y} ||\Gamma_{r+1,i} - \Gamma_{r,i}||_\infty , \tag{4.33}$$

where Γ represents F, G, Θ and Ω.

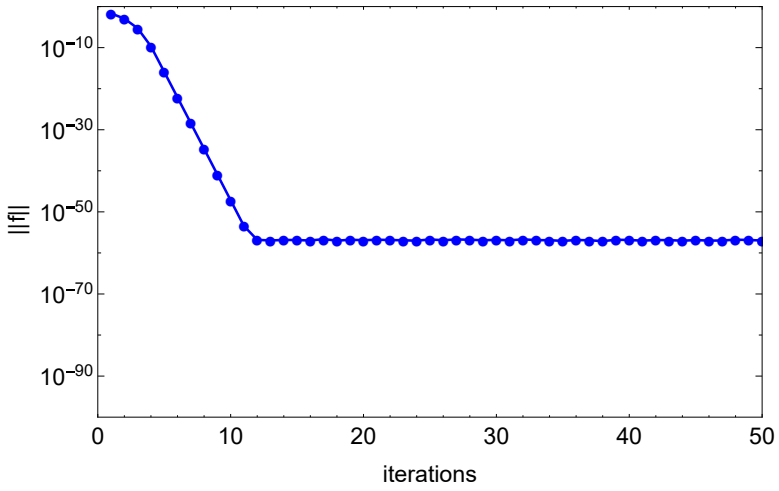

Figure 4.2: Effect of iterations on the solution error for F

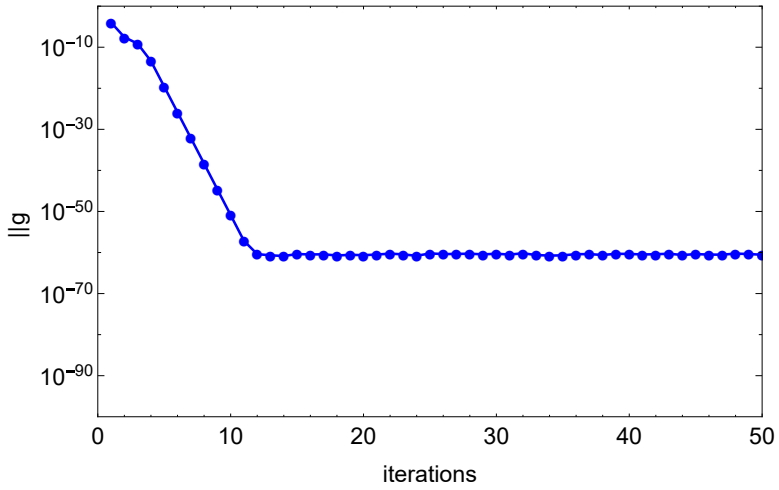

Figure 4.3: Effect of iterations on the solution error for G

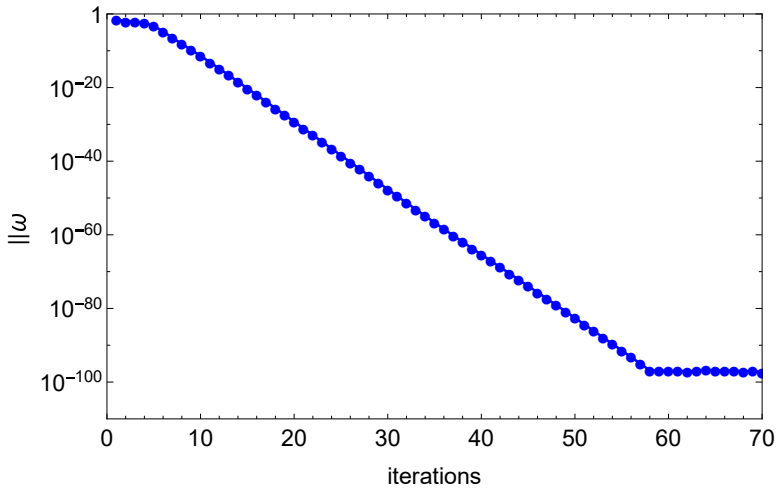

Figure 4.4: Effect of iterations on the solution error for ω

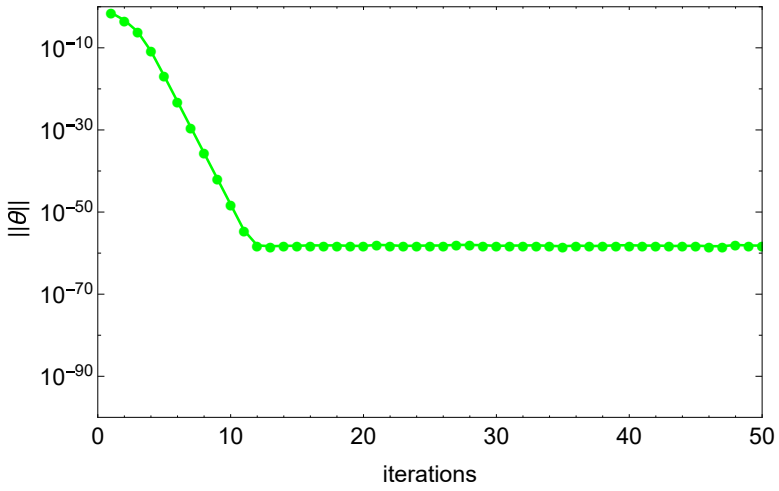

Figure 4.5: Effect of iterations on the solution error for θ

It is observed from Figures 4.2 to 4.5 that as iterations increase, there is a corresponding decrease in the error between successive iterations, until a point where further iteration has no further effect on the error. We say at this point that the method has converged, and we observe from the figures that the error at this point is very small.

4.4.3 Accuracy

Residual error is used in testing the closeness of numerical approximation to the exact solution. The residual error is generated by applying the approximate solutions obtained using the PQLM back into the original equations in the form

$$\mathbf{Res}(\mathbf{F}) = \max_{0\le i\le M_t}\left|\left|(1+K)\,\mathbf{f}_i^{'''}+K\omega_i^{'}-2\mathbf{f}_i^{'2}+3\mathbf{f}_i\mathbf{f}_i^{''}\right.\right.$$
$$\left.\left.+2\zeta\left(\mathbf{f}_i^{''}\frac{\partial\mathbf{f}_i}{\partial\zeta}-\mathbf{f}_i^{'}\frac{\partial\mathbf{f}_i^{'}}{\partial\zeta}\right)+\theta_i-\frac{2M\zeta}{\beta_h^2+\beta_e^2}\left[\beta_h\mathbf{f}_i^{'}+\beta_e\mathbf{g}_i\right]\right|\right|_\infty, \tag{4.34}$$

$$\mathbf{Res}(\mathbf{G}) = \max_{0\le i\le M_t}\left|\left|(1+K)\,\mathbf{g}_i^{''}-2\mathbf{f}_i^{'}\mathbf{g}_i+3\mathbf{f}_i\mathbf{g}_i^{'}+2\zeta\left(\mathbf{g}_i^{'}\frac{\partial\mathbf{f}_i}{\partial\zeta}-\mathbf{f}_i^{'}\frac{\partial\mathbf{g}_i}{\partial\zeta}\right)\right.\right.$$
$$\left.\left.-\frac{2M\zeta}{\beta_h^2+\beta_e^2}\left[\beta_e\mathbf{f}_i^{'}-\beta_h\mathbf{g}_i\right]\right|\right|_\infty, \tag{4.35}$$

$$\mathbf{Res}(\Omega) = \max_{0\le i\le M_t}\left|\left|\gamma\omega_i^{''}+\frac{2KG_r^{-1/2}}{a_j}\zeta\left(2\omega_i-\mathbf{f}_i^{''}\right)-\mathbf{f}_i^{'}\omega_i+3\mathbf{f}_i\omega_i^{'}+2\zeta\left(\omega_i^{'}\frac{\partial\mathbf{f}_i}{\partial\zeta}-\mathbf{f}^{'}\frac{\partial\omega_i}{\partial\zeta}\right)\right|\right|_\infty, \tag{4.36}$$

$$\mathbf{Res}(\Theta) = \max_{0\le i\le M_t}\left|\left|\theta_i^{''}+2Pr\zeta\left[(Q-R_d)\,\theta_i+R_d\right]+3Pr\mathbf{f}_i\theta_i^{'}+2Pr\zeta\left(\theta_i^{'}\frac{\partial\mathbf{f}_i}{\partial\zeta}-\mathbf{f}_i^{'}\frac{\partial\theta_i}{\partial\zeta}\right)\right|\right|_\infty. \tag{4.37}$$

The results are for effect of increasing iterations on the residual errors for the system (4.13) − (4.16) are shown in Figures 4.6 to 4.9

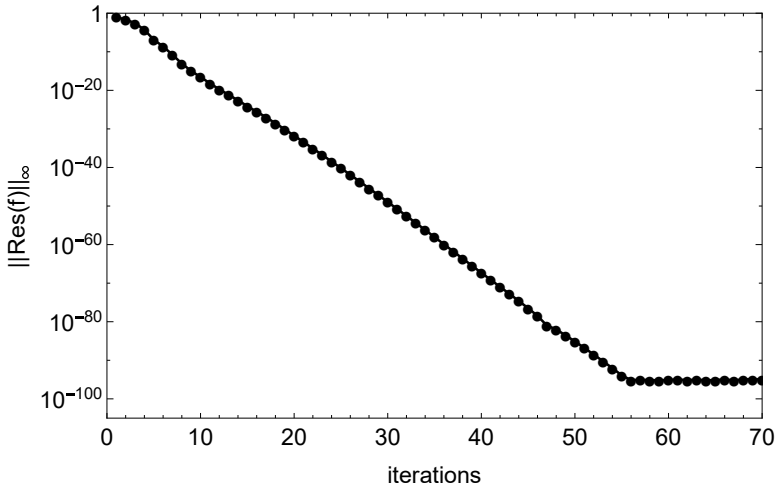

Figure 4.6: Effect of iterations on the residual error for θ

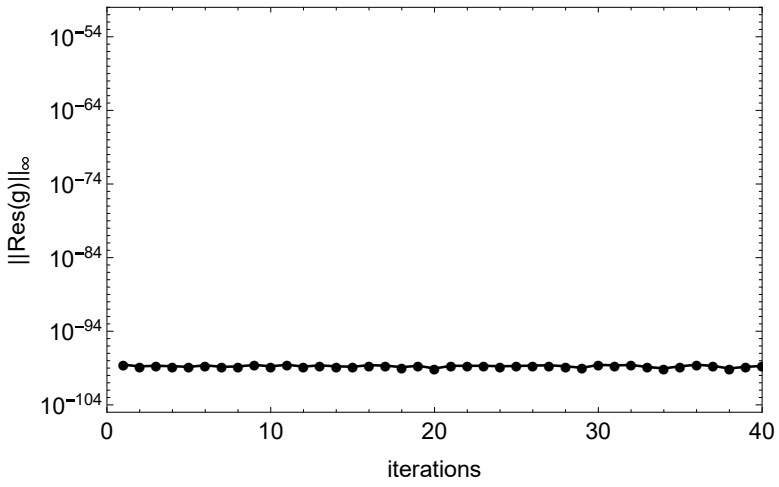

Figure 4.7: Effect of iterations on the residual error for θ

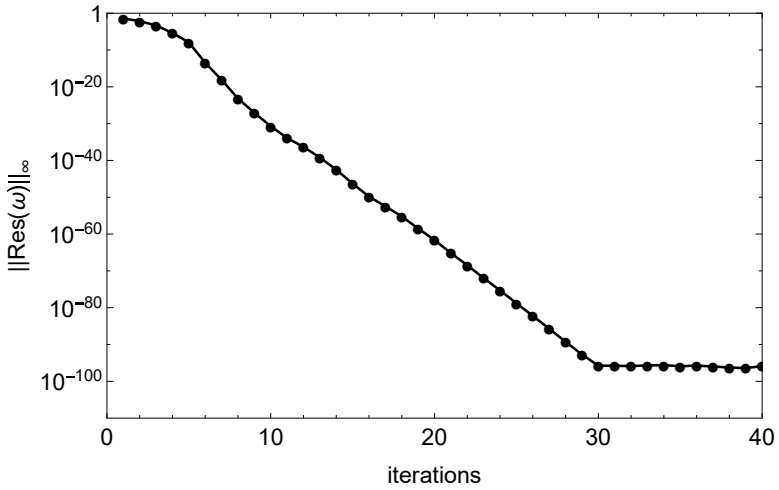

Figure 4.8: Effect of iterations on the residual error for θ

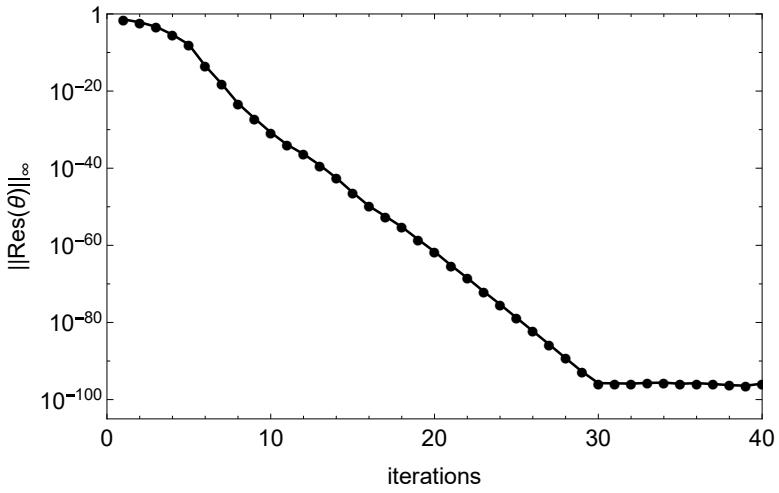

Figure 4.9: Effect of iterations on the residual error for θ

We observe from Figures 4.6 to 4.9 that the residual errors range between 10^{-95} and 10^{-100} and this finding shows the PQLM is an efficient method for solving fluid flow problems such as in this given system of equations. As we iterate further, the accuracy shown in Figures 4.6, 4.8 and 4.9 all improve until they converge, however, the accuracy of Figure 4.7 is seen to be consistent, which is a result of Equation (4.14) being linear in g and its derivatives.

4.4.4 Skin friction, wall shear stress and wall temperature gradient

The table displayed below is generated using the values $N = 0.5,\ Pr = 0.72,\ Gr = 1,\ m = 0.1,\ M = 3,$ and $a_j = 0.01$.

Table 4.5: Skin friction, wall shear stress and wall temperature gradient

β_i	β_e	R_d	Q	$f''(\zeta,0)$	$g'(\zeta,0)$	$\theta'(\zeta,0)$
0	2	0.5	0.25	0.439047190	0.220243940	0.220664870
1	2	0.5	0.25	0.514144260	0.092154159	0.173117860
3	2	0.5	0.25	0.575648250	0.028205931	0.136126550
5	2	0.5	0.25	0.600455680	0.013091335	0.122163130
2	0	0.5	0.25	0.334838890	0.075327620	0.325888190
2	1	0.5	0.25	0.495244240	0.052819281	0.186758460
2	3	0.5	0.25	0.580537630	0.039522869	0.133214190
2	5	0.5	0.25	0.606755300	0.028725222	0.118630380
2	2	0	0.25	0.415348440	0.030151710	-0.134384070
2	2	0.3	0.25	0.524728000	0.044746994	0.091000708
2	2	0.7	0.25	0.570860960	0.048965558	0.181194950
2	2	1	0.25	0.587471040	0.050496505	0.202387620
2	2	0.5	0	0.503324570	0.044443134	-0.140334920
2	2	0.5	0.1	0.522256140	0.045583395	-0.030575555
2	2	0.5	0.3	0.563752760	0.047945946	0.213920780
2	2	0.5	0.4	0.586416060	0.049165457	0.350245160

It is observed from the results in Table 4.5 that as the ion-slip parameter β_i is increased, $f''(\zeta,0)$ increases as well, while $g'(\zeta,0)$ and $\theta'(\zeta,0)$ both decrease. A similar pattern is observed to be the case when the Hall parameter β_e is increased; we see a corresponding increase for $f''(\zeta,0)$ and decrease for $g'(\zeta,0)$ and $\theta'(\zeta,0)$. This implies that as both β_i and β_e increase, the decrease in the temperature of the fluid increases viscosity thereby causing friction between the liquid and wall to

increase and the shear stress to decrease. As the radiation parameter R_d is increased, temperature around the wall of the plate and the fluid will increase. The fluid is being passed up a vertical plate so an increase in R_d combined with the direction of flow of the fluid will lead to a corresponding increase in the skin friction and shear stress. A similar trend can be seen when the heat source/sink parameter Q is increased. Figures 4.10 to 4.25 display the various effects of radiation, ion-slip, Hall and heat sink/source on the velocity, component velocity, microrotation and temperature profiles, respectively. In Figures 4.10 to 4.13, we observe the influence of the radiation parameter *Rd* on the various profiles.

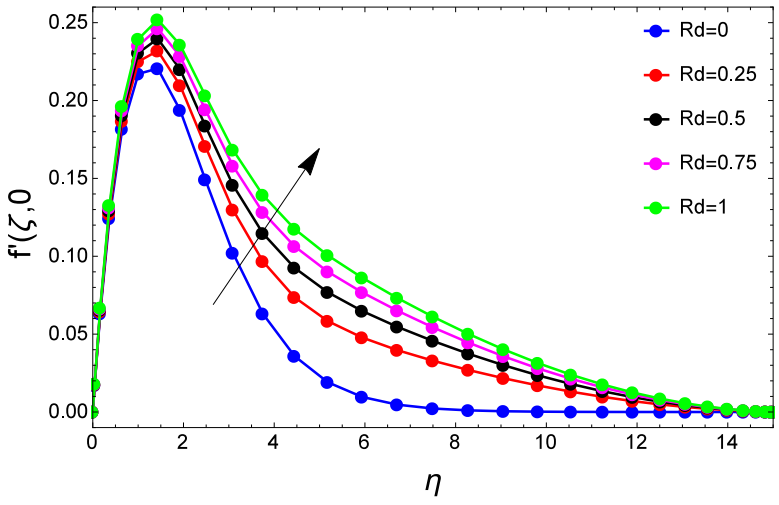

Figure 4.10: Effect of Radiation parameter R_d on velocity profile $f^{'}(\eta,0)$

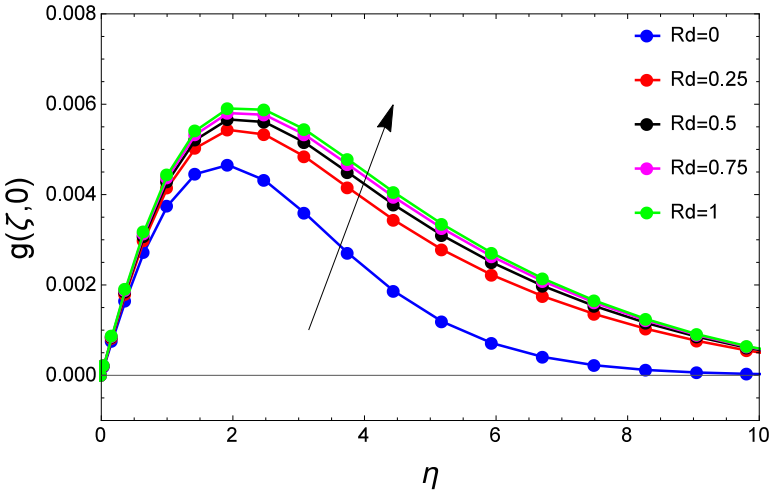

Figure 4.11: Effect of Radiation parameter R_d on component velocity profile $g(\eta,0)$

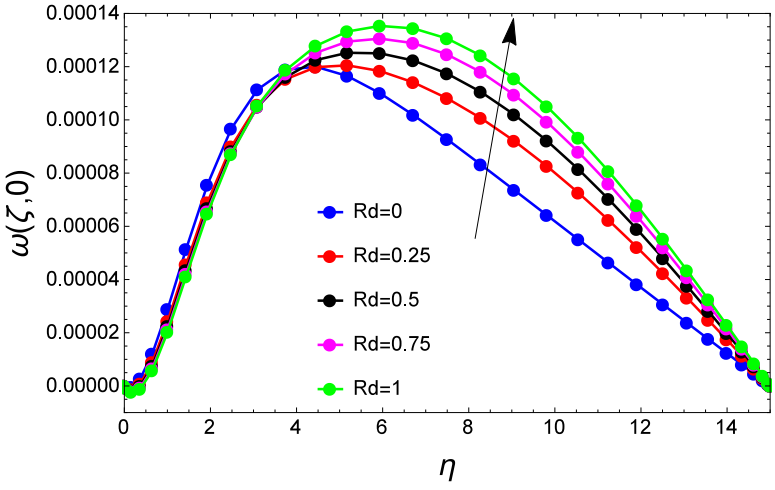

Figure 4.12: Effect of Radiation parameter R_d on microrotation profile $\omega(\eta,0)$

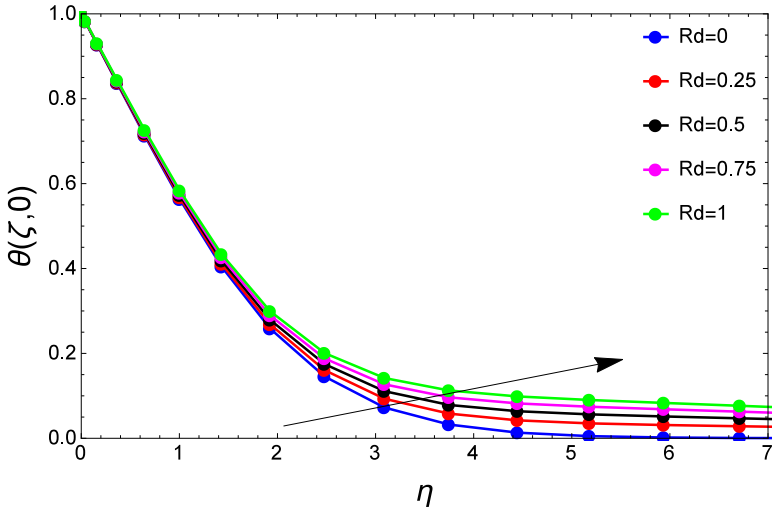

Figure 4.13: Effect of Radiation parameter R_d on temperature profile $\theta(\eta,0)$

We observe from Figures 4.10 to 4.13 that as radiation increases, the profiles all increase. This is because an increase in the radiation leads to more transfer of heat from the plate to the fluid and the boundary layer thickness hereby influencing the velocity, temperature and microrotation. We note from Figure 3.11 that in the absence of radiation, microrotation is at its highest point for $0 \leq \eta \leq 4$ and lowest for $0 \leq \eta \leq 15$.

In Figures 4.14 to 4.17, we observe the influence of the ion-slip parameter β_i on the various profiles.

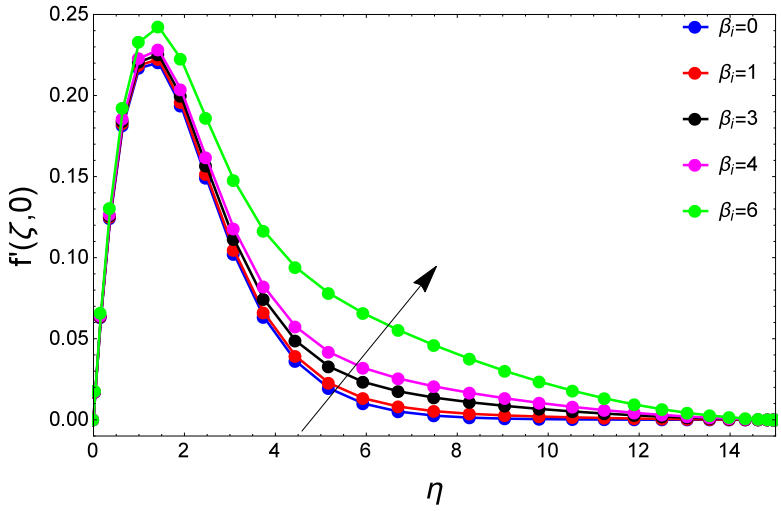

Figure 4.14: Effect of ion-slip parameter β_i on velocity profile $f^{'}(\eta,0)$

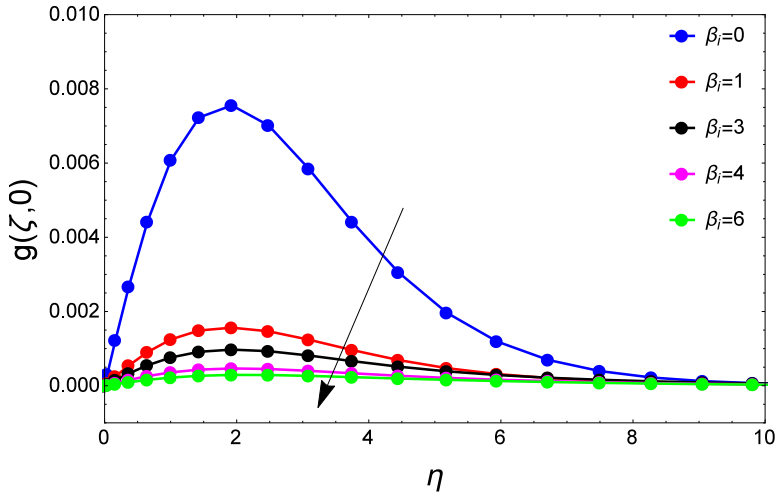

Figure 4.15: Effect of ion-slip parameter β_i on component velocity profile $g(\eta,0)$

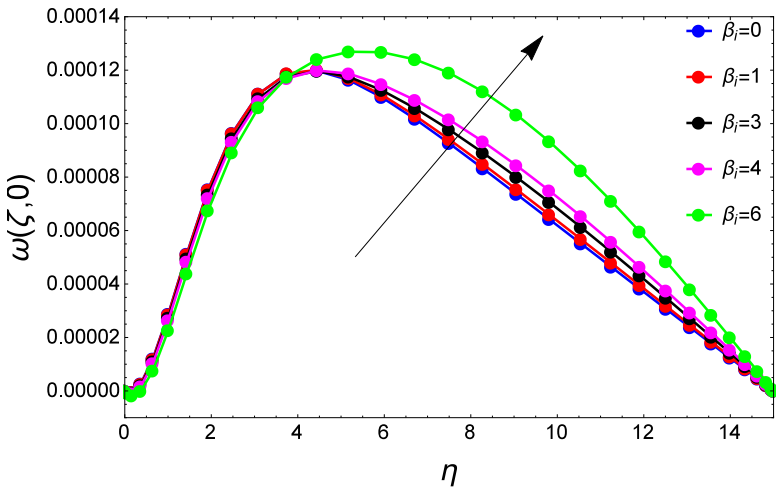

Figure 4.16: Effect of ion-slip parameter β_i on microrotation profile $\omega(\eta, 0)$

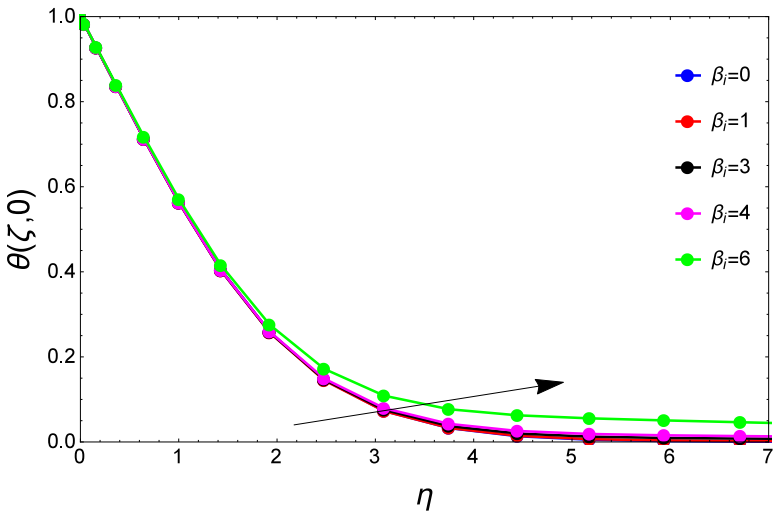

Figure 4.17: Effect of ion-slip parameter β_i on temperature profile $\theta(\eta, 0)$

The effects of the ion-slip parameter on the various flow profiles are observed in Figures 4.14 to 4.17. It is observed from Figure 4.15 that the induced flow in the z-direction decreases with increasing the ion-slip parameter. It is also observed that the introduction of the ion-slip on the component velocity greatly decreases the profile; the larger the parameter, the closer the profile gets to 0. However, for the velocity, temperature and microrotation, we see a reverse pattern. An increase in the ion-slip leads to a corresponding increase in the profiles for f', θ and ω. In Figure

4.16, we note that there seems to be no significant effect on the profiles for $\eta \in [0,4]$ but for $\eta > 4$, profiles steadily increase as β_i increases.

Figures 4.18 to 4.21 display the influence of the Hall parameter on the velocity, component velocity, microrotation and temperature profiles, respectively.

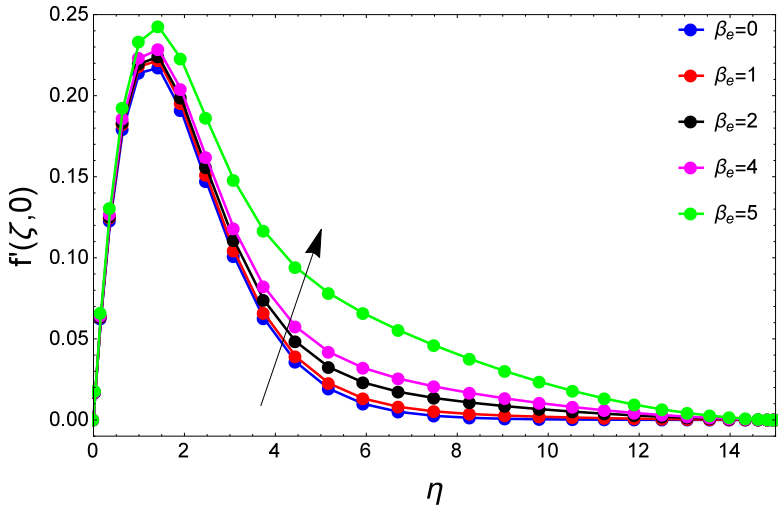

Figure 4.18: Effect of Hall parameter β_e on velocity profile $f^{'}(\eta,0)$

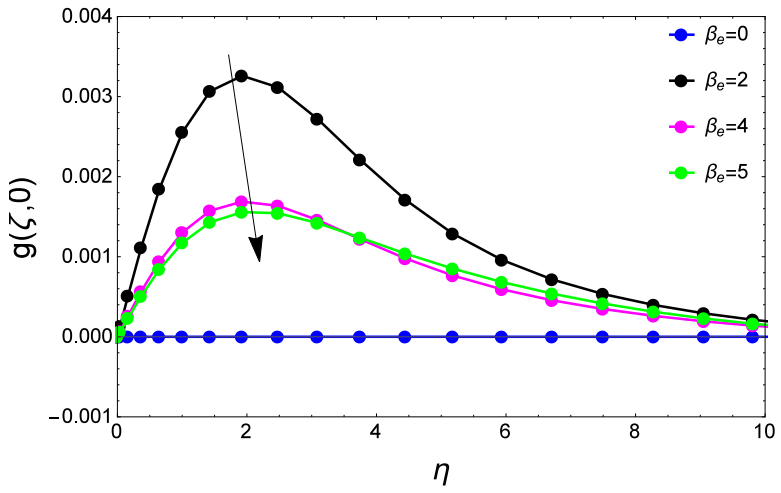

Figure 4.19: Effect of Hall parameter β_e on component velocity profile $g(\eta,0)$

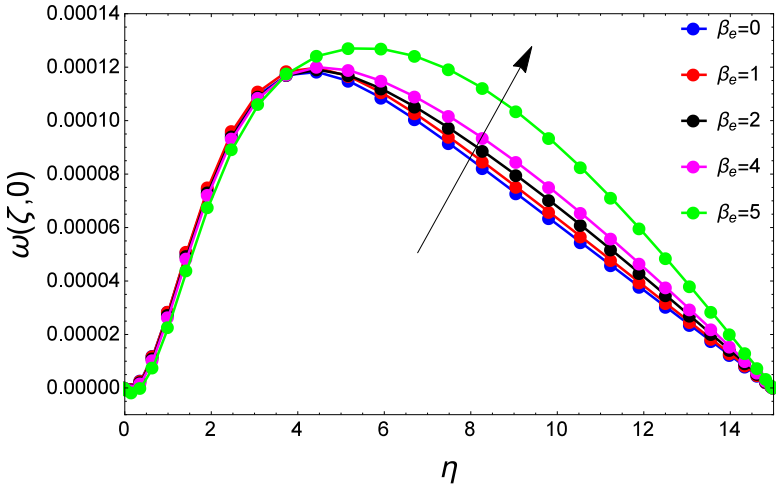

Figure 4.20: Effect of Hall parameter β_e on microrotation profile $\omega(\eta,0)$

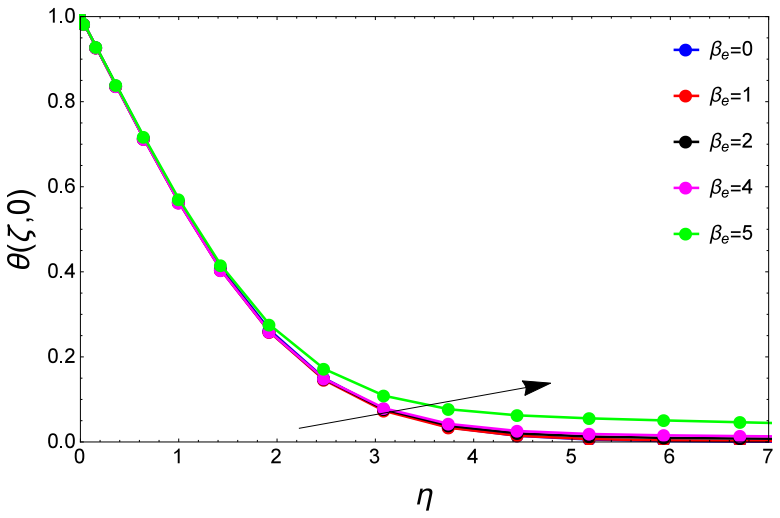

Figure 4.21: Effect of Hall parameter β_e on temperature profile $\theta(\eta,0)$

It is observed that as β_e increases, $f^{'}-$, $\omega-$ and $\theta-$profiles increase while Figure 4.19 shows that the larger β_e gets, the closer the profile gets to 0. We also see that the component velocity depends on the Hall parameter as we observe in Figure 4.19 that when $\beta_e = 0$, the component velocity $g = 0$ for all η. This happens because as the magnetic force terms approach zero for very large values of β_e (imposed magnetic field normal to the flow direction which gives rise to a resistive force and slows down the movement of the fluid is less). It is seen in Figure 4.20 that the Hall parameter has

significant effect on microrotation when $\eta > 0$.

Figures 4.22 to 4.25 display the effect of heat sink/source parameter Q on the profiles for velocity, component velocity, microrotation and temperature, respectively.

4.4.5 Effect of heat/sink source parameter Q

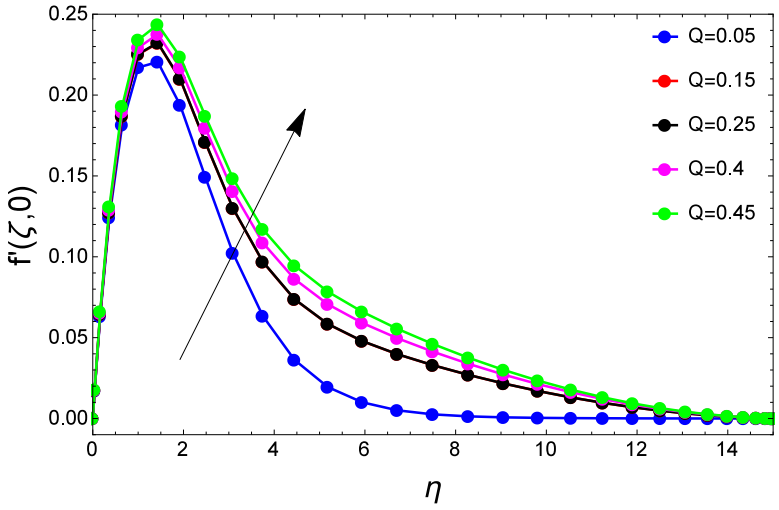

Figure 4.22: Effect of heat/sink source parameter Q on velocity profile $f^{'}(\eta,0)$

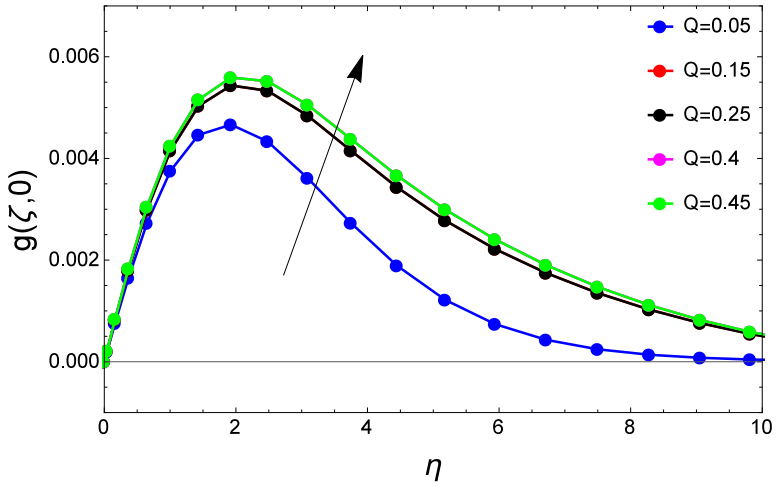

Figure 4.23: Effect of heat/sink source parameter Q component on velocity profile $g(\eta,0)$

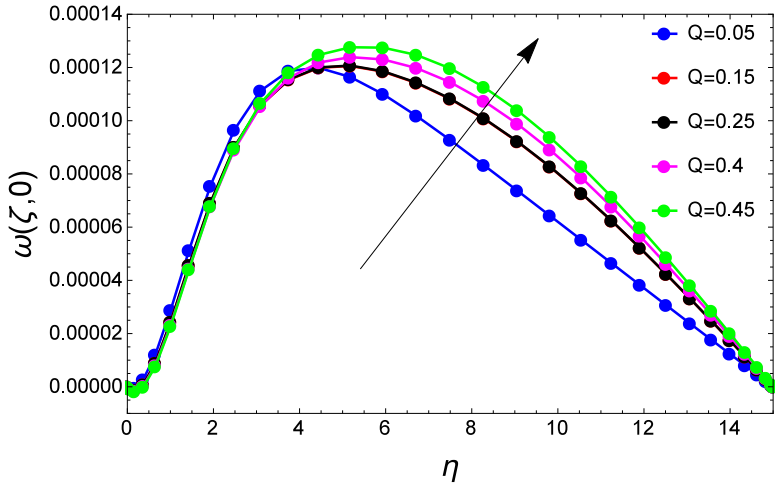

Figure 4.24: Effect of heat/sink source parameter Q on microrotation profile $\omega(\eta,0)$

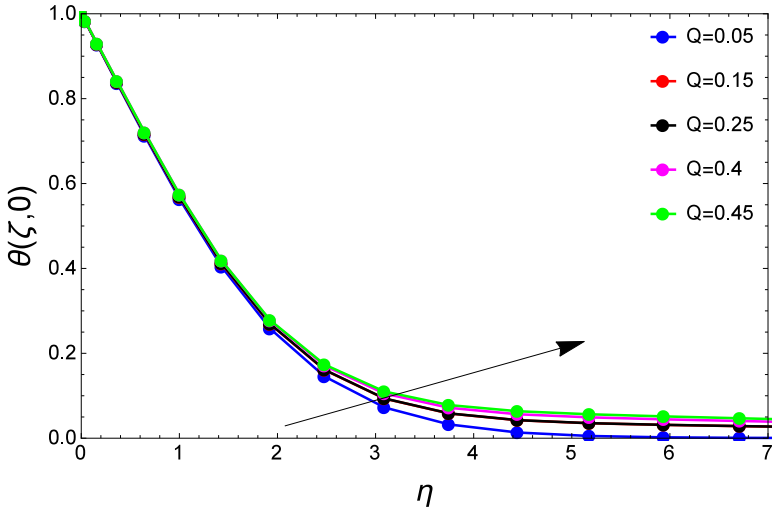

Figure 4.25: Effect of heat/sink source parameter Q on temperature profile $\theta(\eta,0)$

Internal heat generated increases the velocity profiles and temperature profiles. Physically when heat is absorbed, the buoyancy force decreases and retards the flow rate, which, thereby, gives rise to the decrease in the velocity profiles. As more heat is generated within the fluid, the fluid temperature increases the temperature gradient between the fluid and the plate surface. Increase in internal heat generation parameter increases the thermal boundary layer thickness.

4.5 Summary

In this study, an investigation was carried out on the combined influence of radiation, Hall and ion-slip effects on MHD free convective heat generating flow past a semi-infinite vertical flat plate. The governing equations were transformed to highly nonlinear partial differential equations using a similarity transformation and were solved numerically using the paired quasilinearization method (PQLM). The convergence and accuracy of the method were both verified. The physical effects of some parameters such as the heat source/sink parameter, radiation parameter, Hall and ion-slip parameters on the velocity, temperature, and microrotation profiles are shown and discussed in this study. The local skin-friction on both velocity components and local Nusselt number increase as the radiation parameter and heat source/sink parameters increase. It is also observed that the skin friction on main flow increases with increase in the Hall and ion-slip parameters whereas the skin friction caused by induced velocity component and on local Nusselt number decreases.

Chapter 5

Double diffusive mixed convection flow of a nanofluid near a vertical cone embedded in a porous medium with Soret and Dufour effects

5.1 Introduction

Many geothermal, geophysical and industrial applications have necessitated the study of double-diffusive convection by buoyancy due to temperature, concentration and nanoparticle gradients in a fluid-saturated porous medium. Such systems arise in the migration of moisture through air contained in fibrous insulations, underground spreading of chemical contaminants through water-saturated soil, separation processes in chemical industries and storage of radioactive nuclear waste etc. Theories and experiments on thermal convection in porous media with their practical applications are detailed in the books by Nield and Bejan [108], Vafai [109], Pop and Ingham [110], Ingham and Pop [111] and an article by Bejan and Khair [112].

There have been numerous studies concerning fluid flow in the presence of a cone. Cheng et al. [113] presented similarity and non-similarity solutions for a full and truncated cone, respectively, in natural convection flow in a porous medium at high Rayleigh numbers. Yih [114] reported a

study on natural convection flow with buoyancy effects alongside a truncated cone in a saturated medium. Chamkha et al. [115] performed a boundary layer analysis on the hydromagnetic natural convection flow over a vertical cone and wedge embedded in a uniform porous medium. The concept of selecting a proper realm for the flow type and geometry is central for relevant to the real-life applications. Design and erection of several types of industrial equipment like heat exchangers for thermal cooling processes, canisters designed to store nuclear waste disposal and fluid flow mechanics in geothermal reservoirs, depend on first understanding the applications of convective heat and mass transfer over a rotating cone and a flat plate. A mathematical formulation for wing-body combinations for aircraft at supersonic speeds was first lodged by Woodward [116]. Taking this into account, an exact finite-difference solution for the problem was developed by Thomas et al. [117] for steady inviscid, supersonic flow over smooth three dimensional bodies. This inspired Lin and Rubin [118], to investigate numerically, three-dimensional flow over a cone at some moderate incidence by considering the viscous dissipation effects. Vigneron et al. [119] extended Lin and Rubin's [118] work and studied the flow over a sharp subsonic edge (having a geometric structure of a sharp-edged of the cone) by using the central approximation scheme.

Following the pioneering works mentioned above, researchers have initiated rigorous studies on different types of fluid flow over conical structures under various conditions. The steady free convection boundary layer flow over a vertical cone embedded in a porous medium filled with a non-Newtonian fluid with an exponential decaying internal heat generation was investigated by Grosan [120]. Cheng [121] examined non-similar boundary layer analysis about variable viscosity effects on the double-diffusive convection near a vertical truncated cone in a fluid-saturated porous medium with constant wall temperature and concentration. Hady et al. [122] studied the effect of heat generation/absorption on natural convection boundary layer flow over a downward-pointing vertical cone in a porous medium saturated with a non-Newtonian nanofluid in the presence of heat generation/absorption. Awad et al. [123] determined numerical solutions for convection from an inverted cone in a porous medium with cross-diffusion in the presence of Dufour energy flux and Soret mass effects. Khan and Aziz [124] studied double-diffusive natural convective boundary

layer flow in a porous medium saturated with a nanofluid over a vertical plate, considering prescribed surface heat, solute, and nanoparticle fluxes. An analysis of the effect of uniform transpiration velocity on free convection boundary layer flow of a non-Newtonian fluid over a permeable vertical cone embedded in a porous medium saturated with a nanofluid was scrutinized by Rashad et al. [125]. Chamkha and Rashad [126] considered the problem of natural convection boundary layer flow over a permeable vertical cone embedded in a porous medium saturated with a nanofluid, subjected to uniform heat and nanoparticles volume fraction fluxes in the presence of a uniform lateral mass flux effect. Cheng [127] studied the natural convection boundary layer flow over a truncated cone embedded in a porous medium saturated by a nanofluid with constant wall temperature and constant wall nanoparticle volume fraction. The problem of steady, laminar, mixed convection boundary layer flow over a vertical cone embedded in a porous medium saturated with a nanofluid was studied by Chamkha et al. [128] in the presence of thermal radiation incorporating the effects of Brownian motion and thermophoresis with Rosseland diffusion approximation.

The effect of uniform lateral mass flux on non-Darcy natural convection flow for a non-Newtonian nanofluid over cone saturated in a porous medium with uniform heat and volume fraction fluxes was investigated by Chamkha et al. [129]. A numerical investigation was carried out by Raju and Sandeep [130] to analyze the flow, heat, and mass transfer characteristics of gyrotactic microorganisms contained in magneto-hydrodynamic Casson fluid flow towards a vertical rotating cone/plate in a porous medium. Siddiqa et al. [131] presented numerical results for the natural convection flow of a two-phase dusty nanofluid along a vertical wavy frustum of a cone. Khan et al. [132] examined the influence of chemically reactive species and mixed convection on the magnetohydrodynamic (MHD) Williamson nanofluid induced by a non-isothermal cone and plate in a porous medium. Raju et al. [133] carried out numerical simulations to investigate the effect of viscous dissipation, temperature dependent viscosity and heat source/sink on a magnetohydrodynamic (MHD) unsteady Carreaue nanofluid over a cone filled with different alloy nanoparticles. Sulochana et al. [134] investigated the flow, heat, and mass transfer behavior of magnetohydrodynamic flow over a vertical rotating cone through a porous medium in the presence of thermal radiation, chemical reaction and Soret effects. The natural convective flow of an electrically conducting nanofluid

adjacent to a spinning downward-pointing vertical cone in the presence of a transverse magnetic field was studied by Mohammad et al. [135], considering three different types of water-based nanofluid with copper, aluminium oxide (alumina) and titanium dioxide (titania) as nanoparticles. The laminar free-convective flow and heat transfer of an electrically conducting nanofluid in the presence of a transverse magnetic field over a rotating down-pointing vertical cone was examined by Dinarvand and Pop [136].

The present analysis broadens the work by Khan and Aziz [124] in considering the flow over an isothermal cone with Soret and Dufour effects. The coupled nonlinear partial differential equations representing the flow are non-dimensionalized and put into the homogeneous form. An authentic numerical result of highly non-linear partial differential equations is obtained using the paired quasi-linearization method (PQLM). The PQLM [20, 137] is a numerical method that makes use of quasilinearization to linearize two functions and their corresponding derivatives from a system of differential equations. This process effectively decouples the system into smaller subsystems/pairs that are solved using the spectral collocation method. The convergence and accuracy of the PQLM is confirmed by performing solution and residual error analysis, respectively. Modification of the flow, heat and mass transfer by different controlling parameter are presented by means of graphs.

5.2 Mathematical Formulation

Consider two-dimensional steady buoyancy induced Darcy's flow of a viscous incompressible nanofluid along an isothermal vertical cone embedded in the porous medium. The $x-$ and $y-$ axes are taken along and normal to the inclined surface, respectively. The present formulation permits the angle of inclination to range from 0 to close to $\pi/2$ radians from the horizontal. The surface of the sheet is maintained at uniform temperature and concentration, T_w and C_w, respectively, and these values are assumed to be greater than the ambient temperature and concentration, T_∞ and C_∞, respectively. It is assumed that both the fluid phase and nanoparticles are in a state of thermal equilibrium. Further, we assume that

1. the physical properties are constant except for the density variation with the body force,

2. the flow is sufficiently slow that the convective fluid and the porous matrix are in local thermodynamic equilibrium, and

3. the Boussinesq approximation applies.

Under the given assumptions, the boundary layer equations governing the flow are as follows:

The continuity equation

$$\frac{\partial(ru)}{\partial x}+\frac{\partial(rv)}{\partial y}=0. \tag{5.1}$$

The momentum equation

$$\frac{\partial u}{\partial y}=\frac{(1-C_\infty)\rho_{f\infty}g_1 K cos\gamma}{\mu}\left(\beta_T\frac{\partial T}{\partial y}+\beta_C\frac{\partial C}{\partial y}\right)-\frac{(\rho_p-\rho_{f\infty})g_1 K cos\gamma}{\mu}\frac{\partial\phi}{\partial y}. \tag{5.2}$$

The energy equation

$$u\frac{\partial T}{\partial x}+v\frac{\partial T}{\partial y}=\alpha\frac{\partial^2 T}{\partial y^2}+\tau\left[D_B\frac{\partial\phi}{\partial y}\frac{\partial T}{\partial y}+\frac{D_T}{T_\infty}\left(\frac{\partial T}{\partial y}\right)^2\right]+\sigma D_{TC}\frac{\partial^2 C}{\partial y^2}. \tag{5.3}$$

The concentration equation

$$u\frac{\partial C}{\partial x}+v\frac{\partial C}{\partial y}=D_{SM}\frac{\partial^2 C}{\partial y^2}+D_{CT}\frac{\partial^2 T}{\partial y^2}. \tag{5.4}$$

The nanoparticle concentration equation

$$u\frac{\partial\phi}{\partial x}+v\frac{\partial\phi}{\partial y}=D_B\frac{\partial^2\phi}{\partial y^2}+\frac{D_T}{T_\infty}\frac{\partial^2 T}{\partial y^2}, \tag{5.5}$$

where u and v are velocity components along x and y directions, respectively.
$g_1,\beta,K,\alpha,\nu,\rho,c,(\rho c)_p,(\rho c)_f,D_B,D_T,\tau,D_{ct},D_{tc}$ and D_{sm} are, respectively, acceleration due to gravity, coefficient of thermal expansion, permeability of the porous medium, thermal diffusivity, kinematic viscosity, mass density, specific heat, effective heat capacity of the nanoparticle material,

heat capacity of the fluid, Brownian diffusion coefficient, thermophoresis diffusion coefficient, a parameter defined by $(\rho c)_p / (\rho c)_f$, Soret diffusivity, Dufour diffusivity and solutal diffusivity of the porous medium.

The associated boundary conditions are

$$\text{At } y = 0: \; v = 0; \; T = T_w; \; C = C_w, \; \phi = \phi_w, \tag{5.6}$$

$$\text{As } y \to \infty: \; u = U_\infty; \; T = T_\infty; \; C = C_\infty; \; \phi = \phi_\infty. \tag{5.7}$$

Now, we introduce the following group of transformations:

$$\left.\begin{aligned} &\eta = (y/x)\,(Pe_x)^{1/2}\chi^{-1}, \; \chi = \left\{1+\left(\frac{Ra_x}{Pe_x}\right)^{1/2}\right\}^{-1}, \\ &\psi(x,y) = \alpha(Pe_x)^{1/2}\chi^{-1}S(\eta,\chi), \\ &\theta(\eta,\chi) = \frac{T-T_\infty}{T_w-T_\infty}, \; h(\eta,\chi) = \frac{C-C_\infty}{C_w-C_\infty}, \; g(\eta,\chi) = \frac{\phi-\phi_\infty}{\phi_w-\phi_\infty}, \end{aligned}\right\} \tag{5.8}$$

where $f(\eta,\chi)$ is the stream function satisfying continuity equation, $\theta(\eta,\chi)$ is dimensionless temperature, $g(\eta,\chi)$ is dimensionless concentration function. m is the mixed convection parameter, η is the similarity variable,
$Ra_x = \left\{(1-\phi_\infty)\rho_{f_\infty} g_1 \beta_T K(T_w-T_\infty)x\right\}/(\mu\alpha)$ and $Pe_x = U_\infty x/\alpha$ are the modified local thermal

Rayleigh and local Peclet number, respectively. Equations (5.2) − (5.5), under the transformation (5.8), take the form

$$\frac{\partial^2 S}{\partial \eta^2} = (1-\chi)^2 \left\{ \frac{\partial \theta}{\partial \eta} + Nc \frac{\partial h}{\partial \eta} - Nr \frac{\partial g}{\partial \eta} \right\}, \tag{5.9}$$

$$\frac{\partial^2 \theta}{\partial \eta^2} + 0.5(1+m\chi) S \frac{\partial \theta}{\partial \eta} + Nb \frac{\partial g}{\partial \eta} \frac{\partial \theta}{\partial \eta} + Nt \left(\frac{\partial \theta}{\partial \eta} \right)^2 + Nd \frac{\partial^2 h}{\partial \eta^2} = \tag{5.10}$$
$$0.5m\chi(1-\chi) \left\{ \frac{\partial S}{\partial \eta} \frac{\partial \theta}{\partial \chi} - \frac{\partial \theta}{\partial \eta} \frac{\partial S}{\partial \chi} \right\},$$

$$\frac{\partial^2 h}{\partial \eta^2} + 0.5Le(1+m\chi) S \frac{\partial h}{\partial \eta} + Ld \frac{\partial^2 \theta}{\partial \eta^2} = \tag{5.11}$$
$$0.5mLe\chi(1-\chi) \left\{ \frac{\partial S}{\partial \eta} \frac{\partial h}{\partial \chi} - \frac{\partial h}{\partial \eta} \frac{\partial S}{\partial \chi} \right\},$$

$$\frac{\partial^2 g}{\partial \eta^2} + 0.5Ln(1+m\chi) S \frac{\partial g}{\partial \eta} + \frac{Nt}{Nb} \frac{\partial^2 \theta}{\partial \eta^2} = \tag{5.12}$$
$$0.5mLn\chi(1-\chi) \left\{ \frac{\partial S}{\partial \eta} \frac{\partial g}{\partial \chi} - \frac{\partial g}{\partial \eta} \frac{\partial S}{\partial \chi} \right\},$$

and the associated boundary conditions become

$$(1+m\chi) S(0,\chi) + m\chi(1-\chi) \frac{\partial S(0,\chi)}{\partial \chi} = 0,\ \theta(0,\chi) = 1, \tag{5.13}$$

$$h(0,\chi) = 1,\ g(0,\chi) = 1, \tag{5.14}$$

$$\frac{\partial S(\infty,\chi)}{\partial \eta} = \chi^2,\ \theta(\infty,\chi) = 0,\ h(\infty,\chi) = 0,\ g(\infty,\chi) = 0, \tag{5.15}$$

where

$$\left.\begin{aligned} Nr &= \frac{(\rho_p - \rho_{f_\infty})(\phi_w - \phi_\infty)}{\rho_{f_\infty} \beta_T (T_w - T_\infty)(1-\phi_\infty)}, \\ Nb &= \frac{\tau D_B (\phi_w - \phi_\infty)}{\alpha},\ Ln = \frac{\alpha}{D_B},\ Le = \frac{\alpha}{D_{sm}}, \\ Nt &= \frac{\tau D_T (T_w - T_\infty)}{\alpha T_\infty},\ Ld = \frac{D_{ct}(T_w - T_\infty)}{D_{sm}(C_w - C_\infty)}, \\ Nd &= \frac{\sigma D_{tc}(C_w - C_\infty)}{\alpha (T_w - T_\infty)}, Nc = \frac{\beta_C (C_w - C_\infty)}{\beta_T (T_w - T_\infty)}, \end{aligned}\right\} \text{governing parameters}$$

where $Nr, Nb, Nt, Le, Ln, Ld, Nd$ and Nc are, respectively, buoyancy ratio, Brownian motion parameter, thermophoresis parameter, Lewis number, nanofluid Lewis number, Dufour-solutal Lewis number, modified Dufour parameter and regular double diffusive buoyancy parameter.

The physical quantities of interest, the local skin friction coefficient Cf_x, the local Nusselt number Nu_x, the local Sherwood number Sh_x, and the local nanofluid Sherwood number Sh_{xn} are defined as:

$$Nu_x \left(Pe_x^{1/2}+Ra_x^{1/2}\right)^{-1} = -\frac{\partial\theta}{\partial\eta}\bigg|_{\eta=0}, \tag{5.16}$$

$$Sh_x \left(Pe_x^{1/2}+Ra_x^{1/2}\right)^{-1} = -\frac{\partial h}{\partial\eta}\bigg|_{\eta=0}, \tag{5.17}$$

$$Sh_{xn} \left(Pe_x^{1/2}+Ra_x^{1/2}\right)^{-1} = -\frac{\partial g}{\partial\eta}\bigg|_{\eta=0}. \tag{5.18}$$

5.3 Method of solution

In this section, we discuss the application of the paired quasilinearization method (PQLM) on the system of partial differential equations (5.9) − (5.12). We express equations (5.9) − (5.12) as

$$s'' - (1-\chi)^2\theta' - Nc(1-\chi)^2 h' + Nr(1-\chi)^2 g' = 0, \tag{5.19}$$

$$\theta'' + 0.5(1+m\chi)s\theta' + Nbg'\theta' + Nt\theta'^2 + Ndh'' = \tag{5.20}$$
$$0.5m\chi(1-\chi)\left(s'\frac{\partial\theta}{\partial\chi} - \theta'\frac{\partial s}{\partial\chi}\right),$$

$$h'' + 0.5Le(1+m\chi)sh' + Ld\theta'' = 0.5mLe\chi(1-\chi)\left(s'\frac{\partial h}{\partial\chi} - h'\frac{\partial s}{\partial\chi}\right), \tag{5.21}$$

$$g'' + 0.5Ln(1+m\chi)sg' + \frac{Nt}{Nb}\theta'' = 0.5mLn\chi(1-\chi)\left(s'\frac{\partial g}{\partial\chi} - g'\frac{\partial s}{\partial\chi}\right), \tag{5.22}$$

and the associated boundary conditions become

$$(1+m\chi)s(0,\chi) + m\chi(1-\chi)\frac{\partial s(0,\chi)}{\partial\chi} = 0,\ \theta(0,\chi) = 1, \tag{5.23}$$

$$h(0,\chi) = 1,\ g(0,\chi) = 1,$$

$$s'(\infty,\chi) = \chi^2,\ \theta(\infty,\chi) = 0,\ h(\infty,\chi) = 0,\ g(\infty,\chi) = 0, \tag{5.24}$$

where $s,\ \theta,\ ,h\ \&\ g$ are functions of η and χ, and $'$ denotes differentiation with respect to η.

We next present the PQLM numerical scheme for solving the nonlinear system of equations. The PQLM involves solving two functions from two equations simultaneously and using their updated

solutions in subsequent equation pairs. Based on findings by Otegbeye and Motsa [137], we apply linearization on equations (5.19) and (5.20) for s, θ, and their corresponding derivatives. Linearization is performed using the Taylor series expansion to the first order and we obtain

$$s''_{r+1}+(a_1)\,\theta'_{r+1}=a_2, \tag{5.25}$$

$$[b_1]\,s'_{r+1}+[b_2]\,s_{r+1}+\theta''_{r+1}+[b_3]\,\theta'_{r+1}=[b_4]\,\frac{\partial s_{r+1}}{\partial\chi}+[b_5]\,\frac{\partial\theta_{r+1}}{\partial\chi}+b_6, \tag{5.26}$$

where

$$\begin{aligned}
&a_1=-1(1-\chi)^2,\ \ a_2=Nc(1-\chi)^2h'_r-Nr(1-\chi)^2g'_r,\\
&b_1=-0.5m\chi(1-\chi)\frac{\partial\theta_r}{\partial\chi},\ \ b_2=0.5(1+m\chi)\theta'_r,\\
&b_3=0.5(1+m\chi)s_r+Nbg'_r+2Nt\theta'_r+0.5m\chi(1-\chi)\frac{\partial s_r}{\partial\chi},\\
&b_4=-0.5m\chi(1-\chi)\theta'_r,\ \ b_5=0.5m\chi(1-\chi)s'_r,\\
&b_6=0.5(1+m\chi)s_r\theta'_r+Nt\theta'^2_r-Ndh''_r\\
&\qquad -0.5m\chi(1-\chi)s'_r\frac{\partial\theta_r}{\partial\chi}+0.5m\chi(1-\chi)\theta'_r\frac{\partial s_r}{\partial\chi}.
\end{aligned}$$

We express the second equation pair, (5.21) and (5.22), compactly as

$$h''_{r+1}+[c_1]\,h'_{r+1}=[c_2]\,\frac{\partial h_{r+1}}{\partial\chi}+c_3, \tag{5.27}$$

$$g''_{r+1}+[e_1]\,g'_{r+1}=[e_2]\,\frac{\partial g_{r+1}}{\partial\chi}+e_3, \tag{5.28}$$

where

$$\begin{aligned}
&c_1=0.5Le(1+m\chi)s_{r+1}+\ 0.5mLe\chi(1-\chi)\frac{\partial s_{r+1}}{\partial\chi},\\
&c_2=0.5mLe\chi(1-\chi)s'_{r+1},\ \ c_3=-Ld\theta''_{r+1},\\
&e_1=0.5Ln(1+m\chi)s_{r+1}+0.5mLn\chi(1-\chi)\frac{\partial s_{r+1}}{\partial\chi},\\
&e_2=0.5mLn\chi(1-\chi)s'_{r+1},\ \ e_3=-\frac{Nt}{Nb}\theta''_{r+1}.
\end{aligned}$$

The linearized system is solved using the Chebyshev spectral method. Boyd [16] gives more explanation on the implementation of spectral methods.

To solve the pairs {(5.25) and (5.26)} and {(5.27) and (5.28)}, we begin by transforming the physical domains of $\eta \in [0,\infty)$ and $\chi \in [0,1)$ to $x \in [-1,1]$ and $t \in [-1,1]$, respectively. The solutions of $s(x,t),\ g(x,t),\ \theta(x,t)$ and $h(x,t)$ are approximated using the Lagrange interpolating polynomials of the form

$$\begin{aligned}
s(x,t) &= \sum_{i=0}^{Mx}\sum_{j=0}^{Mt} s\left(x_i,t_j\right) L_i(x)L_j(t),\\
g(x,t) &= \sum_{i=0}^{Mx}\sum_{j=0}^{Mt} g\left(x_i,t_j\right) L_i(x)L_j(t),\\
h(x,t) &= \sum_{i=0}^{Mx}\sum_{j=0}^{Mt} h\left(x_i,t_j\right) L_i(x)L_j(t),\\
\theta(x,t) &= \sum_{i=0}^{Mx}\sum_{j=0}^{Mt} \theta\left(x_i,t_j\right) L_i(x)L_j(t),
\end{aligned} \tag{5.29}$$

where L_i and L_j are Lagrange cardinal functions defined as

$$\begin{aligned}
L_i(x) &= \prod_{i=0,i\neq k}^{M_x} \frac{x-x_k}{x_i-x_k},\\
L_j(t) &= \prod_{j=0,j\neq k}^{M_t} \frac{t-t_k}{t_j-t_k},
\end{aligned} \tag{5.30}$$

where

$$\begin{aligned}
L_i\left(x_k\right) = \delta_{ik} &= \begin{cases} 0 \text{ if } i \neq k \\ 1 \text{ if } i = k \end{cases},\\
L_j\left(t_k\right) = \delta_{jk} &= \begin{cases} 0 \text{ if } j \neq k \\ 1 \text{ if } j = k \end{cases}.
\end{aligned} \tag{5.31}$$

Gauss-Chebyshev-Lobatto points are selected as grid-points x_i and t_j, given their smooth conversion of continuous time and spatial derivatives into discrete derivatives. The points are generated thus:

$$\begin{aligned}
x_i &= \cos\frac{\pi i}{M_x}, \quad i = 0,1,\ldots,M_x,\\
t_j &= \cos\frac{\pi j}{M_t}, \quad i = 0,1,\ldots,M_t
\end{aligned} \tag{5.32}$$

Differentiation matrices (denoted D and d) are used to collocate and are applied in the form

$$\begin{aligned}
\left.\frac{\partial s^{(p)}}{\partial x^{(p)}}\right|_{x_i,t_j} &= \mathbf{D}^{(p)} S_i, \quad \left.\frac{\partial s}{\partial t}\right|_{x_i,t_j} = \sum_{j=0}^{M_t} \mathbf{d}_{ij} S_j, \\
\left.\frac{\partial^{(p)} \theta}{\partial x^{(p)}}\right|_{x_i,t_j} &= \mathbf{D}^{(p)} \Theta_i, \quad \left.\frac{\partial \theta}{\partial t}\right|_{x_i,t_j} = \sum_{j=0}^{M_t} \mathbf{d}_{ij} \Theta_j, \\
\left.\frac{\partial^{(p)} g}{\partial x^{(p)}}\right|_{x_i,t_j} &= \mathbf{D}^{(p)} G_i, \quad \left.\frac{\partial g}{\partial t}\right|_{x_i,t_j} = \sum_{j=0}^{M_t} \mathbf{d}_{ij} G_j, \\
\left.\frac{\partial^{(p)} h}{\partial x^{(p)}}\right|_{x_i,t_j} &= \mathbf{D}^{(p)} H_i, \quad \left.\frac{\partial h}{\partial t}\right|_{x_i,t_j} = \sum_{j=0}^{M_t} \mathbf{d}_{ij} H_j,
\end{aligned} \tag{5.33}$$

where S, Θ, G and H are vectors of the form

$$\begin{aligned}
S &= \left[s\left(x_0,t_j\right), s\left(x_1,t_j\right), \ldots, s\left(x_{N_x},t_j\right)\right]^T, \\
\Theta &= \left[\theta\left(x_0,t_j\right), \theta\left(x_1,t_j\right), \ldots, \theta\left(x_{N_x},t_j\right)\right]^T, \\
G &= \left[g\left(x_0,t_j\right), g\left(x_1,t_j\right), \ldots, g\left(x_{N_x},t_j\right)\right]^T, \\
H &= \left[h\left(x_0,t_j\right), h\left(x_1,t_j\right), \ldots, h\left(x_{N_x},t_j\right)\right]^T.
\end{aligned}$$

Applying the concept given by (5.33) in the system of pairs {(5.25) & (5.26)} and {(5.27) & (5.28)}, we obtain

$$\left[\mathbf{D}^2\right] \mathbf{S}_{r+1,i} + [(a_1)]\, \Theta_{r+1,i} = \mathbf{R}_{1,i}, \tag{5.34}$$

$$\begin{aligned}
&\left[[\mathbf{b}_1]\, \mathbf{D} + [\mathbf{b}_2] - [\mathbf{b}_4] \sum_{j=0}^{N_{y-1}} \mathbf{d}_{ij}\right] \mathbf{S}_{r+1,i} + \\
&\left[\mathbf{D}^2 + [\mathbf{b}_3]\, \mathbf{D} - [\mathbf{b}_5] \sum_{j=0}^{N_{y-1}} \mathbf{d}_{ij}\right] \Theta_{r+1,i} = \mathbf{R}_{2,i},
\end{aligned} \tag{5.35}$$

and

$$\left[\mathbf{D}^2 + [\mathbf{c}_1]\, \mathbf{D} - [\mathbf{c}_2] \sum_{j=0}^{N_{y-1}} \mathbf{d}_{ij}\right] \mathbf{H}_{r+1,i} = \mathbf{R}_{3,i}, \tag{5.36}$$

$$\left[\mathbf{D}^2 + [\mathbf{e}_1]\, \mathbf{D} - [\mathbf{e}_2] \sum_{j=0}^{N_{y-1}} \mathbf{d}_{ij}\right] \mathbf{G}_{r+1,i} = \mathbf{R}_{4,i}, \tag{5.37}$$

where

$$\mathbf{R}_{1,i} = \mathbf{a}_2,$$
$$\mathbf{R}_{2,i} = \mathbf{b}_4 d_{i,N_y} S_{N_y} + \mathbf{b}_5 d_{i,N_y} \Theta_{N_y} + \mathbf{b}_6,$$
$$\mathbf{R}_{3,i} = \mathbf{c}_2 d_{i,N_y} H_{N_y} + \mathbf{c}_3,$$
$$\mathbf{R}_{4,i} = \mathbf{e}_2 d_{i,N_y} G_{N_y} + \mathbf{e}_3,$$

5.4 Results and Discussion

In this section, we present some numerical results obtained for the system of partial differential equations using the PQLM. We also investigate the influence of mixed convection, Dufour effect, thermophoresis, buoyancy ratio and Brownian motion on the respective velocity, temperature, concentration and nanoparticle concentration profiles. To generate these results, we used 50 grid-points in space and 20 grid-points in time, because these were found to be adequate in generating solutions consistent to 9 decimal places. We begin by verifying the convergence, speed of convergence and accuracy of the BPQLM.

5.4.1 Convergence

To display accuracy and convergence, we set $m = 0.03$, $Nc = 0.01$, $Nr = 0.01$, $Nb = 0.1$, $Nt = 0.1$, $Nd = 0.02$, $Le = 5$, $Ld = 1$ and $Ln = 4$. Table 5.1 below displays the convergence of solutions after 10 iterations. We observe that the PQLM converges quickly, requiring only 6 iterations to converge to 9 decimal places. We also observe the computational time to be less than 13 seconds for 10 iterations which affirms our belief that the method is computationally efficient in dealing with complex problems.

To further investigate the convergence of our numerical scheme, the solution error norm is calculated. This is done by the difference between solutions obtained with successive iterations. If the

Table 5.1: Convergence of $s''(\chi,0)$, $\theta'(\chi,0)$, $h'(\chi,0)$ and $g'(\chi,0)$ to 9 decimal places and time taken after 10 iterations

Iterations	$s''(\chi,0)$	$\theta'(\chi,0)$	$h'(\chi,0)$	$g'(\chi,0)$
1	-0.004961300	-0.500808340	-0.889759470	-1.014471700
2	-0.004538623	-0.450105410	-0.904672420	-1.027788000
3	-0.004529744	-0.449299380	-0.905241910	-1.028334900
4	-0.004529508	-0.449285800	-0.905255780	-1.028348900
5	-0.004529505	-0.449285510	-0.905256110	-1.028349200
6	-0.004529505	-0.449285510	-0.905256110	-1.028349300
⋮				⋮
10	-0.004529505	-0.449285510	-0.905256110	-1.028349300
Total Time (sec)	12.73,	12.73,	12.73,	12.73,

error between the solutions gets smaller until a point where further increase in iterations does not change the error, we say our method converges. The solution error norms are generated thus;

$$||\Omega||_\infty = \max_{0\leq i\leq N_y} ||\Omega_{r+1,i} - \Omega_{r,i}||_\infty, \tag{5.38}$$

where Ω represents S, G, Θ and H.

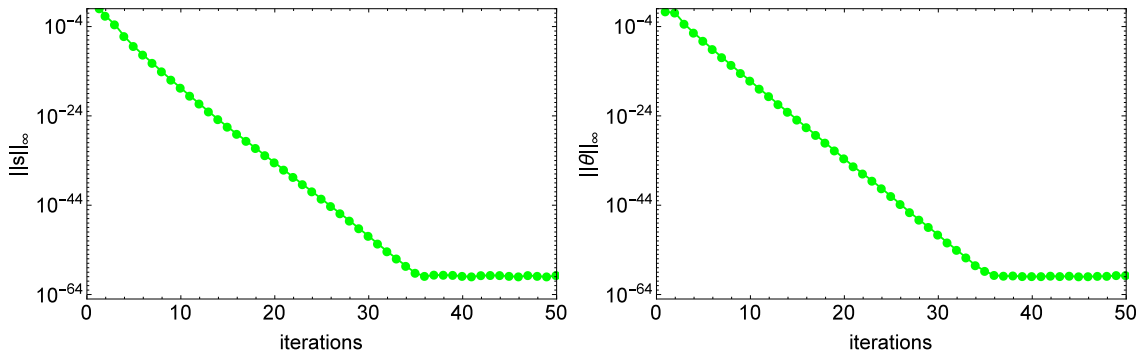

(a) Solution error norm of **S**

(b) Solution error norm of Θ

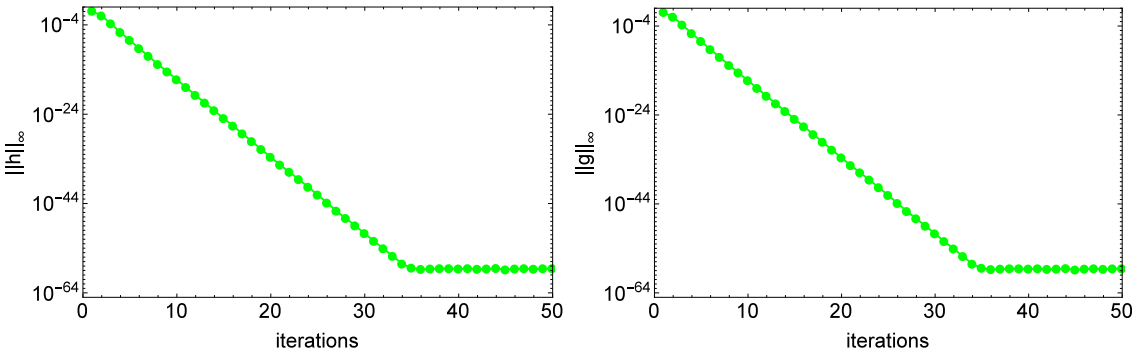

(c) Solution error norm of **H**

(d) Solution error norm of **G**

Figure 5.1: Effect of iterations on the solution error norms when $\chi = 0.4$

We observe from Figure 5.1 that as the number of iterations increase, the solution error on all four graphs reduces until the 35^{th} iteration, to a solution error of 10^{-60}. This indicates that the PQLM converges.

5.4.2 Accuracy

To verify the accuracy of the PQLM, we calculate the residual error by substituting the approximate solutions obtained into the original system of equations. This shows us the proximity of our solutions to the analytical solutions of the system of differential equations. We define the residual

errors as

$$\mathbf{Res}(\mathbf{S}) = \max_{0\leq i\leq M_t} \left|\left| \mathbf{s}_i^{''} - (1-\chi)^2 \theta_i^{'} - Nc\,(1-\chi)^2 \mathbf{h}_i^{'} + Nr\,(1-\chi)^2 \mathbf{g}_i^{'} \right|\right|_{\infty}, \tag{5.39}$$

$$\mathbf{Res}(\Theta) = \max_{0\leq i\leq M_t} \left|\left| \theta_i^{''} + \frac{1}{2}(1+m\chi)\mathbf{s}_i\theta_i^{'} + Nb\mathbf{g}_i^{'}\theta_i^{'} + Nt\theta_i^{'2} + Nd\mathbf{h}_i^{''} - \frac{1}{2}m\chi(1-\chi)\left(\mathbf{s}_i^{'}\frac{\partial\theta_i}{\partial\chi} - \theta_i^{'}\frac{\partial\mathbf{s}_i}{\partial\chi}\right) \right|\right|_{\infty}, \tag{5.40}$$

$$\mathbf{Res}(\mathbf{H}) = \max_{0\leq i\leq M_t} \left|\left| \mathbf{h}_i^{''} + \frac{1}{2}Le(1+m\chi)\mathbf{s}_i\mathbf{h}_i^{'} + Ld\theta_i^{''} - \frac{1}{2}mLe\chi(1-\chi)\left(\mathbf{s}_i^{'}\frac{\partial\mathbf{h}_i}{\partial\chi} - \mathbf{h}_i^{'}\frac{\partial\mathbf{s}_i}{\partial\chi}\right) \right|\right|_{\infty}, \tag{5.41}$$

$$\mathbf{Res}(\mathbf{G}) = \max_{0\leq i\leq M_t} \left|\left| \mathbf{g}_i^{''} + \frac{1}{2}Ln(1+m\chi)\mathbf{s}_i\mathbf{g}_i^{'} + \frac{Nt}{Nb}\theta_i^{''} - \frac{1}{2}mLn\chi(1-\chi)\left(\mathbf{s}_i^{'}\frac{\partial\mathbf{g}_i}{\partial\chi} - \mathbf{g}_i^{'}\frac{\partial\mathbf{s}_i}{\partial\chi}\right) \right|\right|_{\infty}. \tag{5.42}$$

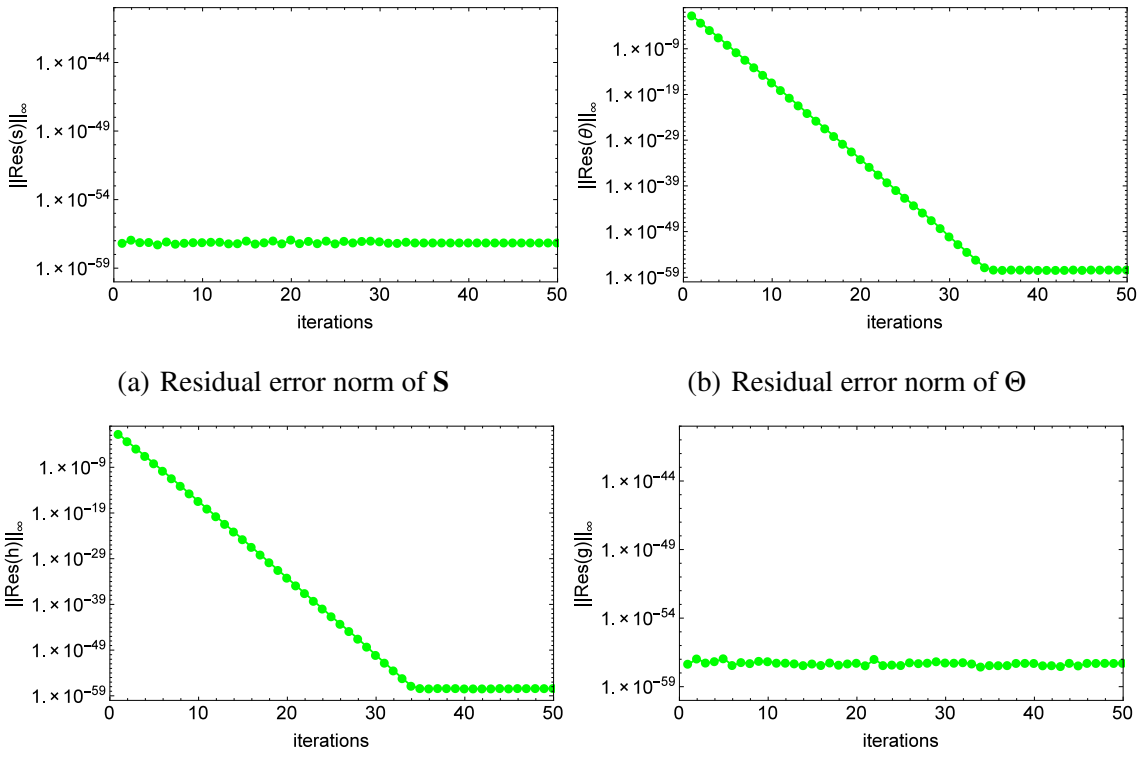

(a) Residual error norm of $\mathbf{S}$

(b) Residual error norm of Θ

(c) Residual error norm of $\mathbf{H}$

(d) Residual error norm of $\mathbf{G}$

Figure 5.2: Effect of iterations on the residual error norms when $\chi = 0.4$

Figure 5.2 displays the accuracy of the PQLM at a fixed time as number of iterations are increased. We observe all the accuracies to be around 10^{-58} which indicates that the PQLM is a highly

accurate method for solving similar problems.

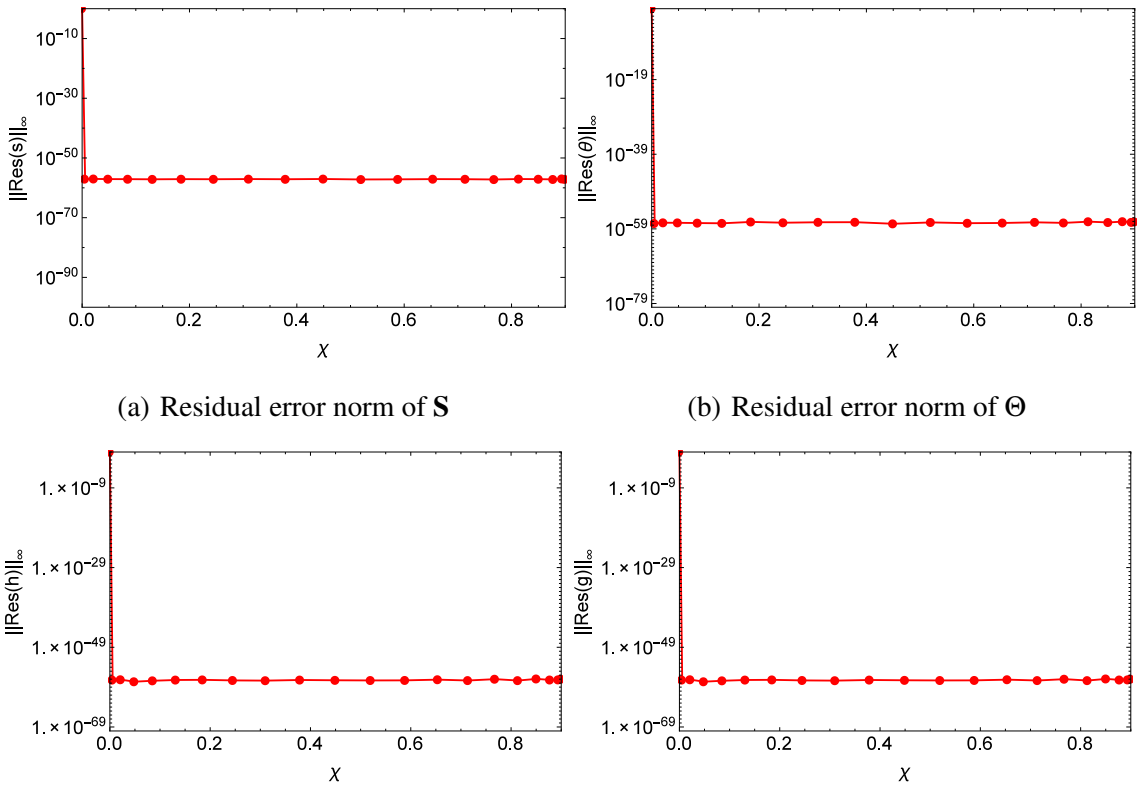

(a) Residual error norm of **S**

(b) Residual error norm of Θ

(c) Residual error norm of **H**

(d) Residual error norm of **G**

Figure 5.3: Effect of χ on the residual error norms at the 30^{th} iteration

Figure 5.3 displays the effect of χ on the residual error of the PQLM at the 30^{th} iteration. We observe that the accuracy is constant for $0 \leq \chi \leq 1$, indicating that for any set of solutions that is needed at a particular point in that domain, the PQLM gives accurate results.

Figures 5.4 to 5.7 show results used to examine the impact of the mixed convection parameter χ on fluid velocity $s'(\eta,\chi)$, fluid temperature $\theta(\eta,\chi)$, mass concentration $h(\eta,\chi)$ and nanoparticle concentration $g(\eta,\chi)$ when $Nb = 0.1$, $m = 0.03$, $Nc = 0.01$, $Nr = 0.01$, $Nt = 0.1$, $Nd = 0.02$, $Le = 4$, $Ld = 1$ and $Ln = 5$.

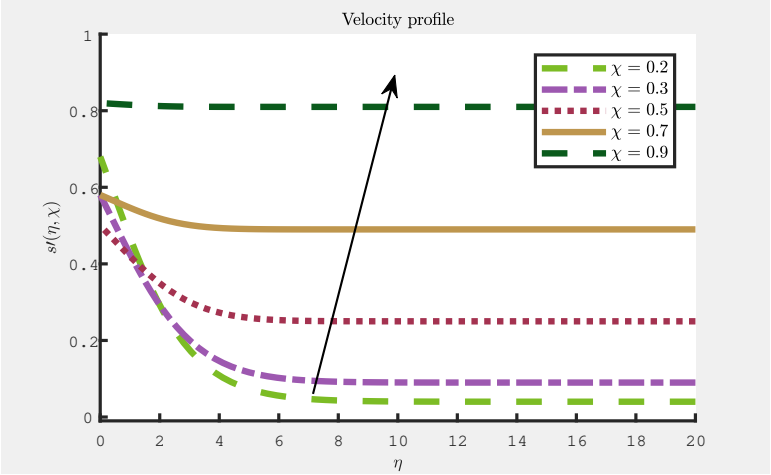

Figure 5.4: Effect of χ on the velocity profile

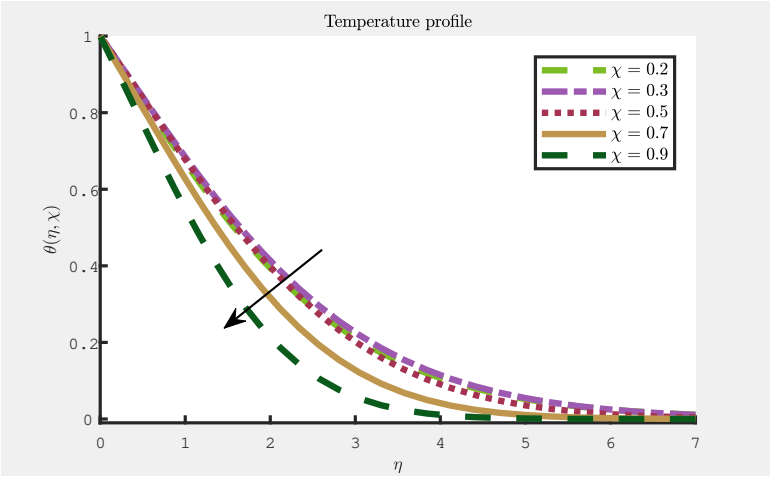

Figure 5.5: Effect of χ on the temperature profile

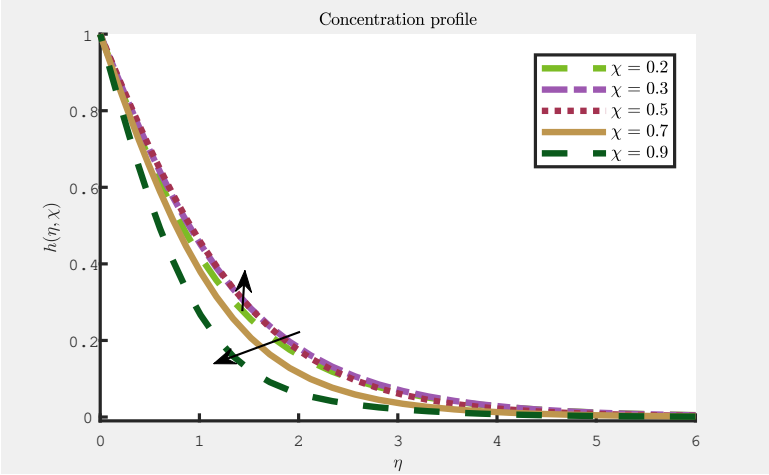

Figure 5.6: Effect of χ on the concentration profile

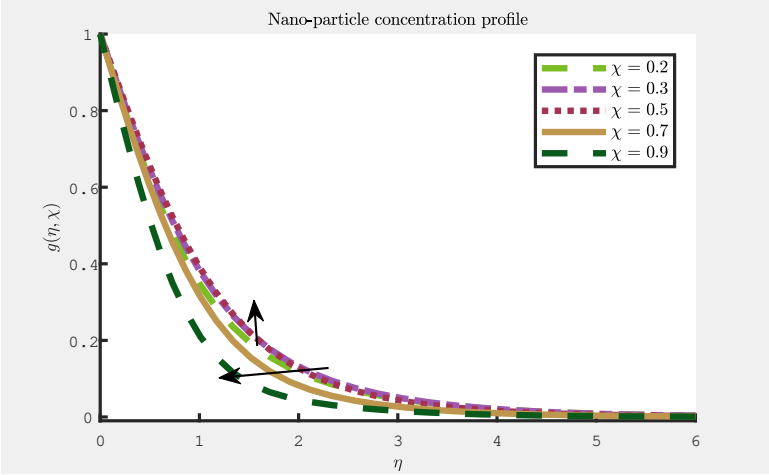

Figure 5.7: Effect of χ on the nanoparticle concentration profile

From the definition of χ given by equation (5.8), t is found that an increase in the value of χ, close to unity which represent a forced convection regime, means small values of Ra_x/Pe_x. On the other hand, large values of Ra_x/Pe_x imply a decrease in the mixed convection parameter χ. From equation 5.9, it is evident that for pure forced convection $(i.e\ \chi = 1)$ the flow is uncoupled from thermal, mass and nanoparticle concentration. Figure 5.4 shows that variations in the flow is insignificant when the values of $\chi \to 1$. Momentum boundary layer thickness decreases for smaller

values of χ. Fluid temperature decreases with χ. Figure 5.6 and 5.7 depict a slight increase in mass and nanoparticle concentration as tending to mixed to free convection regime. Similarly, a decrease in mass and nanoparticle concentration can be interpreted as the system moving from mixed to a forced convection regime.

Figures 5.8 and 5.9 indicate the influence of the Brownian motion parameter Nb and thermophoresis parameter Nt on the fluid temperature when $m = 0.03$, $Nc = 0.01$, $Nr = 0.01$, $Nt = 0.1$,$Nb = 0.01$, $Nd = 0.02$, $Le = 4$, $Ld = 1$ and $Ln = 5$.

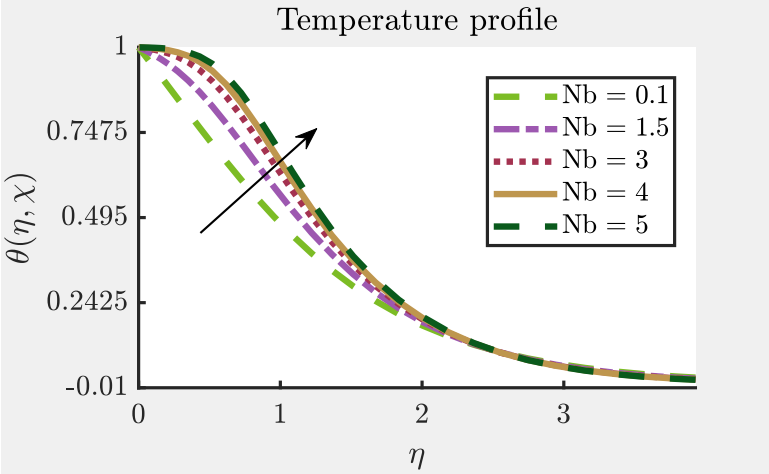

Figure 5.8: Effect of Brownian motion parameter Nb on the temperature profile

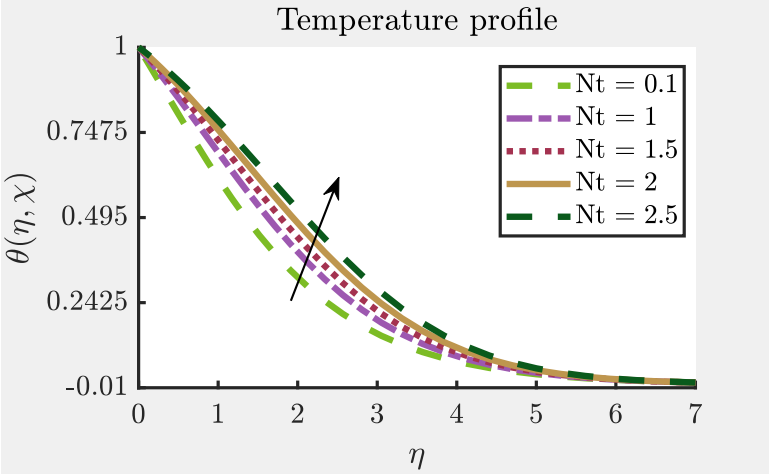

Figure 5.9: Effect of thermophoresis parameter Nt on temperature profile

It is observed from Figure 5.8 that an increase in the Brownian motion parameter Nb results in a corresponding increase in the temperature profile, which is more pronounced near the surface. We observe from Figure 5.9 that an increase in the thermophoresis parameter Nt results in thickening of thermal boundary layer. The increment in the fluid temperature profiles is due to the thermophoretic force induced by the temperature gradient and this causes a rapid flow away from the surface. Consequently, hot fluid moves toward a region having a relatively low temperature. These results are consistent with the results reported by Chamkha and Rashad [126]. A consequent reduction in local Nusselt number $Nu_x \left(Pe_x^{1/2} + Ra_x^{1/2}\right)^{-1}$ for Nb and Nt is perceived.

Figure 5.10 below displays the influence of buoyancy ratio Nr on $s'(\eta,\chi)$ when $m = 0.03$, $Nc = 0.01$, $Nt = 0.1$, $Nb = 0.1$, $Nd = 0.02$, $Le = 4$, $Ld = 1$ and $Ln = 5$.

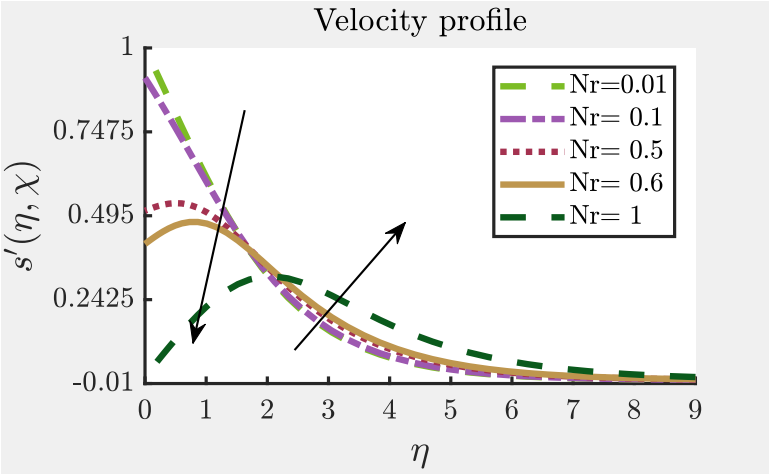

Figure 5.10: Effect of buoyancy ratio Nr on the velocity profile

A significant influence of the buoyancy ratio Nr near the surface of cone on fluid velocity is evident in Figure 5.10. Fluid flow decreases with the increase in Nr. Graphs of $\theta(\eta,\chi)$, $h(\eta,\chi)$ and $g(\eta,\chi)$ are not mentioned here because the impact of Nr on these profiles is not substantial.

Figures 5.11 to 5.14 display the influence of double diffusive buoyancy parameter Nc on $s'(\eta,\chi)$, $\theta(\eta,\chi)$, $h(\eta,\chi)$ and $g(\eta,\chi)$ when $m = 0.03$, $Nt = 0.1$, $Nb = 0.1$, $Nd = 0.02$, $Le = 4$, $Ld = 1$ and $Ln = 5$.

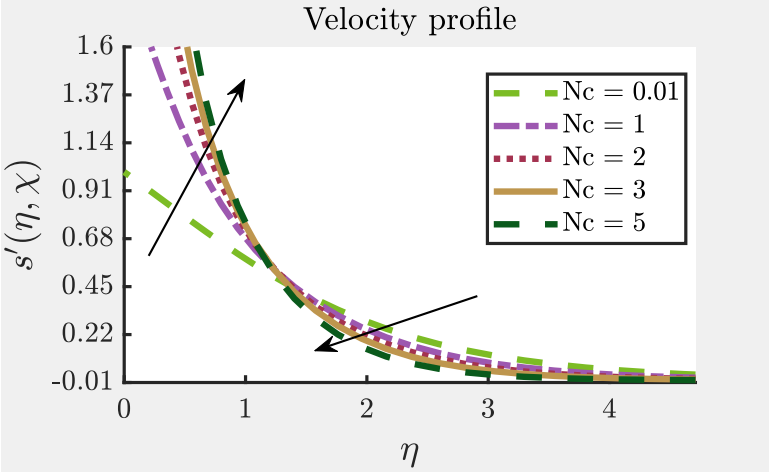

Figure 5.11: Effect of *Nc* on the velocity profile

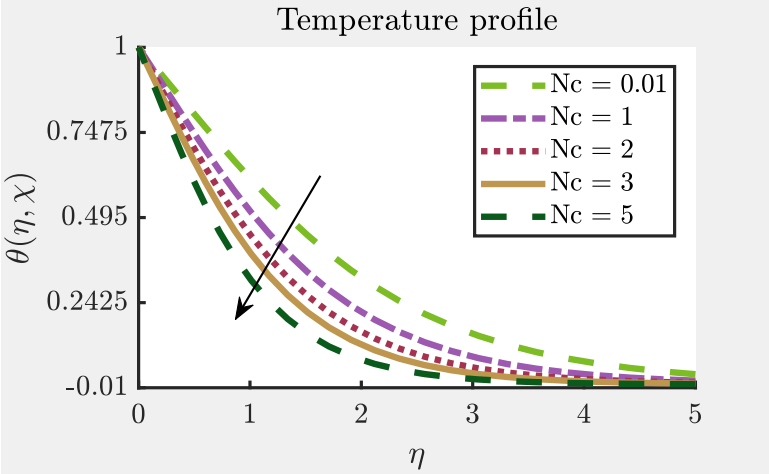

Figure 5.12: Effect of *Nc* on the temperature profile

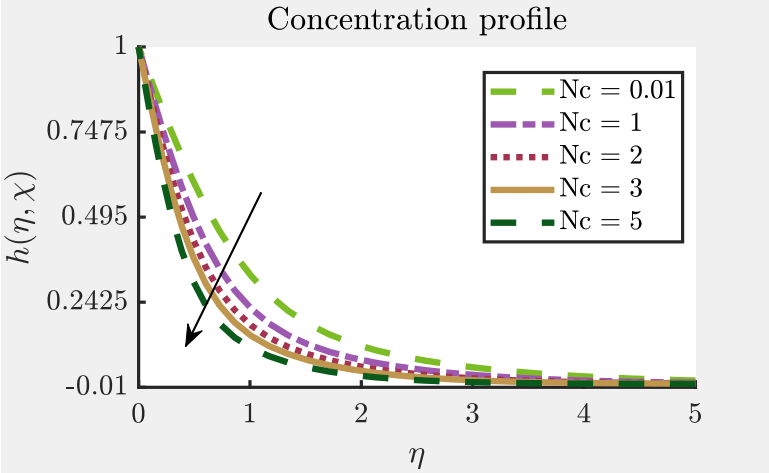

Figure 5.13: Effect of Nc on the concentration profile

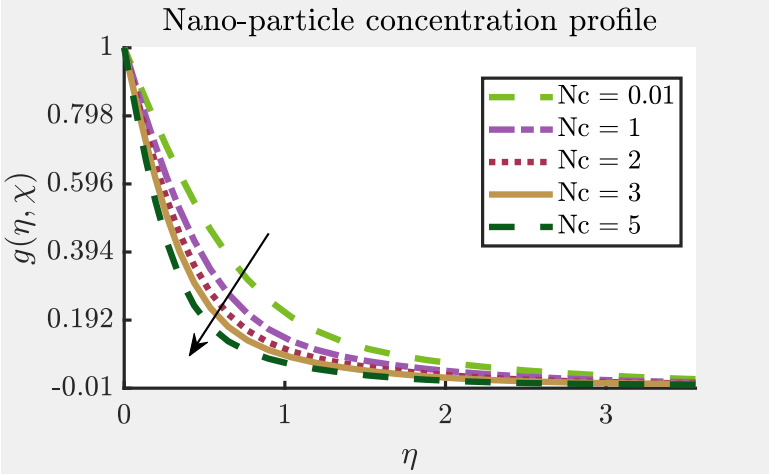

Figure 5.14: Effect of Nc on the nanoparticle profile

We observe that an increase in Nc leads to a decrease in the velocity, temperature, concentration and nanoparticle concentration profiles.

Figures 5.15 to 5.18 display the influence of Dufour number on $s'(\eta,\chi)$, $\theta(\eta,\chi)$, $h(\eta,\chi)$ and $g(\eta,\chi)$ when $m = 0.03$, $Nt = 0.1$, $Nb = 0.1$, $Nc = 0.01$, $Le = 4$, $Ld = 1$ and $Ln = 5$.

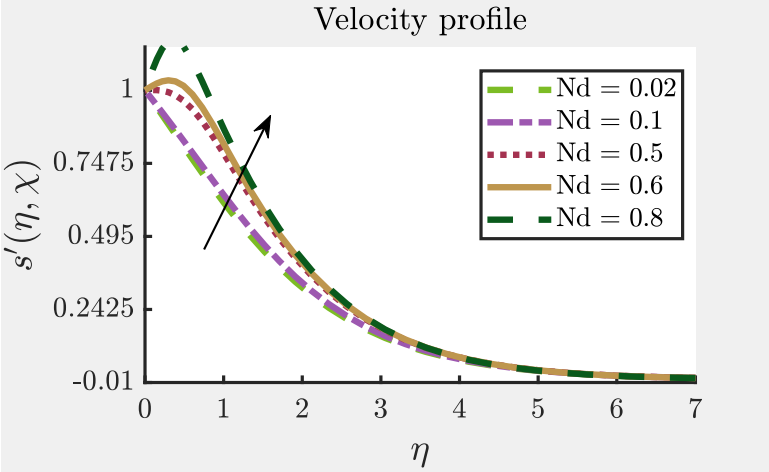

Figure 5.15: Effect of Dufour number *Nd* on the velocity profile

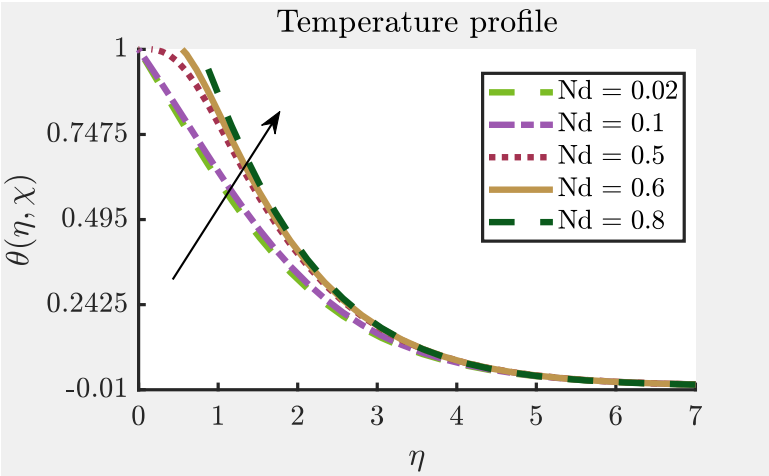

Figure 5.16: Effect of Dufour number *Nd* on the temperature profile

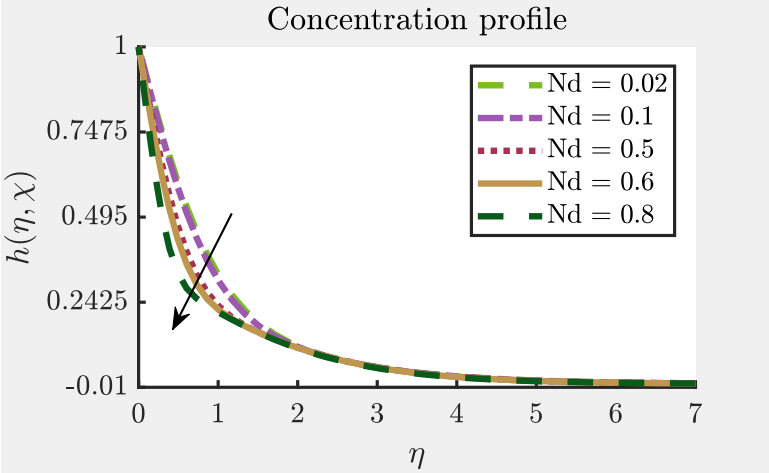

Figure 5.17: Effect of Dufour number *Nd* on the concentration profile

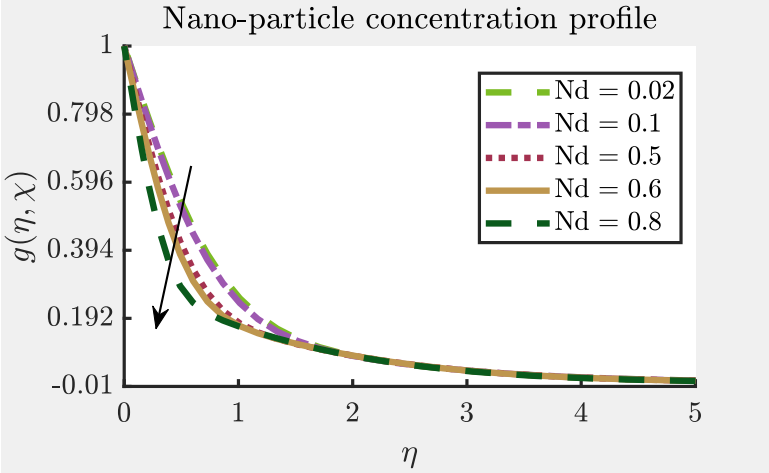

Figure 5.18: Effect of Dufour number *Nd* on the nanoparticle profile

The Dufour number represents the contribution of concentration gradients to the thermal energy flux in the flow. It is observed that an increase in *Nd* increases the velocity and temperature profiles in Figures 5.15 and 5.16 while the concentration and nanoparticle concentration profiles decrease in Figures 5.17 and 5.18.

5.5 Summary

In this chapter, we explored the influence of Brownian motion, Dufour number, mixed convection, thermophoresis and buoyancy ratio on the hydrodynamic boundary layer flow and heat transfer past a vertical isothermal cone in a porous medium through an ambient nanofluid. The governing equations were transformed into highly non-linear partial differential equations using an appropriate transformation, and solved numerically using the paired quasilinearization method (PQLM). The PQLM was found to be convergent and able to give very accurate results. It was seen that increasing the mixed convection parameter increased the velocity, temperature, concentration, and nanoparticle concentration profiles. An increase in the Brownian motion and thermophoresis parameters increases the thermal boundary layer thickness. Influence of Dufour number is to enhance velocity and temperature profiles while it retards concentration and nanoparticle concentration in the boundary layer region. The local Nusselt number decreases with the thermophoresis parameter and the Brownian motion parameter whereas it increases slightly with the double diffusive buoyancy parameter and the buoyancy ratio.

Chapter 6

A paired quasilinearization method for solving MHD mixed convection flow of micropolar fluid through a truncated cone in a Non-Darcy porous medium

6.1 Introduction

Micropolar convection flows have been analyzed by many authors following the seminal work of Eringen [138], who introduced the micropolar fluid. A subclass of these fluids introduced by Eringen [104] is the micropolar fluids, which exhibit the micro-rotational effects observed in colloidal solutions, blood, dielectric fluids, plasmas, liquid crystals etc. Other monographs on the theory and applications of micropolar fluids has been published by Ariman et al. [139], Ariman et al. [140], and Lukaszewicz [141]. Industrial applications of micropolar fluids are found in the purification of crude oil, polymer technologies, centrifugal separation processes, cooling tower dynamics, chemical engineering, metallurgical drawing out of filaments and solar energy systems, among others.

Another field of growing importance in many manufacturing and environmental systems, is combined heat and mass transfer in fluid-saturated porous media. Applications include heat exchanger

devices, petroleum reservoirs, grain storage systems, heat pipes, chemical catalytic reactors, distillation towers, ion exchange columns, subterranean chemical waste migration, solar power absorbers. Thorough discussions of such applications are available in the monographs of Ingham and Pop [111] and Nield et al. [108].

Most studies pertinent to porous media have been based on Darcy's law, which states that the volume-averaged velocity is proportional to the pressure gradient. In many practical applications, for example packed sphere beds, the porous medium, however, is bounded by an impermeable wall, has high flow rates, and reveals nonhomogeneous porosity variation near the wall; thus, making Darcy's law inapplicable [142]. The non-Darcian phenomenon of convective heat transport in porous media has interested many researchers. Inertial effects on porous media transport have been generally studied using the Darcy-Forchheimer model, which uses a quadratic impedance term for inertial drag.

In the literature, flow about a full cone or frustum has been treated quite extensively by Na and Chiou [143] and Chamkha et al. [115] to mention two. Pullepu et al. [144] studied unsteady laminar free convection from a vertical cone with uniform surface heat flux. In this numerical study, they showed that as the semi-vertical angle of the cone increase, so the velocity of the flow decreases. Mohiddin et al. [145] studied, also numerically, unsteady free convective heat and mass transfer in a Walters-B viscoelastic flow along a vertical cone. In this study, it was reported that an increase in Schmidt number significantly decreases both flow velocity and concentration. More recently, free convection from a truncated cone subject to constant wall heat flux in a micropolar fluid was examined by Postelnicu [146]. In his analysis, he used results from a local non-similarity numerical method to complement his previous work [147]. Radiation effects on mixed convection about a cone embedded in a porous medium filled with a nanofluid were later studied by Chamkha [128], taking into account the effects of Brownian motion and thermophoresis with Rosseland diffusion approximation.

Pătrulescu et al. [148] considered the development in a nanofluid of the steady mixed convection boundary layer flow on a vertical impermeable frustum of a cone. They reported the existence

of dual solutions for opposing flows. It was also reported that the range of the mixed convection parameter for which the equations' solution exists increases in the presence of the nanofluids.

In the present analysis, we consider the MHD micropolar chemically-reactive convective heat and mass transfer over a vertical frustum of a cone embedded in a non-Darcian saturated porous medium. In this analysis, a system of non-linear partial differential equations governing the problem are solved numerically using the paired quasilinearization method PQLM [20, 137]. The convergence and accuracy of the PQLM is verified by analysis of the solution error and residual error, respectively. The influence of various physical parameters on the velocities, micro-rotation components, heat and mass transfer are presented in graphical and tabular forms.

6.2 Mathematical formulation of problem

Consider the problem of the chemical reaction effect on mixed convection boundary-layer flow of MHD incompressible micropolar fluid near a vertical truncated cone as shown in Fig.1. Choose

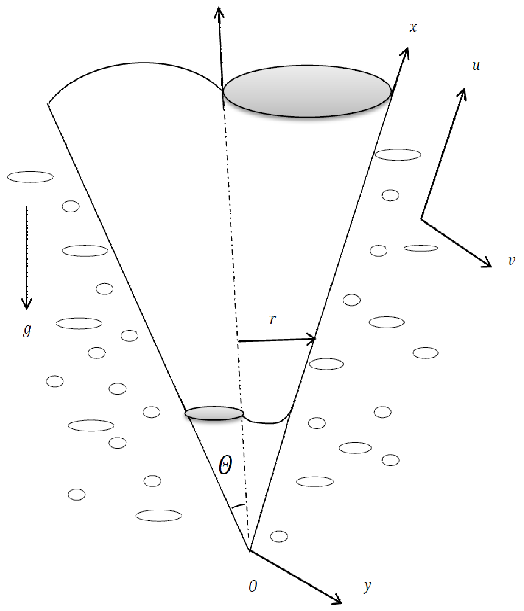

Figure 6.1: Geometry of the flow

the Cartesian coordinate system with the origin O placed at the vertex of the full cone, the x-axis is taken along the vertical frustum of the cone and y-axis is taken as normal to the surface of the truncated cone. The truncated cone is either heated or cooled by convection from a fluid of temperature T_f with $T_f > T_\infty$ (heated surface) and $T_f < T_\infty$ (cooled surface) respectively. The solutal concentration is taken to be constant and is given by C_w. Far away from the truncated cone the velocity in the vertical direction is U_∞, while the temperature and concentration are T_∞, and C_∞, respectively. Under these assumptions, along with the assumptions of Boussinesq and boundary layer approximations, the basic equations of micropolar fluid governing the steady mixed convection boundary layer flow under the influence of a transversely applied magnetic field near a vertical frustum in a Darcy-Forchheimer saturated porous medium can be written as (Pătrulescu [148] and Chamkha [128]):

$$\frac{\partial(ur)}{\partial x}+\frac{\partial(vr)}{\partial y}=0, \tag{6.1}$$

$$u\frac{\partial u}{\partial x}+v\frac{\partial u}{\partial y}=\frac{\mu+\kappa}{\rho}\frac{\partial^2 u}{\partial y^2}+g^*[\beta_T(T-T_0)+\beta_c(C-C_0)]\cos\Theta+\kappa\frac{\partial\Gamma}{\partial y}-\sigma B_0^2 u-\frac{\nu}{K_p}u-\frac{b}{K_p}u^2, \tag{6.2}$$

$$\rho j\left(u\frac{\partial\Gamma}{\partial x}+v\frac{\partial\Gamma}{\partial y}\right)=\gamma\frac{\partial^2\Gamma}{\partial y^2}-2\kappa\Gamma-\kappa\frac{\partial u}{\partial y}, \tag{6.3}$$

$$u\frac{\partial T}{\partial x}+v\frac{\partial T}{\partial y}=\alpha\frac{\partial^2 T}{\partial y^2}+\frac{\mu+\kappa}{\rho C_p}\left(\frac{\partial u}{\partial y}\right)^2+\frac{16\sigma^*}{3(a_r+\sigma_s)\rho C_p}\frac{\partial}{\partial y}\left(T^3\frac{\partial T}{\partial y}\right), \tag{6.4}$$

$$u\frac{\partial C}{\partial x}+v\frac{\partial C}{\partial y}=D\frac{\partial^2 C}{\partial y^2}-K_1(C-C_0), \tag{6.5}$$

where u and v are velocity components in the x and y directions Γ is micro-rotation, ρ is the fluid density, μ, κ and γ are the material constants (viscosity coefficients), g^* is the acceleration due to gravity, K_p is the permeability of the porous medium, σ is electrical conductivity of the fluid, β_T is the coefficient of thermal expansion, β_c is the coefficient of solutal expansion, B_0 magnetic field intensity, α thermal diffusivity, σ^*, a_r, σ_s are the Stefan-Boltzmann constant, scattering coefficient, and the Rosseland mean extinction coefficient, respectively, r is the radius of the vertical frustum

of a cone ($r = x\sin\Theta$), j is the micro-inertia density, C_p is the specific heat, D is the mass diffusivity and K_1 is the chemical reaction parameter.

The boundary conditions are given by

$$u = v = 0, \quad \Gamma = -n\frac{\partial u}{\partial y}, \quad -k\frac{\partial T}{\partial y} = h_f(T_f - T), \quad C = C_w, \text{at} \quad y = 0, \tag{6.6a}$$

$$u = U_\infty, \quad \Gamma = 0, \quad T = T_\infty, \quad C = C_\infty, \text{as} \quad y \to \infty, \tag{6.6b}$$

where $n = 0$ implies the case of micro-elements close to the boundary sticking to the wall, and $n = 1$ corresponds to the turbulent boundary layer, k is thermal conductivity of the fluid and h_f is convective heat transfer coefficient.

Applying the following transformations

$$\Psi = r\nu Re_x^{1/2} f(\zeta,\eta), \quad \zeta = \frac{\bar{x}}{x_0} = \frac{x - x_0}{x_0}, \quad \eta = \frac{y}{\bar{x}} Re_x^{1/2},$$
$$\Gamma = \frac{\nu Re_x^{3/2}}{\bar{x}^2}\omega(\zeta,\eta), \quad \theta(\zeta,\eta) = \frac{T - T_\infty}{T_f - T_\infty}, \quad \phi(\zeta,\eta) = \frac{C - C_\infty}{C_w - C_\infty}, \tag{6.7}$$

where $Re_x = \frac{U_\infty \bar{x}}{\nu}$ is the local Reynolds number, Ψ is the stream function, which is defined as $u = \frac{1}{r}\frac{\partial \Psi}{\partial y}$ and $v = -\frac{1}{r}\frac{\partial \Psi}{\partial x}$. Substituting equation (6.7) into equations (6.1) $-$ (6.5), we obtain the following non-dimensional equations

$$\frac{1}{1-N}f''' + \left(\frac{\zeta}{1+\zeta} + \frac{1}{2}\right) f f'' + \left(\frac{N}{1-N}\right)\omega' + \zeta\lambda(\theta + \Delta\phi) - \zeta\frac{Ha^2}{Re_{xo}} f' - \zeta\frac{1}{D_a Re_{xo}} f' - \zeta\frac{F_s}{D_a} f'^2 = \zeta\left(f'\frac{\partial f'}{\partial \zeta} - f''\frac{\partial f}{\partial \zeta}\right), \tag{6.8}$$

$$\frac{2-N}{2-2N}\omega'' + \left(\frac{\zeta}{1+\zeta} + \frac{1}{2}\right) f\omega' + \frac{1}{2}f'\omega - \zeta\left(\frac{N}{1-N}\right)(2\omega + f'') = \zeta\left(f'\frac{\partial \omega}{\partial \zeta} - \omega'\frac{\partial f}{\partial \zeta}\right), \tag{6.9}$$

$$\theta'' + Pr\left(\frac{\zeta}{1+\zeta} + \frac{1}{2}\right) f\theta' + Pr\delta\left(\frac{1}{1-N}\right)(f'')^2 + \frac{4}{3}RdRe_{xo}\zeta\left\{\theta'[(H-1)\theta + 1]^3\right\}' = Pr\zeta\left(f'\frac{\partial \theta}{\partial \zeta} - \theta'\frac{\partial f}{\partial \zeta}\right), \tag{6.10}$$

$$\frac{1}{Sc}\phi''+\left(\frac{\zeta}{1+\zeta}+\frac{1}{2}\right)f\phi'-K\phi=\zeta\left(f'\frac{\partial\phi}{\partial\zeta}-\phi'\frac{\partial f}{\partial\zeta}\right), \tag{6.11}$$

where the primes denote the differentiation with respect to η, $\lambda=\frac{Gr_{x0}}{Re_{x0}^2}$ is the mixed convection parameter, $G_r=\frac{g*\beta_T(T_f-T_\infty)\bar{x}^3\cos\Theta}{\nu^2}$ is the thermal Grashof number, $G_c=\frac{g*\beta_c(C_w-C_\infty)\bar{x}^3\cos\Theta}{\nu^2}$ is the solutal Grashof number, $Rd=\frac{4\sigma^*T_\infty^3}{k(a_r+\sigma_s}$ is the conduction radiation parameter, $H=\frac{T_w}{T_\infty}$ is the surface temperature excess ratio, $Ha=\frac{\sigma B_0^2d^2}{\mu}$ is the Hartmann number, $D_a=\frac{K_p}{x_0^2}$ is the Darcy number, $F_s=\frac{b}{x_0}$ is the Forchheimer number, $\Delta=\frac{\beta_c(C_w-C_\infty)}{\beta_T(T_f-C_\infty)}$ is the buoyancy ratio, $N=\frac{\kappa}{\mu+\kappa}$ is the coupling number, $\lambda=\frac{Gr_{xo}}{Re_{xo}}$ is the mixed convection parameter, $Pr=\frac{\nu}{\alpha}$ is the Prandtl number, $\delta=\frac{U_\infty^2}{C_p(T_f-T\infty)}$ is the viscous dissipation parameter, $Sc=\frac{\nu}{D_1}$ is the Schmidt number, and $K=\frac{K_1x_o^2}{\nu}$ is chemical reaction parameter.

The boundary conditions now take the form

$$f(\zeta,0)=-\frac{\zeta}{(\frac{\zeta}{\zeta+1}+\frac{1}{2})}\frac{\partial f}{\partial\zeta},\quad f'(\zeta,0)=0,\quad \omega(\zeta,0)=-nf''(\zeta,0), \tag{6.12a}$$

$$\theta'(\zeta,0)=-\zeta^{1/2}Bi(1-\theta(\zeta,0)),\quad \phi(\zeta,0)=1,$$

$$f'(\zeta,\infty)=1,\quad \omega(\zeta,\infty)=0,\quad \theta(\zeta,\infty)=0,\quad \phi(\zeta,\infty)=0,\quad \text{as}\quad \eta\to\infty, \tag{6.12b}$$

where $Bi=\frac{h_fx_o}{kRe_{xo}^{1/2}}$ is the Biot number.
The non-dimensional skin friction, the Nusselt and Sherwood numbers respectively are given by

$$C_fRe_x^{1/2}=\left(\frac{2}{1-N}\right)f''(\zeta,0),$$

$$Nu_x=-Re_x^{1/2}\theta'(\zeta,0),\qquad Sh_x=-Re_x^{1/2}\phi'(\zeta,0). \tag{6.13}$$

6.3 Numerical Scheme

To solve the non-linear system of partial differential equations (6.8) − (6.11), the recently developed method of simplifying large systems called paired quasilinearization method (PQLM) [20] is applied. The PQLM uses the ideas of the popular quasilinearization method (QLM) approach

of Bellman and Kalaba [38], which seeks to simplify a system of equations through Taylor-series linearization before discretizing and solving using numerical methods. The essential differential between the PQLM and the QLM is that the PQLM implements the linearization simultaneously on a pair of equations instead of simultaneous linearization of the full set of equations, as it is often done in the standard QLM. The problem under investigation in this study is well suited for the PQLM because of the nature of the boundary conditions for $f(\zeta,\eta,)$ and $\omega(\zeta,\eta)$, which are also coupled. This coupling suggests that $f(\zeta,\eta,)$ and $\omega(\zeta,\eta)$ should be treated as a pair in the linearization process. Accordingly, an iteration scheme is developed based on the assumption that when solving for f and ω at the current iteration, the values of the other unknowns θ and ϕ obtained from the previous iteration will be used. The iteration scheme is defined as

$$\Omega_1[F_{r+1},W_{r+1},T_r,P_r]=0, \tag{6.14}$$

$$\Omega_2[F_{r+1},W_{r+1},T_r,P_r]=0, \tag{6.15}$$

$$\Omega_2[F_{r+1},W_{r+1},T_{r+1},P_r]=0, \tag{6.16}$$

$$\Omega_3[F_{r+1},W_{r+1},T_{r+1},P_{r+1}]=0. \tag{6.17}$$

where $r+1$ and r denotes the current and previous iteration, respectively, and Ω_1, Ω_2, Ω_3 and Ω_4 are non-linear operators that denote equations (6.8), (6.9), (6.10) and (6.11), respectively, and F,W,T,P are defined as

$$F=\left\{f,\frac{\partial f}{\partial\eta},\frac{\partial^2 f}{\partial\eta^2},\frac{\partial^3 f}{\partial\eta^3},\frac{\partial f}{\partial\zeta},\frac{\partial^2 f}{\partial\zeta\partial\eta}\right\},\quad W=\left\{\omega,\frac{\partial\omega}{\partial\eta},\frac{\partial^2\omega}{\partial\eta^2},\frac{\partial\omega}{\partial\zeta}\right\}, \tag{6.18}$$

$$T=\left\{\theta,\frac{\partial\theta}{\partial\eta},\frac{\partial^2\theta}{\partial\eta^2},\frac{\partial\theta}{\partial\zeta}\right\},H=\left\{\phi,\frac{\partial\phi}{\partial\eta},\frac{\partial^2\phi}{\partial\eta^2},\frac{\partial\phi}{\partial\zeta}\right\}. \tag{6.19}$$

We remark that, at the iteration level $r+1$, once equations (6.14) and (6.15) have been solved simultaneously for the unknowns F_{r+1} and W_{r+1}, equations (6.16) and (6.17) will have only the unknowns T_{r+1} and P_{r+1}, respectively.

The linearization of the equations is applied using the Taylor series expansion of Ω_k about some previous approximation of the solutions denoted by F_r, T_r, H_r, W_r. The assumption used is that the

difference between the current and previous solution is small. The linearization process gives,

$$\frac{1}{1-N}f'''_{r+1}+[a_1]\,f''_{r+1}+[a_2]\,f'_{r+1}+[a_3]\,f_{r+1}+\left(\frac{N}{1-N}\right)\omega'_{r+1}=$$
$$[a_4]\,\frac{\partial f'_{r+1}}{\partial\zeta}+[a_5]\,\frac{\partial f_{r+1}}{\partial\zeta}+a_6, \tag{6.20}$$
$$\left(-\zeta\left(\frac{N}{1-N}\right)\right)f''_{r+1}+[b_1]\,f'_{r+1}+[b_2]\,f_{r+1}+\left(\frac{2-N}{2-2N}\right)\omega''_{r+1}$$
$$+[b_3]\,\omega'_{r+1}+[b_4]\,\omega_{r+1}=[b_5]\,\frac{\partial f_{r+1}}{\partial\zeta}+[b_6]\,\frac{\partial\omega_{r+1}}{\partial\zeta}+b_7, \tag{6.21}$$
$$[c_1]\,\theta''_{r+1}+[c_2]\,\theta'_{r+1}+[c_3]\,\theta_{r+1}=[c_4]\,\frac{\partial\theta_{r+1}}{\partial\zeta}+c_5, \tag{6.22}$$
$$\frac{1}{Sc}\phi''_{r+1}+[e_1]\,\phi'_{r+1}+(-K)\phi_{r+1}=[e_2]\,\frac{\partial\phi_{r+1}}{\partial\zeta}, \tag{6.23}$$

where

$$\alpha_1=\frac{\zeta}{1+\zeta}+\frac{1}{2},\quad \alpha_2=\frac{1}{DaRe_{x_0}},\quad \alpha_3=\frac{4}{3Pr}Re_{x_0},$$
$$\alpha_5=\frac{4}{3}Re_{x_0}Rd,\quad Z=H-1,$$
$$a_1=\alpha_1 f_r+\zeta\frac{\partial f_r}{\partial\zeta},\quad a_2=-\zeta\frac{Ha^2}{Re_{x_0}}-\zeta\alpha_2-2\zeta\frac{Fs}{Da}f'_r-\zeta\frac{\partial f'_r}{\partial\zeta},$$
$$a_3=\alpha_1 f''_r,\quad a_4=\zeta f'_r,\quad a_5=-\zeta f''_r,$$
$$a_6=\alpha_1 f_r f''_r-\zeta\lambda(\theta_r+\Delta\phi_r)-\zeta\frac{Fs}{Da}f'^2_r-\zeta f'_r\frac{\partial f'_r}{\partial\zeta}+\zeta f''_r\frac{\partial f_r}{\partial\zeta},$$
$$b_1=\frac{1}{2}\omega_r-\zeta\frac{\partial\omega_r}{\partial\zeta},\quad b_2=\alpha_1\omega'_r,\quad b_3=\alpha_1 f_r+\zeta\frac{\partial f_r}{\partial\zeta},$$
$$b_4=\frac{1}{2}f'_r-2\zeta\left(\frac{N}{1-N}\right),\quad b_5=-\zeta\omega'_r,\quad b_6=\zeta f'_r,$$
$$b_7=\alpha_1 f_r\omega'_r+\frac{1}{2}f'_r\omega_r-\zeta f'_r\frac{\partial\omega_r}{\partial\zeta}+\zeta\omega'_r\frac{\partial f_r}{\partial\zeta},$$

$$
\begin{aligned}
c_1 &= \frac{1}{Pr}+\alpha_3\zeta\left(1+3Z\theta_r+3Z^2\theta_r^2+Z^3\theta_r^3\right),\\
c_2 &= \alpha_1 f_{r+1}+\alpha_3\zeta\left(6Z\theta_r^{'}+12Z^2\theta_r\theta_r^{'}+6Z^3\theta_r^2\theta_r^{'}\right)+\zeta\frac{\partial f_{r+1}}{\partial\zeta},\\
c_3 &= \alpha_3\zeta\left(6Z^2\theta_r^{'2}+6Z^3\theta_r\theta_r^{'2}+3Z\theta_r^{''}+6Z^2\theta_r^{''}\theta_r+3Z^3\theta_r^{''}\theta_r^2\right),\\
c_4 &= \zeta f_{r+1}^{'},\ \ e_1=\alpha_1 f_{r+1}+\zeta\frac{\partial f_{r+1}}{\partial\zeta},\ \ \ e_2=\zeta f_{r+1}^{'},\\
c_5 &= \left(\frac{-Pr\delta}{1-N}\right)f_{r+1}^{''2}+3\alpha_3\zeta\left(Z\theta_r^{'2}+4Z^2\theta_r\theta_r^{'2}+3Z^3\theta_r^2\theta_r^{'2}+\right.\\
&\quad \left. Z\theta_r\theta_r^{''}+2Z^2\theta_r^{''}\theta_r^2+Z^3\theta_r^{''}\theta_r^3\right),\\
R_1 &= a_6,\ \ R_2=b_7,\ \ R_3=c_5,\ \ R_4=0.
\end{aligned}
$$

Equations (6.20) − (6.23) are now linear and can be solved using any numerical method. In this study, the bivariate spectral method with Chebyshev-Gauss-Lobatto nodes is employed. The discretization with spectral collocation is applied to both the space η and time ξ domains after transforming the original domains to $[-1,1]\times[-1,1]$. Linear transformations are used to transform the physical domains $\eta\in[0,\eta_\infty]$ and $\zeta\in[0,\zeta_\infty)$ to $\xi\in[-1,1]$ and $\tau\in[-1,1]$, respectively. Here η_∞ and ζ_∞ are finite values chosen to be large enough to approximate the behaviour of the flow quantities at a point near infinity. These values are introduced to facilitate the application of the numerical method at infinity. The discretization nodes are defined as

$$
\xi_i=\cos\left(\frac{\pi i}{N_x}\right),\quad \tau_j=\cos\left(\frac{\pi j}{N_\tau}\right),\quad i=0,1,\ldots,N_x;\ \ j=0,1,\ldots,N_\tau. \tag{6.24}
$$

The approximate solutions are assumed to be defined in terms of bivariate Lagrange interpolation polynomial of the form

$$
f(\eta,\zeta)\approx\sum_{m=0}^{N_x}\sum_{j=0}^{N_\tau}f(\xi_m,\tau_j)L_m(\xi)L_j(\tau), \tag{6.25}
$$

which interpolates $f(\eta,\zeta)$ at the Gauss-Lobatto collocation points. Similar expressions are used to define approximate functions for $\theta(\eta,\xi)$, $\phi(\eta,\xi)$ and $\omega(\eta,\xi)$.

The Chebyshev pseudo-spectral method is applied on (6.20) − (6.23) with derivatives of the unknown functions with respect to η and ζ at the collocation points ξ_k and τ_i being defined as:

$$\left.\frac{\partial^n f}{\partial \eta}\right|_{(\xi_k,\tau_i)} = \mathbf{D}^n \mathbf{F}_i, \quad n = 1,2,3 \tag{6.26}$$

$$\left.\frac{\partial f}{\partial \xi}\right|_{(\xi_k,\tau_i)} = \sum_{j=0}^{N_\tau} \mathbf{d}_{ij} \mathbf{F}_j, \tag{6.27}$$

where $\mathbf{d}_{i,j} = (2/\zeta_e) d_{i,j}$ $(i,j = 0,1,\ldots,N_t)$ with $d_{i,j}$ being entries of the standard Chebyshev differentiation matrix $d = [d_{i,j}]$ of size $(N_\tau+1)\times(N_\tau+1)$ (see, for example Trefethen [13]). Similarly, $\mathbf{D} = (2/\eta_e)[D_{r,s}]$ $(r,s = 0,1,2,\ldots,N_x)$ with $[D_{r,s}]$ being an $(N_x+1)\times(N_x+1)$ Chebyshev derivative matrix, and the vector $\mathbf{F}_i$ is defined as

$$\mathbf{F}_i = [f_i(\xi_0), f_i(\xi_1), \ldots, f_i(\xi_{N_x})]^T. \tag{6.28}$$

Similar definitions are obtained for the partial derivatives of the other unknown functions.

The discretized form of equations (6.20) - (6.23) are

$$\mathbf{A}^{(i)}_{1,1}\mathbf{F}_{r+1,i} + \mathbf{A}^{(i)}_{1,2}\mathbf{W}_{r+1,i} + \mathbf{a}_5 \sum_{j=0}^{N_\tau} \mathbf{d}_{i,j}\mathbf{F}_{r+1,j} + \mathbf{a}_4 \sum_{j=0}^{N_\tau} \mathbf{d}_{i,j}\mathbf{D}\mathbf{F}_{r+1,j} = \mathbf{R}_{1,i}, \tag{6.29}$$

$$\mathbf{A}^{(i)}_{2,1}\mathbf{F}_{r+1,i} + \mathbf{A}^{(i)}_{2,2}\mathbf{W}_{r+1,i} + \mathbf{b}_5 \sum_{j=0}^{N_\tau} \mathbf{d}_{i,j}\mathbf{F}_{r+1,j} + \mathbf{b}_6 \sum_{j=0}^{N_\tau} \mathbf{d}_{i,j}\mathbf{W}_{r+1,j} = \mathbf{R}_{2,i}, \tag{6.30}$$

$$\mathbf{A}^{(i)}_{3,3}\Theta_{r+1,i} + \mathbf{c}_4 \sum_{j=0}^{N_\tau} \mathbf{d}_{i,j}\Theta_{r+1,j} = \mathbf{R}_{3,i}, \tag{6.31}$$

$$\mathbf{A}^{(i)}_{4,4}\Phi_{r+1,i} + \mathbf{e}_2 \sum_{j=0}^{N_\tau} \mathbf{d}_{i,j}\Phi_{r+1,j} = \mathbf{R}_{4,i}, \tag{6.32}$$

for $i = 0, 1, 2, \ldots, N_\tau$ where the matrix coefficients and right hand side vectors are defined as

$$
\begin{aligned}
A_{1,1}^{(i)} &= \frac{1}{1-N}\mathbf{D}^3 + [\mathbf{a}_1]\,\mathbf{D}^2 + [\mathbf{a}_2]\,\mathbf{D} + [\mathbf{a}_3] - [\mathbf{a}_4]\,\mathbf{D}\mathbf{d}_{i,i} \quad A_{1,2}^{(i)} = \frac{N}{1-N}\mathbf{D}, \\
A_{2,1}^{(i)} &= \left(-\zeta\left(\frac{N}{1-N}\right)\right)\mathbf{D}^2 + [\mathbf{b}_1]\,\mathbf{D} + [\mathbf{b}_2] - [\mathbf{b}_5]\,\mathbf{d}_{i,i}, \\
A_{2,2}^{(i)} &= \left(\frac{2-N}{2-2N}\right)\mathbf{D}^2 + [\mathbf{b}_3]\,\mathbf{D} + [\mathbf{b}_4] - [\mathbf{b}_6]\,\mathbf{d}_{i,i}, \\
A_{3,3}^{(i)} &= [\mathbf{c}_1]\,\mathbf{D}^2 + [\mathbf{c}_2]\,\mathbf{D} + [\mathbf{c}_3] - [\mathbf{c}_4]\,\mathbf{d}_{i,i}\mathbf{a}_{1,2}^{(1)}, \\
A_{4,4}^{(i)} &= \frac{1}{Sc}\mathbf{D}^2 + [\mathbf{e}_1]\,\mathbf{D} + (-K)\mathbf{I} - [\mathbf{e}_2]\,\mathbf{d}_{i,i},
\end{aligned}
$$

and where $\mathbf{I}$ is an identity matrix of size $(N_x+1)\times(N_x+1)$.

6.4 Results and discussion

In this section, we present some numerical results obtained for the system of partial differential equations using the PQLM. To generate these results, we used 50 grid points in space and 20 grid points in time; these were found to be adequate to generate solutions consistent to 9 decimal places. We first investigated the convergence of the numerical scheme using the solution error norm. The next step was verifying the accuracy of the PQLM. Lastly, the influence of various parameters on the flow profiles of the system of differential equations were investigated.

To display accuracy and convergence, we set $m = 0.03$, $Nc = 0.01$, $Nr = 0.01$, $Nb = 0.1$, $Nt = 0.1$, $Nd = 0.02$, $Le = 5$, $Ld = 1$ and $Ln = 5$. To obtain the solution error norm, the infinity norm of the difference between solutions obtained after successive iterations is calculated. If the error between the solutions gets smaller until a point is reached where further increase in iterations does not change the error, we say our method converges. The solution error norms are generated thus

$$
||\mathbf{V}||_\infty = \max_{0\le i\le N_y} ||\mathbf{V}_{r+1,i} - \mathbf{V}_{r,i}||_\infty, \tag{6.33}
$$

where $\mathbf{V}$ represents F, Ω, Θ and Φ. Figure 6.2 displays the effect of iterations on the solution errors of the system (6.29) − (6.32).

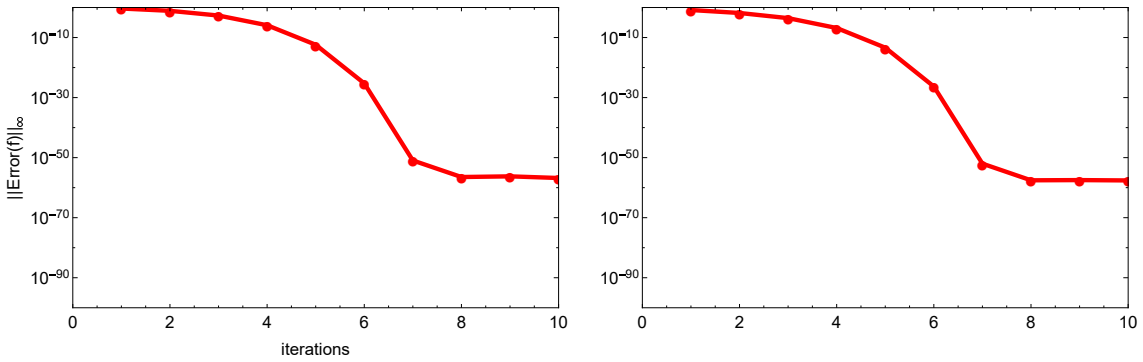

(a) Solution error norm of $\mathbf{F}$

(b) Solution error norm of Φ

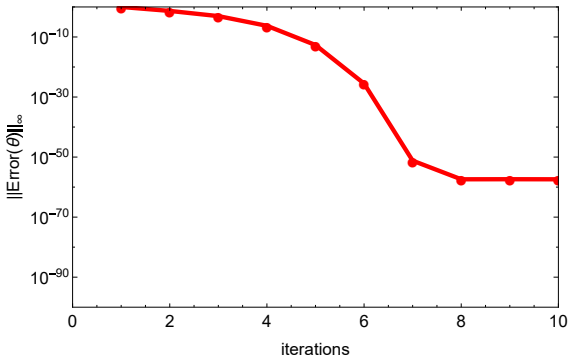

(c) Solution error norm of Θ

Figure 6.2: Effect of iterations on the solution error norms when $\xi = 0.4$

We observe from Figure 6.2 that as the number of iterations increase, the error reduces until the 35^{th} iteration when it reaches a tolerance level of 10^{-60}. This indicates that the PQLM converges.

To verify the accuracy of the PQLM, we calculate the residual error by substituting the original system of equations with the approximate solutions obtained. This shows us the closeness of our solutions to the analytical solutions of the system of differential equations. We define the residual

errors as

$$
\begin{aligned}
\mathbf{Res}(\mathbf{F}) &= \max_{0\leq i\leq M_t}\left|\left|\frac{1}{1-N}\mathbf{f}_i^{'''}+\left(\frac{\xi}{1+\xi}+\frac{1}{2}\right)\mathbf{f}_i\mathbf{f}_i^{''}+\left(\frac{N}{1-N}\right)\omega_i^{'}+\xi\lambda(\theta_i+\Delta\Phi_i)\right.\right.\\
&\left.\left.-\xi\frac{Fs}{Da}\mathbf{f}^{'2}-\xi\frac{1}{DaRe_{x_0}}f^{'}-\xi\left(\mathbf{f}_i^{'}\frac{\partial\mathbf{f}_i^{'}}{\partial\xi}-\mathbf{f}_i^{''}\frac{\partial\mathbf{f}_i}{\partial\xi}\right)\right|\right|_\infty,\\
\mathbf{Res}(\Theta) &= \max_{0\leq i\leq M_t}\left|\left|\theta_i^{''}+Pr\left(\frac{\xi}{1+\xi}+\frac{1}{2}\right)\mathbf{f}_i\theta_i^{'}+Pr\delta\left(\frac{1}{1-N}\right)\mathbf{f}_i^{''2}+\right.\right.\\
&\left.\left.+\frac{4}{3}RdRe_{x_0}\xi\left\{\theta_i^{'}\left[(H-1)\theta_i+1\right]^3\right\}^{'}-Pr\xi\left(\mathbf{f}_i^{'}\frac{\partial\theta_i}{\partial\xi}-\theta_i^{'}\frac{\partial\mathbf{f}_i}{\partial\xi}\right)\right|\right|_\infty,\\
\mathbf{Res}(\Omega) &= \max_{0\leq i\leq M_t}\left|\left|\frac{2-N}{2-2N}\omega_i^{''}+\left(\frac{\xi}{1+\xi}+\frac{1}{2}\right)\mathbf{f}_i\omega_i^{'}+\frac{1}{2}\mathbf{f}_i^{'}\omega_i-\xi\left(\frac{N}{1-N}\right)\left(2\omega_i^{'}+\mathbf{f}_i^{''}\right)-\right.\right.\\
&\left.\left.\xi\left(\mathbf{f}_i^{'}\frac{\partial\omega_i}{\partial\xi}-\phi_i^{'}\frac{\partial\mathbf{f}_i}{\partial\xi}\right)\right|\right|_\infty,\\
\mathbf{Res}(\Phi) &= \max_{0\leq i\leq M_t}\left|\left|\frac{1}{Sc}\phi_i^{''}+\left(\frac{\xi}{1+\xi}+\frac{1}{2}\right)\mathbf{f}_i\phi_i^{'}-K\phi_i-\xi\left(\mathbf{f}_i^{'}\frac{\partial\phi_i}{\partial\xi}-\phi_i^{'}\frac{\partial\mathbf{f}_i}{\partial\xi}\right)\right|\right|_\infty.
\end{aligned}
$$

Figure 6.3 displays the accuracy of the PQLM at a fixed time as number of iterations are increased.

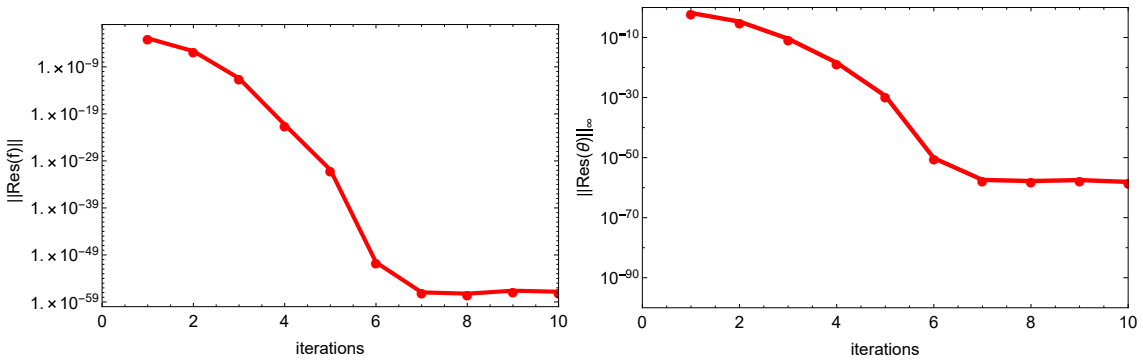

(a) Residual error norm of $\mathbf{F}$ (b) Residual error norm of Θ

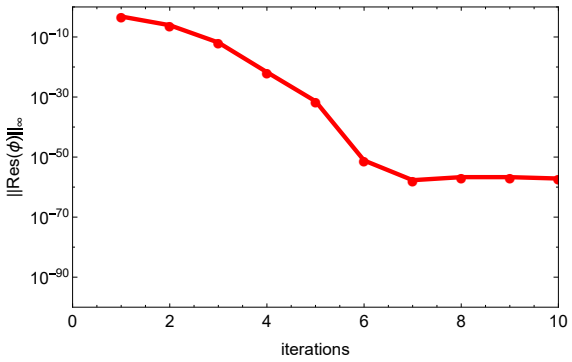

(c) Residual error norm of Φ

Figure 6.3: Effect of iterations on the residual error norms when $\zeta = 0.8$

We observe from Figure 6.3 that all the accuracies‘ are around 10^{-58} which indicates that the PQLM is a highly accurate method for solving similar problems such as in this chapter.

Table 6.1 below displays the effect of mixed convection K, Hartmann number Ha, conduction radiation Rd and Forchheimer number Fs on the skin friction, Nusselt number and Sherwood number. The parameter values used in generating the table were $Re = 0.5$, $n = 0.8$, $\lambda = 0.2$, $\Delta = 0.1$, $Da = \infty$(10 when varying Fs), $Pr = 0.72$, $\delta = 0.1$, $H = 1$, $Sc = 0.22$, $Z = H - 1$ and $N = 0.6$.

Table 6.1: Skin friction, Nusselt number and Sherwood number for various parameter values

K	Ha	Rd	Fs	$\frac{2}{1-N}f''(\xi,0)$	$\frac{2}{1-N}\omega'(\xi,0)$	$-Re_x^{1/2}\theta'(\eta,0)$	$-Re_x^{1/2}\phi'(\eta,0)$
0	0.2	0.1	1	0.423174	-0.217633	-0.074370	-0.233213
0.5	0.2	0.1	1	0.420141	-0.216072	-0.074370	-0.389500
1	0.2	0.1	1	0.418374	-0.215164	-0.074370	-0.505174
2	0.2	0.1	1	0.416216	-0.214054	-0.074369	-0.684176
0.1	0	0.1	1	2.477194	1.301483	0.052504	0.200644
0.1	0.1	0.1	1	2.383719	1.243044	0.052537	0.198243
0.1	0.2	0.1	1	2.111914	1.077212	0.052588	0.190891
0.1	0.3	0.1	1	1.689826	0.832990	0.052505	0.178118
0.1	0.2	1	1	2.119285	1.082616	0.052424	0.191096
0.1	0.2	3	1	2.137405	1.096239	0.051610	0.191542
0.1	0.2	5	1	2.154632	1.109190	0.050730	0.191944
0.1	0.2	7	1	2.170410	1.120998	0.049906	0.192305
0.1	0.2	0.1	0	0.257967	-0.132669	-0.073751	-0.231595
0.1	0.2	0.1	0.1	0.237818	-0.122307	-0.073534	-0.225319
0.1	0.2	0.1	0.3	0.223246	-0.114812	-0.073341	-0.220543
0.1	0.2	0.1	0.4	0.192185	-0.098838	-0.072798	-0.209558

We observe from Table 6.1 that as the chemical reaction increases, skin friction decreases and the Sherwood number increases. There appears to be no visible effect on the Nusselt number. When the Hartmann number is increased, the skin friction and Sherwood number both decrease, while the Nusselt number increases. An increase in radiation however increases the skin friction and Sherwood number while decreasing the Nusselt number. The skin friction, Nusselt number and

Sherwood number all decrease with an increase in the Forchheimer number.

Figures 6.4a to 6.4d, below, display the effect of time ζ on the velocity, micro-rotation, temperature and concentration profiles when $Re = 0.5$, $Rd = 0.5$, $n = 0$, $N = 0.6$, $\Delta = 0.1$, $Ha = 0.2$, $Da = \infty$, $Fs = 1$, $Pr = 0.72$, $\delta = 1$, $\lambda = 0.1$, $H = 1$, $Sc = 0.22$, $K = 0.1$ $Z = H - 1$, and $Bi = \infty$.

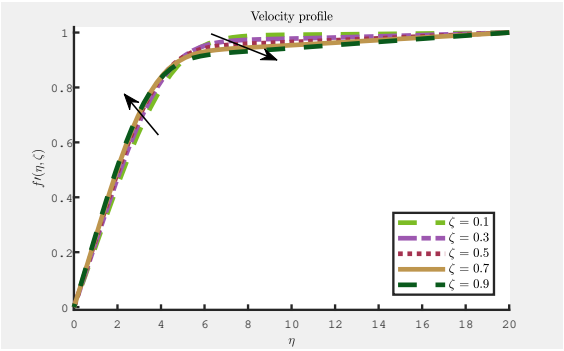

(a) velocity profile

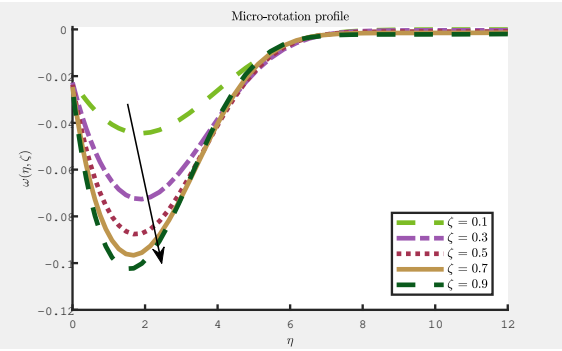

(b) micro-rotation profile

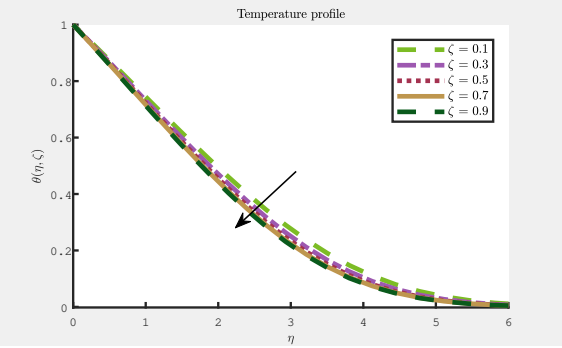

(c) temperature profile

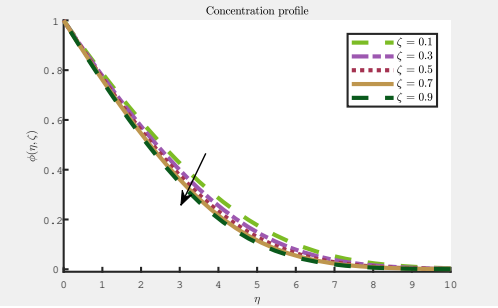

(d) concentration profile

We observe from Figure 6.4a that for $0 \leq \eta \leq 5$, the velocity profiles increase as time increases but decrease when $\eta > 5$. In the remaining three figures (b to d), however, all the profiles are seen to decrease as ζ increases.

The influence of conduction-radiation Rd is observed in the Figures 6.4e to 6.4h, given below, when $\zeta = 0.7$, $Re = 0.5$, $n = 0.8$, $N = 0.6$, $\Delta = 0.1$, $Ha = 0.2$, $Da = \infty$, $Fs = 1$, $Pr = 0.72$, $\delta = 1$, $\lambda = 0.1$, $H = 1$, $Sc = 0.22$, $K = 0.1$ $Z = H - 1$, and $Bi = \infty$

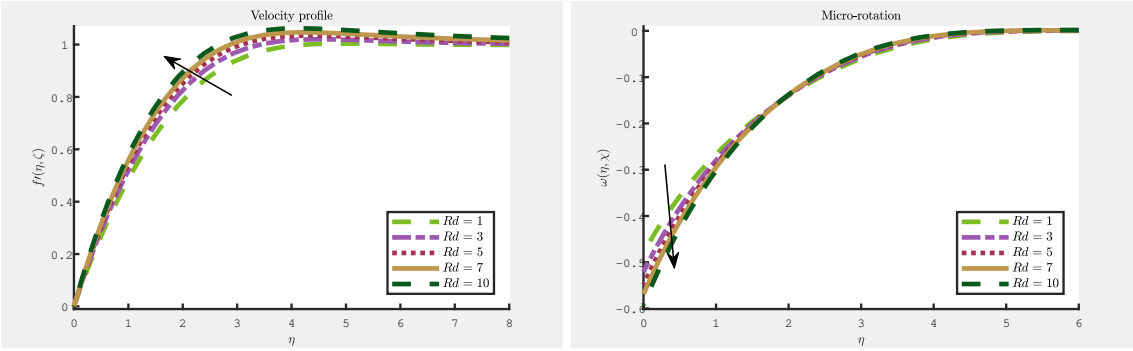

(e) velocity profile

(f) micro-rotation profile

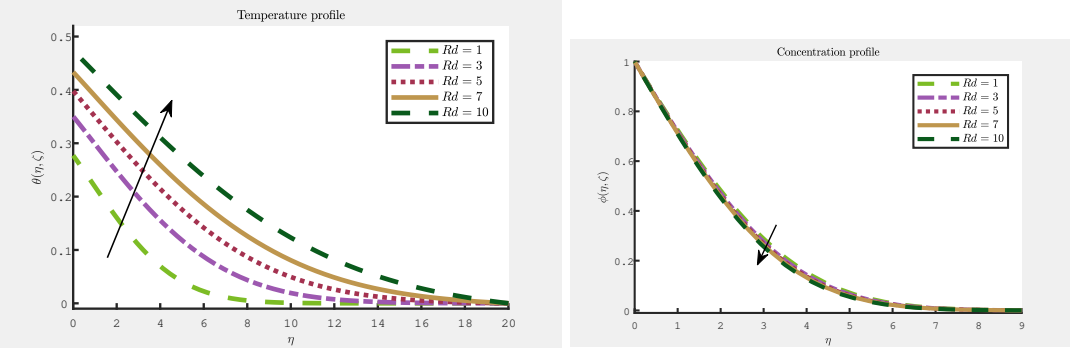

(g) temperature profile

(h) concentration profile

An increase in conduction-radiation Rd is observed to heat the fluid and thereby facilitate the upward flow of the fluid in the cone and reducing microrotation. This is seen in Figures 6.4e and 6.4f where the velocity flow increases while microrotation decreases. With an increase in radiation on the fluid, the fluid heats up thereby increasing temperature within the cone and decreasing concentration of the fluid as diffusion occurs. We see these trends in Figures 6.4g and 6.4h.

Figures 6.4i to 6.4l display the effect of the local Forchheimer parameter on the velocity, micro-rotation, temperature profile and concentration profile when $\zeta = 0.2$, $Re = 0.5$, $n = 0.8$, $N = 0.6$, $\Delta = 0.1$, $Ha = 0.2$, $Da = \infty$, $Rd = 0.5$, $Pr = 0.72$, $\delta = 1$, $\lambda = 0.1$, $H = 1$, $Sc = 0.22$, $K = 0.1$ $Z = H - 1$, and $Bi = \infty$.

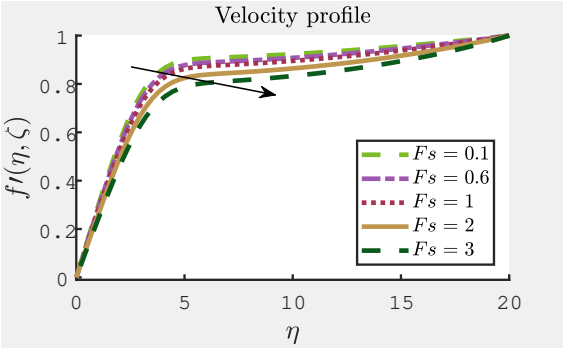

(i) velocity profile

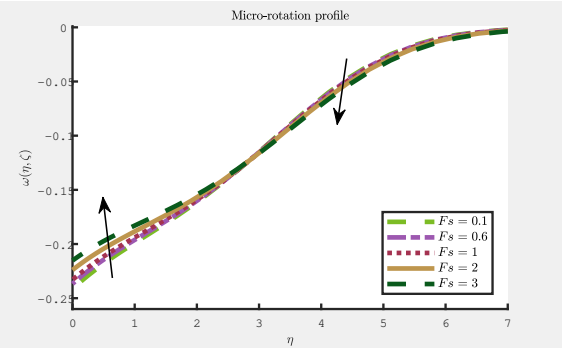

(j) micro-rotation profile

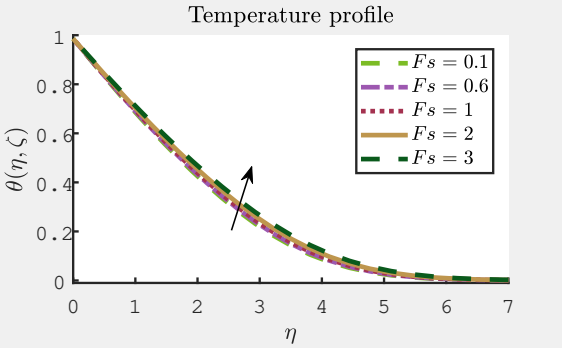

(k) temperature profile

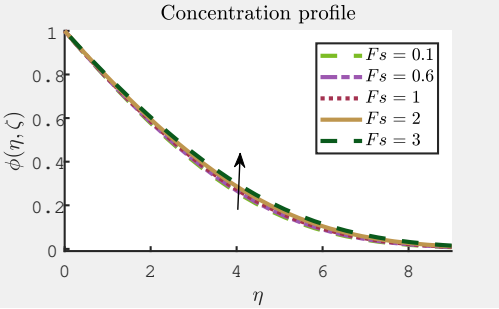

(l) concentration profile

We observe that the velocity profile decreases as Fs increases with less significant effect close to the wall in Figure 6.4i. In Figure 6.4j, we see that for $0 \leq \eta \leq 2$, Fs increases the micro-rotation profile and decreases the profile for $\eta > 2$. The concentration and temperature profiles in Figures 6.4k and 6.4l are observed to increase as Fs increases.

Figures 6.4m to 6.4p display the effect of increasing chemical reaction on the various flow profiles when $\zeta = 0.7$, $Re = 10$, $n = 0.8$, $N = 0.6$, $\Delta = 0.1$, $Ha = 0.2$, $Da = \infty$, $Rd = 0.5$, $Pr = 0.72$, $\delta = 0.1$, $\lambda = 10$, $H = 1$, $Sc = 0.22$, $Fs = 0.1$ $Z = H - 1$, and $Bi = 0.1$.

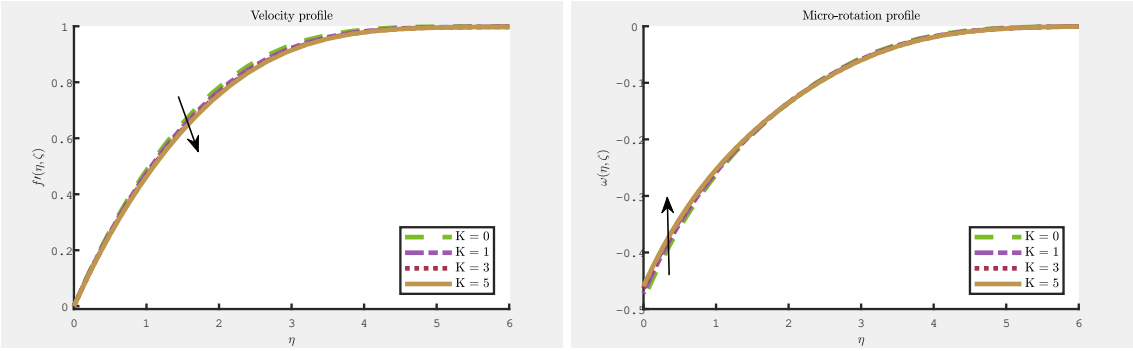

(m) velocity profile

(n) micro-rotation profile

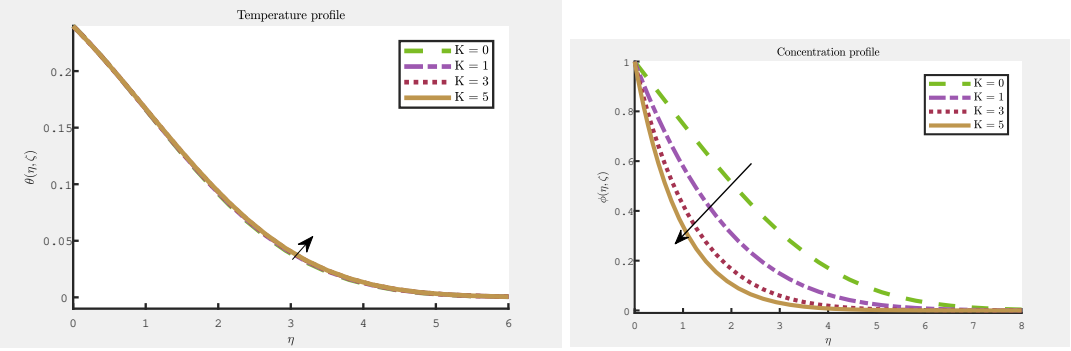

(o) temperature profile

(p) concentration profile

While increase in K decreases the velocity profile, micro-rotation profile is observed to increase. Increasing chemical reaction in the cone will effectively heat up the fluid faster and this reaction will decrease the concentration of the fluid. This expected trend is observed in Figures 6.4o and 6.4p where we observe an increment in the temperature profile and decrease in the concentration profile as K is increased.

Figures 6.4q to 6.4t, below, show the influence of mixed convection on the various profiles when $\zeta = 0.7$, $Re = 0.5$, $n = 0.8$, $N = 0.6$, $\Delta = 0.1$, $Ha = 0.2$, $Da = \infty$, $Fs = 1$, $Pr = 0.72$, $\delta = 1$, $Rd = 0.1$, $H = 1$, $Sc = 0.22$, $K = 0.1$ $Z = H - 1$, and $Bi = \infty$.

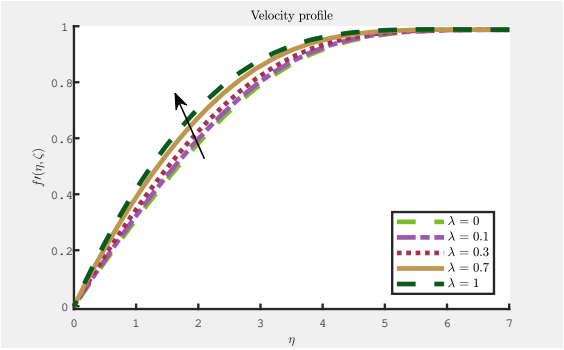

(q) velocity profile

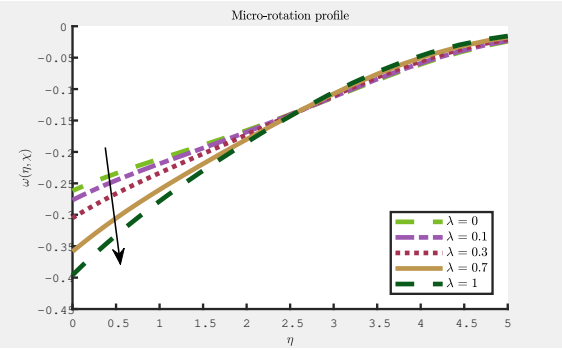

(r) micro-rotation profile

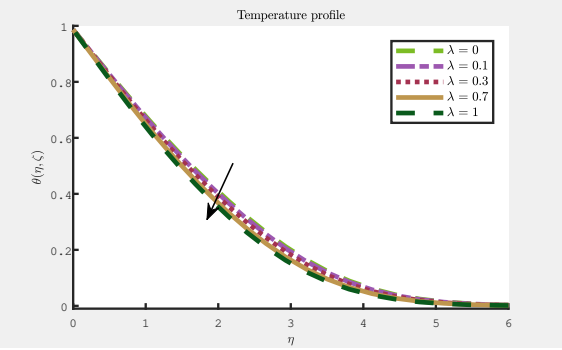

(s) temperature profile

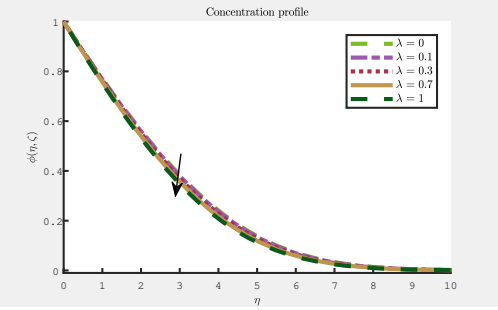

(t) concentration profile

We observe that as λ increases, the velocity flow profile increases while the micro-rotation flow profile decreases in Figures 6.4q and 6.4r, respectively. We also observe that temperature and concentration both decrease with increase in λ.

6.5 Summary

In this study, we have studied the influence of conduction radiation, mixed convection, chemical reaction and Forchheimer parameter on the mixed convection boundary layer flow of an MHD incompressible micropolar fluid near a vertical truncated cone. The study has been conducted using the paired quasilinearization method (PQLM) to generate results. We observe that increased chemical reaction and radiation both increase the temperature and decrease concentration. While

increasing radiation increases the velocity profile and decreases the micro-rotation profile, increasing chemical reaction decreases the velocity profile and increases the micro-rotation profile. We have also discovered that increasing mixed convection decreases micro-rotation, temperature and concentration profiles while increasing velocity profile. We also observed that increasing the Forchheimer parameter both increased and decreased the micro-rotation profile over different domains. It increased both temperature and concentration profiles and decreased the velocity profile.

Chapter 7

Multi-Domain Paired Quasilinearization Method for solving systems of partial differential equations

7.1 Introduction

The increasing complexities in modeling fluid flow problems leads to systems of nonlinear differential equations that are difficult to solve analytically. This necessitates introducing numerical methods, which over the years have been developed to take care of nonlinearities of differential equations used to model the problems more completely. Numerical methods make use of initial approximations that satisfy the given initial or boundary conditions, or both, which after iterations achieve convergence to some consistent solution.

Spectral-based numerical methods have been developed comparatively recently and have been shown to be effective methods for solving fluid flow problems [149]. Both compressible and incompressible fluids have been studied extensively by Peyret and Taylor [150] and Hussaini and Zang [149], who used spectral methods, amongst other numerical methods, to solve several problems. In both publications, the robustness of spectral-based techniques was noted and it was observed that the method demands fewer collocation points to obtain accurate results when compared to finite difference, finite element, and finite volume methods. Spectral methods have also been

established by Colbert-Kelly et al. [151] to be unconditionally stable. Khader and Mziou [152] also performed an analysis on the convergence of spectral methods and found them to converge with the use of appropriate approximating functions.

In dealing with nonlinearities in differential equations, spectral methods have been combined with relaxation, linearization or perturbation techniques with highly positive results. To elaborate, Turkyilmazoglu [153] combined spectral methods with Newton's linearization technique, where a correction term is used when linearizing a nonlinear system of differential equations. It was noted In Turkyilmazoglu's study that with the appropriate initial approximation, solutions could be obtained regardless of the values of parameters involved in the study. This emphasizes the robustness of the spectral method. Analytical coordinate transformations were used by Sharp and Trummer [154] with spectral methods in generating solutions to nonlinear differential equations. They verified that the method was convergent and had high accuracy.

Methods of particular interest to this study, are the spectral local linearization method (SLLM), spectral quasilinearization method (SQLM) and the paired quasilinearization method (PQLM). The SLLM, as introduced by Motsa [18], involves the linearization of a function and its derivative in an equation from a system of nonlinear differential equations and then using updated solutions from the first equation in subsequent equations. This process effectively decouples the system of differential equations. By contrast, the SQLM, also introduced by Motsa [18] involves the linearization of the system of differential equations collectively. Among others, these methods were found by Motsa [18], to be effective in solving fluid flow problems. It was also discovered that the SQLM converged faster than the SLLM, but in some instances to lesser accuracy. This led to the introduction of the PQLM by Motsa and Animasaun [20] that works by linearizing two functions and their corresponding derivatives in two equations and using their updated solutions in subsequent equation pairs. This leads to a decoupled system of coupled pairs of differential equations. The PQLM was found to be effective in solving fluid flow problems and this prompted Otegbeye and Motsa [137] to conduct a comparative study on the PQLM and the SLLM. It was observed that when the PQLM was applied to the pairings that contained more nonlinear terms,

the PQLM converged faster than the SLLM while maintaining the same accuracy level.

Solving systems of partial differential equations that are defined on a large time domain can be computationally demanding and methods like the SLLM and PQLM do not perform well when used on such equations. This challenge has prompted the introduction of time-splitting spectral-based numerical methods. These methods have been successfully implemented and shown to provide convergent numerical solutions with high accuracy. In particular, methods such as the multi-domain bivariate spectral quasilinearization method [50, 155, 156] and the bivariate pseudo-spectral local linearization method [157] have been developed and been shown to be efficient. This prompts the need to improve the PQLM to solve systems of PDEs using domain-splitting.

In this study, we aim to introduce the multi-domain paired quasilinearization method (MD-PQLM) which is an extension of the paired quasilinearization method used by Motsa and Animasaun [20] and Otegbeye and Motsa [137]. We also seek to conduct a comparison test on the different equation pairings in our proposed method to observe their effect on the speed of convergence or accuracy of the method. In the case where it does enhance convergence and accuracy, we try to relate the nonlinearity of the equations modelling the problem to the speed of convergence of the method. To check if our proposed method improves the convergence speed of the bivariate pseudo-spectral linearization method, we compare the different schemes of our proposed method to the method. The speed of convergence is tested using the solution error of the respective methods. The solution error arises by calculating the difference between successive iterations until a point is reached where further iterations do not improve the error. We also test the accuracy of the methods using residual errors. The residual error is generated by rewriting the original set of differential equations using the approximate solutions obtained. Numerical experimentation is carried out on a system of PDEs that model the natural convection over the vertical frustum of a cone in a nanofluid and in the presence of the Soret effect, that had been previously considered by Motsa et al. [157].

7.2 Description of MD-PQLM

In this section, the numerical scheme for the multi-domain paired quasilinearization method (MD-PQLM) is presented for a general system of N nonlinear partial differential equations in N unknowns. Let us consider a partial differential equation that contains its highest derivative of order m_1 in the form

$$f(\zeta, \mathbf{u}_1) = \frac{\partial u_1}{\partial \tau}, \;\; \zeta \in [a,b], \;\; \tau \in [0,T], \tag{7.1}$$

where $\mathbf{u}_1 = \{u_1, u_1^{'}, \ldots, u_1^{m_1-1}, u_1^{m_1}\}$ is a set whose entries are each functions of ζ, $u_1^{'} = \frac{\partial u_1}{\partial \zeta}$ is the first partial derivative with respect to ζ and $u_1^{m_1} = \frac{\partial^{m_1} u_1}{\partial \zeta^{m_1}}$ is the m_1^{th} derivative. We further consider a system of N partial differential equations in N unknowns of the form

$$\mathbf{f}_l(\zeta, \mathbf{u}_1, \mathbf{u}_2, \ldots, \mathbf{u}_N) = \frac{\partial \mathbf{u}_l}{\partial \tau}, \;\; l = 1,2,\ldots,N \tag{7.2}$$

which represents a coupled nonlinear system of partial differential equations with each $\mathbf{f}_l, \;\; l = 1,\ldots,N$, being a nonlinear operator, $\{\mathbf{u}_1, \mathbf{u}_2, \ldots, \mathbf{u}_N\}$ is a set that contains

$$\left(\{u_1^{(0)}, u_1^{(1)}, \ldots, u_1^{(m_1)}\}, \ldots, \{u_N^{(0)}, u_N^{(1)}, \ldots, u_N^{(m_N)}\}\right).$$

For the purpose of consistency, let $m_{l,q}$ represent the highest partial derivative order of entries in $(\mathbf{u}_1, \mathbf{u}_2, \ldots, \mathbf{u}_N)$ with respect to ζ in the l^{th} equation. The MD-PQLM involves linearizing equations from the system (7.2), one pair at a time. To demonstrate how the MD-PQLM is applied on the general system (7.2), an ordered pairing will be performed, but different combinations may be used. The initial process in the MD-PQLM involves the decoupling of the original system (7.2) into pairs with the application of quasilinearization on two sets in $\{\mathbf{u}_1, \mathbf{u}_2, \cdots, \mathbf{u}_N\}$ and their corresponding $\mathbf{f}_l$ equations. If we select $\mathbf{u}_1$ and $\mathbf{u}_2$ as our first pairing, then quasilinearization is applied to equations $f_1(\mathbf{u}_1, \mathbf{u}_2, \cdots, \mathbf{u}_N)$ and $f_2(\mathbf{u}_1, \mathbf{u}_2, \cdots, \mathbf{u}_N)$. This process is continued for other pairs using solutions from previous pairs to update subsequent pairs. To represent this in a general form,

$$f_k(\zeta, \mathbf{u}_1, \cdots, \mathbf{u}_N) = \frac{\partial \mathbf{u}_k}{\partial \tau}, \;\; k = \{1,2\}, \{3,4\}, \ldots, \{N-1, N\} \tag{7.3}$$

In applying the MD-PQLM to the system (7.3), we use quasilinearization on each set of pairs in the system for the purpose of linearizing with the application of the Taylor series expansion. To do

this, initial approximating points $(\mathbf{u}_1, \mathbf{u}_2, \cdots, \mathbf{u}_N)$ are selected and expanded upon such that

$$f_k\left((\mathbf{u}_{1,r},\ldots,\mathbf{u}_{N,r})+\Delta(\mathbf{u}_1,\ldots,\mathbf{u}_N)\right) \approx f_k\left(\mathbf{u}_{1,r},\ldots,\mathbf{u}_{N,r}\right)+\sum_{p=0}^{m_{k,k}} \frac{\partial^{(p)} f_k\left(\mathbf{u}_{1,r},\ldots,\mathbf{u}_{N,r}\right)}{\partial u_k^{(p)}}\left(\Delta \mathbf{u}_k^{(p)}\right), \quad k=\{1,2\},\{3,4\},\ldots,\{N-1,N\} \tag{7.4}$$

where $\Delta \mathbf{u}_k^{(p)} = \mathbf{u}_{k,r+1}^{(p)} - \mathbf{u}_{k,r}^{(p)}$ and each pair $\frac{\partial^{(p)} f_k\left(\mathbf{u}_{q,r}\right)}{\partial \mathbf{u}_k^{(p)}}$ is a 2×2 Jacobian matrix.

The expansion in (7.4) is expressed fully as

$$\begin{aligned} f_k\left((\mathbf{u}_{1,r},\ldots,\mathbf{u}_{N,r})+\Delta(\mathbf{u}_1,\ldots,\mathbf{u}_N)\right) &\approx f_k\left(\mathbf{u}_{1,r},\ldots,\mathbf{u}_{N,r}\right)+\sum_{p=0}^{m_{k,k}} \frac{\partial^{(p)} f_k\left(\mathbf{u}_{1,r},\ldots,\mathbf{u}_{N,r}\right)}{\partial u_k^{(p)}}\left(\mathbf{u}_{k,r+1}^{(p)}\right) \\ -\sum_{p=0}^{m_{k,k}} \frac{\partial^{(p)} f_k\left(\mathbf{u}_{1,r},\ldots,\mathbf{u}_{N,r}\right)}{\partial u_k^{(p)}}&\left(\mathbf{u}_{k,r}^{(p)}\right), \quad k=\{1,2\},\{3,4\},\ldots,\{N-1,N\} \end{aligned} \tag{7.5}$$

The expansion given in (7.5) is substituted into the system (7.3) and we obtain

$$\sum_{p=0}^{m_{k,k}} \frac{\partial^{(p)} f_k\left(\mathbf{u}_{1,r},\ldots,\mathbf{u}_{N,r}\right)}{\partial u_k^{(p)}}\left(\mathbf{u}_{k,r+1}^{(p)}\right) - \frac{\partial \mathbf{u}_{k,r+1}}{\partial \tau} = R_k, \quad k=\{1,2\},\{3,4\},\ldots,\{N-1,N\},\ \ \tau\in[0,T], \tag{7.6}$$

where

$$R_k = \sum_{p=0}^{m_{k,k}} \frac{\partial^{(p)} f_k\left(\mathbf{u}_{1,r},\ldots,\mathbf{u}_{N,r}\right)}{\partial u_k^{(p)}}\left(\mathbf{u}_{k,r}^{(p)}\right) - f_k\left(\mathbf{u}_{1,r},\ldots,\mathbf{u}_{N,r}\right).$$

The time interval of the decoupled system of paired equations (7.6) is decomposed into smaller non-overlapping sub-intervals $\rho_e = [\tau_{e-1}, \tau_e],\ e = 1,2,\ldots,T$ where $\tau \in \rho,\ \rho = [0,T]$. This is the general concept of the multi-domain approach as applied in, amongst others, Motsa et al. [158]. The system (7.6) is solved in each interval $[\tau_{e-1}, \tau_e]$ in the form

$$\sum_{p=0}^{m_{k,k}} \frac{\partial^{(p)} f_k\left(\mathbf{u}_{1,r}^{e},\ldots,\mathbf{u}_{N,r}^{e}\right)}{\partial u_k^{(p)}}\left(\mathbf{u}_{k,r+1}^{(p)e}\right) - \frac{\partial \mathbf{u}_{k,r+1}^{e}}{\partial \tau} = R_k, \quad k=\{1,2\},\{3,4\},\ldots,\{N-1,N\},\ \ \tau\in[0,T]. \tag{7.7}$$

The system (7.7) can be solved using different numerical techniques but due to the advantage of spectral accuracy needing few grid points, we elect to apply the Chebyshev spectral collocation method. Numerous researchers have documented the description and implementation of the

Chebyshev spectral method; for instance Boyd [16], Trefethen [13] and Canuto et al. [17]. In summary, the idea behind the spectral method is using Gauss-Lobatto points as collocation points, applying Lagrange polynomials and differentiation matrices in order to seek a solution. It also involves transforming the physical domains $\zeta \in [a,b]$ and $\tau \in [0,T]$ to $x \in [-1,1]$ and $y \in [-1,1]$, respectively.

$$\sum_{p=0}^{m_{k,k}} \mathbf{diag}\left[\frac{\partial^{(p)} f_k\left(\mathbf{u}^e_{1,j,r},\ldots,\mathbf{u}^e_{N,j,r}\right)}{\partial u^{(p)}_{k,j}}\right]\left(\mathbb{U}^{(p)e}_{k,r+1}\right) - \sum_{q=0}^{N_y} d_{j,q}\mathbf{u}^e_{r+1,k} = \mathbf{R}_{k,j}, \tag{7.8}$$

where

$$\mathbf{diag}\left[\frac{\partial^{(p)} f_k\left(\mathbf{u}^e_{1,j,r},\ldots,\mathbf{u}^e_{N,j,r}\right)}{\partial u^{(p)}_{k,j}}\right] = \begin{bmatrix} \frac{\partial^{(p)} f_k\left(\mathbf{u}^e_{1,j,r}\left(x_0,y_j\right),\ldots,\mathbf{u}^e_{N,j,r}\left(x_0,y_j\right)\right)}{\partial u^{(p)}_{k,j}} & & & \\ & \frac{\partial^{(p)} f_k\left(\mathbf{u}^e_{1,j,r}\left(x_1,y_j\right),\ldots,\mathbf{u}^e_{N,j,r}\left(x_1,y_j\right)\right)}{\partial u^{(p)}_{k,j}} & & \\ & & \ddots & \\ & & & \frac{\partial^{(p)} f_k\left(\mathbf{u}^e_{1,j,r}\left(x_N,y_j\right),\ldots,\mathbf{u}^e_{N,j,r}\left(x_N,y_j\right)\right)}{\partial u^{(p)}_{k,j}} \end{bmatrix} \tag{7.9}$$

and

$$\mathbb{U}^{(p)e}_{k,r+1} = \mathbf{D}^p \mathbf{u}^e_{k,r+1}. \tag{7.10}$$

The coupled linearized system (7.8) can be expressed in matrix form as

$$\begin{bmatrix} \mathbf{A}^e_{k,k} & A^e_{k,k+1} \\ \mathbf{A}^e_{k+1,k} & \mathbf{A}^e_{k+1,k+1} \end{bmatrix}\begin{bmatrix} \mathbf{U}^e_k \\ \mathbf{U}^e_{k+1} \end{bmatrix} = \begin{bmatrix} \mathbf{R}_{k,j} \\ \mathbf{R}_{k+1,j} \end{bmatrix}, \tag{7.11}$$

where each entry of $\mathbf{A}^e_{\{k,k+1\},\{k,k+1\}}$ is a matrix of size $N_y\left(N_x+1\right)\times N_y\left(N_x+1\right)$ and each entry of both $\mathbf{U}^e_k$ and $\mathbf{R}_k$ have $N_y\left(N_x+1\right)$ dimensions.

7.3 Example

In this section, the natural convection over the vertical frustum of a cone in a nanofluid in the presence of the Soret effect, previously studied by Motsa et al. [157] is considered. Motsa et al. [157]

investigated this problem by representing it with a nonlinear system of partial differential equations and applying the bivariate pseudo-spectral local linearization method (BPSLLM) to generate solutions.

$$f''' + \left(R + \frac{3}{4}\right) f f'' - \frac{1}{2} f'^2 + \theta + NcS - Nr\gamma = \xi \left(f' \frac{\partial f'}{\partial \xi} - f'' \frac{\partial f}{\partial \xi} \right), \tag{7.12}$$

$$\frac{1}{Pr}\theta'' + \left(R + \frac{3}{4}\right) f\theta' + Nb\gamma'\theta' + Nt\theta'^2 = \xi \left(f' \frac{\partial \theta}{\partial \xi} - \theta' \frac{\partial f}{\partial \xi} \right), \tag{7.13}$$

$$\frac{1}{Le}\gamma'' + \left(R + \frac{3}{4}\right) f\gamma' + \frac{1}{Le}\frac{Nt}{Nb}\theta'' = \xi \left(f' \frac{\partial \gamma}{\partial \xi} - \gamma' \frac{\partial f}{\partial \xi} \right), \tag{7.14}$$

$$\frac{1}{Sc}S'' + \left(R + \frac{3}{4}\right) fS' + S_T\theta'' = \xi \left(f' \frac{\partial S}{\partial \xi} - S' \frac{\partial f}{\partial \xi} \right), \tag{7.15}$$

with corresponding boundary conditions

$$f(0,\xi) + \frac{\xi}{\left(\frac{3}{4}+R\right)} \frac{\partial f}{\partial \xi} = 0,\ \theta(0,\xi) = S(0,\xi) = \gamma(0,\xi) = 1, \tag{7.16}$$

$$f'(\infty,\xi) = S(\infty,\xi) = \theta(\infty,\xi) = \gamma(\infty,\xi) = 0, \tag{7.17}$$

where Pr is the Prandtl number, Sc the Schmidt number, Le the Lewis number, Nr, Nc the nanofluid and regular buoyancy ratios, respectively, Nt the thermophoresis parameter, S_T the Soret number, $R = \frac{\xi}{1+\xi}$ and prime denotes differentiation with respect to η.

7.3.1 Solution Techniques

In this section, the iteration schemes of the MD-PQLM, BPSLLM and MD-SQLM on the system (7.12) − (7.15) are fully described.

The pairing of equations in the system (7.12) − (7.15) is performed using different combinations.

1. MD-PQLM Case 1: ($\{f,\theta\}$ and $\{\gamma,S\}$) which represents the pairings {(7.12) and (7.13)} and {(7.14) and (7.15)},

2. MD-PQLM Case 2:($\{f,\gamma\}$ and $\{\theta,S\}$) which represents the pairings {(7.12) and (7.14)} and {(7.13) and (7.15)},

3. MD-PQLM Case 3: ($\{f,S\}$ and $\{\theta,\gamma\}$) which represents the pairings {(7.12) and (7.15)} and {(7.13) and (7.14)},

4. Case 4: BPSLLM,

Bivariate pseudo-spectral local linearization method (BPSLLM)

In this section, we present the BPSLLM scheme for the system (7.12) − (7.15). The BPSLLM linearizes equations individually, thereby decoupling a coupled system of equations. Let us consider equation (7.12) that contains the nonlinear terms ff'', f'^2, $f'\frac{\partial f'}{\partial \xi}$ and $f''\frac{\partial f}{\partial \xi}$. We linearize the nonlinear terms using the Taylor series expansion and obtain the linearized equations

$$f'''_{r+1}+\left(R+\frac{3}{4}\right)f_r f''_{r+1}+\left(R+\frac{3}{4}\right)f''_r f_{r+1}-\left(R+\frac{3}{4}\right)f_r f''_r-f'_r f'_{r+1}+\frac{1}{2}f'^2_r+\theta_r+NcS_r-$$
$$Nr\gamma_r=\xi f'_r\frac{\partial f'_{r+1}}{\partial \xi}+\xi\frac{\partial f'_r}{\partial \xi}f'_{r+1}-\xi f'_r\frac{\partial f'_r}{\partial \xi}-\xi f''_r\frac{\partial f_{r+1}}{\partial \xi}-\xi\frac{\partial f_r}{\partial \xi}f''_{r+1}+\xi f''_r\frac{\partial f_r}{\partial \xi}, \tag{7.18}$$

where terms with $r+1-$ and $r-$subscripts are at current and previous iteration levels, respectively. With the solution obtained for equation (7.18), f and its corresponding derivatives are updated and applied at the current iteration level in subsequent equations. We apply the same procedure for the functions in equations (7.13)−(7.15) and we obtain

$$\frac{1}{Pr}\theta''_{r+1}+\left(R+\frac{3}{4}\right)f_{r+1}\theta'_{r+1}+Nb\gamma'_r\theta'_{r+1}+2Nt\theta'_r\theta'_{r+1}-$$
$$Nt\theta'^2_r=\xi f'_{r+1}\frac{\partial \theta_{r+1}}{\partial \xi}-\xi\frac{\partial f_{r+1}}{\partial \xi}\theta'_{r+1}, \tag{7.19}$$
$$\frac{1}{Le}\gamma''_{r+1}+\left(R+\frac{3}{4}\right)f_{r+1}\gamma'_{r+1}+\frac{1}{Le}\frac{Nt}{Nb}\theta''_{r+1}=$$
$$\xi f'_{r+1}\frac{\partial \gamma}{\partial \xi}-\xi\frac{\partial f_{r+1}}{\partial \xi}\gamma'_{r+1}, \tag{7.20}$$
$$\frac{1}{Sc}S''_{r+1}+\left(R+\frac{3}{4}\right)f_{r+1}S'_{r+1}+S_T\theta''_{r+1}=\xi f'_{r+1}\frac{\partial S_{r+1}}{\partial \xi}-\xi\frac{\partial f_{r+1}}{\partial \xi}S'_{r+1}. \tag{7.21}$$

The decoupled system (7.18)−(7.21) can be expressed compactly as;

$$f_{r+1}+[a_1]\,f''_{r+1}+[a_2]\,f'_{r+1}+[a_3]\,f_{r+1}=[a_4]\,\frac{\partial f'_{r+1}}{\partial\xi}+[a_5]\,\frac{\partial f_{r+1}}{\partial\xi}, \tag{7.22}$$

$$\left(\frac{1}{Pr}\right)\theta''_{r+1}+[b_1]\,\theta'_{r+1}=[b_2]\,\frac{\partial\theta_{r+1}}{\partial\xi}+b_3, \tag{7.23}$$

$$\left(\frac{1}{Le}\right)\gamma''_{r+1}+[c_1]\,\gamma'_{r+1}=[c_2]\,\frac{\partial\gamma_{r+1}}{\partial\xi}+c_3, \tag{7.24}$$

$$\left(\frac{1}{Sc}\right)S''_{r+1}+[e_1]\,S'_{r+1}=[e_2]\,\frac{\partial S_{r+1}}{\partial\xi}+e_3, \tag{7.25}$$

where terms in $[\ldots]$ and $(\ldots)$ are vector and scalar quantities, respectively, and

$$a_1=\left(R+\frac{3}{4}\right)f_r+\xi\frac{\partial f_r}{\partial\xi},\ \ a_2=-f'_r-\xi\frac{\partial f'_r}{\partial\xi},\ a_3=\left(R+\frac{3}{4}\right)f''_r,$$

$$a_4=\xi f'_r,\ \ a_5=-\xi f''_r,$$

$$a_6=\left(R+\frac{3}{4}\right)f_r f''_r-\frac{1}{2}f'^2_r-\theta_r-NcS_r-Nr\gamma_r-\xi f'_r\frac{\partial f'_r}{\partial\xi}+\xi f''_r\frac{\partial f_r}{\partial\xi},$$

$$b_1=\left(R+\frac{3}{4}\right)f_{r+1}+Nb\gamma'_r+2Nt\theta'_r+\xi\frac{\partial f_{r+1}}{\partial\xi},\ b_2=\xi f'_{r+1},\ b_3=Nt\theta'^2_r,$$

$$c_1=\left(R+\frac{3}{4}\right)f_{r+1}+\xi\frac{\partial f_{r+1}}{\partial\xi},\ c_2=\xi f'_{r+1},\ c_3=-\frac{Nt}{LeNb}\theta''_{r+1},$$

$$e_1=\left(R+\frac{3}{4}\right)f_{r+1}+\xi\frac{\partial f_{r+1}}{\partial\xi},\ e_2=\xi f'_{r+1},\ e_3=-S_T\theta''_{r+1}.$$

Applying the multi-domain approach as described previously Chapter 1, the system of decoupled linear equations (7.22) − (7.25) can be further expressed as

$$f'''^{(p)}_{r+1}+\left[a_1^{(p)}\right]f''^{(p)}_{r+1}+\left[a_2^{(p)}\right]f'^{(p)}_{r+1}+\left[a_3^{(p)}\right]f^{(p)}_{r+1}=\left[a_4^{(p)}\right]\frac{\partial f'^{(p)}_{r+1}}{\partial\xi}$$
$$+\left[a_5^{(p)}\right]\frac{\partial f^{(p)}_{r+1}}{\partial\xi}+\left[a_6^{(p)}\right], \tag{7.26}$$

$$\left(\frac{1}{Pr}\right)\theta''^{(p)}_{r+1}+\left[b_1^{(p)}\right]\theta'^{(p)}_{r+1}=\left[b_2^{(p)}\right]\frac{\partial\theta^{(p)}_{r+1}}{\partial\xi}+b_3^{(p)}, \tag{7.27}$$

$$\left(\frac{1}{Le}\right)\gamma''^{(p)}_{r+1}+\left[c_1^{(p)}\right]\gamma'^{(p)}_{r+1}=\left[c_2^{(p)}\right]\frac{\partial\gamma^{(p)}_{r+1}}{\partial\xi}+c_3^{(p)}, \tag{7.28}$$

$$\left(\frac{1}{Sc}\right)S''^{(p)}_{r+1}+\left[e_1^{(p)}\right]S'^{(p)}_{r+1}=\left[e_2^{(p)}\right]\frac{\partial S^{(p)}_{r+1}}{\partial\xi}+e_3^{(p)}, \tag{7.29}$$

where p denotes the particular time sub-interval that the equations are being solved in. We further apply the Chebyshev spectral collocation method on the decoupled system (7.26) − (7.29) in the form

$$\left[\mathbf{D}^3+\left[\mathbf{a}_1^{(p)}\right]\mathbf{D}^2+\left[\mathbf{a}_2^{(p)}\right]\mathbf{D}+\left[\mathbf{a}_3^{(p)}\right]\right]\mathbf{F}_{r+1}^{(p)}-\left[\mathbf{a}_4^{(p)}\right]\sum_{k=0}^{N_y}\mathbf{d}_{jk}\mathbf{D}\mathbf{F}_{r+1,k}-$$

$$\left[\mathbf{a}_5^{(p)}\right]\sum_{k=0}^{N_y}\mathbf{d}_{jk}\mathbf{F}_{r+1,k}^{(p)}=\left[\mathbf{a}_6^{(p)}\right], \tag{7.30}$$

$$\left[\left(\frac{1}{Pr}\right)\mathbf{D}^2+\left[\mathbf{b}_1^{(p)}\right]\mathbf{D}\right]\Theta_{r+1,j}-\left[\mathbf{b}_2^{(p)}\right]\sum_{k=0}^{Ny-1}\mathbf{d}_{jk}\Theta_{r+1,k}^{(p)}=\mathbf{b}_3^{(p)}, \tag{7.31}$$

$$\left[\left(\frac{1}{Le}\right)\mathbf{D}^2+\left[\mathbf{c}_1^{(p)}\right]\mathbf{D}\right]\Gamma_{r+1,j}-\left[\mathbf{c}_2^{(p)}\right]\sum_{k=0}^{Ny-1}\mathbf{d}_{jk}\Gamma_{r+1,k}^{(p)}=\mathbf{c}_3^{(p)}, \tag{7.32}$$

$$\left[\left(\frac{1}{Sc}\right)\mathbf{D}^2+\left[\mathbf{e}_1^{(p)}\right]\mathbf{D}\right]\mathbf{S}_{r+1,j}-\left[\mathbf{e}_2^{(p)}\right]\sum_{k=0}^{Ny-1}\mathbf{d}_{jk}\mathbf{S}_{r+1,k}^{(p)}=\mathbf{e}_3^{(p)}, \tag{7.33}$$

where $[\ldots]$ denotes a diagonal matrix and the differentiation matrix $\mathbf{D}=\frac{2}{L}D$. We further represent the decoupled system of linear equations (7.30) − (7.33) as

$$\mathbf{A}_1\mathbf{F}_{r+1,j}=\mathbf{R}_{1,j}, \tag{7.34}$$

$$\mathbf{A}_2\Theta_{r+1,j}=\mathbf{R}_{2,j}, \tag{7.35}$$

$$\mathbf{A}_3\Gamma_{r+1,j}=\mathbf{R}_{3,j}, \tag{7.36}$$

$$\mathbf{A}_4\mathbf{S}_{r+1,j}=\mathbf{R}_{4,j}, \tag{7.37}$$

where the diagonal and off-diagonal entries of the matrices $\mathbf{A}_1,\ \mathbf{A}_2,\ \mathbf{A}_3$ and $\mathbf{A}_4$ are given as

$$\begin{aligned}
\mathbf{A}_{1\{j,j\}} &= \mathbf{D}^3 + \left[\mathbf{a}_1^{(p)}\right]\mathbf{D}^2 + \left[\mathbf{a}_2^{(p)}\right]\mathbf{D} + \left[\mathbf{a}_3^{(p)}\right] - \left[\mathbf{a}_4^{(p)}\right]\mathbf{d}_{jj}\mathbf{D} - \left[\mathbf{a}_5^{(p)}\right]\mathbf{d}_{jj}, \\
\mathbf{A}_{1\{j,k\}} &=]- \left[\mathbf{a}_4^{(p)}\right]\mathbf{d}_{jk}\mathbf{D} - \left[\mathbf{a}_5^{(p)}\right]\mathbf{d}_{jk}, \qquad (7.38) \\
\mathbf{A}_{2\{j,j\}} &= \left(\frac{1}{Pr}\right)\mathbf{D}^2 + \left[\mathbf{b}_1^{(p)}\right]\mathbf{D} - \left[\mathbf{b}_2^{(p)}\right]\mathbf{d}_{jj}, \\
\mathbf{A}_{2\{j,k\}} &= -\left[\mathbf{b}_2^{(p)}\right]\mathbf{d}_{jk}, \qquad (7.39) \\
\mathbf{A}_{3\{j,j\}} &= \left(\frac{1}{Le}\right)\mathbf{D}^2 + \left[\mathbf{c}_1^{(p)}\right]\mathbf{D} - \left[\mathbf{c}_2^{(p)}\right]\mathbf{d}_{jj}, \\
\mathbf{A}_{3\{j,k\}} &= -\left[\mathbf{c}_2^{(p)}\right]\mathbf{d}_{jk}, \qquad (7.40) \\
\mathbf{A}_{4\{j,j\}} &= \left(\frac{1}{Sc}\right)\mathbf{D}^2 + \left[\mathbf{e}_1^{(p)}\right]\mathbf{D} - \left[\mathbf{e}_2^{(p)}\right]\mathbf{d}_{jk}, \\
\mathbf{A}_{4\{j,k\}} &= -\left[\mathbf{e}_2^{(p)}\right]\mathbf{d}_{jk}, \qquad (7.41)
\end{aligned}$$

and the right-hand sides are defined thus

$$\mathbf{R}_{1,r,j} = \left[\mathbf{a}_4^{(p)}\right]\mathbf{d}_{jN_y}\mathbf{D}\mathbf{F}_{N_y,r}^{(p)} + \left[\mathbf{a}_5^{(p)}\right]\mathbf{d}_{jN_y}\mathbf{F}_{N_y,r}^{(p)} + \mathbf{a}_{6,j}^{(p)}, \qquad (7.42)$$

$$\mathbf{R}_{2,r,j} = \left[\mathbf{b}_2^{(p)}\right]\mathbf{d}_{jN_y}\Theta_{N_y,r}^{(p)} + \mathbf{b}_{3,j}^{(p)}, \qquad (7.43)$$

$$\mathbf{R}_{3,r,j} = \left[\mathbf{c}_2^{(p)}\right]\mathbf{d}_{jN_y}\Gamma_{N_y,r}^{(p)} + \mathbf{c}_{3,j}^{(p)}, \qquad (7.44)$$

$$\mathbf{R}_{4,r,j} = \left[\mathbf{e}_2^{(p)}\right]\mathbf{d}_{jN_y}\mathbf{S}_{N_y,r}^{(p)} + \mathbf{e}_{3,j}^{(p)}. \qquad (7.45)$$

Multi-domain paired quasilinearization method-CASE 1

We describe the implementation of the paired quasilinearization method on the system (7.12) − (7.15). In section 7.3.1, we described the application of linearization on one function and its corresponding derivatives in one equation and updating its solution in subsequent equations. In the case of the MD-PQLM, however, we apply quasilinearization on two functions and their corresponding derivatives in two equations and update their solutions in subsequent equations. This brings about "pairing" or coupling of equations but at the same time effectively decoupling the large system.

For the first case, we apply quasilinearization to equations (7.12) and (7.13) to obtain the pair

$$f'''_{r+1}+\left(R+\frac{3}{4}\right)f_r f''_{r+1}+\left(R+\frac{3}{4}\right)f''_r f_{r+1}-\left(R+\frac{3}{4}\right)f_r f''_r-f'_r f'_{r+1}+\frac{1}{2}f'^2_r+\theta_{r+1}+NcS_r$$
$$-Nr\gamma_r=\xi f'_r\frac{\partial f'_{r+1}}{\partial\xi}+\xi\frac{\partial f'_r}{\partial\xi}f'_{r+1}-\xi f'_r\frac{\partial f'_r}{\partial\xi}-\xi f''_r\frac{\partial f_{r+1}}{\partial\xi}-\xi\frac{\partial f_r}{\partial\xi}f''_{r+1}+\xi f''_r\frac{\partial f_r}{\partial\xi}, \tag{7.46}$$

$$\frac{1}{Pr}\theta''_{r+1}+\left(R+\frac{3}{4}\right)f_r\theta'_{r+1}+\left(R+\frac{3}{4}\right)\theta'_r f_{r+1}-\left(R+\frac{3}{4}\right)f_r\theta'_r+Nb\gamma'_r\theta'_{r+1}+2Nt\theta'_r\theta'_{r+1}$$
$$-Nt\theta'^2_r=\xi f'_r\frac{\partial\theta_{r+1}}{\partial\xi}+\xi\frac{\partial\theta_r}{\partial\xi}f'_{r+1}-\xi f'_r\frac{\partial\theta_r}{\partial\xi}-\xi\theta'_r\frac{\partial f_{r+1}}{\partial\xi}-\xi\frac{\partial f_r}{\partial\xi}\theta'_{r+1}+\xi\theta'_r\frac{\partial f_r}{\partial\xi}. \tag{7.47}$$

Updated solutions for f, θ and their corresponding derivatives are used in the second pair of equations (7.14) and (7.15) which leads to the linear coupled pair

$$\frac{1}{Le}\gamma''_{r+1}+\left(R+\frac{3}{4}\right)f_{r+1}\gamma'_{r+1}+\frac{1}{Le}\frac{Nt}{Nb}\theta''_{r+1}=\xi f'_{r+1}\frac{\partial\gamma_{r+1}}{\partial\xi}-\xi\frac{\partial f_{r+1}}{\partial\xi}\gamma'_{r+1}, \tag{7.48}$$

$$\frac{1}{Sc}S''_{r+1}+\left(R+\frac{3}{4}\right)f_{r+1}S'_{r+1}+S_T\theta''_{r+1}=\xi f'_{r+1}\frac{\partial S_{r+1}}{\partial\xi}-\xi\frac{\partial f_{r+1}}{\partial\xi}S'_{r+1}. \tag{7.49}$$

The pairs $\{(7.46)\ \&\ (7.47)\}$ and $\{(7.48)\ \&\ (7.49)\}$ represent a decoupled system of coupled equations and can be expressed compactly as

$$f'''_{r+1}+[a_1]f''_{r+1}+[a_2]f'_{r+1}+[a_3]f_{r+1}+\theta_{r+1}=[a_4]\frac{\partial f'_{r+1}}{\partial\xi}+[a_5]\frac{\partial f_{r+1}}{\partial\xi}+a_6, \tag{7.50}$$

$$[b_1]f'_{r+1}+[b_2]f_{r+1}+\frac{1}{Pr}\theta''_{r+1}+[b_3]\theta'_{r+1}=[b_4]\frac{\partial f_{r+1}}{\partial\xi}+[b_5]\frac{\partial\theta_{r+1}}{\partial\xi}+b_6, \tag{7.51}$$

and

$$\frac{1}{Le}\gamma''_{r+1}+[c_1]\gamma'_{r+1}=[c_2]\frac{\partial\gamma_{r+1}}{\partial\xi}+c_3, \tag{7.52}$$

$$\frac{1}{Sc}S''_{r+1}+[e_1]S'_{r+1}=[e_2]\frac{\partial S_{r+1}}{\partial\xi}+e_3, \tag{7.53}$$

where

$$
\begin{aligned}
&a_1 = \left(R+\frac{3}{4}\right) f_r + \xi \frac{\partial f_r}{\partial \xi},\ a_2 = -f_r^{'} - \xi \frac{\partial f_r^{'}}{\partial \xi},\\
&a_3 = \left(R+\frac{3}{4}\right) f_r^{''},\ a_4 = \xi f_r^{'},\ a_5 = -\xi f_r^{''},\\
&a_6 = -\frac{1}{2} f_r^{'2} + \left(R+\frac{3}{4}\right) f_r f_r^{''} - NcS_r + Nr\gamma_r - \xi f_r^{'} \frac{\partial f_r^{'}}{\partial \xi} + \xi f_r^{''} \frac{\partial f_r}{\partial \xi},\\
&b_1 = -\xi \frac{\partial \theta_r}{\partial \xi},\ b_2 = \left(R+\frac{3}{4}\right) \theta_r^{'},\ b_3 = \left(R+\frac{3}{4}\right) f_r + Nb\gamma_r^{'} + 2Nt\theta_r^{'} + \xi \frac{\partial f_r}{\partial \xi},\\
&b_4 = -\xi \theta_r^{'},\ b_5 = \xi f_r^{'},\ b_6 = \left(R+\frac{3}{4}\right) f_r \theta_r^{'} + Nt\theta_r^{'2} - \xi f_r^{'} \frac{\partial \theta_r}{\partial \xi} + \xi \theta_r^{'} \frac{\partial f_r}{\partial \xi},\\
&c_1 = \left(R+\frac{3}{4}\right) f_{r+1} + \xi \frac{\partial f_{r+1}}{\partial \xi},\ c_2 = \xi f_r^{'},\ c_3 = -\frac{1}{Le}\frac{Nt}{Nb} \theta_{r+1}^{''},\\
&e_1 = \left(R+\frac{3}{4}\right) f_{r+1} + \xi \frac{\partial f_{r+1}}{\partial \xi},\ e_2 = \xi f_{r+1},\ e_3 = -S_T \theta_{r+1}^{''}.
\end{aligned}
$$

The multi-domain approach is applied on the pairs in the form

$$
f_{r+1}^{'''(p)} + \left[a_1^{(p)}\right] f_{r+1}^{''(p)} + \left[a_2^{(p)}\right] f_{r+1}^{'(p)} + \left[a_3^{(p)}\right] f_{r+1}^{(p)} + \theta_{r+1}^{(p)} = \left[a_4^{(p)}\right] \frac{\partial f_{r+1}^{'(p)}}{\partial \xi} + \left[a_5^{(p)}\right] \frac{\partial f_{r+1}^{(p)}}{\partial \xi} + a_6^{(p)}, \tag{7.54}
$$

$$
\left[b_1^{(p)}\right] f_{r+1}^{'(p)} + \left[b_2^{(p)}\right] f_{r+1}^{(p)} + \frac{1}{Pr} \theta_{r+1}^{''(p)} + \left[b_3^{(p)}\right] \theta_{r+1}^{'(p)} = \left[b_4^{(p)}\right] \frac{\partial f_{r+1}^{(p)}}{\partial \xi} + \left[b_5^{(p)}\right] \frac{\partial \theta_{r+1}^{(p)}}{\partial \xi} + b_6^{(p)}, \tag{7.55}
$$

and

$$
\frac{1}{Le} \gamma_{r+1}^{''(p)} + \left[c_1^{(p)}\right] \gamma_{r+1}^{'(p)} = \left[c_2^{(p)}\right] \frac{\partial \gamma_{r+1}^{(p)}}{\partial \xi} + c_3^{(p)}, \tag{7.56}
$$

$$
\frac{1}{Sc} S_{r+1}^{''(p)} + \left[e_1^{(p)}\right] S_{r+1}^{'(p)} = \left[e_2^{(p)}\right] \frac{\partial S_{r+1}^{(p)}}{\partial \xi} + e_3^{(p)}. \tag{7.57}
$$

The Chebyshev spectral collocation method is used to integrate the decoupled pairs and we get

$$\left[\mathbf{D}^3+\left[\mathbf{a}_1^{(p)}\right]\mathbf{D}^2+\left[\mathbf{a}_2^{(p)}\right]\mathbf{D}+\left[\mathbf{a}_3^{(p)}\right]\right]\mathbf{F}_{r+1}^{(p)}-\left[\mathbf{a}_4^{(p)}\right]\sum_{k=0}^{N_y}\mathbf{d}_{jk}\mathbf{D}\mathbf{F}_{r+1,k}^{(p)}$$
$$-\left[\mathbf{a}_5^{(p)}\right]\sum_{k=0}^{N_y}\mathbf{d}_{jk}\mathbf{F}_{r+1,k}^{(p)}+[\mathbf{I}]\,\Theta_{r+1}^{(p)}=a_6^{(p)}, \tag{7.58}$$

$$\left[\left[\mathbf{b}_1^{(p)}\right]\mathbf{D}+\left[\mathbf{b}_2^{(p)}\right]\right]\mathbf{F}_{r+1}^{(p)}-\left[\mathbf{b}_4^{(p)}\right]\sum_{k=0}^{N_y}\mathbf{d}_{jk}\mathbf{F}_{r+1,k}^{(p)}+\left[\frac{1}{Pr}\mathbf{D}^2+\left[\mathbf{b}_3^{(p)}\right]\mathbf{D}\right]\Theta_{r+1}^{(p)}$$
$$-\left[\mathbf{b}_5^{(p)}\right]\sum_{k=0}^{N_y}\mathbf{d}_{jk}\Theta_{r+1,k}^{(p)}=b_6^{(p)}, \tag{7.59}$$

and

$$\left[\frac{1}{Le}\mathbf{D}^2+\left[\mathbf{c}_1^{(p)}\right]\mathbf{D}\right]\Gamma_{r+1}^{(p)}-\left[\mathbf{c}_2^{(p)}\right]\sum_{k=0}^{N_y}\mathbf{d}_{jk}\Gamma_{r+1,k}^{(p)}=c_3^{(p)}, \tag{7.60}$$

$$\left[\frac{1}{Sc}\mathbf{D}^2+\left[\mathbf{e}_1^{(p)}\right]\mathbf{D}\right]\mathbf{S}_{r+1}^{(p)}-\left[\mathbf{e}_2^{(p)}\right]\sum_{k=0}^{N_y}\mathbf{d}_{jk}\mathbf{S}_{r+1,k}^{(p)}=e_3^{(p)}. \tag{7.61}$$

The pairs are solved in the form

$$\begin{bmatrix}\mathbf{A}_{11} & \mathbf{A}_{12}\\ \mathbf{A}_{21} & \mathbf{A}_{22}\end{bmatrix}\times\begin{bmatrix}\mathbf{F}_{r+1}\\ \Theta_{r+1}\end{bmatrix}=\begin{bmatrix}\mathbf{R}_{1,r,j}\\ \mathbf{R}_{2,r,j}\end{bmatrix}, \tag{7.62}$$

and

$$\begin{bmatrix}\mathbf{B}_{11} & \mathbf{B}_{12}\\ \mathbf{B}_{21} & \mathbf{B}_{22}\end{bmatrix}\times\begin{bmatrix}\Gamma_{r+1}\\ \mathbf{S}_{r+1}\end{bmatrix}=\begin{bmatrix}\mathbf{R}_{3,r,j}\\ \mathbf{R}_{4,r,j}\end{bmatrix}, \tag{7.63}$$

where the matrices $\mathbf{A}_{l,k}$ and $\mathbf{B}_{l,k}$ $l,k = 1,2$ consists of different entries on the diagonal and off-diagonal defined thus:

$$
\begin{aligned}
\mathbf{A}_{11\{j,j\}} &= \mathbf{D}^3 + \left[\mathbf{a}_1^{(p)}\right]\mathbf{D}^2 + \left[\mathbf{a}_2^{(p)}\right]\mathbf{D} + \left[\mathbf{a}_3^{(p)}\right] - \left[\mathbf{a}_4^{(p)}\right]\mathbf{d}_{jj}\mathbf{D} - \left[\mathbf{a}_5^{(p)}\right]\mathbf{d}_{jj}, \\
\mathbf{A}_{11\{j,k\}} &= -\left[\mathbf{a}_4^{(p)}\right]\mathbf{d}_{jk}\mathbf{D} - \left[\mathbf{a}_5^{(p)}\right]\mathbf{d}_{jk}, \\
\mathbf{A}_{12\{j,j\}} &= \mathbf{I}, \\
\mathbf{A}_{21\{j,j\}} &= \left[\mathbf{b}_1^{(p)}\right]\mathbf{D} + \left[\mathbf{b}_2^{(p)}\right] - \left[\mathbf{b}_4^{(p)}\right]\mathbf{d}_{jj}, \\
\mathbf{A}_{21\{j,k\}} &= -\left[\mathbf{b}_4^{(p)}\right]\mathbf{d}_{jk}, \\
\mathbf{A}_{22\{j,j\}} &= \frac{1}{Pr}\mathbf{D}^2 + \left[\mathbf{b}_3^{(p)}\right]\mathbf{D} - \left[\mathbf{b}_5^{(p)}\right]\mathbf{d}_{jj}, \\
\mathbf{A}_{22\{j,k\}} &= -\left[\mathbf{b}_5^{(p)}\right]\mathbf{d}_{jk}, \\
\mathbf{B}_{21\{j,j\}} &= \frac{1}{Le}\mathbf{D}^2 + \left[\mathbf{c}_1^{(p)}\right]\mathbf{D} - \left[\mathbf{c}_2^{(p)}\right]\mathbf{d}_{jj}, \\
\mathbf{B}_{21\{j,k\}} &= -\left[\mathbf{c}_2^{(p)}\right]\mathbf{d}_{jk}, \\
\mathbf{B}_{22\{j,k\}} &= \frac{1}{Sc}\mathbf{D}^2 + \left[\mathbf{e}_1^{(p)}\right]\mathbf{D} - \left[\mathbf{e}_2^{(p)}\right]\mathbf{d}_{jj}, \\
\mathbf{B}_{22\{j,k\}} &= -\left[\mathbf{e}_2^{(p)}\right]\mathbf{d}_{jk}, \\
\mathbf{A}_{12\{j,k\}} &= \mathbf{B}_{12} = \mathbf{B}_{21} = \mathbf{0},
\end{aligned}
$$

and;

$$\mathbf{R}_{1,j,r} = \left[\mathbf{a}_4^{(p)}\right]\mathbf{d}_{jN_y}\mathbf{D}\mathbf{F}_{N_y}^{(p)} + \left[\mathbf{a}_5^{(p)}\right]\mathbf{d}_{jN_y}\mathbf{F}_{N_y}^{(p)} + a_6^{(p)}, \tag{7.64}$$

$$\mathbf{R}_{2,j,r} = \left[\mathbf{b}_4^{(p)}\right]\mathbf{d}_{jN_y}\mathbf{F}_{N_y}^{(p)} + \left[\mathbf{b}_5^{(p)}\right]\mathbf{d}_{jN_y}\Theta_{N_y}^{(p)} + b_6^{(p)}, \tag{7.65}$$

$$\mathbf{R}_{3,j,r} = \left[\mathbf{c}_2^{(p)}\right]\mathbf{d}_{jN_y}\Gamma_{N_y}^{(p)} + c_3^{(p)}, \tag{7.66}$$

$$\mathbf{R}_{4,j,r} = \left[\mathbf{e}_2^{(p)}\right]\mathbf{d}_{jN_y}\mathbf{S}_{N_y}^{(p)} + e_3^{(p)}. \tag{7.67}$$

Multi-domain paired quasilinearization method-CASE 2

Pairing is performed on equations (7.12) and (7.14) by linearizing the nonlinear functions f, γ and their corresponding derivatives and we obtain the pair

$$f_{r+1}^{'''}+\left(R+\frac{3}{4}\right)f_r f_{r+1}^{''}+\left(R+\frac{3}{4}\right)f_r^{''}f_{r+1}-\left(R+\frac{3}{4}\right)f_r f_r^{''}-f_r^{'}f_{r+1}^{'}+\frac{1}{2}f_r^{'2}-Nr\gamma_{r+1}+$$
$$NcS_r+\theta_r=\xi f_r^{'}\frac{\partial f_{r+1}^{'}}{\partial\xi}+\xi\frac{\partial f_r^{'}}{\partial\xi}f_{r+1}^{'}-\xi f_r^{'}\frac{\partial f_r^{'}}{\partial\xi}-\xi f_r^{''}\frac{\partial f_{r+1}}{\partial\xi}-\xi\frac{\partial f_r}{\partial\xi}f_{r+1}^{''}+\xi f_r^{''}\frac{\partial f_r}{\partial\xi}, \tag{7.68}$$
$$\frac{1}{Le}\gamma_{r+1}+\left(R+\frac{3}{4}\right)f_r\gamma_{r+1}^{'}+\left(R+\frac{3}{4}\right)\gamma_r^{'}f_{r+1}-\left(R+\frac{3}{4}\right)f_r\gamma_r^{'}+\frac{1}{Le}\frac{Nt}{Nb}\theta_r^{''}$$
$$=\xi f_r^{'}\frac{\partial\gamma_{r+1}}{\partial\xi}+\xi\frac{\partial\gamma_r}{\partial\xi}f_{r+1}^{'}-\xi f_r^{'}\frac{\partial\gamma_r}{\partial\xi}-\xi\gamma_r^{'}\frac{\partial f_{r+1}}{\partial\xi}-\xi\frac{\partial f_r}{\partial\xi}\gamma_{r+1}^{'}+\xi\gamma_r^{'}\frac{\partial f_r}{\partial\xi}. \tag{7.69}$$

Updated solutions for f, γ and their corresponding derivatives are used in the second pair of equations and we obtain

$$\frac{1}{Pr}\theta_{r+1}^{''}+\left(R+\frac{3}{4}\right)f_{r+1}\theta_{r+1}^{'}+Nb\gamma_{r+1}^{'}\theta_{r+1}^{'}+2Nt\theta_r^{'}\theta_{r+1}^{'}=\xi f_{r+1}^{'}\frac{\partial\theta_{r+1}}{\partial\xi}-\xi\frac{\partial f_{r+1}}{\partial\xi}\theta_{r+1}^{'}, \tag{7.70}$$
$$\frac{1}{Sc}S_{r+1}^{''}+\left(R+\frac{3}{4}\right)f_{r+1}S_{r+1}^{'}+S_T\theta_{r+1}^{''}=\xi f_{r+1}^{'}\frac{\partial S_{r+1}}{\partial\xi}-\xi\frac{\partial f_{r+1}}{\partial\xi}S_{r+1}^{'}. \tag{7.71}$$

The pairs $\{7.68\ \&\ 7.69\}$ and $\{7.70\ \&\ 7.71\}$ represent coupled sub-systems of a decoupled large system and can be expressed compactly as

$$f_{r+1}^{'''}+[a_1]f_{r+1}^{''}+[a_2]f_{r+1}^{'}+[a_3]f_{r+1}+(-Nr)\gamma_{r+1}=$$
$$[a_4]\frac{\partial f_{r+1}^{'}}{\partial\xi}+[a_5]\frac{\partial f_{r+1}}{\partial\xi}+a_6, \tag{7.72}$$
$$[b_1]f_{r+1}^{'}+[b_2]f_{r+1}+\frac{1}{Le}\gamma_{r+1}^{''}+[b_3]\gamma_{r+1}^{'}=[b_4]\frac{\partial f_{r+1}}{\partial\xi}+[b_5]\frac{\partial\gamma_{r+1}}{\partial\xi}+b_6, \tag{7.73}$$

and

$$\frac{1}{Pr}\theta_{r+1}^{''}+[c_1]\theta_{r+1}^{'}=[c_2]\frac{\partial\theta_{r+1}}{\partial\xi}+c_3, \tag{7.74}$$
$$(S_T)\theta_{r+1}^{''}+\frac{1}{Sc}S_{r+1}^{''}+[e_1]S_{r+1}^{'}=[e_2]\frac{\partial S_{r+1}}{\partial\xi}, \tag{7.75}$$

where

$$a_1 = \left(R+\frac{3}{4}\right) f_r + \xi \frac{\partial f_r}{\partial \xi},\ a_2 = -f_r^{'} - \xi \frac{\partial f_r^{'}}{\partial \xi},$$
$$a_3 = \left(R+\frac{3}{4}\right) f_r^{''},\ a_4 = \xi f_r^{'},\ a_5 = -\xi f_r^{''},$$
$$a_6 = -\frac{1}{2} f_r^{'2} + \left(R+\frac{3}{4}\right) f_r f_r^{''} - \theta_r - NcS_r - \xi f_r^{'} \frac{\partial f_r^{'}}{\partial \xi} + \xi f_r^{''} \frac{\partial f_r}{\partial \xi},$$
$$b_1 = -\xi \frac{\partial \gamma_r}{\partial \xi},\ b_2 = \left(R+\frac{3}{4}\right) \gamma_r^{'},\ b_3 = \left(R+\frac{3}{4}\right) f_r + \xi \frac{\partial f_r}{\partial \xi},$$
$$b_4 = -\xi \gamma_r^{'},\ b_5 = \xi f_r^{'},\ b_6 = \left(R+\frac{3}{4}\right) f_r \gamma_r^{'} - \xi f_r^{'} \frac{\partial \gamma_r}{\partial \xi} + \xi \gamma_r^{'} \frac{\partial f_r}{\partial \xi},$$
$$c_1 = \left(R+\frac{3}{4}\right) f_{r+1} + Nb\gamma_{r+1}^{'} + 2Nt\theta_r^{'} + \xi \frac{\partial f_{r+1}}{\partial \xi},\ c_2 = \xi f_{r+1}^{'},\ c_3 = Nt\theta_{r+1}^{'2},$$
$$e_1 = \left(R+\frac{3}{4}\right) f_{r+1} + \xi \frac{\partial f_{r+1}}{\partial \xi},\ e_2 = \xi f_{r+1}^{'},$$

Implementing multi-domain on the pairs, we obtain

$$f_{r+1}^{'''(p)} + \left[a_1^{(p)}\right] f_{r+1}^{''(p)} + \left[a_2^{(p)}\right] f_{r+1}^{'(p)} + \left[a_3^{(p)}\right] f_{r+1}^{(p)} + (-Nr)\gamma_{r+1}^{(p)} =$$
$$\left[a_4^{(p)}\right] \frac{\partial f_{r+1}^{'(p)}}{\partial \xi} + \left[a_5^{(p)}\right] \frac{\partial f_{r+1}^{(p)}}{\partial \xi} + a_6^{(p)}, \tag{7.76}$$
$$\left[b_1^{(p)}\right] f_{r+1}^{'(p)} + \left[b_2^{(p)}\right] f_{r+1}^{(p)} + \frac{1}{Le} \gamma_{r+1}^{''(p)} + \left[b_3^{(p)}\right] \gamma_{r+1}^{'(p)} =$$
$$\left[b_4^{(p)}\right] \frac{\partial f_{r+1}^{(p)}}{\partial \xi} + \left[b_5^{(p)}\right] \frac{\partial \gamma_{r+1}^{(p)}}{\partial \xi} + b_6^{(p)}, \tag{7.77}$$

and

$$\frac{1}{Pr} \theta_{r+1}^{''(p)} + \left[c_1^{(p)}\right] \theta_{r+1}^{'(p)} = \left[c_2^{(p)}\right] \frac{\partial \theta_{r+1}^{(p)}}{\partial \xi} + c_3^{(p)}, \tag{7.78}$$
$$(S_T)\, \theta_{r+1}^{''(p)} + \frac{1}{Sc} S_{r+1}^{''(p)} + \left[e_1^{(p)}\right] S_{r+1}^{'(p)} = \left[e_2^{(p)}\right] \frac{\partial S_{r+1}^{(p)}}{\partial \xi}, \tag{7.79}$$

where p denotes the sub-interval of the time-domain. Chebyshev spectral collocation method is applied on the decoupled system of equations (7.76) − (7.79) and we obtain

$$\left[\mathbf{D}^3+\left[\mathbf{a}_1^{(p)}\right]\mathbf{D}^2+\left[\mathbf{a}_2^{(p)}\right]\mathbf{D}+\left[\mathbf{a}_3^{(p)}\right]\right]\mathbf{F}_{r+1}^{(p)}-\left[\mathbf{a}_4^{(p)}\right]\sum_{k=0}^{N_y}\mathbf{d}_{jk}\mathbf{D}\mathbf{F}_{r+1,k}-$$

$$\left[\mathbf{a}_5^{(p)}\right]\sum_{k=0}^{N_y}\mathbf{d}_{jk}\mathbf{F}_{r+1,k}+[(-Nr\mathbf{I})]\,\Gamma_{r+1}^{(p)}=a_6^{(p)}, \tag{7.80}$$

$$\left[\left[\mathbf{b}_1^{(p)}\right]\mathbf{D}+\left[\mathbf{b}_2^{(p)}\right]\right]\mathbf{F}_{r+1}^{(p)}-\left[\mathbf{b}_4^{(p)}\right]\sum_{k=0}^{N_y}\mathbf{d}_{jk}\mathbf{F}_{r+1,k}+\left[\frac{1}{Le}\mathbf{D}^2+\left[\mathbf{b}_3^{(p)}\right]\mathbf{D}\right]\Gamma_{r+1}^{(p)}-$$

$$\left[\mathbf{b}_5^{(p)}\right]\sum_{k=0}^{N_y}\mathbf{d}_{jk}\Gamma_{r+1,k}=b_6^{(p)}, \tag{7.81}$$

and

$$\left[\frac{1}{Pr}\mathbf{D}^2+\left[\mathbf{c}_1^{(p)}\right]\mathbf{D}\right]\Theta_{r+1}^{(p)}-\left[\mathbf{c}_2^{(p)}\right]\sum_{k=0}^{N_y}\mathbf{d}_{jk}\Theta_{r+1,k}=c_3^{(p)}, \tag{7.82}$$

$$\left[(S_T)\,\mathbf{D}^2\right]\Theta_{r+1}^{(p)}+\left[\frac{1}{Sc}\mathbf{D}^2+\left[\mathbf{e}_1^{(p)}\right]\mathbf{D}\right]\mathbf{S}_{r+1}^{(p)}-\left[\mathbf{e}_2^{(p)}\right]\sum_{k=0}^{N_y}\mathbf{d}_{jk}\mathbf{S}_{r+1,k}=\mathbf{0}. \tag{7.83}$$

Multi-domain paired quasilinearization method-CASE 3

In this section, we linearize equations (7.12) and (7.15) to obtain

$$f_{r+1}^{'''}+\left(R+\frac{3}{4}\right)f_r f_{r+1}^{''}+\left(R+\frac{3}{4}\right)f_r^{''}f_{r+1}-\left(R+\frac{3}{4}\right)f_r f_r^{''}-f_r^{'}f_{r+1}^{'}+\frac{1}{2}f_r^{'2}-Nr\gamma_r+$$

$$NcS_{r+1}+\theta_r=\xi f_r^{'}\frac{\partial f_{r+1}^{'}}{\partial\xi}+\xi\frac{\partial f_r^{'}}{\partial\xi}f_{r+1}^{'}-\xi f_r^{'}\frac{\partial f_r^{'}}{\partial\xi}-\xi f_r^{''}\frac{\partial f_{r+1}}{\partial\xi}-\xi\frac{\partial f_r}{\partial\xi}f_{r+1}^{''}+\xi f_r^{''}\frac{\partial f_r}{\partial\xi}, \tag{7.84}$$

$$\frac{1}{Sc}S_{r+1}+\left(R+\frac{3}{4}\right)f_r S_{r+1}^{'}+\left(R+\frac{3}{4}\right)S_r^{'}f_{r+1}-\left(R+\frac{3}{4}\right)f_r S_r^{'}+S_T\theta_r^{''} \tag{7.85}$$

$$=\xi f_r^{'}\frac{\partial S_{r+1}}{\partial\xi}+\xi\frac{\partial S_r}{\partial\xi}f_{r+1}^{'}-\xi f_r^{'}\frac{\partial S_r}{\partial\xi}-\xi S_r^{'}\frac{\partial f_{r+1}}{\partial\xi}-\xi\frac{\partial f_r}{\partial\xi}S_{r+1}^{'}+\xi S_r^{'}\frac{\partial f_r}{\partial\xi}. \tag{7.86}$$

Updated solutions for f, S and their corresponding derivatives are used in the second pair of equations and we obtain

$$\frac{1}{Pr}\theta_{r+1}^{''}+\left(R+\frac{3}{4}\right)f_{r+1}\theta_{r+1}^{'}+Nb\gamma_{r+1}^{'}\theta_{r+1}^{'}+2Nt\theta_r^{'}\theta_{r+1}^{'}=\xi f_{r+1}^{'}\frac{\partial\theta_{r+1}}{\partial\xi}-\xi\frac{\partial f_{r+1}}{\partial\xi}\theta_{r+1}^{'}, \tag{7.87}$$

$$\frac{1}{Le}\gamma_{r+1}^{''}+\left(R+\frac{3}{4}\right)f_{r+1}\gamma_{r+1}^{'}+\frac{1}{Le}\frac{Nt}{Nb}\theta_{r+1}^{''}=\xi f_{r+1}^{'}\frac{\partial\gamma_{r+1}}{\partial\xi}-\xi\frac{\partial f_{r+1}}{\partial\xi}\gamma_{r+1}^{'}, \tag{7.88}$$

The pairs (7.84) & (7.86) and (7.87) & (7.88) are compactly expressed as

$$f_{r+1}^{'''(p)}+\left[a_1^{(p)}\right]f_{r+1}^{''(p)}+\left[a_2^{(p)}\right]f_{r+1}^{'(p)}+\left[a_3^{(p)}\right]f_{r+1}^{(p)}+(Nc)S_{r+1}^{(p)}=\left[a_4^{(p)}\right]\frac{\partial f_{r+1}^{'(p)}}{\partial\xi}+\left[a_5^{(p)}\right]\frac{\partial f_{r+1}^{(p)}}{\partial\xi}+a_6^{(p)}, \tag{7.89}$$

$$\left[b_1^{(p)}\right]f_{r+1}^{'(p)}+\left[b_2^{(p)}\right]f_{r+1}^{(p)}+\frac{1}{Sc}S_{r+1}^{''(p)}+\left[b_3^{(p)}\right]S_{r+1}^{'(p)}=\left[b_4^{(p)}\right]\frac{\partial f_{r+1}^{(p)}}{\partial\xi}+\left[b_5^{(p)}\right]\frac{\partial S_{r+1}^{(p)}}{\partial\xi}+b_6^{(p)} \tag{7.90}$$

and

$$\frac{1}{Pr}\theta_{r+1}^{''(p)}+\left[c_1^{(p)}\right]\theta_{r+1}^{'(p)}+\left[c_2^{(p)}\right]\gamma_{r+1}^{'(p)}=\left[c_3^{(p)}\right]\frac{\partial\theta_{r+1}^{(p)}}{\partial\xi}+c_4^{(p)}, \tag{7.91}$$

$$\left(\frac{1}{Le}\frac{Nt}{Nb}\right)\theta_{r+1}^{''(p)}+\frac{1}{Le}\gamma_{r+1}^{''(p)}+\left[e_1^{(p)}\right]\gamma_{r+1}^{'(p)}=\left[e_2^{(p)}\right]\frac{\partial\gamma_{r+1}^{(p)}}{\partial\xi}, \tag{7.92}$$

where p denotes the time sub-interval and

$$\begin{aligned}
&a_1=\left(R+\frac{3}{4}\right)f_r+\xi\frac{\partial f_r}{\partial\xi},\ a_2=-f_r^{'}-\xi\frac{\partial f_r^{'}}{\partial\xi},\\
&a_3=\left(R+\frac{3}{4}\right)f_r^{''},\ a_4=\xi f_r^{'},\ a_5=-\xi f_r^{''},\\
&a_6=-\frac{1}{2}f_r^{'2}+\left(R+\frac{3}{4}\right)f_rf_r^{''}-\theta_r+Nr\gamma_r-\xi f_r^{'}\frac{\partial f_r^{'}}{\partial\xi}+\xi f_r^{''}\frac{\partial f_r}{\partial\xi},\\
&b_1=-\xi\frac{\partial S_r}{\partial\xi},\ b_2=\left(R+\frac{3}{4}\right)S_r^{'},\ b_3=\left(R+\frac{3}{4}\right)f_r+\xi\frac{\partial f_r}{\partial\xi},\\
&b_4=-\xi S_r^{'},\ b_5=\xi f_r^{'},\ b_6=\left(R+\frac{3}{4}\right)f_rS_r^{'}-\xi f_r^{'}\frac{\partial S_r}{\partial\xi}+\xi S_r^{'}\frac{\partial f_r}{\partial\xi},\\
&c_1=\left(R+\frac{3}{4}\right)f_{r+1}+Nb\gamma_{r+1}^{'}+2Nt\theta_r^{'}+\xi\frac{\partial f_{r+1}}{\partial\xi},\ c_2=Nb\theta_r^{'},\ c_3=\xi f_r^{'},\ c_4=Nt\theta_{r+1}^{'2}+Nb\gamma_r^{'}\theta_r^{'},\\
&e_1=\left(R+\frac{3}{4}\right)f_{r+1}+\xi\frac{\partial f_{r+1}}{\partial\xi},\ e_2=\xi f_{r+1}^{'}.
\end{aligned}$$

The Chebyshev spectral collocation method is applied on the decoupled system of paired equations in the form

$$\left[\mathbf{D}^3+\left[\mathbf{a}_1^{(p)}\right]\mathbf{D}^2+\left[\mathbf{a}_2^{(p)}\right]\mathbf{D}+\left[\mathbf{a}_3^{(p)}\right]\right]\mathbf{F}_{r+1}^{(p)}-\left[\mathbf{a}_4^{(p)}\right]\sum_{k=0}^{N_y}\mathbf{d}_{jk}\mathbf{D}\mathbf{F}_{r+1,k}-$$
$$\left[\mathbf{a}_5^{(p)}\right]\sum_{k=0}^{N_y}\mathbf{d}_{jk}\mathbf{F}_{r+1,k}+[(Nc\mathbf{I})]\mathbf{S}_{r+1}^{(p)}=a_6^{(p)}, \tag{7.93}$$
$$\left[\left[\mathbf{b}_1^{(p)}\right]\mathbf{D}+\left[\mathbf{b}_2^{(p)}\right]\right]\mathbf{F}_{r+1}^{(p)}-\left[\mathbf{b}_4^{(p)}\right]\sum_{k=0}^{N_y}\mathbf{d}_{jk}\mathbf{F}_{r+1,k}+\left[\frac{1}{Sc}\mathbf{D}^2+\left[\mathbf{b}_3^{(p)}\right]\mathbf{D}\right]\mathbf{S}_{r+1}^{(p)}-$$
$$\left[\mathbf{b}_5^{(p)}\right]\sum_{k=0}^{N_y}\mathbf{d}_{jk}\mathbf{S}_{r+1,k}=b_6^{(p)} \tag{7.94}$$

and

$$\left[\frac{1}{Pr}\mathbf{D}^2+\left[\mathbf{c}_1^{(p)}\right]\mathbf{D}\right]\Theta_{r+1}^{(p)}-\left[\mathbf{c}_2^{(p)}\right]\sum_{k=0}^{N_y}\mathbf{d}_{jk}\Theta_{r+1,k}=c_3^{(p)}, \tag{7.95}$$
$$\left[\left(\frac{1}{Le}\frac{Nt}{Nb}\right)\mathbf{D}^2\right]\Theta_{r+1}^{(p)}+\left[\frac{1}{Le}\mathbf{D}^2+\left[\mathbf{e}_1^{(p)}\right]\mathbf{D}\right]\Gamma_{r+1}^{(p)}-\left[\mathbf{e}_2^{(p)}\right]\sum_{k=0}^{N_y}\mathbf{d}_{jk}\Gamma_{r+1,k}=\mathbf{0}, \tag{7.96}$$

where $\mathbf{I}$ is an identity matrix of size $(N_x+1)\times(N_x+1)$.

7.4 Results and Discussion

In this section, we discuss the results obtained using the multi-domain paired quasilinearization method cases and compare them against those obtained using the bivariate pseudo-spectral local linearization method. To perform error and residual analysis on the different numerical schemes, unless specified differently, we set parameter values to $Nc = 0.5$, $Nr = 0.5$, $Pr = 1$, $Nb = 0.2$, $Nt = 0.3$, $Le = 10$, $Sc = 0.6$, and $St = 1$. We also fix the number of grid-points in time and space, respectively, to be $N_t = 10$ and $N_x = 30$ as these were found to be sufficient to give accurate and convergent solutions.

7.4.1 Convergence

Table 7.1 below displays the number of iterations needed for each method to give solutions that were converged to 9 decimal places. To further show how fast the MD-PQLM converges, we compare it against the multi-domain spectral quasilinearization method that is documented to converge quadratically and with few iterations.

Table 7.1: Convergence of skin friction $f''(\xi,0)$ to 9 decimal places and time taken to attain convergence using the MD-PQLM cases, MDSQLM and BPSLLM.

ξ	**BPSLLM**	**MDSQLM**	**MD−PQLM CASE 1**	**MD−PQLM CASE 2**	**MD−PQLM CASE 3**
6	1.035143700	1.035143700	1.035143700	1.035143700	1.035143700
12	1.021716500	1.021716500	1.021716500	1.021716500	1.021716500
18	1.016593900	1.016593900	1.016593900	1.016593900	1.016593900
Total Time (sec)	84.14	135.22	101.26	102.36	105.44
Convergence speed	21	4	10	13	9
Convergence time (sec)	54.97	17.66	32.2	42.30	29.74

where total time is the time taken for all the methods to perform 20 iterations while convergence time is the time taken for the solutions to converge.

We observe from the data in Table 7.1 that the multi-domain spectral quasilinearization method (MDSQLM) converges fastest, that is after just 4 iterations, while the BPSLLM requires 21 iterations for convergence. This implies the MD-PQLM schemes all converge faster than the BPSLLM; in particular we observe that case 3 converges after only 9 iterations, while cases 1 and 2 converge after 10 and 13 iterations, respectively. Due to the coupling nature of the MDSQLM, it is observed that the total computational time is much higher than for the other methods, but because it takes only 4 iterations to converge, it has the shortest convergence time. In practice however, we need to allow a numerical scheme to run for a certain number of iterations, hence the advantage of the

MD-PQLM. The total computational time for the MD-PQLM is more than for the BPSLLM, but the time needed for it to attain convergence is smaller for all three cases than for the BPSLLM. The more rapid convergence of the MD-PQLM in comparison with that of the BPSLLM is further supported by the solution error graphs.

The solution error test is performed by obtaining the difference between successive iterations until a point where consistency in the error is attained. At this point, convergence has been achieved. We note that our solution set is a vector, so we elect to choose the maximum error to be given as

$$||\Omega||_\infty = \max_{0\leq i\leq N_y} ||\Omega_{r+1,i} - \Omega_{r,i}||_\infty , \tag{7.97}$$

where Ω represents F, S, Θ and Γ. Figures 7.1 to 7.4 below display the solution errors obtained using the different numerical schemes.

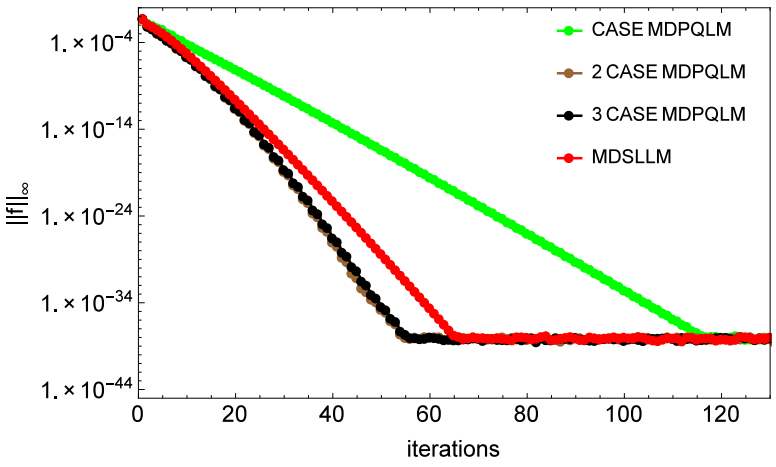

Figure 7.1: Effect of iterations on the solution error norm for **F** when $\xi = 1.5$

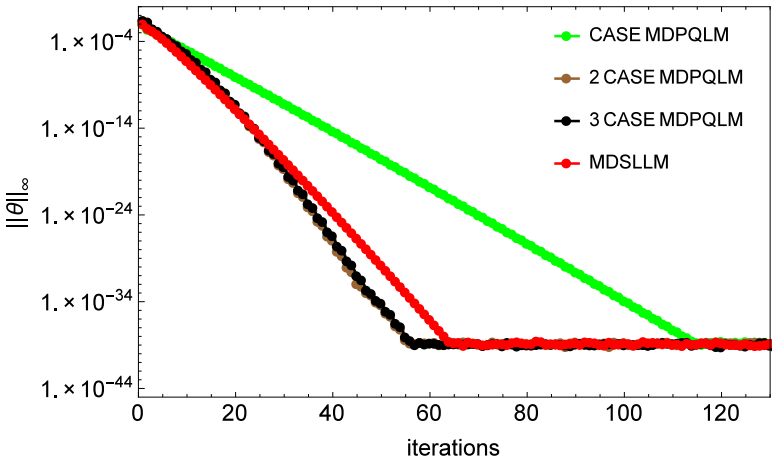

Figure 7.2: Effect of iterations on the solution error norm for Θ when $\xi = 1.5$

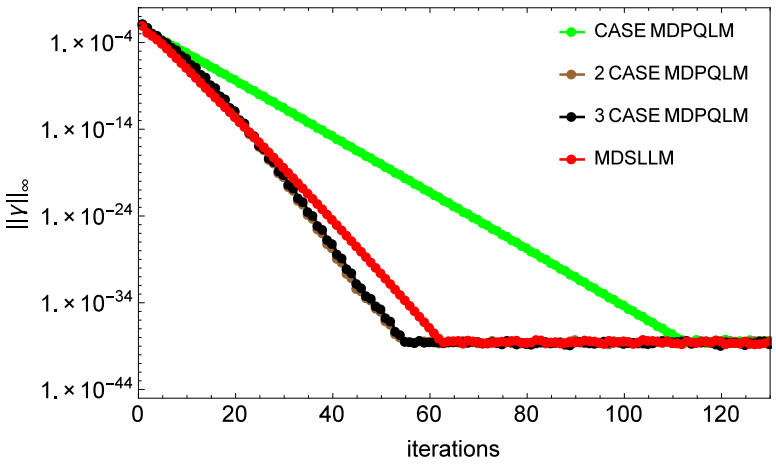

Figure 7.3: Effect of iterations on the solution error norm for Γ when $\xi = 1.5$

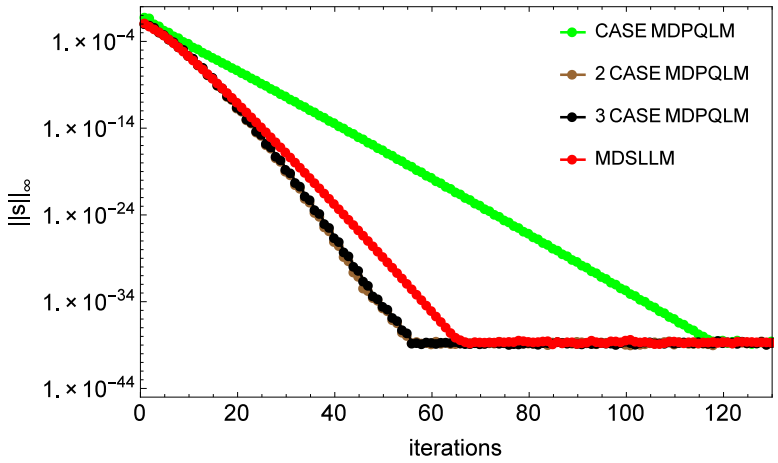

Figure 7.4: Effect of iterations on the solution error norm for $\mathbf{S}$ when $\xi = 1.5$

We observe in the four figures above that the solution error decreases with an increase in iterations until consistency is achieved. Linearizing the large system in pairs is observed to significantly improve the speed of convergence of MD-PQLM cases 2 and 3 as both are seen to converge faster than the BPSLLM. This signifies that the MD-PQLM improves the convergence speed of the BPSLLM.

7.4.2 Accuracy

To test accuracy of the approximate solutions, we make use of the residual error obtained using the different numerical schemes. We use the residual error to determine the proximity of the approximate solution to the actual solution. We note that this is not the same as the actual error between the exact solution and approximate solution. As noted earlier, with the solutions being vector sets, we choose to extract the maximum error, which explains the choice of the infinity norm

in defining the residual error. We define the residual error as

$$\mathbf{Res}(\mathbf{F}) = \max_{0\le i\le N_y} \left\| \mathbf{f}_i''' + \left(R+\frac{3}{4}\right)\mathbf{f}_i\mathbf{f}_i'' - \frac{1}{2}\mathbf{f}_i'^2 + \theta_i + Nc\mathbf{s}_i - Nr\gamma_i - \xi\left(\mathbf{f}_i'\frac{\partial \mathbf{f}_i'}{\partial \xi} - \mathbf{f}_i''\frac{\partial \mathbf{f}_i}{\partial \xi}\right)\right\|_\infty,$$

$$\mathbf{Res}(\Theta) = \max_{0\le i\le N_y} \left\| \frac{1}{Pr}\Theta_i'' + \left(R+\frac{3}{4}\right)\mathbf{f}_i\theta_i' + Nb\gamma_i'\theta_i' + Nt\theta_i'^2 - \xi\left(\mathbf{f}_i'\frac{\partial \theta_i}{\partial \xi} - \theta_i'\frac{\partial \mathbf{f}_i}{\partial \xi}\right)\right\|_\infty,$$

$$\mathbf{Res}(\Gamma) = \max_{0\le i\le N_y} \left\| \frac{1}{Le}\gamma_i'' + \left(R+\frac{3}{4}\right)\mathbf{f}_i\gamma_i' + \frac{1}{Le}\frac{Nt}{Nb}\theta_i'' - \xi\left(\mathbf{f}_i'\frac{\partial \gamma_i}{\partial \xi} - \gamma_i'\frac{\partial \mathbf{f}_i}{\partial \xi}\right)\right\|_\infty,$$

$$\mathbf{Res}(\mathbf{S}) = \max_{0\le i\le N_y} \left\| \frac{1}{sc}\mathbf{s}_i'' + \left(R+\frac{3}{4}\right)\mathbf{f}_i\mathbf{s}_i' + S_T\theta_i'' - \xi\left(\mathbf{f}_i'\frac{\partial \mathbf{s}_i}{\partial \xi} - \mathbf{s}_i'\frac{\partial \mathbf{f}_i}{\partial \xi}\right)\right\|_\infty.$$

Figures 7.5 to 7.8 display the residual error obtained using the different numerical schemes.

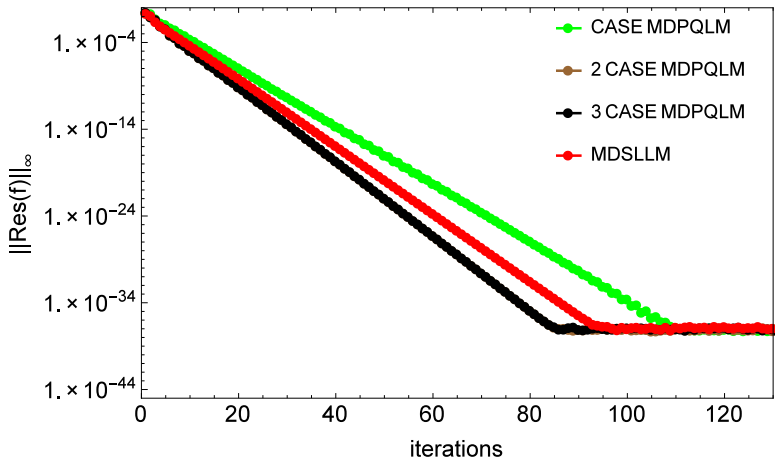

Figure 7.5: Effect of iterations on the residual error norm for $\mathbf{F}$ when $\xi = 1.5$

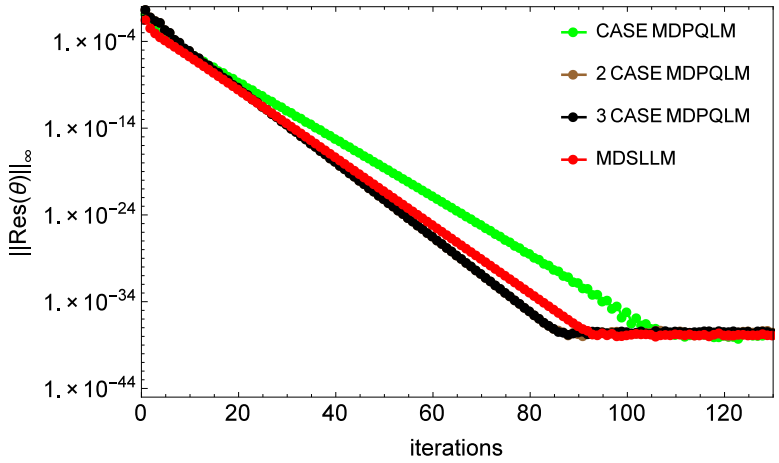

Figure 7.6: Effect of iterations on the residual error norm for Θ when $\xi = 1.5$

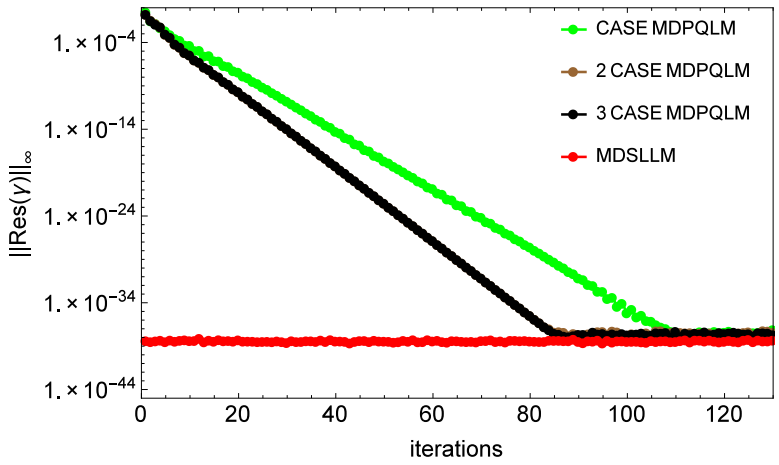

Figure 7.7: Effect of iterations on the residual error norm for Γ when $\xi = 1.5$

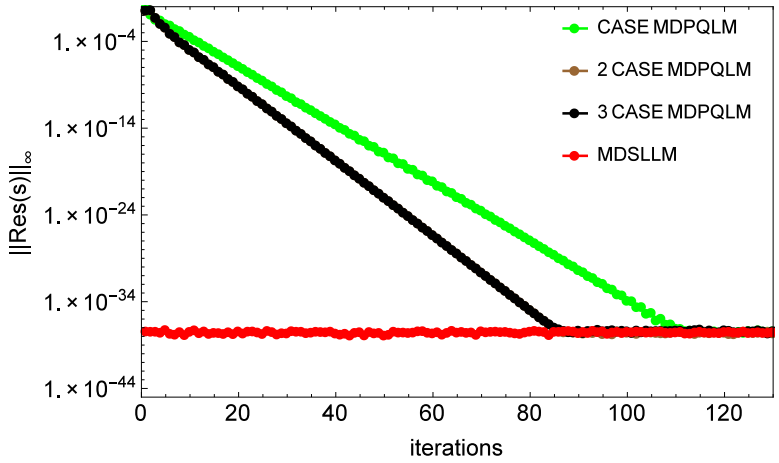

Figure 7.8: Effect of iterations on the residual error norm for $\mathbf{S}$ when $\xi = 1.5$

We observe in Figures 7.5 to 7.8 that as iterations increase, the methods display better accuracy until convergence is attained. In Figures 7.7 and 7.8, we observe that the BPSLLM shows an error of 10^{-40} at all iteration levels. This is due to equations (7.14) and (7.15) being linear. In Figures 7.5 and 7.6, it is seen that the MD-PQLM cases 2 and 3 converge to an error of 10^{-40} quicker than does the BPSLLM.

7.5 Summary

In this study, we have described the multi-domain paired quasilinearization method for a general system of partial differential equations. We found the MD-PQLM to be convergent and accurate. From the results obtained and following observation by Otegbeye and Motsa [137], it was shown that the pairings that gave high nonlinearities converged faster than the BPSLLM. We also noted that the accuracy of the MD-PQLM was the same as for the BPSLLM. The computational efficiency of the MD-PQLM is also displayed as it reduces the time taken for generating solutions. In summary, the MD-PQLM has been shown to be an accurate and convergent method that works better with pairings that have the most nonlinear terms.

Chapter 8

Conclusion

This thesis has presented new and innovative approaches for solving nonlinear fluid flow problems that are modeled using ordinary and partial differential equations. Using the local linearization methods and pairings of functions within a system of differential equations, we introduced some numerical schemes that we could show numerically to be convergent and accurate. We also performed comparative studies with a method that was already in existence and obtained some results. We demonstrated the application of the methods on generalized systems of ordinary and partial differential equations. These methods include the paired quasilinearization method (PQLM) for ordinary differential equations, paired quasilinearization method (PQLM) for partial differential equations and the multi-domain paired quasilinearization method (MD-PQLM). Highlights of the results obtained in each chapter include;

1 In Chapter 2, the paired quasilinearization method for solving ordinary differential equations was found to converge faster than the spectral local linearization method and to be equally as accurate. Time taken to attain convergence of solutions was also observed to be comparable to the SLLM.

2 Chapter 3 was largely based on a comparative study of the paired quasilinearization method that had been recently introduced. The PQLM solved partial differential equations in space and time using a spectral method. The comparative study showed that the pairings that had the most number of nonlinear terms generally converged fastest and they also converged faster than the bivariate spectral local linearization method (BSLLM) while maintaining the

same high accuracy level.

3 Chapter 4 focused on the effect of Hall, ion-slip and radiation on the MHD free convective heat generating flow past a semi-infinite vertical flat plate, as modeled by a system of partial differential equations. We used the PQLM to investigate how varying parameter values influenced the various flow profiles. Based on the findings, we were able to ascertain that the PQLM is an effective method for solving equations that describe flow properties.

4 In Chapter 5, we considered a new problem that modeled the combined influence of radiation, Hall and ion effects on MHD free convective heat generating flow past a semi-infinite vertical flat plate. Using the PQLM from the previous chapter, we successfully investigated the effect of certain parameters on the various profiles of the problem and it further validated the applicability of the method.

5 In Chapter 6, the influence of conduction radiation, mixed convection, chemical reaction and Forchheimer parameters on a mixed convection boundary layer flow of an MHD incompressible micropolar fluid near a vertical truncated cone were examined using the PQLM. This study showed the robustness of the PQLM as it was able to handle fluid problems of different variations. The analysis carried out generated interesting results that clearly displayed the effects of various parameters.

6 Chapter 7 saw the introduction of the multi-domain paired quasilinearization method (MD-PQLM) for solving systems of partial differential equations. It was observed that the MD-PQLM converged faster, and took less computational time to converge, than did than the BPSLLM. It was also noted that the method was very accurate while generating solutions.

We observe that the numerical schemes are all easy to implement and they all provide high accuracy. We also observe that a small number of grid points are needed in obtaining numerical solutions compared to methods like finite difference. To test the paired approach more, there is the need to delve into solving elliptic differential equations and fractional differential equations. Success in those areas will further show the approach of pairing equations to be truly robust.

References

[1] F. S. Acton. *Numerical methods that usually work*. Mathematical Association of America, Washington DC, 1990.

[2] S. Liao. *Beyond perturbation: introduction to the homotopy analysis method*. CRC Press, Boca Raton, 2003.

[3] J. G. Simmonds and J. E. Mann. *A first look at perturbation theory*. Courier Corporation, New York, 1985.

[4] J. B. Keller and H. Cebeci. Accurate numerical methods for boundary layer flows in two dimensional laminar flows. *In Proceedings of the Second International Conference on Numerical Methods in Fluid Dynamics*. 92-100, 1971.

[5] R. Courant, K. Friedrichs, and H. Lewy. Über die partiellen differenzengleichungen der mathematischen physik. *Mathematische Annalen*, 100(1):32–74, 1928.

[6] K. O. Friedrichs. A finite difference scheme for the Neumann and the Dirichlet problem. Technical report, New York Univ., New York. Atomic Energy Commission Computing and Applied Mathematics Center, 1962.

[7] K. Feng. Finite difference schemes based on variational principles. *Applied Mathematics and Computation*, 2:238–262, 1965.

[8] K. O. Friedrichs and H. B. Keller. A finite difference scheme for generalized Neumann problems. *Numerical Solution of Partial Differential Equations*, 1(1):1, 1966.

[9] Z. Alterman and F. C. Karal. Propagation of elastic waves in layered media by finite difference methods. *Bulletin of the Seismological Society of America*, 58(1):367–398, 1968.

[10] R. Seshadri, N. Sreeshylan, and G. Nath. Unsteady mixed convection flow in the stagnation region of a heated vertical plate due to impulsive motion. *International Journal of Heat and Mass Transfer*, 45(6):1345–1352, 2002.

[11] K. Lipnikov, G. Manzini, J. D. Moulton, and M. Shashkov. The mimetic finite difference method for elliptic and parabolic problems with a staggered discretization of diffusion coefficient. *Journal of Computational Physics*, 305:111–126, 2016.

[12] S. B. Yuste and L. Acedo. An explicit finite difference method and a new von Neumann-type stability analysis for fractional diffusion equations. *SIAM Journal on Numerical Analysis*, 42(5):1862–1874, 2005.

[13] L. N. Trefethen. *Spectral methods in MATLAB*, volume 10. Society for Industrial and Applied Mathematics, Philadelphia, 2000.

[14] C. I. Gheorghiu. Spectral methods for differential problems. *Casa Cartii de Stiinta Publishing House, Cluj-Napoca*, 2007.

[15] F. N. Van de Vosse and P. D. Minev. Spectral elements methods: Theory and applications. Technical report, EUT Report 96-W-001 ISBN 90-236-0318-5, Eindhoven University of Technology, Eindhoven, 1996.

[16] J. P. Boyd. *Chebyshev and Fourier spectral methods*. Courier Dover Publications, New York, 2001.

[17] C. Canuto, M. Y. Husseini, A. Quarteroni, and T. A. Zang. *Spectral Methods in Fluid Dynamics*. Springer-Verlag, Berlin, 1988.

[18] S. S. Motsa. A new spectral local linearization method for nonlinear boundary layer flow problems. *Journal of Applied Mathematics*, 2013. vol. 2013, Article ID 423628, 15 pages, 2013. doi:10.1155/2013/423628.

[19] S.S. Motsa, V. M. Magagula, and P. Sibanda. A bivariate chebyshev spectral collocation quasilinearization method for nonlinear evolution parabolic equations. *The Scientific World Journal*, 2014, Article ID 581987, 13 pages, 2014. http://dx.doi.org/10.1155/2014/581987.

[20] S. S. Motsa and I. L. Animasaun. Paired quasi-linearisation analysis of heat transfer in unsteady mixed convection nanofluid containing both nanoparticles and gyrotactic microorganisms due to impulsive motion. *Journal of Heat Transfer*, 138(11):114503–114511, 2016.

[21] S. S. Motsa, O. D. Makinde, and S. Shateyi. On the successive linearisation approach to flow of reactive third-grade liquid in a channel with isothermal walls. *Mathematical Problems in Engineering*, 2013. vol. 2013, Article ID 635392, 7 pages, 2013. doi:10.1155/2013/635392.

[22] S. S. Motsa and I. L. Animasaun. A new numerical investigation of some thermo-physical properties on unsteady MHD non-Darcian flow past an impulsively started vertical surface. *Thermal Science*, 19(1):249–258, 2015.

[23] O. Otegbeye. On decoupled quasi-linearization methods for solving systems of nonlinear boundary value problems. Unpublished M.Sc dissertation, University of KwaZulu-Natal, 2014. http://hdl.handle.net/10413/12114.

[24] D. Gottlieb and S. A. Orszag. *Numerical analysis of spectral methods: theory and applications*. Society for Industrial and Applied Mathematics, Philadelphia, 1977.

[25] J. S. Hesthaven, S. Gottlieb, and D. Gottlieb. *Spectral methods for time-dependent problems*, volume 21. Cambridge University Press, Cambridge, 2007.

[26] E. Tadmor. Spectral methods for time dependent problems. ICASE Interim Report 14, Institute for Computer Applications in Science and Engineering, NASA, Hampton, publisher = United States, year=1990.

[27] L. N. Trefethen. *Finite difference and spectral methods for ordinary and partial differential equations*. Cornell University [Department of Computer Science and Center for Applied Mathematics], New York, 1996.

[28] S. Gottlieb and D. Gottlieb. Spectral methods. *Scholarpedia*, 4(9):7504, 2009. revision 91796.

[29] R. Baltensperger and J-P. Berrut. The errors in calculating the pseudospectral differentiation matrices for Chebyshev-Gauss-Lobatto points. *Computers & Mathematics with Applications*, 37(1):41–48, 1999.

[30] B. S. Ogundare. On the pseudo-spectral method of solving linear ordinary differential equations. *Journal of Mathematics and Statistics*, 5(2):136–140, 2009.

[31] E. Babolian, M. Bromilow, R. England, and M. Saravi. A modification of pseudo-spectral method for solving a linear ODEs with singularity. *Applied Mathematics and Computation*, 188(2):1260–1266, 2007.

[32] N. V. Mantzaris, P. Daoutidis, and F. Srienc. Numerical solution of multi-variable cell population balance models. II. spectral methods. *Computers & Chemical Engineering*, 25 (11):1441–1462, 2001.

[33] L. Cueto-Felgueroso and R. Juanes. Adaptive rational spectral methods for the linear stability analysis of nonlinear fourth-order problems. *Journal of Computational Physics*, 228 (17):6536–6552, 2009.

[34] L. N. Trefethen and M. R. Trummer. An instability phenomenon in spectral methods. *SIAM Journal on Numerical Analysis*, 24(5):1008–1023, 1987.

[35] H-M. H. Juang and M. Kanamitsu. The NMC nested regional spectral model. *Monthly Weather Review*, 122(1):3–26, 1994.

[36] İ. Çelik. Collocation method and residual correction using Chebyshev series. *Applied Mathematics and Computation*, 174(2):910–920, 2006.

[37] A. H. D. Cheng, M. A. Golberg, E. J. Kansa, and G. Zammito. Exponential convergence and H-C multiquadric collocation method for partial differential equations. *Numerical Methods*

for Partial Differential Equations, 19(5):571–594, 2003. ISSN 1098-2426. doi: 10.1002/num.10062.

[38] R. E. Bellman and R. E. Kalaba. Quasilinearization and nonlinear boundary-value problems. *American Elsevier, New York*, 1965.

[39] V. B. Mandelzweig and F. Tabakin. Quasilinearization approach to nonlinear problems in physics with application to nonlinear ODEs. *Computer Physics Communications*, 141(2): 268–281, 2001.

[40] R. Krivec and V. B. Mandelzweig. Numerical investigation of quasilinearization method in quantum mechanics. *Computer Physics Communications*, 138(1):69–79, 2001.

[41] K. Parand, H. Yousefi, and M. Delkhosh. A numerical approach to solve Lane-Emden type equations by the fractional order of rational Bernoulli functions. *Romanian Journal of Physics*, 62(104):1–24, 2017.

[42] R. Bellman, J. Jacquez, R. Kalaba, and S. Schwimmer. Quasilinearization and the estimation of chemical rate constants from raw kinetic data. *Mathematical Biosciences*, 1(1):71–76, 1967.

[43] N. Shazad and A. S. Vatsala. Extension of the method of generalized quasilinearization for second order boundary value problems. *Applicable Analysis*, 58(1-2):77–83, 1995.

[44] B. Ahmad, J. J. Nieto, and N. Shahzad. The Bellman–Kalaba–Lakshmikantham quasilinearization method for neumann problems. *Journal of Mathematical Analysis and Applications*, 257(2):356–363, 2001.

[45] J. Nieto. Generalized quasilinearization method for a second order ordinary differential equation with dirichlet boundary conditions. *Proceedings of the American Mathematical Society*, 125(9):2599–2604, 1997.

[46] B. Ahmad, J. J. Nieto, and N. Shahzad. Generalized quasilinearization method for mixed boundary value problems. *Applied Mathematics and Computation*, 133(2):423–429, 2002.

[47] V. Lakshmikantham, N. Shahzad, and J. J. Nieto. Methods of generalized quasilinearization for periodic boundary value problems. *Nonlinear Analysis: Theory, Methods & Applications*, 27(2):143–151, 1996.

[48] V. Lakshmikantham. An extension of the method of quasilinearization. *Journal of Optimization Theory and Applications*, 82(2):315–321, 1994.

[49] H. Jaddu. Direct solution of nonlinear optimal control problems using quasilinearization and Chebyshev polynomials. *Journal of the Franklin Institute*, 339(4):479–498, 2002.

[50] T.M. Agbaje, S. Mondal, S. S. Motsa, and P. Sibanda. A numerical study of unsteady non-Newtonian Powell-Eyring nanofluid flow over a shrinking sheet with heat generation and thermal radiation. *Alexandria Engineering Journal*, 56(1):81–91, 2017.

[51] H. Kushner and P. G. Dupuis. *Numerical methods for stochastic control problems in continuous time*. Springer Science & Business Media, New York, 2013.

[52] D. Xiu. *Numerical methods for stochastic computations: a spectral method approach*. Princeton University Press, Princeton, New Jersey, 2010.

[53] F. G. Shuman. Numerical methods in weather prediction: Smoothing and filtering. *Monthly Weather Review*, 85(11):357–361, 1957.

[54] H. B. Keller. Numerical methods in boundary-layer theory. *Annual Review of Fluid Mechanics*, 10(1):417–433, 1978.

[55] S. Wang and Y. Lin. A finite-difference solution to an inverse problem for determining a control function in a parabolic partial differential equation. *Inverse Problems*, 5:631–642, 1989. doi:10.1088/0266-5611/5/4/013.

[56] B. Hu, Y. Xu, and J. Hu. Crank-nicolson finite difference scheme for the Rosenau-Burgers equation. *Applied Mathematics and Computation*, 204(1):311–316, 2008.

[57] G. Sun and C. W. Trueman. Efficient implementations of the crank-nicolson scheme for the finite-difference time-domain method. *Microwave Theory and Techniques, IEEE Transactions on*, 54(5):2275–2284, 2006.

[58] P. G. Dlamini, S. S. Motsa, and M. Khumalo. Higher order compact finite difference schemes for unsteady boundary layer flow problems. *Advances in Mathematical Physics*, 2013. vol. 2013, Article ID 941096, 10 pages, 2013. doi:10.1155/2013/941096.

[59] E. M. A. Elbashbeshy and M. A. A. Bazid. Heat transfer over an unsteady stretching surface with internal heat generation. *Applied Mathematics and Computation*, 138(23):239 – 245, 2003. ISSN 0096-3003. doi: http://dx.doi.org/10.1016/S0096-3003(02)00106-6. URL http://www.sciencedirect.com/science/article/pii/S0096300302001066.

[60] E. M. A. Elbashbeshy and M. A. A. Bazid. Heat transfer over an unsteady stretching surface. *Heat and Mass Transfer*, 41(1):1–4, 2004. ISSN 0947-7411. doi: 10.1007/s00231-004-0520-x. URL http://dx.doi.org/10.1007/s00231-004-0520-x.

[61] H. Xu and S. J. Liao. Series solutions of unsteady magnetohydrodynamic flows of non-Newtonian fluids caused by an impulsively stretching plate. *Journal of Non-Newtonian Fluid Mechanics*, 129(1):46 – 55, 2005. ISSN 0377-0257. doi: http://dx.doi.org/10.1016/j.jnnfm.2005.05.005. URL http://www.sciencedirect.com/science/article/pii/S0377025705001102.

[62] A. Mehmood and A. Ali. Analytic solution of generalized three-dimensional flow and heat transfer over a stretching plane wall. *International Communications in Heat and Mass Transfer*, 33(10):1243 – 1252, 2006.

[63] S. Liao. An analytic solution of unsteady boundary-layer flows caused by an impulsively stretching plate. *Communications in Nonlinear Science and Numerical Simulation*, 11(3):326 – 339, 2006.

[64] M. Kumari and G. Nath. Analytical solution of unsteady three-dimensional MHD boundary layer flow and heat transfer due to impulsively stretched plane surface. *Communications*

in Nonlinear Science and Numerical Simulation, 14(8):3339 – 3350, 2009. ISSN 1007-5704. doi: http://dx.doi.org/10.1016/j.cnsns.2008.11.011. URL http://www.sciencedirect.com/science/article/pii/S1007570408004188.

[65] A. Ishak, R. Nazar, and I. Pop. Unsteady mixed convection boundary layer flow due to a stretching vertical surface. *Arabian Journal for Science & Engineering (Springer Science & Business Media B.V.)*, 31(2B):165 – 182, 2006. ISSN 13198025.

[66] R. Nazar, N. Amin, and I. Pop. Unsteady boundary layer flow due to a stretching surface in a rotating fluid. *Mechanics Research Communications*, 31(1):121–128, 2004. ISSN 0093-6413. doi: http://dx.doi.org/10.1016/j.mechrescom.2003.09.004. URL http://www.sciencedirect.com/science/article/pii/S009364130300106X.

[67] F. M. Ali, R. Nazar, and N. M. Arafin. Numerical solutions of unsteady boundary layer flow due to an impulsively stretching surface. *Journal of Applied Computer Science and Mathematics*, 8(4):25–30, 2010. ISSN 2066-3129. doi: 10.1007/BF00945764. URL http://dx.doi.org/10.1007/BF00945764.

[68] R. Nazar, N. Amin, and I. Pop. Unsteady mixed convection boundary layer flow near the stagnation point on a vertical surface in a porous medium. *International Journal of Heat and Mass Transfer*, 47(1213):2681 – 2688, 2004. ISSN 0017-9310. doi: http://dx.doi.org/10.1016/j.ijheatmasstransfer.2004.01.002. URL http://www.sciencedirect.com/science/article/pii/S0017931004000067.

[69] C. Lanczos. Trigonometric interpolation of empirical and analytical functions. *Journal of Mathematics and Physics*, 17(1-4):123–199, 1938. doi: 10.1002/sapm1938171123. URL https://onlinelibrary.wiley.com/doi/abs/10.1002/sapm1938171123.

[70] M. Y. Hussaini and T. A. Zang. *Spectral methods in fluid dynamics*. Institute for Computer Applications in Science and Engineering, NASA Langley Research Center, 1986.

[71] B. Fornberg. *A practical guide to pseudospectral methods*, volume 1. Cambridge university press, 1998.

[72] S. S. Motsa. A new spectral relaxation method for similarity variable nonlinear boundary layer flow systems. *Chemical Engineering Communications*, 201(2):241–256, 2013. doi: 10.1080/00986445.2013.766882. URL http://www.tandfonline.com/doi/abs/10.1080/00986445.2013.766882.

[73] S. S. Motsa, P. Sibanda, J. M. Ngnotchouye, and G. T. Marewo. A spectral relaxation approach for unsteady boundary-layer flow and heat transfer of a nanofluid over a permeable stretching/shrinking sheet. *Advances in Mathematical Physics*, 2014. vol. 2014, Article ID 564942, 10 pages, 2014. doi:10.1155/2014/564942.

[74] Z. G. Makukula, S. S. Motsa, and S. Shateyi. Numerical analysis for the synthesis of biodiesel using spectral relaxation method. *Mathematical Problems in Engineering*, 2014. vol. 2014, Article ID 601374, 6 pages, 2014. doi:10.1155/2014/601374.

[75] P. K. Kameswaran, Z. G. Makukula, P. Sibanda, S. S. Motsa, and P. V. S. N. Murthy. A new algorithm for internal heat generation in nanofluid flow due to a stretching sheet in a porous medium. *International Journal of Numerical Methods for Heat & Fluid Flow*, 24 (5):1020–1043, 2014.

[76] S. S. Motsa, P. G. Dlamini, and M. Khumalo. Solving hyperchaotic systems using the spectral relaxation method. *Abstract and Applied Analysis*, 2013. vol. 2012, Article ID 203461, 18 pages, 2012. doi:10.1155/2012/203461.

[77] S. S. Motsa, Z. G. Makukula, and S. Shateyi. Spectral local linearisation approach for natural convection boundary layer flow. *Mathematical Problems in Engineering*, 2013. vol. 2013, Article ID 765013, 7 pages, 2013. doi:10.1155/2013/765013.

[78] P. G. Dlamini, S. S. Motsa, and M. Khumalo. On the comparison between compact finite difference and pseudospectral approaches for solving similarity boundary layer problems. *Mathematical Problems in Engineering*, 2013. vol. 2013, Article ID 746489, 15 pages, 2013. doi:10.1155/2013/746489.

[79] A Raees, H. Xu, Q. Sun, and I. Pop. Mixed convection in gravity-driven nano-liquid film containing both nanoparticles and gyrotactic microorganisms. *Applied Mathematics and Mechanics*, 36(2):163–178, 2015.

[80] T. E. Hull, W. H. Enright, B. M. Fellen, and A. E. Sedgwick. Comparing numerical methods for ordinary differential equations. *SIAM Journal on Numerical Analysis*, 9(4):603–637, 1972.

[81] D. K. R. Babajee and M. Z. Dauhoo. An analysis of the properties of the variants of Newtons method with third order convergence. *Applied Mathematics and Computation*, 183(1):659 – 684, 2006. ISSN 0096-3003. doi: http://dx.doi.org/10.1016/j.amc.2006.05.116. URL http://www.sciencedirect.com/science/article/pii/S0096300306006011.

[82] J. F. Traub. *Iterative methods for the solution of equations*. Chelsea Publishing Company, New York, 1982.

[83] O. C. Zienkiewicz, R. L. Taylor, and J. Z. Zhu. The finite element method: Its basis and fundamentals. *Butterworth-Heinemann*, 132:1987–1993, 2005.

[84] C. Y. Kai and O. C. Zienkiewicz. *The finite element method in structural and continuum mechanics, numerical solution of problems in structural and continuum mechanics*. McGraw-Hill, London, 1967.

[85] R. Eymard, T. Gallouët, and R. Herbin. Finite volume methods. *Handbook of numerical analysis*, 7:713–1018, 2000.

[86] H. K. Versteeg and W. Malalasekera. *An introduction to computational fluid dynamics: the finite volume method*. Pearson Education, Harlow, England, 2007.

[87] R. J. LeVeque. *Finite difference methods for ordinary and partial differential equations: steady-state and time-dependent problems*. Society for Industrial and Applied Mathematics, Philadelphia, 2007.

[88] G. Ben-Yu. *Spectral methods and their applications*. World Scientific, Singapore, 1998.

[89] W. Zhong-Qing and S. Chang-Tao. An *hp*-spectral collocation method for nonlinear volterra integral equations with vanishing variable delays. *Mathematics of Computation*, 85(298): 635–666, 2016.

[90] V. M. Magagula, S. S. Motsa, and P. Sibanda. On the multi-domain bivariate spectral local linearisation method for solving system of non-similar boundary layer equations. In *Conference Abstracts*, volume 1, 2016.

[91] T. Hayat and M. Qasim. Effects of thermal radiation on unsteady magnetohydrodynamic flow of a micropolar fluid with heat and mass transfer. *Zeitschrift für Naturforschung A*, 65 (11):950–960, 2010.

[92] K. Ahmad, R. Nazar, A. Ishak, and I. Pop. Unsteady three-dimensional boundary layer flow due to a stretching surface in a micropolar fluid. *International Journal for Numerical Methods in Fluids*, 68(12):1561–1573, 2012.

[93] S.K. Ghosh and I. Pop. Hall effects on unsteady hydromagnetic flow in a rotating system with oscillating pressure gradient. *International Journal of Applied Mechanics and Engineering*, 8(1):43–56, 2003.

[94] E.M. Abo-Eldahab and A. M. Salem. Hall effects on MHD free convection flow of a non-Newtonian power-law fluid at a stretching surface. *International Communications in Heat and Mass Transfer*, 31:343–354, 2004.

[95] G.C. Shit. Hall effects on MHD free convective flow and mass transfer over a stretching sheet. *International Journal of Applied Mathematics and Mechanics*, 5(8):22–38, 2009.

[96] M.A. Seddeek. Effects of radiation and variable viscosity on a MHD free convection flow past a semi-infinite flat plate with an aligned magnetic field in the case of unsteady flow. *International Journal of Heat and Mass Transfer*, 45(4):931–935, 2002.

[97] M. A. Seddeek and E. M. Aboeldahab. Radiation effects on unsteady MHD free convection with Hall current near an infinite vertical porous plate. *International Journal of Mathematics and Mathematical Sciences*, 26(4):249–255, 2001.

[98] V. S. Rao and L. A. Babu. Finite element analysis of radiation and mass transfer flow past semi-infinite moving vertical plate with viscous dissipation. *ARPN Journal of Engineering and Applied Sciences*, 5(11), 2010.

[99] V.M. Soundalgekar and H. S. Takhar. Radiation convective flow past a semi-infinite vertical plate. *Modelling Measurements and Control*, 51:31–41, 1993.

[100] A.J. Chamkha, H. S. Takhar, and V. M. Soundalgekar. Radiation effects on free convection flow past a semi-infinite vertical plate with mass transfer. *Chemical Engineering Journal*, 84(3):335–342, 2001.

[101] J.C. Ericksen. Anisotropic fluids. *Archive for Rational Mechanics and Analysis*, 4(1):231–237, 1959.

[102] J.C. Ericksen. Transversely isotropic fluids. *Colloid & Polymer Science*, 173(2):117–122, 1960.

[103] Hoyt J.W. and A. G. Fabula. The effect of Additives on Fluid Friction. US Naval Ordinance Test Station Report, 1964.

[104] A.C. Eringen. Theory of micropolar fluids. *Journal of Mathematics and Mechanics*, 16(1): 1–18, 1966.

[105] A.C. Eringen. Theory of thermomicrofluids. *Journal of Mathematical analysis and Applications*, 38(2):480–496, 1972.

[106] A. C. Cogley, W. G. Vincenti, and S. E. Gilles. Differential approximation for radiation transfer in a nongray near equilibrium. *American Institute of Aeronautics and Astronautics Journal*, 6:551–553, 1968. URL https://doi.org/10.2514/3.4538.

[107] E. M. Abo-Eldahab and M. A. El Aziz. Viscous dissipation and joule heating effects on MHD-free convection from a vertical plate with power-law variation in surface temperature in the presence of hall and ion-slip currents. *Applied Mathematical Modelling*, 29(6):579–595.

[108] D. A. Nield and A. Bejan. *Convection in porous media*. (3rd ed) Springer, New York, 2006.

[109] K. Vafai. *Handbook of porous media*. CRC Press, Boca Raton, 2015.

[110] I. Pop and D. B. Ingham. *Convective heat transfer: mathematical and computational modelling of viscous fluids and porous media*. Elsevier, Oxford, 2001.

[111] D. B. Ingham and I. Pop. *Transport phenomena in porous media*. Elsevier, Oxford, 1998.

[112] A. Bejan and K. R. Khair. Heat and mass transfer by natural convection in a porous medium. *International Journal of Heat and Mass Transfer*, 28(5):909–918, 1985.

[113] P. Cheng, T. T. Le, and I. Pop. Natural convection of a Darcian fluid about a cone. *International communications in heat and mass transfer*, 12(6):705–717, 1985.

[114] K. A. Yih. Coupled heat and mass transfer in mixed convection over a VHF/VMF wedge in porous media: the entire regime. *Acta Mechanica*, 137(1-2):1–12, 1999.

[115] A. J. Chamkha, A. Khaled, and O. Al-Hawaj. Simultaneous heat and mass transfer by natural convection from a cone and a wedge in porous media. *Journal of Porous Media*, 3 (2), 2000.

[116] F. A. Woodward. Analysis and design of wing-body combinations at subsonic and supersonic speeds. *Journal of Aircraft*, 5(6):528–534, 1968.

[117] P.D. Thomas, M. R. Vinokur, B. A. Bastianon, and R. J. Conti. Numerical solution for three-dimensional inviscid supersonic flow. *AIAA Journal*, 10(7):887–894, 1972.

[118] T. C. Lin and S. G. Rubin. Viscous flow over a cone at moderate incidence, hypersonic tip region. *Computers & Fluids*, 1(1):37–57, 1973.

[119] Y. Vigneron, J. Tannehill, and J. Rakich. Calculation of supersonic viscous flow over delta wings with sharp subsonic leading edges. In *11th Fluid and Plasma Dynamics Conference*, page 1137, 1978.

[120] T. Grosan, A. Postelnicu, and I. Pop. Free convection boundary layer over a vertical cone in a non-Newtonian fluid saturated porous medium with internal heat generation. *Technische Mechanik*, 24(4):91–104, 2004.

[121] C-Y. Cheng. Nonsimilar boundary layer analysis of double-diffusive convection from a vertical truncated cone in a porous medium with variable viscosity. *Applied Mathematics and Computation*, 212(1):185–193, 2009.

[122] F. M. Hady, F. S. Ibrahim, S. M. Abdel-Gaied, and M. R. Eid. Effect of heat generation/absorption on natural convective boundary-layer flow from a vertical cone embedded in a porous medium filled with a non-Newtonian nanofluid. *International Communications in Heat and Mass Transfer*, 38(10):1414–1420, 2011.

[123] F. G. Awad, P. Sibanda, S. S. Motsa, and O. D. Makinde. Convection from an inverted cone in a porous medium with cross-diffusion effects. *Computers & Mathematics with Applications*, 61(5):1431–1441, 2011.

[124] W. A. Khan and A. Aziz. Double-diffusive natural convective boundary layer flow in a porous medium saturated with a nanofluid over a vertical plate: Prescribed surface heat, solute and nanoparticle fluxes. *International Journal of Thermal Sciences*, 50(11):2154–2160, 2011.

[125] A. M. Rashad, M. A. El-Hakiem, and M. M. M. Abdou. Natural convection boundary layer of a non-newtonian fluid about a permeable vertical cone embedded in a porous medium saturated with a nanofluid. *Computers & Mathematics with Applications*, 62(8):3140–3151, 2011.

[126] A. J. Chamkha and A.M. Rashad. Natural convection from a vertical permeable cone in a nanofluid saturated porous media for uniform heat and nanoparticles volume fraction fluxes. *International Journal of Numerical Methods for Heat & Fluid Flow*, 22(8):1073 – 1085, 2012.

[127] C-Y. Cheng. Natural convection boundary layer flow over a truncated cone in a porous medium saturated by a nanofluid. *International Communications in Heat and Mass Transfer*, 39(2):231–235, 2012.

[128] A. J. Chamkha, S. Abbasbandy, A. M. Rashad, and K. Vajravelu. Radiation effects on mixed convection about a cone embedded in a porous medium filled with a nanofluid. *Meccanica*, 48(2):275–285, 2013.

[129] A. J. Chamkha, S. Abbasbandy, and A. M. Rashad. Non-darcy natural convection flow for non-Newtonian nanofluid over cone saturated in porous medium with uniform heat and volume fraction fluxes. *International Journal of Numerical Methods for Heat & Fluid Flow*, 25(2):422–437, 2015.

[130] C. S. K. Raju and N. Sandeep. Heat and mass transfer in MHD non-Newtonian bioconvection flow over a rotating cone/plate with cross diffusion. *Journal of Molecular Liquids*, 215:115–126, 2016.

[131] S. Siddiqa, N. Begum, M. A. Hossain, and R. S. R. Gorla. Numerical solutions of natural convection flow of a dusty nanofluid about a vertical wavy truncated cone. *Journal of Heat Transfer*, 139(2):022503, 2017.

[132] M. Khan, M. Y. Malik, T. Salahuddin, K. U. Rehman, M. Naseer, et al. Mhd flow of Williamson nanofluid over a cone and plate with chemically reactive species. *Journal of Molecular Liquids*, 231:580–588, 2017.

[133] C. S. K. Raju, M. M. Hoque, N. N. Anika, S. U. Mamatha, and P. Sharma. Natural convective heat transfer analysis of MHD unsteady Carreau nanofluid over a cone packed with alloy nanoparticles. *Powder Technology*, 317:408–416, 2017.

[134] C. Sulochana, S.P. Samrat, and N. Sandeep. Numerical investigation of magnetohydrodynamic (MHD) radiative flow over a rotating cone in the presence of soret and chemical reaction. *Propulsion and Power Research*, 7(1):91 – 101, 2018. ISSN 2212-540X. doi: https:

//doi.org/10.1016/j.jppr.2018.01.001. URL http://www.sciencedirect.com/science/article/pii/S2212540X18300014.

[135] A. Mohammad, E. Y. Mohammad, D. Saeed, and I. Pop. Tiwari-Das nanofluid model for magnetohydrodynamics (MHD) natural-convective flow of a nanofluid adjacent to a spinning down-pointing vertical cone. *Propulsion and Power Research*, 7(1):78 – 90, 2018. ISSN 2212-540X. doi: https://doi.org/10.1016/j.jppr.2018.02.002. URL http://www.sciencedirect.com/science/article/pii/S2212540X18300075.

[136] S. Dinarvand and I. Pop. Free-convective flow of copper/water nanofluid about a rotating down-pointing cone using tiwari-Das nanofluid scheme. *Advanced Powder Technology*, 28 (3):900 – 909, 2017. ISSN 0921-8831. doi: https://doi.org/10.1016/j.apt.2016.12.016. URL http://www.sciencedirect.com/science/article/pii/S0921883116303880.

[137] O. Otegbeye and S. S. Motsa. A paired quasilinearization method for solving boundary layer flow problems. In *American Institute of Physics Conference Proceedings*, pages 1975(1), 030020. AIP Publishing, 2018.

[138] A. C. Eringen. Simple microfluids. *International Journal of Engineering Science*, 2(2): 205–217, 1964.

[139] T. Ariman, M. A. Turk, and N. D. Sylvester. Microcontinuum fluid mechanics: a review. *International Journal of Engineering Science*, 11(8):905–930, 1973.

[140] T. Ariman, M. A. Turk, and N. D. Sylvester. Applications of microcontinuum fluid mechanics. *International Journal of Engineering Science*, 12(4):273–293, 1974.

[141] G. Lukaszewicz. *Micropolar fluids: theory and applications*. Springer Science & Business Media, 1999.

[142] C. Chien-Hsin and C. Cha'o-Kuang. Non-Darcian mixed convection along a vertical plate embedded in a porous medium. *Applied Mathematical Modelling*, 14(9):482 – 488, 1990.

ISSN 0307-904. doi: https://doi.org/10.1016/0307-904X(90)90173-3. URL http://www.sciencedirect.com/science/article/pii/0307904X90901733.

[143] T. Na and J. P. Chiou. Laminar natural convection over a frustum of a cone. *Applied Scientific Research*, 35(5-6):409–421, 1979.

[144] B. Pullepu, K. Ekambavanan, and A. J. Chamkha. Unsteady laminar free convection from a vertical cone with uniform surface heat flux. *Nonlinear Analysis: Modelling and Control*, 13(1):47–60, 2008.

[145] S. G. Mohiddin, V. R. Prasad, S. V. K. Varma, and O. A. Bég. Numerical study of unsteady free convective heat and mass transfer in a Walters-B viscoelastic flow along a vertical cone. *International Journal of Applied Mathematics and Mechanics*, 6(15):88–114, 2010.

[146] A. Postelnicu. Free convection from a truncated cone subject to constant wall heat flux in a micropolar fluid. *Meccanica*, 47(6):1349–1357, 2012.

[147] A. Postelnicu. Free convection about a vertical frustum of a cone in a micropolar fluid. *International Journal of Engineering Science*, 44(10):672–682, 2006.

[148] F. O. Pătrulescu, T. Groşan, and I. Pop. Mixed convection boundary layer flow from a vertical truncated cone in a nanofluid. *International Journal of Numerical Methods for Heat & Fluid Flow*, 24(5):1175–1190, 2014.

[149] M. Y. Hussaini and T. A. Zang. Spectral methods in fluid dynamics. *Annual review of fluid mechanics*, 19(1):339–367, 1987.

[150] R. Peyret and T. D. Taylor. *Computational methods for fluid flow*. Springer Science & Business Media, 2012.

[151] S. Colbert-Kelly, G. B. McFadden, D. Phillips, and J. Shen. Numerical analysis and simulation for a generalized planar Ginzburg-Landau equation in a circular geometry. *Communications in Mathematical Sciences*, 15(2):329–357, 2017.

[152] M. M. Khader and S. Mziou. Chebyshev spectral method for studying the viscoelastic slip flow due to a permeable stretching surface embedded in a porous medium with viscous dissipation and non-uniform heat generation. *Boundary Value Problems*, 2017(1):37, 2017.

[153] M. Turkyilmazoglu. MHD fluid flow and heat transfer due to a stretching rotating disk. *International Journal of Thermal Sciences*, 51:195–201, 2012.

[154] N. Sharp and M. Trummer. A spectral collocation method for systems of singularly perturbed boundary value problems. *Procedia Computer Science*, 108:725–734, 2017.

[155] V. M. Magagula, S. S. Motsa, and P. Sibanda. A multi-domain bivariate pseudospectral method for evolution equations. *International Journal of Computational Methods*, 14(04): 1750041, 2017.

[156] S. Mondal, S. P. Goqo, P. Sibanda, and S. S. Motsa. Efficient multi-domain bivariate spectral collocation solution for MHD laminar natural convection flow from a vertical permeable flat plate with uniform surface temperature and thermal radiation. *International Journal of Computational Methods*, 2018.

[157] S. S. Motsa, C. RamReddy, and C. V. Rao. Non-similarity solution for soret effect on natural convection over the vertical frustum of a cone in a nanofluid using new bivariate pseudospectral local linearisation method. *Applied Mathematics and Computation*, 314:439–455, 2017.

[158] S. S. Motsa, Y. Khan, and S. Shateyi. Application of piecewise successive linearization method for the solutions of the Chen chaotic system. *Journal of Applied Mathematics*, 2012, 2012.